Technische Universität München

TUM School of Life Sciences

Identification and investigation of F-box proteins affecting carbohydrate utilization in *Neurospora crassa*

Lisa T. Meyer, M. Sc.

Vollständiger Abdruck der von der TUM School of Life Sciences
der Technischen Universität München zur Erlangung des akademischen Grades einer

Doktorin der Naturwissenschaften

genehmigten Dissertation.

Vorsitz:	Prof. Dr. Wolfgang Liebl
Prüfende der Dissertation:	1. Prof. Dr. Johan Philipp Benz
	2. Prof. Dr. Gustavo Goldman

Die Dissertation wurde am 09.09.2024 bei der Technische Universität München eingereicht und durch die TUM School of Life Sciences am 20.10.2024 angenommen.

Pre-publications of the dissertation

Parts of the results of this work have been pre-published in the following contributions:

L. T. Meyer, G. H. Goldman, J. P. Benz, Focus Group: Fungal Sensing and Signaling of the Environment (oral presentation). TUM Institute for Advanced Study General Assembly, digital, June 2021

L. T. Meyer, M. A. Crivelente Horta, G. H. Goldman, J. P. Benz, Identification of F-Box proteins involved in the regulation of sugar metabolism (oral presentation). Annual Conference of the Association for General and Applied Microbiology 2022, Düsseldorf/Jülich digital conference, Germany, February 2022

L. T. Meyer, M. A. Crivelente Horta, G. H. Goldman, J. P. Benz, Identification of F-Box proteins involved in the regulation of sugar metabolism (poster presentation). TUM Institute for Advanced Study General Assembly, Garching, Germany, May 2022

L. T. Meyer, M. A. Crivelente Horta, G. H. Goldman, J. P. Benz, Fungal Sensing and Signaling of the Environment – Identification of F-Box proteins involved in the regulation of sugar metabolism (poster presentation). Symposium Molecular Biology of Fungi 2022, Kaiserslautern, Germany, September 2022

Summary

Filamentous fungi naturally thrive on decaying plant matter. Due to their ability to secrete a range of enzymes required for the deconstruction of lignocellulosic material, filamentous fungi are of particular interest for biotechnological processes based on the biotransformation of plant biomass, a renewable resource for the circular bioeconomy. A natural break in fungal hydrolytic enzyme production is carbon catabolite repression (CCR), a highly conserved and multi-faceted process leading to the repression of genes involved in lignocellulose utilization in the presence of easily metabolizable carbon sources such as glucose.

The proteins involved in CCR are known to be regulated, among other things, by targeted degradation, an important regulatory process that creates new cellular or metabolic states. F-box proteins act as key factors within this process and are known to be involved in many metabolic adjustments including CCR. They target proteins for the proteasomal degradation process, allowing the regulation of new cellular or metabolic processes. F-box proteins are found in all eukaryotes. In fungi, they are, among other functions, involved in glucose sensing and induction of cellulolytic genes. Nevertheless, the targets and functions of most of the F-box proteins present in filamentous fungi remains enigmatic.

To specifically identify F-box proteins involved in the switch between CCR and lignocellulose utilization, the genetic reference organism *Neurospora crassa* was employed. Putative *N. crassa* F-box proteins were identified through database search for relevant domains and an ortholog search for known *Aspergillus nidulans* F-box proteins. Based on this identity search, *N. crassa* deletion strains of 40 genes with putative F-box protein domains were investigated and several mutants were identified showing significant CCR-repressed or de-repressed phenotypes. Six candidate genes potentially involved in the regulation of lignocellulose signaling pathways were identified. Four of the encoding proteins were subjected to immunoprecipitation experiments to identify potential interactors by using mass spectrometry. Additionally, transcriptional profiling was used for three of the corresponding *fbx* gene deletion strains during the switch from repressed to de-repressed state and *vice versa*.

Collectively, the results of these experiments allowed a better understanding of the function of F-Box proteins during carbohydrate metabolic switches in general and will be essential to allow rational strain modifications, leading to improved enzyme-producing strains of high interest for the industry.

Zusammenfassung

Filamentöse Pilze wachsen auf natürliche Weise auf zerfallenden Pflanzenmaterialien. Aufgrund ihrer Fähigkeit, eine Reihe von Enzymen abzusondern, die für den Abbau von lignozellulosehaltigem Material erforderlich sind, sind filamentöse Pilze von besonderem Interesse für biotechnologische Prozesse, die auf der Umwandlung pflanzlicher Biomasse beruhen, die eine erneuerbare Ressource für die zirkuläre Bioökonomie darstellt. Eine natürliche Einschränkung der hydrolytischen Enzymproduktion von Pilzen ist die Katabolitrepression, ein hochkonservierter und vielschichtiger Prozess, der zur Unterdrückung von Genen führt, die an der Lignocellulose-Verwertung beteiligt sind und in Gegenwart von leicht verstoffwechselbaren Kohlenstoffquellen wie Glucose ausgelöst wird. Es ist bekannt, dass die an der Katabolitrepression beteiligten Proteine unter anderem durch gezielten Abbau reguliert werden, ein wichtiger regulatorischer Prozess, um Platz für neue zelluläre oder metabolische Gegebenheiten zu schaffen. F-Box-Proteine agieren als Schlüsselfaktoren innerhalb dieses Prozesses und sind bekanntermaßen an vielen Stoffwechselregulierungen einschließlich Katabolitrepression beteiligt. Sie bestimmen Proteine für den proteasomalen Abbau, zum Beispiel um Platz für neue zelluläre oder metabolische Bedingungen zu schaffen. F-Box-Proteine kommen in allen Eukaryonten vor. In Pilzen sind sie unter anderem an der Glukose-Wahrnehmung und an der Induzierung von zellulolytischen Genen beteiligt. Dennoch ist die spezifische Funktion der meisten F-Box Proteine in filamentösen Pilzen nach wie vor unerforscht.

Um speziell F-Box Proteine zu identifizieren, die an der Umstellung zwischen Katabolitrepression und Lignocellulose-Nutzung beteiligt sind, wurde der genetische Referenzorganismus *Neurospora crassa* verwendet. Zunächst wurden putative *N. crassa* F-box Proteine durch eine Datenbanksuche nach relevanten Domänen und eine Ortholog-Suche nach bekannten F-Box Proteinen von *Aspergillus nidulans* identifiziert. Anschließend wurden durch die Kombination zweier Screening-Experimente *N. crassa* Deletionsstämme von 40 Genen mit putativer F-Box Protein Funktion untersucht, wobei festgestellt wurde, dass mehrere Deletionsstämme signifikante katabolit-reprimierte oder -dereprimierte Phänotypen ausprägten. Schließlich wurden sechs Kandidatengene identifiziert, die für die Regulierung von Lignocellulose-Signalwegen von großer Bedeutung sein könnten. Vier vielversprechende F-Box Protein Kandidaten, die für die Regulierung von Lignozellulose-Signalwegen von erheblicher Bedeutung sein könnten, wurden Immunpräzipitations-experimenten unterzogen, um potenzielle Interaktoren durch anschließende Massenspektrometrie zu identifizieren. Parallel dazu wurden die transkriptomischen Veränderungen in drei der entsprechenden *fbx* Deletionsstämme während des Wechsels von einer repressiven zu einer de-repressiven Wachstumsbedingung und umgekehrt durch

RNS-Sequenzierung analysiert, um ihren regulatorischen Einfluss auf die Kohlenstoffverwertung zu untersuchen.
Die Ergebnisse dieser Arbeit ermöglichen ein besseres Verständnis der Funktion von F-Box Proteinen bei der Umstellung des Stoffwechsels im Allgemeinen und tragen wesentlich dazu bei, gezielte Stammveränderungen zu ermöglichen, die zu verbesserten enzymproduzierenden Stämmen von großem Interesse für die Industrie führen.

Table of contents

Pre-publications of the dissertation ..... **I**

Summary ..... **II**

Zusammenfassung ..... **III**

List of figures ..... **X**

List of tables ..... **XIII**

1. Introduction **1**

1.1. Importance of lignocellulosic biomass as sustainable raw material for energy and fuels 1

1.2. Structure of lignocellulose and enzymatic decomposition 2

1.3. The filamentous fungus *Neurospora crassa* 4

1.4. Fungal sensing of the environment and regulation of carbon utilization 5

1.5. Targeted protein degradation 7

1.5.1. E3 ubiquitin ligase mediated proteasomal degradation 7

1.5.2. F-box proteins – the substrate recognizing subunit of the SCF complex .. 8

1.6. Function of F-box proteins across eukaryotes with a focus on *Neurospora crassa* ……..11

1.7. Gap of knowledge and objectives 12

2. Results **14**

2.1. Putative F-box proteins of *Neurospora crassa* 14

2.1.1. Identification of putative *fbx* genes in *Neurospora crassa* 14

2.1.2. Transcriptional response of *N. crassa fbx* genes during perception of different carbon sources 17

2.2. Screening for F-box proteins involved in the regulation of sugar metabolism.....20

2.2.1. Cellulolytic response of *N. crassa* to different sugar concentrations 20

2.2.2. Screening for F-box genes involved in the integration of cellulose perception ……..22

2.2.3. Biomass formation of *N. crassa fbx* deletion strains in presence of allyl alcohol…….25

2.2.4. Selection of putative F-box protein candidates for further investigations . 26

2.3. Characterization of selected F-box candidates 29

2.3.1. Developmental phenotypes and growth rates of selected *fbx* deletion strains 29

2.3.2. Transcriptional response to carbon source switches by *N. crassa* 32

2.4. Identification of F-box interaction partners 56

2.4.1. Complementation of selected F-box candidates and analysis of functionality of the constructs 56

2.4.2. Identification of putative F-box interaction partners via immunoprecipitation and mass spectrometry 59

2.4.3. Investigation of putative interaction partners and screening for CCR-phenotypes 67

3. Discussion 71

3.1. Putative F-box proteins of *Neurospora crassa* 71

3.2. Screening for F-box proteins involved in the regulation of sugar metabolism 73

3.2.1. Altering glucose levels affect *Neurospra crassa* cellulolytic response 73

3.2.2. F-box deletion affects the cellulolytic response in *Neurospora crassa* and leads to CCR-related defects 74

3.3. Characterization of selected F-box candidates 76

3.3.1. Global transcriptional response to carbon source switches by *N. crassa fbx* deletion strains results in altered gene enrichment 76

3.3.2. Comparative analysis of transcriptomes between *N. crassa* WT, Δ*fbx17/41* and ΔNCU05033 mutants distinguishes clusters of genes co-regulated in response to carbon source switches 80

3.4. Identification of F-box interaction partners 84

3.4.1. Localization events could cause functional consequences of complemented strains 84

3.4.2. Three F-box candidates assemble within the SCF complex – one might functions in a SCF-independent manner 84

3.4.3. Fbx40 might influence anastomosis through HAM-14 85

3.4.4. Putative transcriptional regulator targeted by NCU05033 is part of the CRE-1 regulon 86

3.4.5. NCW-1 protein levels might contribute to the repressed phenotype of ΔNCU05033 86

3.4.6. Fbx41 might indirectly influence the concentration of cellulose signaling molecules 88

3.4.7. Fbx17 could indirectly influence glucose-6-phosphate levels 90

4. Concluding remarks and outlook 91

5. Materials and methods 93

5.1. Equipment, chemicals and strains 93

5.1.1. Software and instruments 93

5.1.2. Chemicals and consumables 96

5.1.3. Buffers and media 100

5.1.4. Primers and plasmids 104

5.1.5. Utilized organisms and strains 108

5.2. Physiological methods 111

5.2.1. Propagation of *N. crassa* 111

5.2.2. Glycerol stocks 111

5.2.3. *N. crassa* growth assays 111

5.2.4. Determination of mycelial dry weight 114

5.2.5. Homokaryotization of *N. crassa* via microconidia isolation 114

5.2.6. Crossing of *N. crassa* strains 115

5.2.7. Race tube assay 116

5.3. Molecular biological methods 116

5.3.1. PCR for cloning using Phusion polymerase 116

5.3.2. Genotyping PCR using Taq polymerase 117

5.3.3. Agarose gel electrophoresis 118

5.3.4. DNA gel extraction and purification 118

5.3.5. Restriction digest and ligation cloning of *N. crassa* expression cassettes 118

5.3.6. *Escherichia coli* transformation 119
5.3.7. *E. coli* plasmid miniprep and sequencing 120
5.3.8. *N. crassa* transformation by electroporation 120
5.3.9. gDNA extraction from *N. crassa* conidia 121
5.3.10. RNA extraction from *N. crassa* biomass 121
5.3.11. Quality control of RNA samples 122
5.3.12. cDNA synthesis and quantitative PCR 123
5.4. Biochemical methods 124
5.4.1. Protein quantification assay according to Bradford 124
5.4.2. Determination of enzymatic activity of *endo*-1.4-β-D-glucanase (cellulase) 124
5.4.3. Sodium dodecyl sulfate polyacrylamide gel electrophoresis (SDS-PAGE) 125
5.4.4. Silver staining of protein gels 126
5.4.5. Coomassie Blue staining of protein gels 126
5.4.6. Protein extraction and immunoprecipitation 127
5.4.7. Fusion protein detection by Western Blotting 127
5.4.8. Trypsin in-gel digestion of protein samples after immunoprecipitation 128
5.4.9. Mass spectrometry 130
5.5. Transcriptome analysis 130
5.5.1. RNA sequencing 130
5.5.2. Hierarchical clustering of transcriptome data 132
5.6. Statistical and computational methods 132
5.6.1. Determination of F-box proteins and protein domains 132
5.6.2. Statistical methods 132
5.6.3. Quantitative analysis of mass spectrometry data using MaxQuant and Perseus 133
5.6.4. Qualitative analysis of mass spectrometry data 133
6. Appendix 134
6.1. Abbreviations 134

6.2. Supplementary figures 136

6.3. Supplementary tables.....150

6.4. Plasmid maps.....162

References 166

Acknowledgements 178

List of figures

Figure 1-1: Conversion of lignocellulose biomass for the production of chemicals and fuels. 2
Figure 1-2: Key enzymes for cellulose, hemicellulose and lignin depolymerization. 4
Figure 1-3: 5
Figure 1-4: Examples of F-box motif consensus sequence variants from literature given in single-letter amino acid code. 9
Figure 2-1: Domain architectures of the putative *N. crassa* F-box proteins. 15
Figure 2-2: Phylogenetic tree of all known putative F-box proteins in *N. crassa* and *A. nidulans*. 17
Figure 2-3: Transcriptional response of putative *N. crassa fbx* genes during perception of different carbon sources. 18
Figure 2-4: Transcriptional response of putative *fbx* genes available as deletion strain. 19
Figure 2-5: Cellulase activity of *N. crassa* WT culture supernatants. 21
Figure 2-6: Enzymatic activity profiles of *N. crassa fbx* deletion strains grown in 1% Avicel supplemented with 0.5% glucose. 22
Figure 2-7: Protein profile of culture supernatants from *N. crassa* WT and Δ*fbx23*. 23
Figure 2-8: Cellulase activity versus protein amount of *N. crassa fbx* deletion mutants. 24
Figure 2-9: Biomass formation of *N. crassa fbx* deletion strains in presence of allyl alcohol. 25
Figure 2-10: *N. crassa* growth phenotype in 24-deep well plate. 26
Figure 2-11: Growth phenotypes of *N. crassa* strains in agar slants. 30
Figure 2-12: Growth rate of deletion strains of selected *fbx* candidates compared to WT and Δ*cre-1*. 30
Figure 2-13: Developmental deficits of Δ*fbx17* and Δ*fbx22*. 31
Figure 2-14: *cbh-1* expression of selected *fbx* mutants. 32
Figure 2-15: Venn diagrams of significant DEGs within each strain at different time points. 34
Figure 2-16: Comparison of expression levels of RNA-seq data. 40
Figure 2-17: Hierarchical clustering analysis of RNA-sequencing data from *N. crassa* Δ*fbx17* and WT strains. 44
Figure 2-18: Hierarchical clustering analysis of RNA-sequencing data from *N. crassa* Δ*fbx41* and WT strains. 47
Figure 2-19: Hierarchical clustering analysis of RNA-sequencing data from *N. crassa* ΔNCU05033 and WT strains. 49
Figure 2-20: Hierarchical clustering of CAZymes. 52

Figure 2-21: Hierarchical clustering of sugar transporter genes. 54
Figure 2-22: Cellulase activity of complemented strains grown in 1% Avicel supplemented with 0.5% glucose. 57
Figure 2-23: Biomass formation of *N. crassa* complemented strains in presence of allyl alcohol. 58
Figure 2-24: Volcano plot of F-box::GFP bait proteins for Fbx17 and Fbx41 (derepressed phenotype). 60
Figure 2-25: Volcano plot of F-box::GFP bait proteins for Fbx40 and NCU05033 (repressed phenotype). 61
Figure 2-26: Venn diagram of qualitative analysis of MS data. 62
Figure 2-27: GO analysis of putative interactors of Fbx40 and NCU05033. 63
Figure 2-28: GO analysis of putative interactors of Fbx17 and Fbx41. 64
Figure 2-29: Biomass formation of putative interactor deletion strains in presence of allyl alcohol. 68
Figure 2-30: Cellulase activity of putative interactor deletion strains grown in 1% Avicel supplemented with 0.5% glucose. 69
Figure 3-1: Model of F-box protein NCU05033 indirectly influencing the cellulolytic capacity in *Neurospora crassa*. 88

Figure S 6-1: Determined protein amount of culture supernatants. 136
Figure S 6-2: Protein profile of culture supernatants from *N. crassa*. 137
Figure S 6-3: Repetition of enzymatic activity profiles of selected *N. crassa fbx* deletion strains grown in 1% Avicel supplemented with 0.5% glucose. 138
Figure S 6-4: *N. crassa* conidia. 139
Figure S 6-5: Race tube assay of selected *N. crassa* deletion strains compared to WT and Δ*cre-1*. 139
Figure S 6-6: Fluorescent microscopy of *N. crassa* WT, *fbx40*-comp and *cre-1*-comp. ..140
Figure S 6-7: Fluorescent microscopy of *N. crassa* WT, *fbx41*-comp and NCU05033-comp. 140
Figure S 6-8: Quality control of *N. crassa* WT samples for IP and MS analysis. 141
Figure S 6-9: Quality control of *N. crassa* GFP control samples for IP and MS analysis.141
Figure S 6-10: Quality control of *N. crassa fbx17*-comp samples for IP and MS analysis. 141
Figure S 6-11: Quality control of *N. crassa fbx40*-comp samples for IP and MS analysis. 142
Figure S 6-12: Quality control of *N. crassa fbx41*-comp samples for IP and MS analysis. 142

Figure S 6-13: Quality control of *N. crassa* NCU05033-comp samples for IP and MS analysis. 142
Figure S 6-14: Quality control of *N. crassa pdr-1*-comp samples for IP and MS analysis. 143
Figure S 6-15: Quality control of *N. crassa cre-1*-comp samples for IP and MS analysis. 143
Figure S 6-16: Volcano plot of both transcription factors CRE-1::GFP and PDR-1::GFP. 144
Figure S 6-17: Volcano plot F-box::GFP bait proteins whose deletions showed a derepressed phenotype. 145
Figure S 6-18: Volcano plot F-box::GFP bait proteins whose deletions showed a repressed phenotype. 146
Figure S 6-19: Venn and network diagram of putative interactors identified via qualitative analysis of MS data across all conditions for the investigated F-box proteins. 147
Figure S 6-20: Venn and network diagram of putative interactors identified via qualitative analysis of MS data across all conditions for the investigated F-box proteins and CRE-1. 147
Figure S 6-21: Growth phenotype of deletion strains of putative interactors of Fbx17. 148
Figure S 6-22: Total protein amount in culture supernatants of putative interactor deletion strains grown in 1% Avicel supplemented with 0.5% glucose. 148
Figure S 6-23: Protein profile of culture supernatants from *N. crassa* Fbx interactor deletion strains. 149
Figure S 6-24: Map of *Neurospora* expression vector pCCG::C-Gly::GFP. 162
Figure S 6-25: Map of *Neurospora* expression vector pLK052, pCCG::NCU07521::C-Gly::GFP. 162
Figure S 6-26: Map of *Neurospora* expression vector pLK053, pCCG::NCU05939::C-Gly::GFP. 163
Figure S 6-27: Map of *Neurospora* expression vector pLK054, pCCG::NCU04540::Gly-GFP 163
Figure S 6-28: Map of *Neurospora* expression vector pLK055, pCCG::NCU03462::Gly-GFP. 164
Figure S 6-29: Map of *Neurospora* expression vector pLK056, pCCG::NCU00471::C-Gly::GFP. 164
Figure S 6-30: Map of *Neurospora* expression vector pLK057, pCCG::NCU05033::C-Gly::GFP. 165
Figure S 6-31: Map of *Neurospora* expression vector pLK058, pCCG::NCU08807::Gly-GFP. 165

List of tables

Table 2-1: Interesting carbon utilization genes which were first (F) and second (S) neighbor of the corresponding *fbx* gene in the co-expression network. 27
Table 2-2: Summary of scores for *N. crassa* putative F-box proteins and the transcription factor CRE-1 27
Table 2-3: List of putative F-box protein interactors involved in carbon utilization and regulation. 65
Table 5-1: List of used software and online tools for data processing and analysis. 93
Table 5-2: List of used instruments. 95
Table 5-3: List of used chemicals and carbon sources. 96
Table 5-4: List of used consumables and kits 98
Table 5-5: List of buffers and media. 100
Table 5-6: List of antibiotics and supplements 103
Table 5-7: List of used primers. 104
Table 5-8: List of plasmids used in this study. 106
Table 5-9: List of used organisms and strains. 108
Table 5-10: Culturing procedure and time points for first qPCR experiment. 113
Table 5-11: Culturing procedure and time points for second qPCR and RNA-seq experiment. 114
Table 5-12: Phusion polymerase PCR amplification reaction master mix. 116
Table 5-13: Thermocycler protocol for Phusion polymerase PCR amplification 117
Table 5-14: Taq polymerase PCR amplification reaction master mix. 117
Table 5-15: Thermocycler protocol for Taq polymerase PCR amplification. 117
Table 5-16: Composition of restriction digest approach 118
Table 5-17: Required insert DNA mass per T4 ligation approach. 119
Table 5-18: T4 ligation assembly approach 119
Table 5-19: Pipetting schedule for BSA calibration standard for Bradford assay. 124
Table 5-20: Composition of acrylamide separating gel for SDS-PAGE. 125
Table 5-21: Composition of a stacking gel for SDS-PAGE. 126
Table 5-22: Metadata of the submitted RNA samples to the chair of Animal Physiology and Immunology (TUM) for performing sequencing. 130

Table S 6-1: Number of differentially expressed genes of RNA-sequencing analysis (switch from CC-derepressing to CC-repressing condition). 150
Table S 6-2: Number of differentially expressed genes from RNA-sequencing analysis (switch from CC-repressing to CC-derepressing condition). 150

Table S 6-3: Generation of histidine auxotrohic *N. crassa* strains through mating. 150
Table S 6-4: *N. crassa* strains used for immunoprecipitation experiments (chapter 2.4.2). 151
Table S 6-5: Samples used for immunoprecipitation and mass spectrometry analysis. . 151
Table S 6-6: List of interactors identified for several bait proteins via quantitative analysis. 152
Table S 6-7: List of interactors identified exclusively for one bait protein via quantitative analysis. 153
Table S 6-8: Qualitative analysis of NCU05033::GFP MS data. 155
Table S 6-9: Qualitative analysis of Fbx17::GFP MS data. 156
Table S 6-10: Qualitative analysis of Fbx40::GFP MS data. 157
Table S 6-11: Qualitative analysis of Fbx41::GFP MS data. 157
Table S 6-12: Qualitative analysis of CRE-1::GFP MS data. 158
Table S 6-13: List of interactors identified within several F-box samples via qualitative analysis of the MS data. 158
Table S 6-14: List of interactors identified within several F-box samples and CRE-1 via qualitative analysis of the MS data. 160

1. Introduction

1.1. Importance of lignocellulosic biomass as sustainable raw material for energy and fuels

Fossil fuels are the primary energy source used across the world, since they provide a high energy content. However, their combustion leads to the emission of greenhouse gases. [Osman et al. 2023] Globally, the highest carbon dioxide emission emerges in the energy sector with 14.6 gigatons, followed by approximately 9 gigatons from industrial emissions and approximately 8 gigatons from transport [IEA 2023]. To combat the resulting climate change, there is a high need for energy obtained from renewable sources, since combustion of biofuels is cleaner than gasoline, resulting in decreased greenhouse gas emissions [Wang et al. 2007]. Therefore, to decrease greenhouse gas emissions in the transport sector, biofuels are a potential alternative, since only three percent of the energy used for global transport are covered by liquid biofuels [Clauser et al. 2021]. Dependent on the biomass source used to produce liquid biofuels, there are three classes of liquid biofuels. First-generation biofuels are generated from biomass of the food chain, containing high amounts of starches, sugars and fats. The raw material used for second-generation biofuels are inedible residues from plants like lignocellulosic biomass e.g. from agriculture. Therefore, there is no competition with food production when producing second-generation biofuels. Algae and cyanobacteria are employed to produce third-generation biofuels, which is rather on a pilot level. [Clauser et al. 2021; Maliha and Abu-Hijleh 2022]

Greenhouse gas emissions from fuel combustion are dependent from the used feedstock. The highest decrease of greenhouse gas emissions can be achieved by fuels produced using cellulosic biomass, offering 86% reduction. [Wang et al. 2007] Lignocellulose is the main component of plant biomass, the most abundant raw material on Earth and a renewable resource [Guerriero et al. 2015]. The major challenge of second-generation biofuels production is the complex structure of lignocellulosic biomass, which consists of three main components lignin, cellulose and hemicellulose [Wilson and Lee 2016].

The production of biofuels from biomass is differentiated between the thermochemical or syngas route and the sugar fermentation (Figure 1-1) [Wilson and Lee 2016; Clauser et al. 2021]. Disadvantages of thermo-chemical production methods are that they are unspecific and destructive, resulting in loss of components with potential value. Other limitations of biomass pyrolysis include the high water and oxygen content of the bio-oil produced, as well as a low calorific value, high viscosity and immiscibility with regular fuels. One challenge in the biochemical process is that lignocellulose cannot be utilized directly. First, the individual components lignin, hemicellulose and cellulose must be separated from each

other. Separation methods used are acid or base hydrolysis, steam explosion or organosolv treatments. [Wilson and Lee 2016]

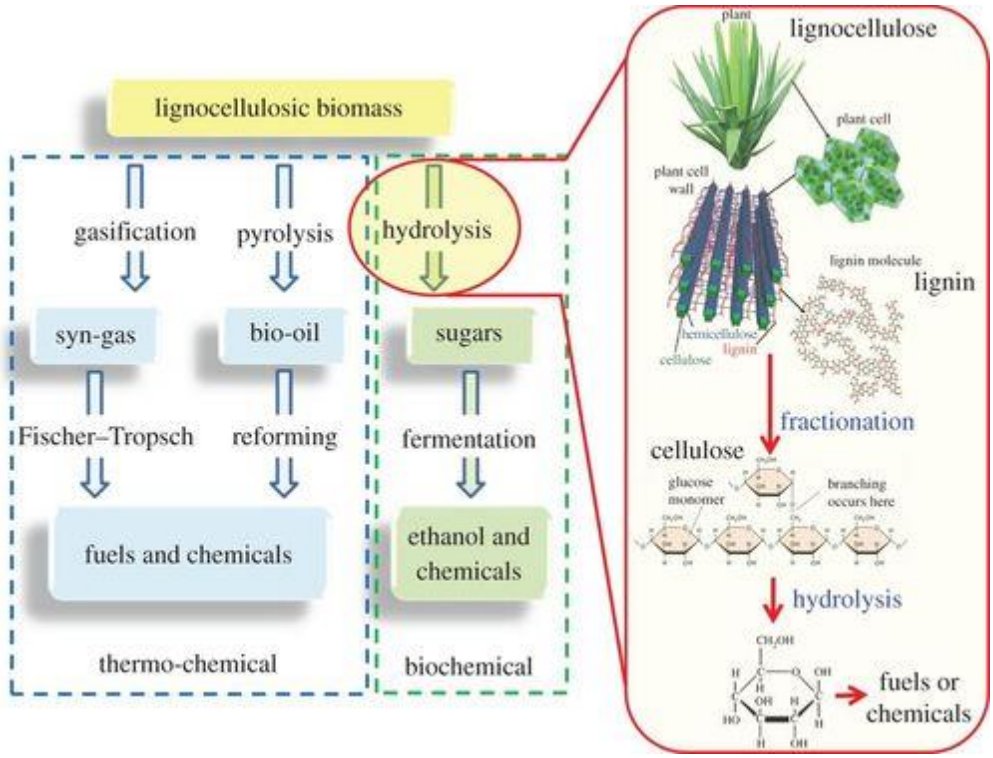

Figure 1-1: Conversion of lignocellulose biomass for the production of chemicals and fuels. Within the biochemical route, lignocellulose has to be segregated into its individual components to hydrolyze cellulose to glucose. This figure was published by Wilson and Lee [Wilson and Lee 2016].

Within the biochemical process, microorganisms and enzymes are utilized to convert the cell wall polysaccharides to fermentable sugars. Advantages of this method are lower energy consumption and that aggressive chemicals are not necessary. The great expenditure of time is the major disadvantage of the biological method, which makes its commercial use impracticable. [Devi et al. 2022] Therefore, rational strain modifications, leading to improved enzyme-producing strains would be of high interest for the industry [Gabriel et al. 2021].

1.2. Structure of lignocellulose and enzymatic decomposition

The plant cell wall, which constitutes more than 50% of the dry weight of the plant, provides mechanical strength by means of its rigid structure and is therefore essential for the plants sedentary life [Kubicek 2013].

Normally, plant cell walls consist of a total of three layers. The primary cell wall, which consists of growing cells and mainly of the polysaccharides cellulose, hemicellulose and pectin. The secondary cell wall, which forms a barrier within the primary cell wall, often consists of hemicellulose, mostly xylan, cellulose and lignin. The third and oldest layer, the

middle lamella, forms the outermost layer and consists mainly of pectin. [Taiz and Zeiger 2002; Kubicek 2013]

Lignocellulosic biomass comprises of polyphenol lignin and the three polysaccharides pectin, cellulose and hemicellulose, which makes it highly complex for enzymatic degradation [Glass et al. 2013; Andlar et al. 2018]. The composition and amount of the constituents vary dependant from the origin of the plant matter. The linear polymer cellulose, which is the most abundant polysaccharide of lignocellulose, consists of cellobiose dimers, which are linked through hydrogen bonds and van der Waals forces. Each cellobiose dimer consist of two β-1,4-glycosidic bound D-glucose units. [Frey-Wyssling 1954; Varner and Lin 1989; Sánchez 2009]Hemicellulose is the second most abundant polysaccharide, consisting of a diverse group of branched polysaccharides with the ability to connect onto the surface of cellulose fibrils via hydrogen bonds [Varner and Lin 1989; Somerville et al. 2004]. The main monomers and heteropolymers of hemicellulose are e. g. xylans, consisting of β-1,4-linked D-xylose residues as backbone, mannans, composed of D-mannose units, arabinan, containing L-arabinose, and galactan which is made up of D-galactose [Bastawde 1992].

The polyphenol lignin comprises about 15 to 30% of the lignocellulosic matrix and is covalently bound to plant polysaccharides like cellulose and mainly consists of three phenylpropanoid alcohols [Taiz and Zeiger 2002; van den Bosch et al. 2018].

The major components of pectin are uronic acids. Homogalacturonan is the most abundant polysaccharide of pectin and consists of α-linked D-galacturonic acids. Homogalacturonan with substitutions of β-linked xylose at O-3 is designated xylogalacturonan. Approximately 20 to 35% of pectin consists of rhamnogalacturonan I, which is comprised of the repetitive disaccharide D-galacturonic acid and L-rhamnose. The D-galacturonic acid and L-rhamnose backbone is connected with side chains of D-galactose, L-arabinose, L-rhamnose and also polymers like arabinan and arabinogalactan. Rhamnogalacturonan II has the highest complexity. It accounts for about 10% of pectin. In total, it is composed of about twelve different monomers. [Schols et al. 1990; Somerville et al. 2004; Mohnen 2008]

Crucial for the recalcitrance of plant biomass is the degree of interlacing of the cellulose by the hemicellulose, the high cistallinity and the high degree of polymerization of the cellulose and the lignin content [Andlar et al. 2018]. Prior to the hydrolysis of cellulose, hemicellulose and lignin need to be modified or depolymerized, for a better access to cellulose. The deconstruction of lignocellulose requires a suite of carbohydrate-active enzymes, including cellulases, hemicellulases, and lignin-modifying enzymes such as peroxidases, laccases, and ferulic acid esterases. These enzymes act together to break down the complex structure of lignocellulose and convert it into simple sugars that can be used for the production of biofuels and other products. [Guerriero et al. 2015]

Generally, two different types of enzymes are utilized extracellularly by fungi. Oxidative enzymes open phenyl rings to degrade lignin and hydrolytic enzymes, which cleave polysaccharides (Figure 1-2). [Sánchez 2009; Andlar et al. 2018; Østby et al. 2020]

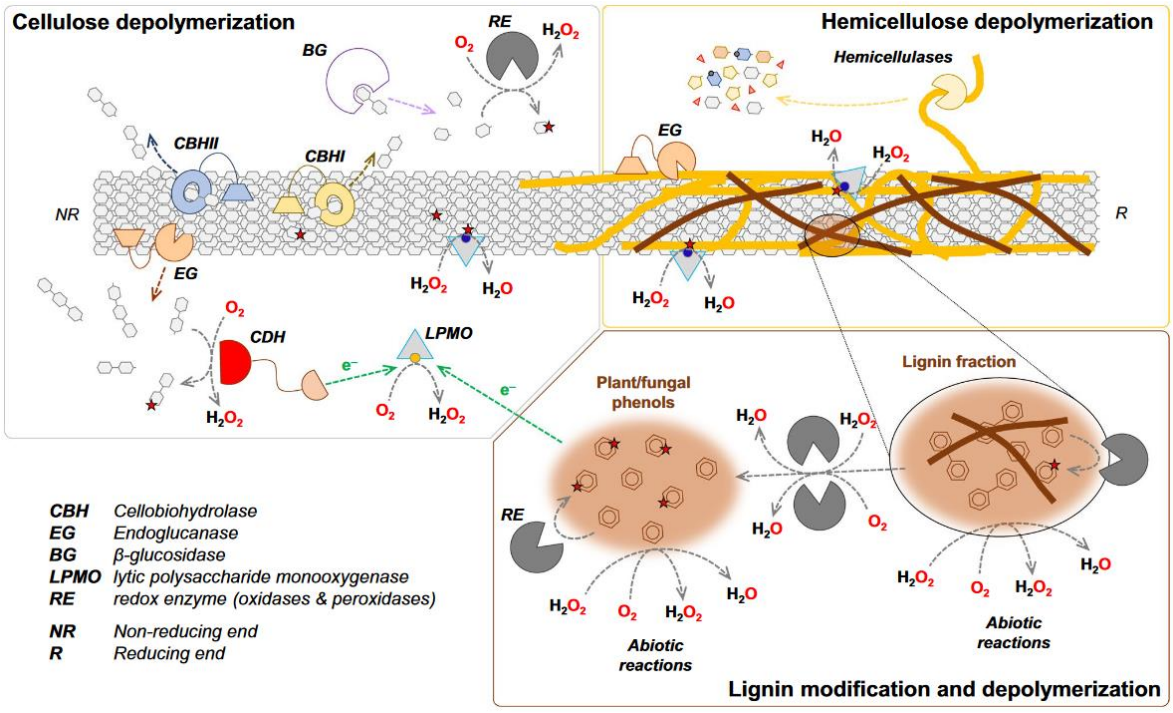

Figure 1-2: Key enzymes for cellulose, hemicellulose and lignin depolymerization.
According to Østby *et al.* the most important enzymes are depicted for lignocellulose degradation. The oxidation via lytic polysaccharide monooxygenases, which are represented as triangles, is depicted as star. Cu(I) is represented by blue spheres and Cu(II) by orange ones. Cellobiohydrolases are responsible for the cleavage of cellobiose from cellulose chain ends, while endoglucanases cleave the cellulose polymer into smaller fractions like oligomers at random sites. The resulting non-reducing β-D-glucosyl residues are hydrolysed by β-glucosidases, releasing D-glucose. This figure was published by Østby *et al.* [Østby et al. 2020].

1.3. The filamentous fungus *Neurospora crassa*

Neurospora crassa is an orange mold which belongs to the phylum Ascomycota (Figure 1-3). *N. crassa* was initially described as a contamination in French bakeries in 1843 as *Monilia sitophila*. [Shear and Dodge 1927; Davis and Perkins 2002] *N. crassa* has often been isolated from burned plant matter in tropical or subtropical regions [Jacobson et al. 2006]. Within early studies of *Neurospora*, Bernard O. Dodge discovered its potential use for genetics and identified two mating types [Davis and Perkins 2002]. The haploid fungus has a heterothallic life cycle which contains an asexual and a sexual phase [Griffin 1994].

In 1941, George Beadle and Edward Tatum proposed the, nowadays known as, “one gene–one enzyme hypothesis” while working on *N. crassa* enzyme-encoding genes, for which they received the Nobel Prize in 1958 [Beadle and Tatum 1941]. The whole genome was sequenced in 2003 and comprises approximately 10,000 protein coding genes [Galagan et al. 2003]. *N. crassa* is also known for its capabilities to degrade lignocellulosic biomass [Tian et al. 2009]. Additionally, there are extensive opportunities of genetic and molecular tools to work with *N. crassa*, e. g. arrayed mutants of nearly full genome deletion strains are available from the Fungal Genetic Stock Center (FGSC) [Colot et al. 2006; Dunlap et al. 2007; McCluskey et al. 2010].

Figure 1-3: *Neurospora crassa* growth phenotype on 2% sucrose.

Since *N. crassa* synthesizes and secretes all enzyme types involved in cellulose hydrolysis as well as different enzymes for hemicellulose degradation and in addition has a very fast growth rate, it is a very promising candidate for the industrial utilization of renewable resources, such as cellulosic plant biomass [Dogaris et al. 2013].

1.4. Fungal sensing of the environment and regulation of carbon utilization

Filamentous fungi are specialized on decaying plant matter. Due to their ability to secrete a range of enzymes required for the deconstruction of lignocellulosic material, filamentous fungi are of particular interest for biotechnological processes based on the biotransformation of plant biomass, a renewable resource for the circular bioeconomy. [Meyer et al. 2020]

The transcriptional response triggered by different carbon sources has been studied in, e. g. *N. crassa*, *Aspergillus niger* and *Trichoderma reesei*, concluding that low amounts of a set of extracellular enzymes is generating degradation products, which are leading to an increased expression of the proteins needed to degrade and transport the identified carbon source [Tian et al. 2009; Delmas et al. 2012; Ries et al. 2013]. This pattern has been recognized in all species tested, and can be split into three main steps of coordination. In absence of inducers, like carbohydrate monomers, enzymes are expressed at low levels, so called “scouting enzymes”. This sensing and perception step triggers signal transduction, which causes, in a third step, the response of the fungus mediated by transcriptional activators and repressors. [Tian et al. 2009; Delmas et al. 2012; Ries et al. 2013; Daly et al. 2016] For instance, the gene expression of carbohydrate-active enzymes (CAZymes [Cantarel et al. 2009]) is under the control of transcription factors which activate transcription when lignocellulosic biomass is sensed in the environment [Huberman et al. 2016]. Only

little is known about the initial singaling steps right after induction, but phosphorylation events seem to play a crucial role within this process [Horta et al. 2019].

In general, fungi recognize the availability of glucose, for instance by means of the cAMP-dependent protein kinase A (PKA) signaling pathway. Here, two main mechanisms can be distinguished. One is the phosphorylation of the imported glucose, and the other G protein-coupled receptors (GPCR). [Brown et al. 2014] Li and Borkovich described the link between carbon source sensing and the PKA pathway in *N. crassa*, and the importance of the GPCR GPR-4 for the regulation of cAMP levels during medium switches [Li and Borkovich 2006].

In presence of easily metabolizable carbon sources such as glucose, a natural break in fungal hydrolytic enzyme production is enabled, called *carbon catabolite repression* (CCR), a highly conserved and multi-faceted process leading to the repression of genes involved in lignocellulose utilization [Ebbole 1998; Delmas et al. 2012; Assis et al. 2018]. Glucose is favored over more complex carbon sources, since it represents the most energetically efficient carbon source [Ries et al. 2016].

One known mediator of CCR is the transcription factor CreA/CRE-1/Mig1 (*Aspergillus nidulans*/*N. crassa*/*Saccharomyces cerevisiae*), which has been firstly identified and described in *Aspergillus nidulans* [Arst and Cove 1973; Bailey and Arst 1975]. CreA was shown to interact and form a complex with the corepressors SsnF and RcoA, which is essential for the functionality [Hicks et al. 2001; García et al. 2008; Assis et al. 2018]. The CreA ortholog in *S. cerevisiae*, Mig1, recruits the repressor complex Tup1-Ssn6, which is orthologous to SsnF and RcoA in *A. nidulans* [Treitel and Carlson 1995]. The *N. crassa* orthologs of Tup1-Ssn6, RCO-1 and RCM-1, were investigated, but there was no conclusion made on a physical interaction of RCO-1 and RCM-1 with CRE-1 [Cupertino et al. 2015].

In presence of the carbon catabolite derepressing condition xylan, CreA was found to be degraded by the help of the F-box protein Fbx23 (AN5593) in a ubiquitylation-dependent manner in *A. nidulans* [Assis et al. 2018]. It is still unclear, however, if CreA itself or an interaction partner is ubiquitinated. In carbon catabolite derepressing conditions, CreA was found to interact physically with two kinases, GskA and CkiA. Both kinases were found to phosphorylate CreA, which is crucial for its localization and DNA binding abilities. [Assis et al. 2018; Assis et al. 2021]

Additionally involved in CCR in *A. nidulans* are CreB, a deubiquitinating enzyme, CreC, a WD-40 repeat protein, and CreD, an arrestin motif protein [Hynes and Kelly 1977; Todd et al. 2000; Alam and Kelly 2017]. It has been assumed that the CreB-CreC deubiquitination complex regulates CreA. In presence of CreB, there is active CreA, and therefore repression. CreB and CreC interact *in vivo*, while CreC prevents CreB proteolysis. It has been demonstrated that CreB overexpression is able to compensate loss of CreC, which was not working *vice versa*. [Lockington and Kelly 2002] Alam and Kelly aimed to reveal the

link between CreA and CreB with regard to their involvement in CCR [Alam and Kelly 2017]. Within this study, the suggestion was made that CreB could be involved in CCR through the Histone transcription regulator 3 (Hir3) regulatory process or Hir3 modification [Alam and Kelly 2017]. Nevertheless, previous studies showed the requirement of ubiquitylation for CreA degradation [Lockington and Kelly 2002; Ries et al. 2016].

In *N. crassa*, the expression of cellulases was suggested to be regulated at least through three pathways. One is the CLR-mediated induction of cellulases through the interplay of transcriptional regulators. The others are CCR, including the involvement of CRE-1, and the hyperosmotic response (OS) MAP kinase pathway. Within the OS pathway, the histidine kinase OS-1 is able to sense the osmolarity of the environment and activates the OS MAP kinase cascade after an increase of osmolarity. As consequence, the internal osmolarity is increased to adapt to the environment, leading to the repression of genes like cellulases. [Coradetti et al. 2012; Huberman et al. 2017; Wu et al. 2020; Kerkaert and Huberman 2023]

1.5. Targeted protein degradation

1.5.1. E3 ubiquitin ligase mediated proteasomal degradation

Post-translational modifications (PTMs) are essential for metabolic adjustments and for the adaption to environmental changes. To date, over 200 divers PTMs have been discussed in literature, reversible and irreversible ones, which open a wide range of functions (reviewed in [Salas-Lloret and González-Prieto 2022] with focus on ubiquitin and SUMO). In 1975 ubiquitin was discovered, a polypeptide chain consisting of 76 amino acid residues, which received its name because it was found being ubiquitously existent among living cells [Goldstein et al. 1975; Vijay-Kumar et al. 1987]. Polyubiquitin serves as proteolytic signal within the ubiquitin-proteasome system: Within a first step, an ubiquitin activating enzyme, enzyme-1 (E1), activates ubiquitin in an adenosine triphosphate (ATP)-dependent manner. The activated ubiquitin is transferred to an ubiquitin-conjugating enzyme (E2). With the help of an E3 ubiquitin ligase, the substrate protein is ubiquitinated and a minimum of four attached ubiquitins is necessary for the recognition by the 26S proteasome and subsequent degradation of the substrate protein. [Hershko et al. 1983; Scheffner et al. 1995; Thrower et al. 2000; Welchman et al. 2005]

In general, three main families of E3 ubiquitin ligases are distinguished on basis of the catalytic mechanism. The really interesting new gene (RING) E3 ligases, the Homologous to E6-AP C-Terminus (HECT) E3 ligases and the RING-between-RING (RBR) E3 ligases. [Berndsen and Wolberger 2014; Zheng and Shabek 2017; Wang et al. 2023] The RING E3 ligases directly mediate transfer of the ubiquitin from E2 ubiquitin-conjugating enzyme to the substrate, while the RING domain binds the E2 enzyme, which leads to a closed

conformation essential for the reaction to split off ubiquitin from the E2 enzyme [Potuschak et al. 1998; Metzger et al. 2012; Wang et al. 2023]. A two-step reaction is catalyzed by the HECT E3 ligases, in which ubiquitin is first transferred from an active cysteine to a catalytic cysteine in the HECT C-lobe. In a second step, ubiquitin is transferred from the HECT C-lobe to the substrate protein. [Huibregtse et al. 1995; Kamadurai et al. 2009; Wang et al. 2023] The RBR E3 ligases contain three zinc-binding domains: RING1, in-between RING (IBR) and RING2. In general, RBR E3 ligases are described as hybrids of RING and HECT E3 ligases. Like RING ligases, RBR ligases bind the E2 enzyme using the RING1 domain, but do not induce the essential closed E2-ubiquitin conformation, like RING E3s. Instead, RBR E3s support an open E2-ubiquitin conjugate conformation. For the transfer of ubiquitin from the E2 to the RBR E3, RBR E3s align the active site cysteine in their RING2 domain with the E2-ubiquitin thioester. Subsequently, analogous to the mechanism used by HECT E3 ligases, ubiquitin is transferred to the substrate. [Wenzel et al. 2011; Metzger et al. 2012; Berndsen and Wolberger 2014; Wang et al. 2023]

The RING-type E3s include different architectures, like the tetrameric Skp1-Cullin-F-Box (SCF) E3 ubiquitin ligases [Zheng et al. 2002; Metzger et al. 2014]. The mediation of protein degradation of ubiquitinated proteins through the SCF E3 ubiquitin ligase, which belongs to the Cullin-based E3 ubiquitin ligases, was originally characterized in *S. cerevisiae* [Bai et al. 1996]. The multi-protein complex consists of three components: the RING-box 1 (Rbx1) protein, which connects the E2 enzyme with the carboxy-terminus of the Cullin subunit functioning as scaffold. The amino-terminus of Cullin is connected to the adapter protein S-phase kinase-associated protein 1 (Skp1). Skp1 interacts with the F-box protein, the subunit which recognizes the substrate and therefore can target other proteins for degradation. [Jin et al. 2004; Thompson et al. 2021]

1.5.2. F-box proteins – the substrate recognizing subunit of the SCF complex

F-box proteins play a crucial role in targeted protein degradation. They are the subunit within the SCF complex responsible for substrate recognition. The F-box motif was named by Bai *et al.* on the basis of the presence of the motif in Cyclin F [Bai et al. 1996]. The F-box domain is usually located at the amino-terminus of the protein, while different domains, whose function mainly is protein interaction with the targeted protein, are located at the carboxy-terminus of the F-box protein [Bai et al. 1996; Skowyra et al. 1997]. F-box proteins are differentiated into three major classes based on the domains identified besides the F-box domain [Jin et al. 2004]. The class of FBXWs are F-box proteins harbouring WD40 domains, which have a length of approximately 40 amino acids, a conserved core of tryptophan-aspartic acid (W-D) dipeptide repeats and terminating with a WD repeat [Neer et al. 1994;

Jin et al. 2004]. F-box proteins containing additionally a leucine-rich repeat (LRR) domain were classified as FBXL. If neither a WD40 repeat, nor LRR is present, the F-box protein is classified as FBXO. [Cenciarelli et al. 1999; Winston et al. 1999; Jin et al. 2004]

The F-box domain consists of approximately 40 to 50 conserved amino acids and mediates the interaction with the adaptor Skp1 [Kipreos and Pagano 2000; Schulman et al. 2000]. Within several studies, the consensus sequence of the F-box motif has been described or reviewed (Figure 1-4) [Kumar and Paietta 1998; Kipreos and Pagano 2000; Jonkers and Rep 2009; Schmidt et al. 2009]. Kumar and Paietta described a highly conserved Leucine-Proline dipeptide and the conservation of amino acids with hydrophobic side chains. Especially Valine, Leucine and Isoleucine can often be found within the F-box motif at twelve positions and two Tryptophan residues are often positioned at the carboxy-terminus of the F-box motif. At positions nine and 37, Kumar and Paietta described “nearly invariant” Leucine and Valine. [Kumar and Paietta 1998] Two years later, Kipreos and Pagano published variants of the F-box consensus sequence and also pointed out that the lack of a strict consensus sequence makes identification by eye difficult, as well as the issue that not all databases are able to recognize the motif [Kipreos and Pagano 2000].

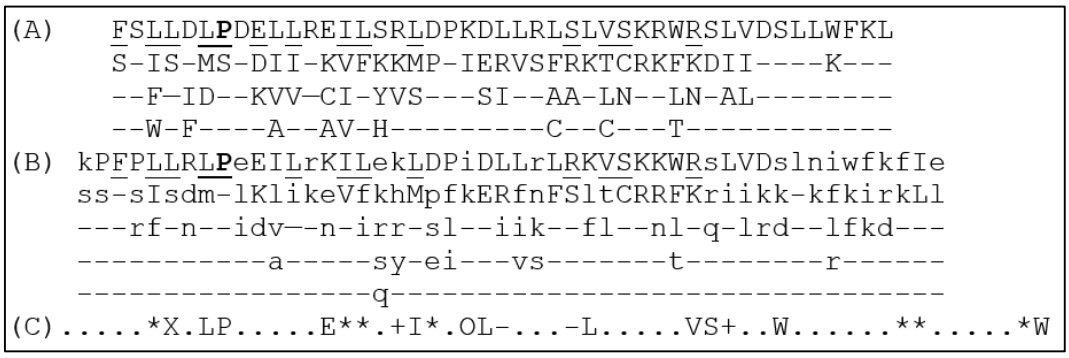

Figure 1-4: Examples of F-box motif consensus sequence variants from literature given in single-letter amino acid code.

(A) F-box consensus sequence published by Jonkers and Rep in 2009. According to their analysis, underlined amino acids are highly conserved [Jonkers and Rep 2009]. (B) F-box consensus sequence published by Kipreos and Pagano in 2000. According to these authors, bold and underlined capital letters represent significant residues identified in more than 40% of the sequences tested. Bold, not underlined capital letters were identified in 20-40%; bold, lower case letters in 15-19%; and lower case letters, not bold, in 10-14%. [Kipreos and Pagano 2000] (C) F-box consensus sequence published by Kumar and Paietta in 1998. * labels aliphatic, X hydroxyl- or sulfur-containing amino acids, + basic, – acidic, and O aromatic amino acids. [Kumar and Paietta 1998] Lines in (A) and (B) and dots in (C) are placeholders for amino acids.

It is known that F-box proteins are not exclusive and can target different substrate proteins [Winston et al. 1999]. F-box proteins can bind to Skp1 via their F-box domain, but there were also cases identified, where the F-box domain is not mandatory for the interaction with Skp1 [Bai et al. 1996; Hermand 2006]. Studies investigating the F-box proteins Pop1p and

Pop2p of the fission yeast *Schizosaccharomyces pombe* revealed that at least for Pop2p the F-box was not necessary for degradation of the target protein Rum1p and ploidy control [Seibert et al. 2002]. Additionally, the results of Seibert *et al.* suggested F-box Pop1p and Pop2p perform homo- and heterooligomerization to generate combinational diversity [Seibert et al. 2002]. F-box proteins bound to Skp1 can also function without the complete SCF complex [Hermand 2006]. For instance, at least three non-SCF complexes were described in budding yeast: the CBF3 centromere binding complex, the regulator of the (H^+)-ATPase of the vacuolar and endosomal membranes (RAVE) complex and the soluble NSF attachment protein receptor (SNARE) complex. What these cases have in common is that Skp1 plays an essential role, and the interaction is reminiscent of an SCF complex, but its catalytic subunit is missing, thus no degradation occurs due to lack of ubiquitination. [Hermand 2006]

Known mechanisms of substrate recruitment through SCF complexes were reviewed by Skaar *et al.*, giving a broad overview of at least eight recruitment strategies [Skaar et al. 2013]. Substrate recruitment is also an essential mechanism to regulate the activity of SCF complexes. To adapt to environmental changes, a rapid and targeted binding of F-box proteins to their substrate proteins is crucial. On the contrary, also the release of the interaction can be induced through changing stimuli, making a strict regulation essential on both, the F-box protein itself and the protein interaction interfaces on the substrate. [Skaar et al. 2013] Recognition sites within substrate proteins are defined as degrons [Varshavsky 1991], and the majority of SCF substrates are known to be phosphorylated prior to F-box interaction at the canonical phosphodegron [Ravid and Hochstrasser 2008; Skaar et al. 2013]. Phosphorylation on different sites of the substrate results in an increased specificity of protein interaction. One well-studied example is Sic1 in yeast, which requires a minimum of six from nine phosphorylated amino acids to be recognized by the F-box Cdc4, because the affinity of each single phosphorylated amino acid would be too low to promote binding. This mechanism is known as allovalency. [Kõivomägi et al. 2011; Okoye et al. 2022] Orlicky *et al.* proposed „the term allovalent to describe the ability of multiple weak, spatially separated ligand sites to cooperatively interact with a single receptor site.“ [Orlicky et al. 2003] Phosphorylations can also induce conformational changes in the substrate protein, allowing access for the F-box protein, or serve as priming phosphorylation [Skaar et al. 2013].

Substrate recognition can also be mediated through cofactors. For instance, human Cks1 was found to serve as accessory protein, enhancing the binding ability of the F-box Skp2 to its target protein. [Ganoth et al. 2001; Skaar et al. 2013]

1.6. Function of F-box proteins across eukaryotes with a focus on *Neurospora crassa*

F-box proteins can be found within all eukaryotes and have a wide range of functions. Fungal F-box proteins are known to be involved in cell division, cell cycle, regulation of the adaption to environmental changes, development and much more. [Goh and Surana 1999; Jonkers et al. 2016; Assis et al. 2018; Gabriel et al. 2021; Sarikaya Bayram et al. 2022] In humans and *A. nidulans*, approximately 70 F-box proteins are predicted [Draht et al. 2008; Sarikaya Bayram et al. 2022]. Plants harbour over 800 F-box proteins, while *S. cerevisiae* was found to have 21 [Sarikaya Bayram et al. 2022]. Primarily, fungal F-box proteins were studied in yeasts, thus several targets are already known for some yeast F-box proteins [Jonkers and Rep 2009]. Within mushroom-forming Agaricales an extended number of F-Box genes, similar to plants, has been determined with a mean number of approximately 274 copies [Krizsán et al. 2019].

Studies in *A. nidulans* revealed a link between F-box proteins and CreA-mediated carbon catabolite repression [Assis et al. 2018]. As described previously, the F box protein Fbx23 (AN5593) is thought to be involved in CreA degradation in an ubiquitylation-dependent manner in *A. nidulans*, however it is still unclear if CreA or an interaction partner is ubiquitinated [Assis et al. 2018; Assis et al. 2021]. Sarikaya Bayram *et al.* executed a comprehensive analysis of all identified 74 F-box proteins in *A. nidulans* to investigate their molecular and developmental functions and identified more than 700 potential interaction partners [Sarikaya Bayram et al. 2022].

Even less is known about F-box proteins and their targets in other filamentous fungi. In *N. crassa* for instance, the mutagen sensitive-10 protein (MUS-10, NCU02379), which is orthologous to Fbx30 in *A. nidulans*, plays an important role for mitochondrial function. Its deletion results in instability of mitochondrial DNA, senescence and altered mitochondrial morphology. [Kato et al. 2010] The *N. crassa* F-box/WD-40 domain-containing protein 1 and 2 (FWD-1, NCU04540; FWD-2, NCU07521) are the orthologs of *A. nidulans* Fbx23 and Fbx17, and are known to play a role within the circadian clock [He et al. 2003]. FWD-1 (Fbx23) interacts physically with the period clock protein FREQUENCY (FRQ, NCU02265), which is essential for clock function, while FWD-2 (Fbx17) was suggested to take over the function of Fbx23 in its absence [He et al. 2003; He et al. 2005]. Investigating physical protein−protein interactions, using a yeast two-hybrid approach, Lobo *et al.* identified, amongst others, Fbx23 (FWD-1, NCU04540) as target of the antifungal plant peptide *Pisum sativum* defensin 1 (*Ps*d1) [Lobo et al. 2007]. The F-box protein sulfur controller-2 protein (Scon2) is targeting the regulatory protein Cys-3, which is responsible for the activation of genes required for sulfur utilization [Kumar and Paietta 1998]. Another F-box protein in

N. crassa, EXO-1 (NCU09899), is known to cause a hypersecretion phenotype of amylases in starvation conditions when mutated [Gabriel et al. 2021]. Gabriel *et al.* identified the causative mutation in the classical mutant *exo-1*. They concluded that Δ*exo-1* has a partially impaired CCR response and influences the stability of the transcription factor COL-26, which induces expression of the starch regulon. Transferring the enzyme hypersecretion phenotype via reverse engineering into the industrially important strain *Myceliophthora thermophila* (now: *Thermothelomyces thermophilus*), Gabriel *et al.* demonstrated the great potential of F-box proteins for industrial applications. [Gabriel et al. 2021]
Additionally, the F-box proteins Fbx19 (NCU08642) and Fbx22 (CDC4, NCU05939), were shown to have a defect in CCR and suggested to potentially have an influence on carbon utilization or signaling, especially in high D-glucose concentrations [Horta et al. 2019]. However, despite these few examples of F-box proteins having been described, the majority of the F-box proteins and their specific function still remain enigmatic.

1.7. Gap of knowledge and objectives

As outlined above, CCR remains to be a major drawback in fungal enzyme production. Although F-box proteins have been demonstrated to have a regulatory influence on carbon utilization and CCR [Assis et al. 2018; Horta et al. 2019; Gabriel et al. 2021], only a fraction of fungal F-box proteins have been described, and especially their influence on the ability of fungi to switch between different carbon sources (with different potential to trigger CCR) remains poorly understood. This thesis therefore aimed to elucidate the effects of F-box-mediated post-translational regulation of lignocellulose-degrading enzymes in the transition from conditions with high to conditions with low CCR potential and *vice versa*. The main goal was to provide mechanistic insights through an analysis of the protein-protein interactions governing the regulatory system. The chosen model system for this study was *N. crassa*, for which the majority of F-box proteins remain unknown, but which represents a superior genetic reference system with an almost complete knock-out collection and diverse genetic tools being available.

The following specific objectives were targeted:

The first objective was to make a genomic inventory and identify all putative *fbx* genes in the *N. crassa* genome, compare them amongst each other and with other fungal species and categorize them according to their domain architecture.

Subsequently, a screen was to be developed to test their potential influence on the switch between carbon utilization conditions with a specific focus on CCR.

As a third objective, some selected *fbx* deletion strains were to be further investigated by physiological analyses and RNA-sequencing. This comparative analysis of the transcriptional profiles was aimed to identify aberrant gene expression patterns potentially influenced by the according *fbx* deletion.

Within the fourth objective, selected F-box candidates were tagged with green fluorescent protein (GFP) for immunoprecipitations. By mass spectrometry potential interaction partners were to be identified in two different growth conditions. Moreover, deletion strains of the putative interaction partners should be screened for CCR-related phenotypes and aberrant behaviour compared to the wild type (WT) to verify if these are indeed involved in the same regulatory processes.

The results of these experiments were to provide a better understanding of the function of F-box proteins during carbohydrate metabolic switches in general and to allow rational and targeted strain modifications in the future, leading to improved enzyme-producing strains of high interest for the industry.

2. Results

2.1. Putative F-box proteins of *Neurospora crassa*

Generally, the lack of a strict consensus makes the identification of the F-box motif itself challenging [Kipreos and Pagano 2000]. Several variations of probable F-box motif amino acid sequences can be found in literature (for a general impression of the consensus sequence see Figure 1-4). Although the sequence of the F-box domain is not strictly conserved and can vary to a certain extent, the F-box domain is modular and interchangeable across species [Kumar and Paietta 1998].

2.1.1. Identification of putative *fbx* genes in *Neurospora crassa*

For *Aspergillus nidulans* 74 F-box proteins are known [Draht et al. 2008; Assis et al. 2018; Sarikaya Bayram et al. 2022]. In order to identify putative *fbx* genes in *N. crassa*, an ortholog search was conducted. In total, 28 *A. nidulans fbx* genes were found to have orthologs in *N. crassa* [Horta et al. 2019; Sarikaya Bayram et al. 2022]. Additionally, 21 putative *fbx* genes of *N. crassa* were identified on the platforms FungiDB and Uniprot (Table 5-1) by searching for relevant domains, GO terms and predicted functions.
A list of putative *N. crassa* F-box proteins was compiled, indicating the orthologous *A. nidulans* genes by usage of the corresponding F-box numeration [Draht et al. 2008; Sarikaya Bayram et al. 2022]. Additionally, the predicted domains of the *N. crassa* F-box proteins were visualized (Figure 2-1).

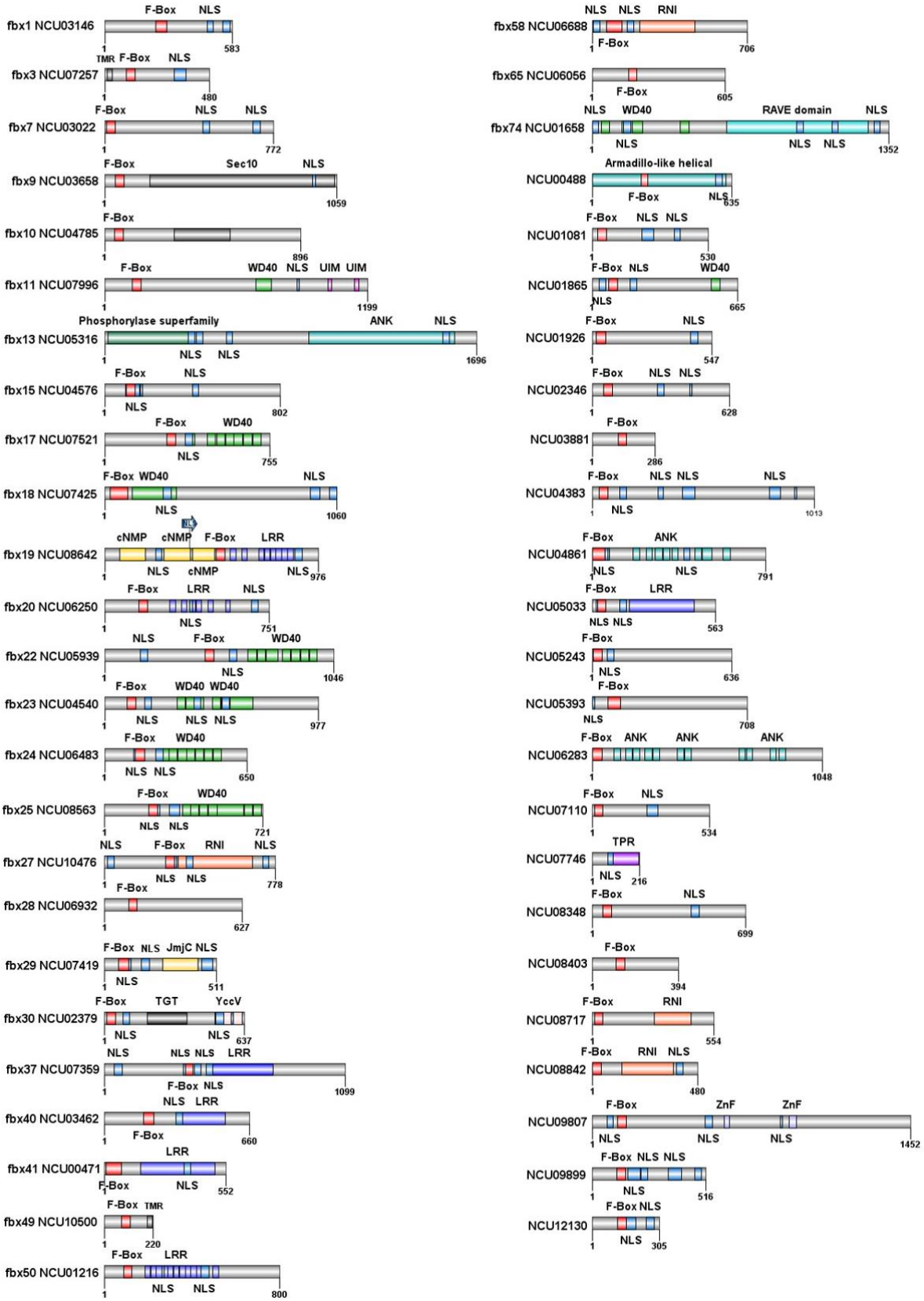

Figure 2-1: Domain architectures of the putative *N. crassa* F-box proteins.
Gene IDs are given on the left-hand side as NCU numbers. In case of an existing *Aspergillus nidulans* ortholog, the corresponding *fbx*-number of the ortholog is listed additionally [Draht et al. 2008]. Numbers below the start and end of each protein indicate its size in amino acids. The locations of the following domains are depicted in the figure: F-box domain, Leucine-rich Repeat (LRR), WD40

domain, Ubiquitin Interacting Motif (UIM), Sec10, Transmembrane region (TMR), Cyclic nucleotide-monophosphate binding domain (cNMP), jumonji domain (JmjC), Transglutaminase-like domain (TGT), YccV-like DNA binding, RNI-like superfamily (RNI), Ankyrin repeats (ANK), Tetratricopeptide repeat domain (TPR), Zinc finger swim domain (ZnF), Nuclear localization signal (NLS). In cases where the F-box domain is labeled below the protein, this indicates that the domain location was determined manually via alignments. Domain architecture was determined as described in chapter 5.6.1.

Some of the putative F-box proteins of *N. crassa* have only a partially conserved F-box domain (Fbx37/40/41/58/65/NCU00488). For those candidates, the probable location of the F-box domain was identified via alignments with F-box proteins harboring true F-box domains, so called “high scoring F-box proteins” [Draht et al. 2008]. Additionally, five known F-box consensus sequences were used to identify the motif [Kipreos and Pagano 2000].
Interestingly, NCU07746 carries the submitted name “F-box domain-containing protein” on FungiDB and UniProt (Table 5-1), but the F-box motif of this protein could not be found in different protein databases. F-box proteins without a canonical F-box domain are described as “low scoring F-box proteins” [Draht et al. 2008]. For a total of three putative F-box proteins, Fbx13, Fbx74 and NCU07746, the probable location of the F-box motif could not be identified.

Domains with high levels of interspecies conservation are thought to reflect important biological functions accomplished by these regions. The F-box proteins of the ascomycete *A. nidulans* have been studied for their developmental and molecular function [Sarikaya Bayram et al. 2022]. Therefore, all known *A. nidulans* and *N. crassa* F-box protein sequences were investigated in a phylogenetic analysis using Clustal Omega protein sequence alignment. A phylogenetic tree was created comprised of all known putative *A. nidulans* and *N. crassa* F-box proteins. The proteins within the phylogenetic tree were color highlighted according to the three major classes, based on the domains identified besides the F-box domain [Jin et al. 2004] (Figure 2-2).
The different distances of the proteins from each other show their divergence, while each node represents the closest common ancestor to its descendants. The majority of the orthologous proteins show a closer relationship, originating from one ancestor. Most of the orthologous F-box proteins were also assigned into the same classes according to their domain architecture (FBXW, FBXL or FBXO, see also 1.5.2), but that was not the case for all of them. For instance, an exception was Fbx10, which shows in *A. nidulans* an additional WD40 domain (AN0460) that is not present in *N. crassa* (NCU04785).

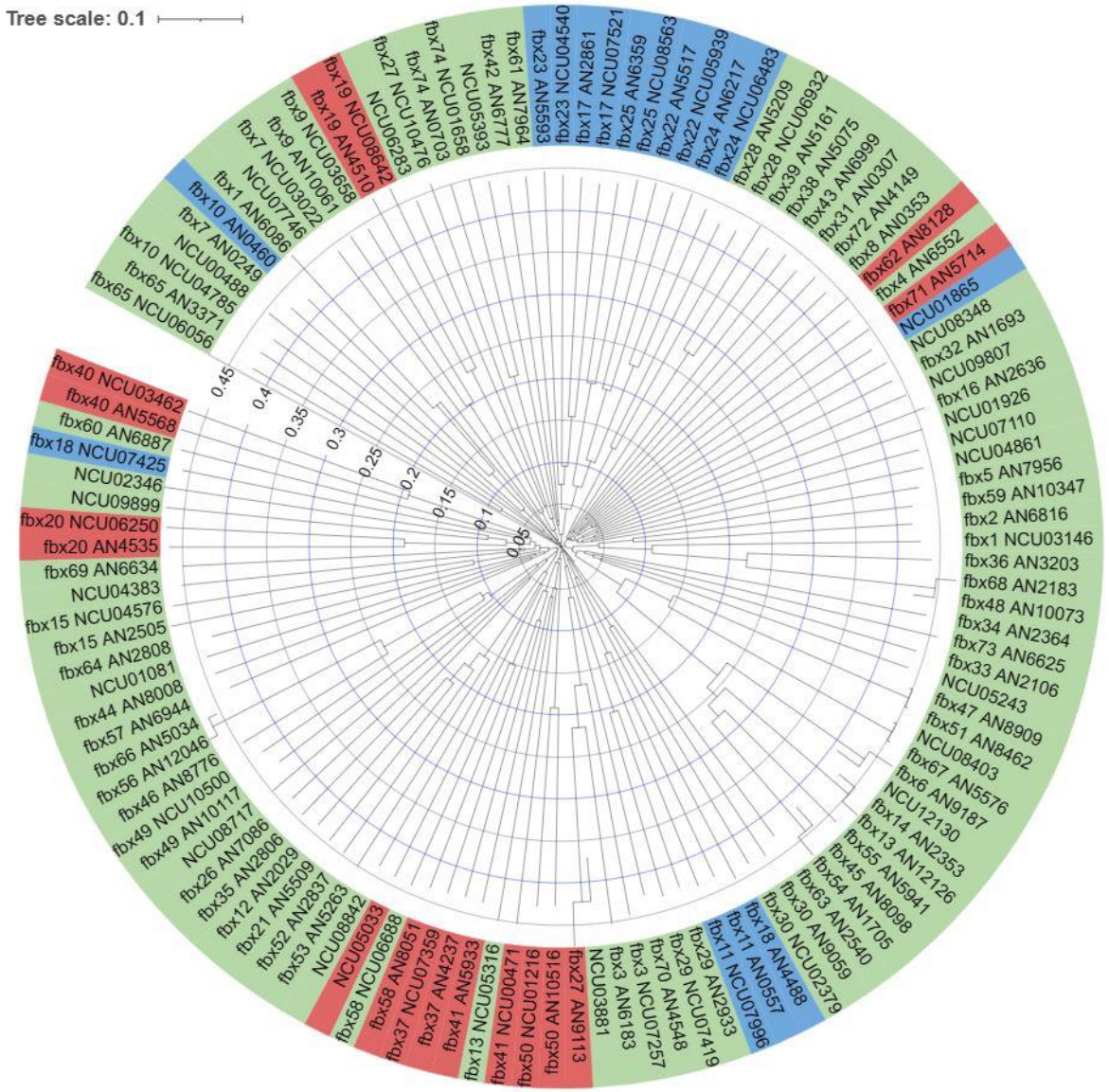

Figure 2-2: Phylogenetic tree of all known putative F-box proteins in *N. crassa* and *A. nidulans*. A phylogenetic analysis of putative *N. crassa* and *A. nidulans* F-box proteins was performed using Clustal Omega protein sequence alignment and visualized using iTOL (Table 5-1). Tree scale is indicated internally. Three main clades are originating from the root. F-box proteins containing a WD40 domain were highlighted in blue (FBXW), those containing LLRs in red (FBXL), and F-box proteins with none or other predicted domains are colored in green (FBXO).

2.1.2. Transcriptional response of *N. crassa fbx* genes during perception of different carbon sources

To get a first insight into which *fbx* genes might be involved in carbon utilization, the transcriptional data of the “Fungal Nutritional ENCODE Project” (Table 5-1), which was funded by the Joint Genome Institute [Glass 2012; Wu et al. 2020], was used to depict the expression. Within this large-scale transcriptomic project, *N. crassa* was pre-grown for 16 hours on minimal medium and subsequently grown for four hours on 72 different carbon sources.

The gene expression of the putative *fbx* genes is shown during the perception of 35 different carbon sources (Figure 2-3).

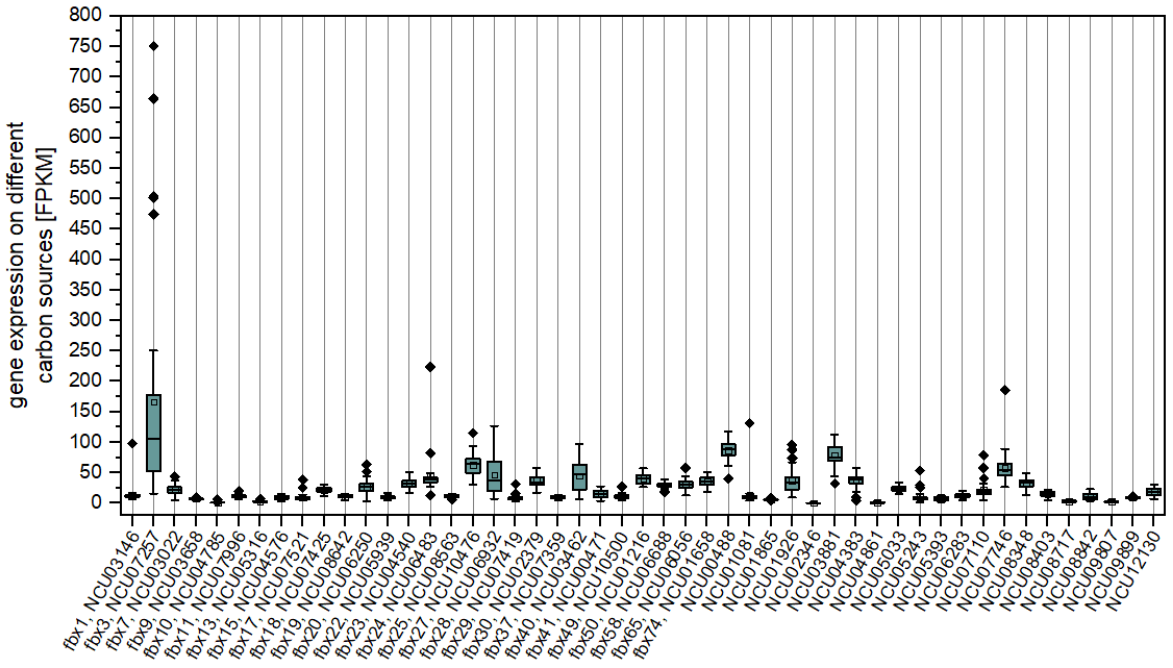

Figure 2-3: Transcriptional response of putative *N. crassa fbx* genes during perception of different carbon sources.
Expression data from the "Fungal Nutritional ENCODE Project" [Glass 2012]. *N. crassa* gene IDs are given on the x-axis as NCU numbers. In case of an existing *Aspergillus nidulans* ortholog, the corresponding *fbx*-number of the ortholog is added additionally [Draht et al. 2008]. Gene expression strength is given in Fragments Per Kilobase per Million mapped fragments (FPKM). Conditions displayed: starvation, 2% sucrose, 1% glucomannan, 2 mM cellobiose, 2mM lignin, 1% galactomannan, 1% pectin, bac cellulose, poly galacturonic acid, 2 mM trehalose, 1% amylopectin, 2 mM maltose, 2 mM sorbose, 2 mM rhamnose, 2 mM xylose, 2 mM mannitol, 2mM glycerol, 1% xylan, 1% galactan, 1% rhamnogalacturonan, 1% Avicel, 1% arabinan, 2 mM glucuronic acid, 2 mM arabinose, 2 mM mannobiose, 2 mM fructose, 2 mM fucose, 2 mM galactose, 2 mM galacturonic acid, 2 mM amylose, 1% xyloglucan, 2 mM inulin, 2 mM ribose, 2 mM mannose, 1% pectin esterified.

The majority of the *fbx* genes were expressed below 100 FPKM on different carbon sources and, except for *fbx3*, the median of each *fbx* gene was below 100 FPKM. The highest variance within these conditions was found for *fbx3* (NCU07257). Especially on sucrose (750 FPKM), amylose (664 FPKM), cellobiose (504 FPKM) and trehalose (474 FPKM), the expression level increased. Generally, *fbx* genes were expressed rather low with only slight variances during perception of different carbon sources.

Figure 2-4 shows the fungal transcriptional ENCODE expression data for only those putative *fbx* genes, which were available as deletion strain from the Fungal Genetic Stock Center (FGSC). This should provide a better overview, which strains could be investigated further and screened for aberrant phenotypes in the deletion strain.

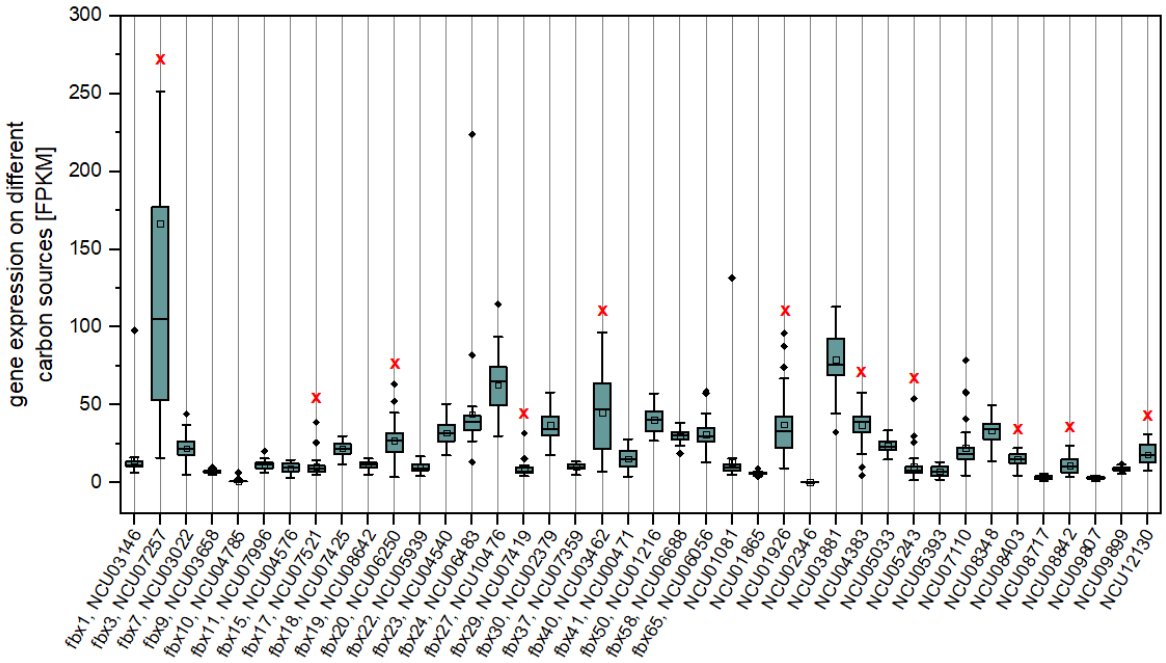

Figure 2-4: Transcriptional response of putative *fbx* genes available as deletion strain. Expression data from the "Fungal Nutritional ENCODE Project" [Glass 2012]. *N. crassa* gene IDs are given on the x-axis as NCU numbers. In case of an existing *Aspergillus nidulans* ortholog, the corresponding *fbx*-number of the ortholog is added additionally [Draht et al. 2008]. Gene expression strength is given in Fragments Per Kilobase of transcript per Million mapped reads (FPKM). Interesting expression patterns were labelled with a red x. Conditions displayed: starvation, 2% sucrose, 1% glucomannan, 2 mM cellobiose, 2mM lignin, 1% galactomannan, 1% pectin, bac cellulose, poly galacturonic acid, 2 mM trehalose, 1% amylopectin, 2 mM maltose, 2 mM sorbose, 2 mM rhamnose, 2 mM xylose, 2 mM mannitol, 2mM glycerol, 1% xylan, 1% galactan, 1% rhamnogalacturonan, 1% Avicel, 1% arabinan, 2 mM glucuronic acid, 2 mM arabinose, 2 mM mannobiose, 2 mM fructose, 2 mM fucose, 2 mM galactose, 2 mM galacturonic acid, 2 mM amylose, 1% xyloglucan, 2 mM inulin, 2 mM ribose, 2 mM mannose, 1% pectin esterified.

Expression patterns that seemed to be interesting regarding CCR and carbon utilization were highlighted with a red x (Figure 2-4). Interesting patterns were varying expressions strengths of putative *fbx* genes across different carbon sources, especially on carbon sources known to trigger CCR and carbon starvation stress response (CSSR). Additionally, the expression values of the *fbx* genes on the glucose time series published by Wang *et al.* was taken into account [Wang et al. 2017]. Interesting expression patterns were, for instance, high expression levels on starvation and low on glucose or *vice versa*. However, most *fbx* genes were rather constitutively expressed on a relatively low expression level.

2.2. Screening for F-box proteins involved in the regulation of sugar metabolism

To identify F-box proteins involved in the switch between CCR and lignocellulose utilization, 40 available *N. crassa* gene deletion strains [Colot et al. 2006; Dunlap et al. 2007] were employed to investigate their function. Avicel, a microcrystalline cellulose, can induce carbon starvation stress response (CSSR). CSSR is a competing metabolic state towards CCR, which can be induced by glucose. Both metabolic states affect the transcriptional response during substrate perception. CSSR is only enabled when the CCR response has decreased significantly. [Szilágyi et al. 2013; Wang et al. 2017; Thieme 2019]
First of all, *N. crassa* wild type (WT) was assessed for enzymatic activity in Avicel supplemented with different glucose concentrations, to set up conditions for a screening.
N. crassa deletion strains were screened to identify aberrant phenotypes related to CCR. Furthermore, six putative F-box proteins were selected harboring potential to be involved in CCR and lignocellulose utilization. The deletion strains of the selected candidates were phenotypically analyzed for growth and developmental deficiencies. Three of these strains were investigated within a transcriptional approach for the response to carbon source switches.

2.2.1. Cellulolytic response of *N. crassa* to different sugar concentrations

In presence of favored carbon sources, like glucose, the production of enzymes needed for the utilization of less-favored carbon sources, like plant cell wall polymers, is reduced or repressed [Adnan et al. 2017]. To examine screening conditions to detect CCR effects, *N. crassa* culture supernatants were investigated for cellulase activity. *N. crassa* WT strain was pre-grown in 2% fructose VMM for 16 h. A medium switch was perfomed into 100 ml 1% Avicel VMM supplemented with different glucose concentrations in 250 ml plastic Erlenmeyer flasks. Culture supernatant was sampled at different time points and cellulase activity was determined (Figure 2-5).

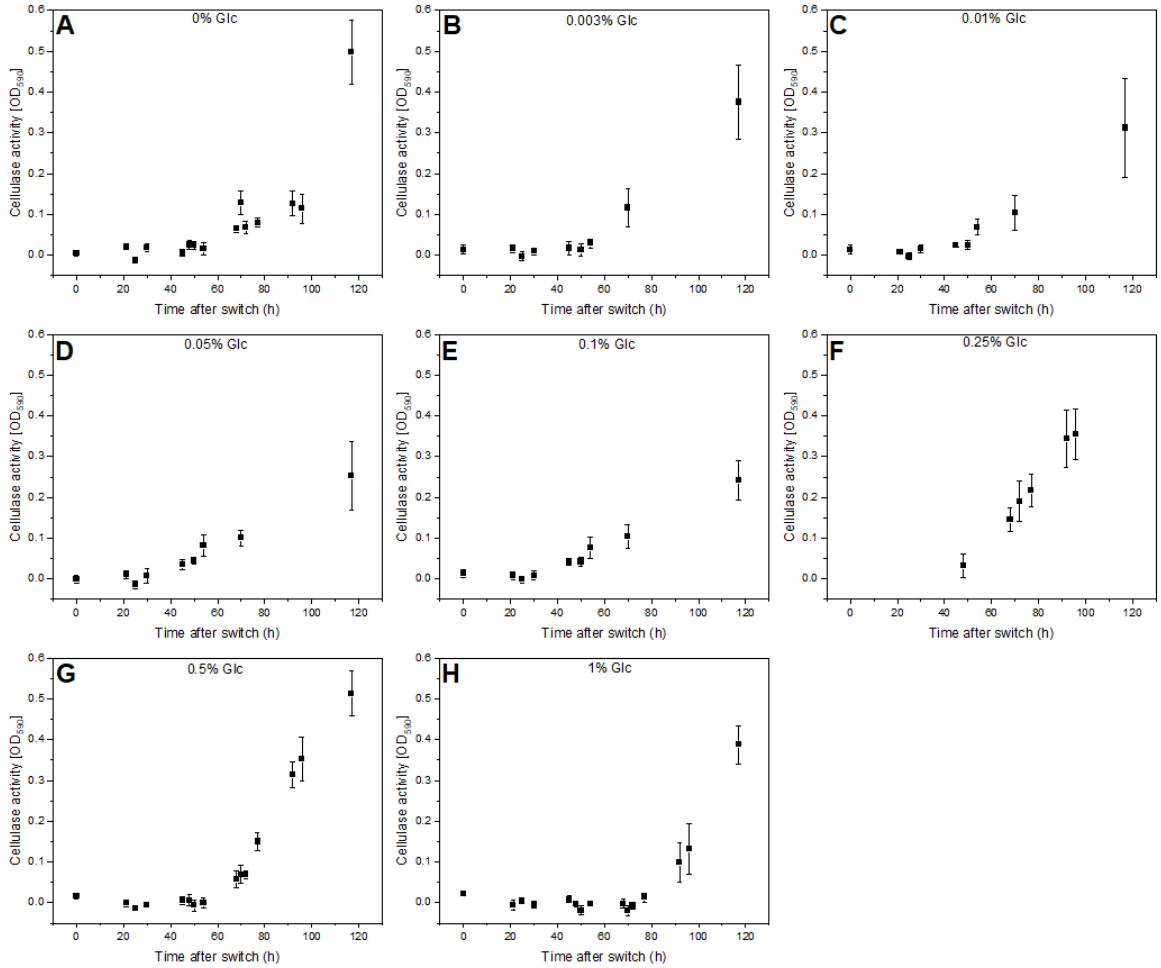

Figure 2-5: Cellulase activity of *N. crassa* WT culture supernatants.
N. crassa WT was grown in liquid cultures using 1% Avicel VMM supplemented with different glucose concentrations (A) 0% glucose, (B) 0.003% glucose, (C) 0.01% glucose, (D) 0.05% glucose, (E) 0.1% glucose, (F) 0.25% glucose, (G) 0.5% glucose, (H) 1% glucose. Culture supernatant was sampled over time to determine cellulase activity.

Figure 2-5 shows enzymatic activity profiles of *N. crassa* WT over time in a carbon catabolite repressing (glucose) and derepressing condition (Avicel). Since the WT can perform regular CCR, glucose is consumed first, therefore nearly no cellulase activity is measurable at the early time points after medium switch. 70 h after medium switch, the cellulase activity started to increase. Higher concentrations of supplemented glucose led to a delayed increase of cellulase activity (Figure 2-5 H) compared to 0% glucose supplementation or lower concentrations.

To screen the *N. crassa fbx* deletion mutants for CCR phenotypes, an experimental setting was needed to detect both, mutants with a derepressed phenotype showing higher cellulase activity at an earlier time point, and mutants with a repressed phenotype with significantly lower cellulase activity compared to the WT. Therefore, the most promising condition was determined to be 1% Avicel supplemented with 0.5% glucose, sampling 40, 60 and 80 h after medium switch. Within this experimental setting, an increase of cellulase activity was

detected over time in the WT (Figure 2-5 G). Another important reason why these conditions were chosen is that glucose should not be completely metabolized. Therefore, the initial glucose concentration should not be too low to detect the effect of CCR.

2.2.2. Screening for F-box genes involved in the integration of cellulose perception

In total, 40 putative *fbx* deletion strains of *N. crassa*, the WT strain, and Δ*cre-1* strain, which served as CCR phenotype control strain, were screened at the settings determined in 2.2.1, to identify aberrant phenotypes related to CCR. Derepressed phenotypes were expected to show higher cellulase activity at an earlier time point, while repressed strains cannot release CCR, and were expected to show lower cellulase activities, compared to the WT.

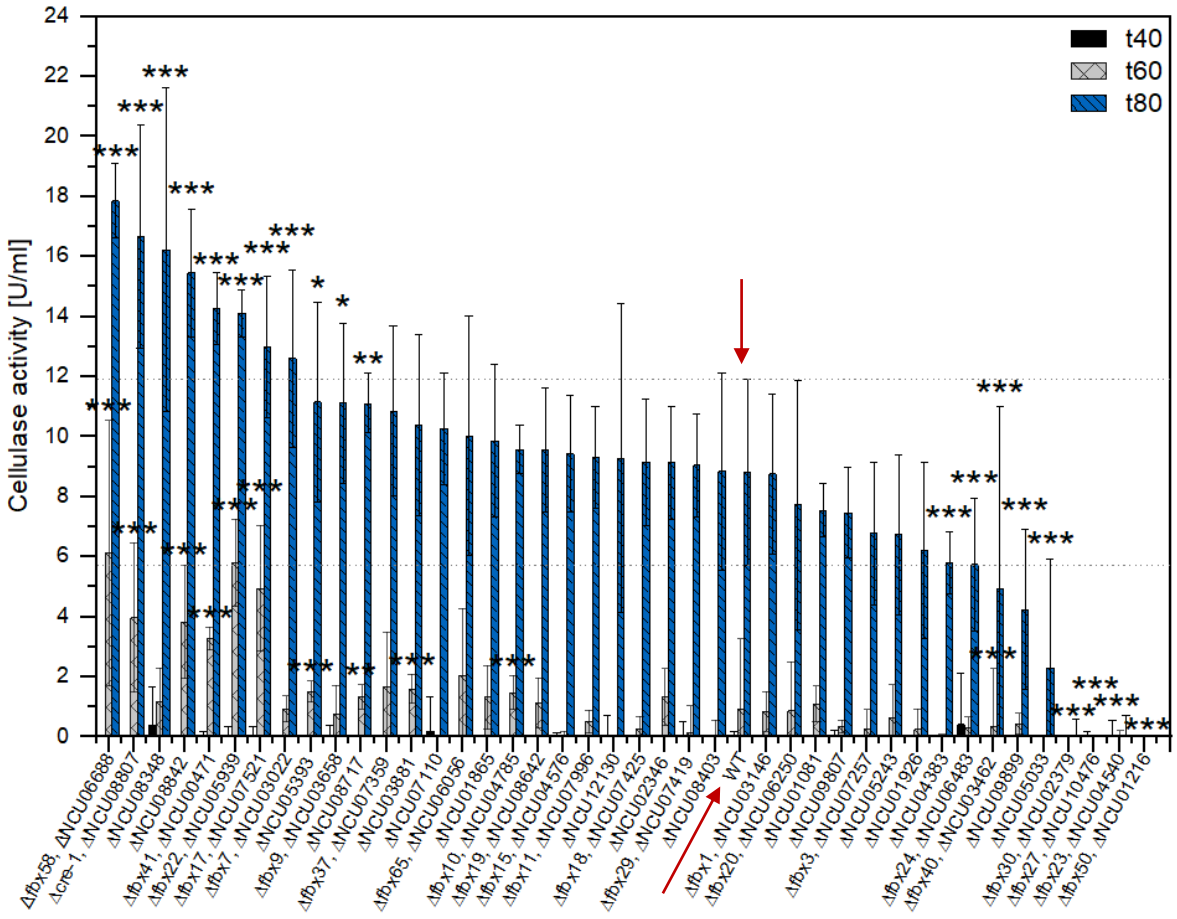

Figure 2-6: Enzymatic activity profiles of *N. crassa fbx* deletion strains grown in 1% Avicel supplemented with 0.5% glucose.
Pre-cultured *N. crassa fbx* deletion strains were switched into liquid medium containing cellulose supplemented with glucose. The enzymatic activity was determined 40 h, 60 h and 80 h after the medium switch. The WT is highlighted by a red arrow. Dotted horizontal lines show standard deviation area of the WT at 80 h after medium switch. Significance levels were determined using a post-hoc test, based on Kruskal-Wallis test. *, $P < 0.05$; **, $P < 0.01$; ***, $P < 0.001$.

The increase over time of cellulase activity of the WT showed that the WT consumed glucose first and subsequently increased cellulase secretion and metabolized cellulose (Figure 2-6, red arrow). Some *fbx* deletion strains, including also Δ*cre-1*, showed significant higher cellulase activity compared to the WT (Figure 2-6). Up to a twofold increased cellulase activity at t80 of deletion mutants compared to WT were determined. A total of ten *fbx* deletion strains showed a derepressed phenotype with significantly higher cellulase activity compared to the WT. On the other side, this experimental setting revealed nine strains with a significant repression of cellulase activity. After 80 h, no cellulase activity could be detected in the supernatant of four deletion strains (Figure 2-6).

To investigate whether the strains show impaired secretion, the total protein amount was determined of the supernatants (Figure S 6-1). Additionally, the supernatant samples of strains which showed a significant difference in biomass formation (Figure 2-9), described in 2.2.3, were separated via SDS-PAGE and silver stained (Figure 2-7 and Figure S 6-2). The quantification and profiling of secreted protein showed a reduction in protein secretion by the Δ*fbx23* strain (Figure 2-7).

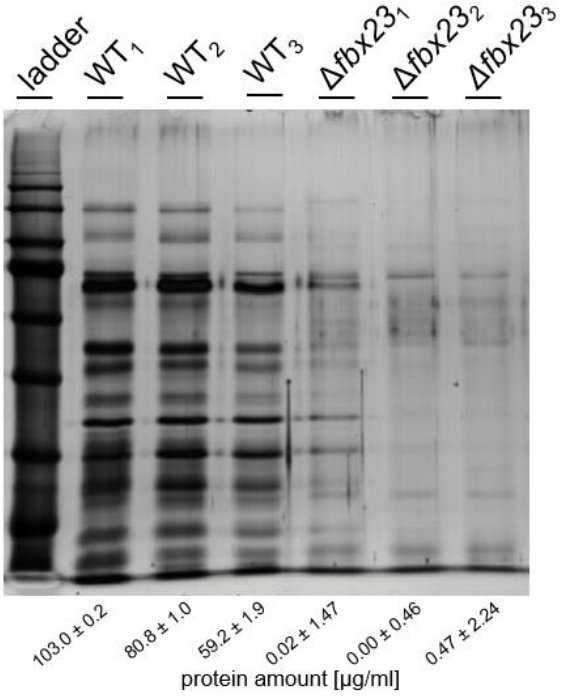

Figure 2-7: Protein profile of culture supernatants from *N. crassa* WT and Δ*fbx23*.
SDS-PAGE from unconcentrated culture supernatants of *N. crassa* WT and Δ*fbx23* deletion strain using same samples as from Figure 2-6, 80 h after medium switch. The number below the strain name is the number of the corresponding replicate. Below the lanes is the determined protein amount and standard deviation in µg/ml of each supernatant sample. The used ladder is BlueStar Prestained Protein Marker (NIPPON Genetics EUROPE GmbH).

Within this experimental setting, a significant difference of cellulase activity in culture supernatants of several deletion strains was found compared to the WT. The protein amount

appeared quite stable, except for few strains, where nearly no protein content was measurable within the culture supernatants, or a higher amount than in the WT supernatant was detected (Figure S 6-1). Nevertheless, for some strains a severe reduction of the total protein amount was observed.

To visualize aberrant phenotypes of the *fbx* deletion strains for both cellulase activity and protein amount, the data were displayed in correlation to each other (Figure 2-8).

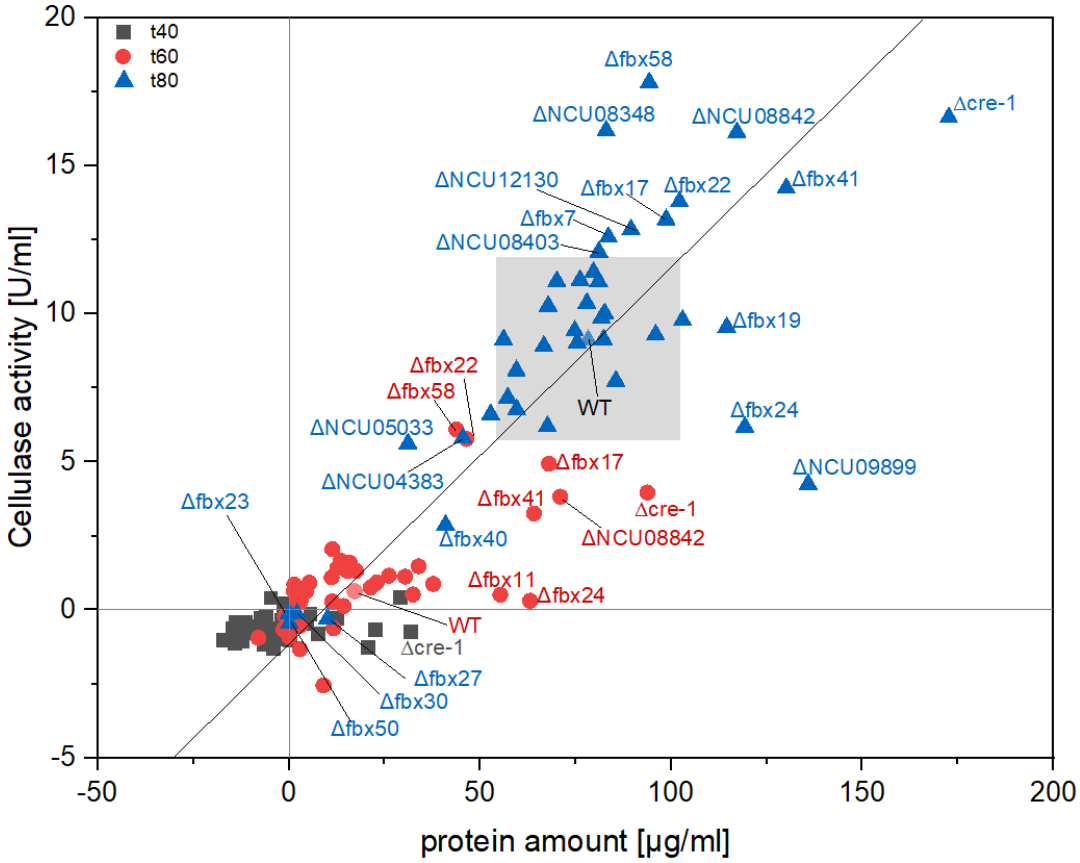

Figure 2-8: Cellulase activity versus protein amount of *N. crassa fbx* deletion mutants.
The determined mean values of the cellulase activities and protein amounts of the screen (without standard deviation) shown above are displayed within this figure. Pre-cultured *N. crassa fbx* deletion strains were switched into liquid medium containing cellulose supplemented with glucose. The enzymatic activity and total protein amount was determined 40 h (black squares), 60 h (red dots) and 80 h (blue triangles) after the medium switch. The grey square indicates the area of standard deviation of WT 80 h after medium switch.

Especially 80 h after medium switch, aberrant phenotypes stood out, as well as derepressed phenotypes 60 h after medium switch (Figure 2-8).

The loss of some F-box proteins had a severe impact on cellulase activity, while the total protein amounts in the supernatants of the deletion strain cultures did show significant differences for only some exceptions. Overall, these results indicate that at least 19 F-box proteins contribute in a direct or indirect way to carbon utilization, growth, protein secretion and enzyme production.

2.2.3. Biomass formation of *N. crassa fbx* deletion strains in presence of allyl alcohol

To verify the potentially CCR-related defects of the *N. crassa fbx* mutants, a second screen was carried out. The deletion and control strains investigated in 2.2.2 were grown in Vogel´s minimal medium (VMM) supplemented with glucose and allyl alcohol.

Allyl alcohol (AA) is known to be converted by (unspecific) alcohol dehydrogenases to the toxic compound acrolein. Since alcohol dehydrogenase is subjected to CCR, in strains with functional CCR, glucose will be first utilized; however, strains that have an impaired CCR would use both carbon sources and will be more sensitive to acrolein. In summary, higher sensitivity of the strain to AA defines a CCR-derepressed phenotype, while functional CCR would result in insensitivity of the strain to AA, which defines a CCR-repressed phenotype. *N. crassa* Δ*cre-1* was chosen as control strain, since this deletion strain is sensitive to AA [Xiong et al. 2014].

The strains were grown in the control condition VMM supplemented with 1% glucose and the test condition VMM supplemented with 1% glucose and 100 mM AA for 24 h. Mycelial dry biomass was determined and normalized with the control condition and statistically compared to the wild-type strain data (Figure 2-9).

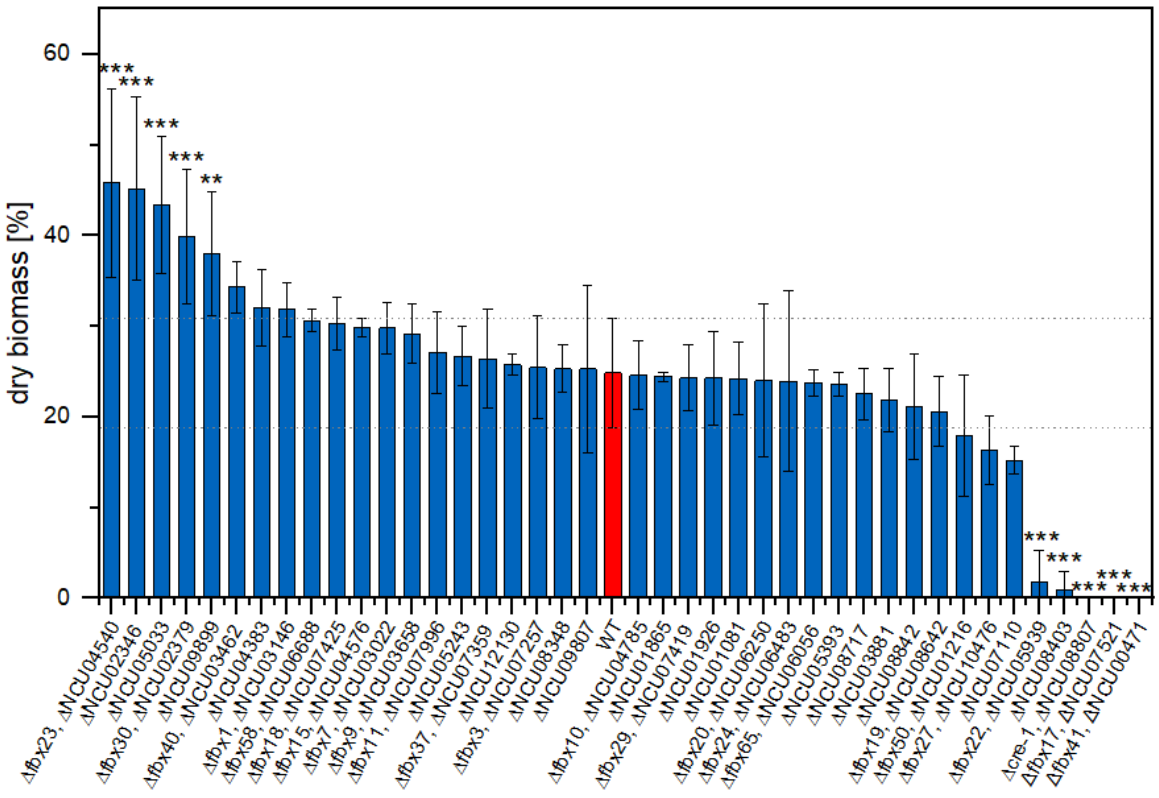

Figure 2-9: Biomass formation of *N. crassa fbx* deletion strains in presence of allyl alcohol. F-box gene deletion strains were grown on glucose medium supplemented with allyl alcohol before the dry biomass was determined of the strains under all conditions, normalized with the control

condition and statistically compared to the WT strain data (red bar). Dotted horizontal lines show standard deviation area of the WT. Significance levels were determined using an ANOVA. *, $P < 0.05$; **, $P < 0.01$; ***, $P < 0.001$.

In total, five strains were significantly less sensitive to AA than the WT, resulting in increased biomass formation in the test condition, and indicating a hyper-repressed CCR. Five other strains, including the Δ*cre-1* control strain, showed a significantly higher sensitivity to AA compared to the WT, suggesting to be de-repressed. These strains were only able to grow in the control condition and could barely grow in the test condition in the presence of AA, (Figure 2-10).

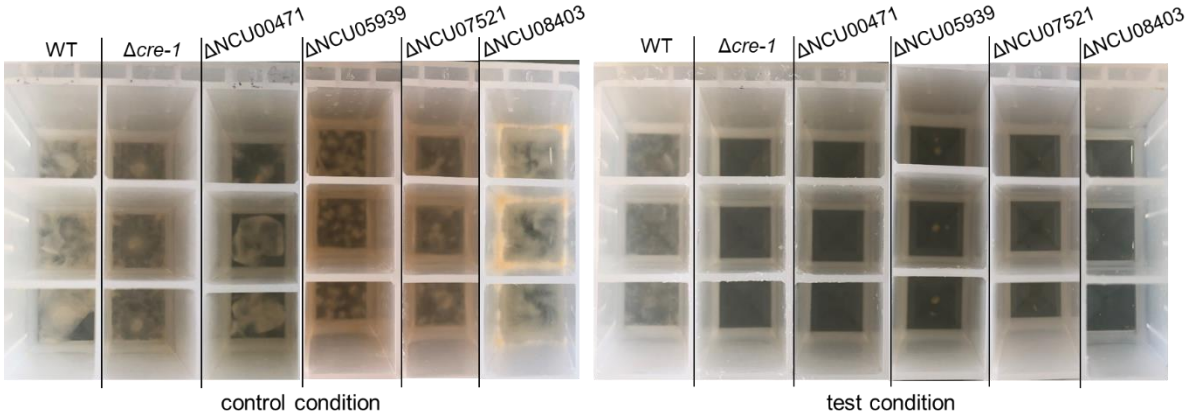

Figure 2-10: *N. crassa* growth phenotype in 24-deep well plate.
Image of *N. crassa* WT and deletion strains that showed a significantly increased sensitivity to AA. Strains were grown in 1% glucose VMM (control condition) and in 1% glucose VMM supplemented with 100 mM AA (test condition) for 24 h (triplicates per strain and condition, 3 ml liquid medium per well).

2.2.4. Selection of putative F-box protein candidates for further investigations

Some deletion strains, which were found to be CCR-derepressed in the cellulose perception screen (Figure 2-6) showed also higher sensitivity to allyl alcohol (Figure 2-9), which confirms the derepressed phenotype for these strains. Especially Δ*fbx22*, Δ*fbx17* and Δ*fbx41* showed significant difference compared to the WT in both screenings (Figure 2-6 and Figure 2-9). Interestingly, ΔNCU08403 was highly sensitive to AA, but did not show increased cellulase activity compared to the WT (Figure 2-6). In contrast, Δ*fbx58* and ΔNCU06688 showed significantly higher enzymatic activity, while the sensitivity of the strain to AA was at WT level.

Some strains showing a CCR-repressed phenotype in cellulose perception (Figure 2-6) were also significantly less sensitive to AA compared to the WT (Figure 2-9), like Δ*fbx23*, ΔNCU05033, Δ*fbx30* and ΔNCU09899. The Δ*fbx40* deletion strain showed a significantly decreased cellulase activity, but only a slightly repressed phenotype in presence of AA.

The ΔNCU09899 deletion strain showed a significantly lower cellulase activity (Figure 2-6), but in contrast the determined protein amount in the supernatant was slightly higher than in the WT (Figure S 6-1). The *N. crassa* deletion strains of the 40 genes with putative F-box protein function were screened to identify aberrant phenotypes related to CCR (see above), while significant difference compared to the WT was rated with scores. Higher significant difference resulted in a higher score value.

Additionally, interesting expression patterns of the *fbx* genes on different carbon sources were assessed and also rated with scores (Figure 2-4, highlighted with a red x), as well as the presence of CCR-relevant proteins in the co-expression network using PlaNet (Table 5-1) of each F-box protein (Table 2-1).

Table 2-1: Interesting carbon utilization genes which were first (F) and second (S) neighbor of the corresponding *fbx* gene in the co-expression network.

***fbx* gene**	**Interesting CCR/ carbon utilization genes**
fbx17, NCU07521	NCU07788, *col-26* (S)
fbx20, NCU06250	NCU07788, *col-26* (S)
fbx24, NCU06483	NCU07788, *col-26* (S)
fbx3, NCU07257	NCU03887, *creD* (F) and NCU08378, *creB* (S)

The scores for significantly different phenotypes in cellulose perception (2.2.2), biomass formation in presence of allyl alcohol (2.2.3), interesting co-expressions (Table 2-1) and expression patterns on different carbon sources (Figure 2-4) were summed up and F-box candidates were ranked according to the score counts (Table 2-2). Additionally, the CCR phenotype found in chapter 2.2.3 is listed in the last column.

Table 2-2: Summary of scores for *N. crassa* putative F-box proteins and the transcription factor CRE-1

Δ*cre-1* additionally served as control. Summary of scores for significant difference, interesting co-expressed genes and expression patterns on different carbon sources is given in the third column. hp = hypothetical protein.

***A. nidulans* ortholog *fbx* gene, Genotype**	**gene name**	**Score**	**CCR phenotype**
Δ*fbx17*, ΔNCU07521	*fwd-2*; F-box/WD-40 domain-containing protein 2	16	derepressed
ΔNCU05033	hp	13	repressed
Δ*fbx22*, ΔNCU05939	*cdc4*; cell division control protein 4	12	derepressed
Δ*fbx23*, ΔNCU04540	*fwd-1*; F-box/WD-40 domain-containing protein 1	12	repressed
Δ*fbx30*, ΔNCU02379	*mus-10*; mutagen sensitive-10 protein	12	
Δ*fbx41*, ΔNCU00471	hp	12	derepressed
Δ*cre-1*, ΔNCU08807	DNA-binding protein *cre-1*	9	derepressed

***A. nidulans* ortholog *fbx* gene, Genotype**	**gene name**	**Score**	**CCR phenotype**
Δ*fbx50*, ΔNCU01216	*hpth-1*; ubiquitin ligase complex F-box protein GRR1	9	
ΔNCU08842	hp	9	
Δ*fbx27*, ΔNCU10476	hp	9	
Δ*fbx40*, ΔNCU03462	leucine Rich Repeat domain-containing protein	8	Slightly repressed
ΔNCU05393	hp	7	
Δ*fbx24*, ΔNCU06483	F-box and WD repeat-containing protein	7	
ΔNCU04383	hp	7	
ΔNCU12130	hp	7	
Δ*fbx58*, ΔNCU06688	F-box domain-containing protein	6	
ΔNCU02346	hp	6	repressed
ΔNCU07110	hp	6	
ΔNCU08348	hp	6	
ΔNCU09899	*exo-1* (*frp1*)	5	Slightly repressed
Δ*fbx15*, ΔNCU04576	hp	5	
Δ*fbx3*, ΔNCU07257	F-box domain-containing protein	5	
Δ*fbx29*, ΔNCU07419	F-box domain-containing protein	4	
ΔNCU08403	hp	4	derepressed
ΔNCU08717	hp	4	
Δ*fbx1*, ΔNCU03146	F-box protein *pof7*	3	
Δ*fbx10*, ΔNCU04785	hp (hypothetical protein)	3	
Δ*fbx18*, ΔNCU07425	hp	3	
Δ*fbx19*, ΔNCU08642	cyclic nucleotide-binding domain-containing protein	3	
Δ*fbx20*, ΔNCU06250	F-box/LRR repeat containing protein 2	3	
Δ*fbx37*, ΔNCU07359	hp	3	
Δ*fbx7*, ΔNCU03022	F-box domain-containing protein	3	
ΔNCU03881	hp	3	
ΔNCU09807	hp	3	
ΔNCU01926	hp	2	
Δ*fbx9*, ΔNCU03658	*spp-1*; secretory pathway protein-1	1	
ΔNCU05243	hp	1	
Δ*fbx11*, ΔNCU07996	F-box and WD domain-containing protein	0	
Δ*fbx65*, ΔNCU06056	hp	0	
ΔNCU01081	hp	0	
ΔNCU01865	hp	0	

The plan was to investigate three de-repressed and three repressed F-box candidates involved in the switch between CCR and lignocellulose utilization in more detail. To this end, the first four *fbx* genes with the highest score numbers in the screenings were selected for

further investigation: *fbx17* (NCU07521), NCU05033, *fbx22* (NCU05939) and *fbx23* (NCU04540).

The deletion strain of *fbx41* (NCU00471) had also shown a Δ*cre-1*-like phenotype within all assays, including sensitivity to allyl alcohol, and a higher protein amount and cellulase activity compared to the WT. Therefore, it was also chosen for further investigations. To choose one more repressed strain, Δ*fbx50* (ΔNCU01216), Δ*fbx27* (ΔNCU10476) and Δ*fbx40* (ΔNCU03462) were compared:

Within the cellulase activity assay (Figure 2-6), Δ*fbx27/40/50* showed significantly decreased cellulase activity compared to the WT and therefore a repressed phenotype. This phenotype was confirmed for Δ*fbx40* within the AA assay (Figure 2-9). In contrast, Δ*fbx27/50* were more sensitive to AA than the WT, indicating a slightly derepressed phenotype, which was however not significant. Taking the results of both screening methods into account (2.2.2, 2.2.3), *fbx40* was the most interesting candidate for the purpose of this study compared to *fbx27/50*. In addition, *fbx40* showed an interesting expression pattern within the RNA-sequencing dataset containing glucose gradients and time series published by Wang *et al.* [Wang et al. 2017], in which *fbx40* (NCU03462) displayed a clear repression in presence of glucose [Wang et al. 2017].

Overall, three *fbx* genes were selected, for which the corresponding deletion strains showed a repressed phenotype: *fbx23* (NCU04540), NCU05033, and *fbx40* (NCU03462) - and three which showed a deprepressed phenotype when deleted: *fbx17* (NCU07521), *fbx22* (NCU05939), and *fbx41* (NCU00471). To verify the phenotype through an independent cellulose perception assay, the culturing procedure and the determination of the enzymatic activity profiles, as described in chapter 2.2.2, were repeated one more time (Figure S 6-3).

2.3. Characterization of selected F-box candidates

2.3.1. Developmental phenotypes and growth rates of selected *fbx* deletion strains

In *A. nidulans*, *fbx* deletions can cause growth and developmental defects [Sarikaya Bayram et al. 2022]. The *N. crassa* deletion strains of the finally selected candidates (2.2.4) were therefore also characterized for growth phenotypes and compared to the WT strain and Δ*cre-1* (Figure 2-11).

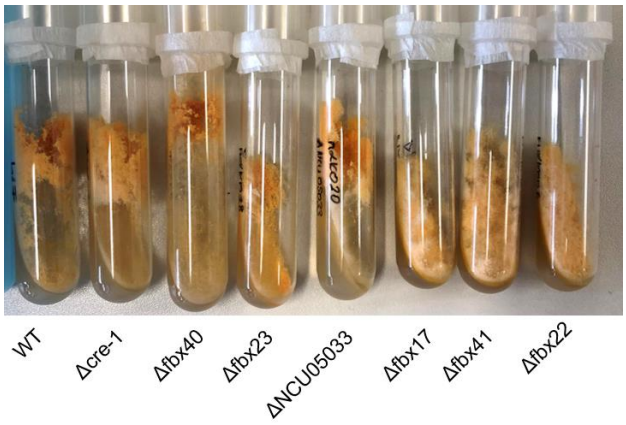

Figure 2-11: Growth phenotypes of *N. crassa* strains in agar slants.
N. crassa strains indicated below the corresponding slant were grown on VMM with 2% sucrose for two days in the dark at 30 °C, followed by day:night 12:12 incubation cycles at 25 °C for seven days.

A reduced formation of conidia was clearly visible for Δ*fbx23/17/22/41*, indicating a direct or indirect involvement of those F-box proteins at some point in the development of aerial hyphae or conidia formation. Observing the asexual conidia with an optical microscope, it was very remarkable that most of the conidia of Δ*fbx22* had an abnormal shape, which was rather elliptic than round (Figure S 6-4).

To assess to growth rate of these strains, a race tube assay was conducted. The deletion strains and the WT were grown on 2% sucrose VMM in tubes (Figure S 6-5). The growth is depicted in millimeter (mm) over time in Figure 2-12. Additionally, the average growth rate in millimeter per day was calculated and is shown in the diagram next to the corresponding strain.

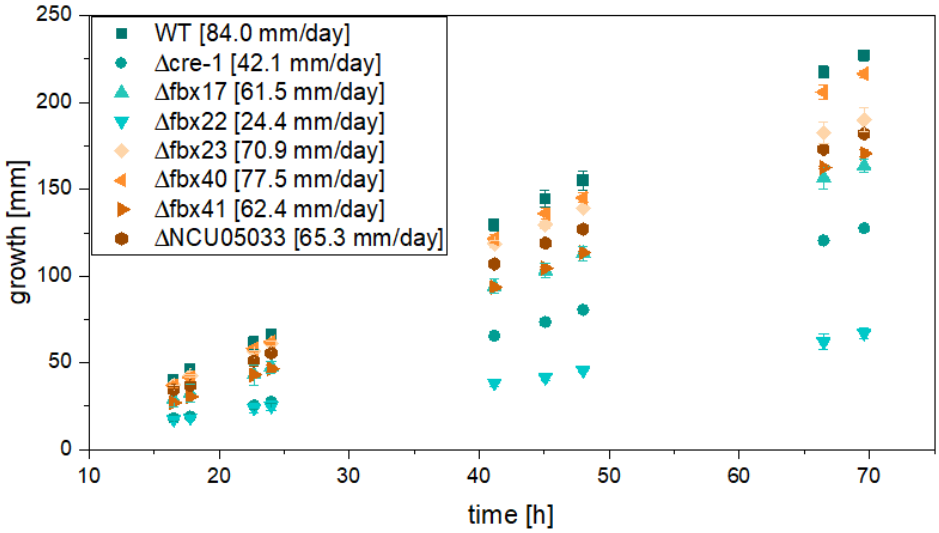

Figure 2-12: Growth rate of deletion strains of selected *fbx* candidates compared to WT and Δ*cre-1.*
Growth of the hyphal growth front is shown in millimeter over hours. Average growth rate is shown in millimeter per day, next to the corresponding strain. Time represents the time after transition from constant dark to constant light.

The average growth rate of the WT strain was the highest, followed by Δ*fbx40/23/41/17* and ΔNCU05033. The Δ*cre-1* strain grew only half as fast as the WT, while Δ*fbx22* only showed ~29% of the WT growth rate.

To prepare the strains for complementation constructs, as described in chapter 2.4.1, the strains were crossed with a histidine auxotrophic *N. crassa* WT strain. During these crossings, morphological abnormalities were observed for both Δ*fbx17* and Δ*fbx22* (Figure 2-13). Crosses of these mutants with the histidine auxotrophic *N. crassa* WT strain worked poorly, or the resulting strains did not have the desired genotype.

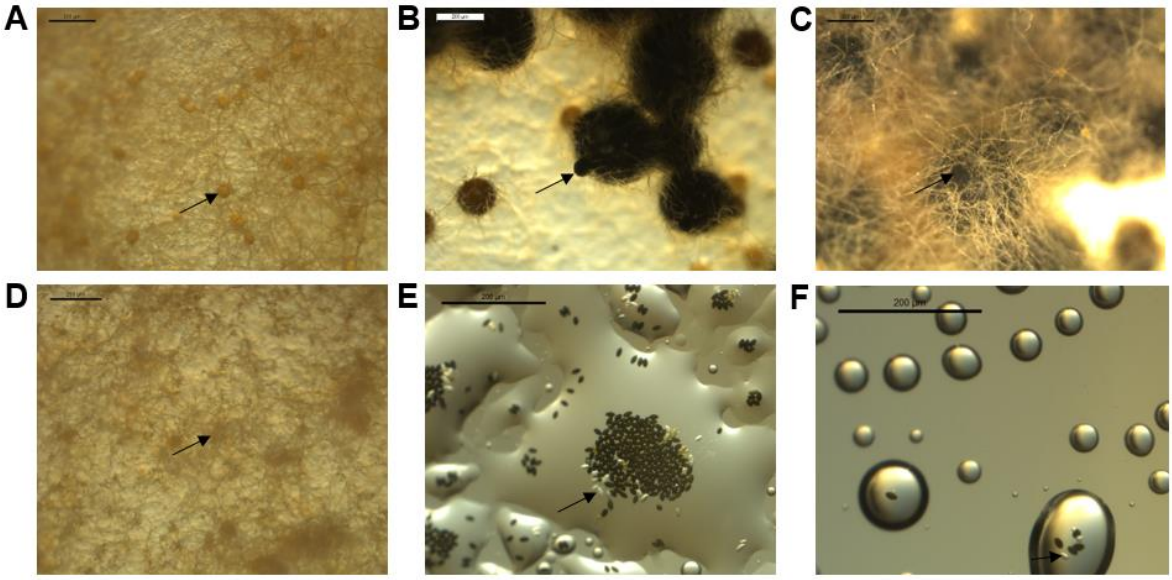

Figure 2-13: Developmental deficits of Δ*fbx17* and Δ*fbx22*.
(A) and (D) show protoperithecia (arrow) of (A) histidine auxotrophic *N. crassa* WT and (D) Δ*fbx22*. Development of perithecia of (B) Δ*fbx17* and (C) Δ*fbx22*, both crossed with histidine auxotrophic *N. crassa* WT. The Arrow in (B) and (C) indicates the beak of the perithecia. Ascospores (arrow), which were shot onto the lid of the petri dish from (E) Δ*fbx17* and (F) Δ*fbx22*, after cross with histidine auxotrophic *N. crassa* WT. (A) to (D) five-fold magnification of strains grown on Westergaard´s medium. (E) and (F) eight-fold magnification. Ruler indicates 200 µm within all figures.

The deletion strain of *fbx22* was not able to form WT-like protoperithecia (Figure 2-13, compare A and D), which were more reminiscent of clumps of hyphae and were not able to serve as female crossing partner. Crosses never resulted in perithecia formation when using Δ*fbx22* as the female part. Even when Δ*fbx22* was used as male mating partner, resulting perithecia exhibited an aberrant phenotype compared to the other strain crossings. The cross of histidine auxotrophic *N. crassa* WT (female) and Δ*fbx22* (male) developed perithecia covered in hyphae and appeared as a “hairy” phenotype (Figure 2-13, C). In general, very few perithecia were formed and as a consequence very few ascospores (Figure 2-13, F).

The morphology of Δ*fbx17* protoperithecia and perithecia did not appear abnormal. Nevertheless, the number of white (sterile) ascospores appeared more compared to other crosses (Figure 2-13, B and E).

To conclude, some *fbx* deletions cause pleiotropic effects. In the context of this investigation and strain selection, the deletion of *fbx22* showed the most severe phenotype concerning growth rate and developmental deficiencies.

2.3.2. Transcriptional response to carbon source switches by *N. crassa*

The deletion of the *fbx* genes Δ*fbx17*, Δ*fbx41* and ΔNCU05033 resulted in either derepressed or repressed phenotypes, which implies an influence of these F-box proteins in carbon utilization or CCR. RNA sequencing was conducted to gain insights into which genes are mis-expressed in these three *fbx* deletion strains during carbon source switches from a carbon catabolite (CC) derepressing to a CC-repressing condition or *vice versa*. To receive an impression of the time frame of transcriptional events taking place after carbon source switches, a quantitative PCR experiment was performed initially to define the experimental setup for the RNA-seq experiment.

Expression of cbh-1 in selected N. crassa fbx mutants

The gene *cbh-1* encodes a major cellulase of *N. crassa*, which is one of the most abundantly secreted proteins [Glass et al. 2013]. Since *cbh-1* expression is also induced in presence of cellulose and cellobiose, this gene was chosen to be investigated in a qPCR experiment (Figure 2-14). Deletion strains, which showed a derepressed phenotype in the previous screening (Table 2-2), were grown on 1% Avicel and switched to 2% Glucose (Figure 2-14 A). Culturing conditions were applied *vice versa* for the strain NCU05033, which showed a repressed phenotype (Figure 2-14 B).

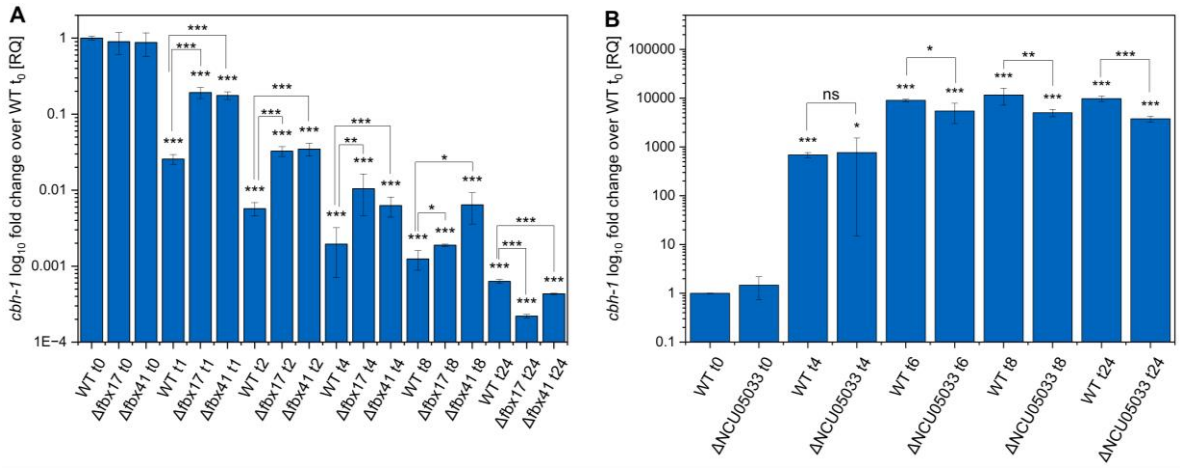

Figure 2-14: *cbh-1* expression of selected *fbx* mutants.

Strains were grown on 1% Avicel and switched to 2% Glucose (A) or *vice versa* (B) before harvested for RNA extraction and qPCR (see Table 5-10 and Table 5-11). The gene of interest, *cbh-1,* is the major cellulase of *N. crassa*. *cbh-1* expression levels were determined in the WT, Δ*fbx17*, Δ*fbx41* and ΔNCU05033 deletion strain. Relative quantification (RQ) was done over housekeeping gene *actin*. Harvesting time points are indicated next to the strain description on the x-axis. Asterisks above the bars indicate significance compared to WT t_0 if not indicated otherwise through lines. Significance levels were determined using a paired t test. *, $P < 0.05$; **, $P < 0.01$; ***, $P < 0.001$.

Deletion of *fbx17*, *fbx41* and NCU05033 resulted in significant changes of *cbh-1* expression (Figure 2-14). Derepressed strains (Δ*fbx17/41*) displayed a slow repression after switch to glucose. The repressed strain (ΔNCU5033) was not able to release CCR in a WT-like manner, since *cbh-1* expression levels were significantly decreased in ΔNCU05033 compared to the WT after switching from glucose to Avicel (Figure 2-14 B).

In general, switching from the derepressed to repressed condition (Figure 2-14 A), the repression of *cbh-1* seems to happen quickly. After 1 h, there is already a strong repression of *cbh-1* detectable. Therefore, the first harvesting time point for the RNA-seq experiment was chosen to be 30 min post transfer to the repressing condition. At t_8, significant differences were detected between the strains. This time point was therefore chosen to additionally detect events happening at a later time point after the switch from Avicel (cellulose) to glucose.

Switching from the repressed (glucose) to the derepressed condition (Avicel) revealed that the derepression requires more time (Figure 2-14 B). Because the derepession seems to happen between four (t_4) and six (t_6) hours, t_5 was chosen as harvesting time point for the RNA-seq experiment. Since also at t_{24} significant differences in *cbh-1* expression were detected, and because the derepression was likewise detected at later time points in the screen for cellulolytic response (see 2.2.2), t_{24} was added as a late time point to investigate in the RNA-seq experiment.

Transcriptional profiling of N. crassa fbx deletion strains – Analysis of differentially expressed genes

Analogous to the qPCR pre-experiment above, the derepressed deletion strains Δ*fbx17* and Δ*fbx41* (see chapter 2.2.4) were switched from a derepressed condition (24 h in 1% Avicel after pre-growth) to a repressed condition (2% glucose). Replicates were harvested after 24 h in 1% Avicel VMM (t_0), 0.5 h ($t_{0.5}$) and 8 h (t_8) after the switch into 2% glucose VMM.

The deletion strain ΔNCU05033, which showed a repressed phenotype (see subchapters of chapter 2.2), was switched in the opposite way: from a repressed condition (24 h in 2% glucose) to a derepressed condition (1% Avicel). Some replicates were harvested after 24 h in 2% glucose VMM, which represents t_0. The remaining replicates were switched to 1% Avicel VMM and harvested five (t_5) and 24 (t_{24}) hours after the medium switch. The

cultivation procedure can be found in 5.2.3, Table 5-11. RNA sequencing and data processing was performed as described in chapter 5.5.

Differentially expressed genes (DEGs) (Table S 6-1, Table S 6-2) which were at least two-fold significantly up- or downregulated over the different time points were compared using Venn diagrams (Figure 2-15).

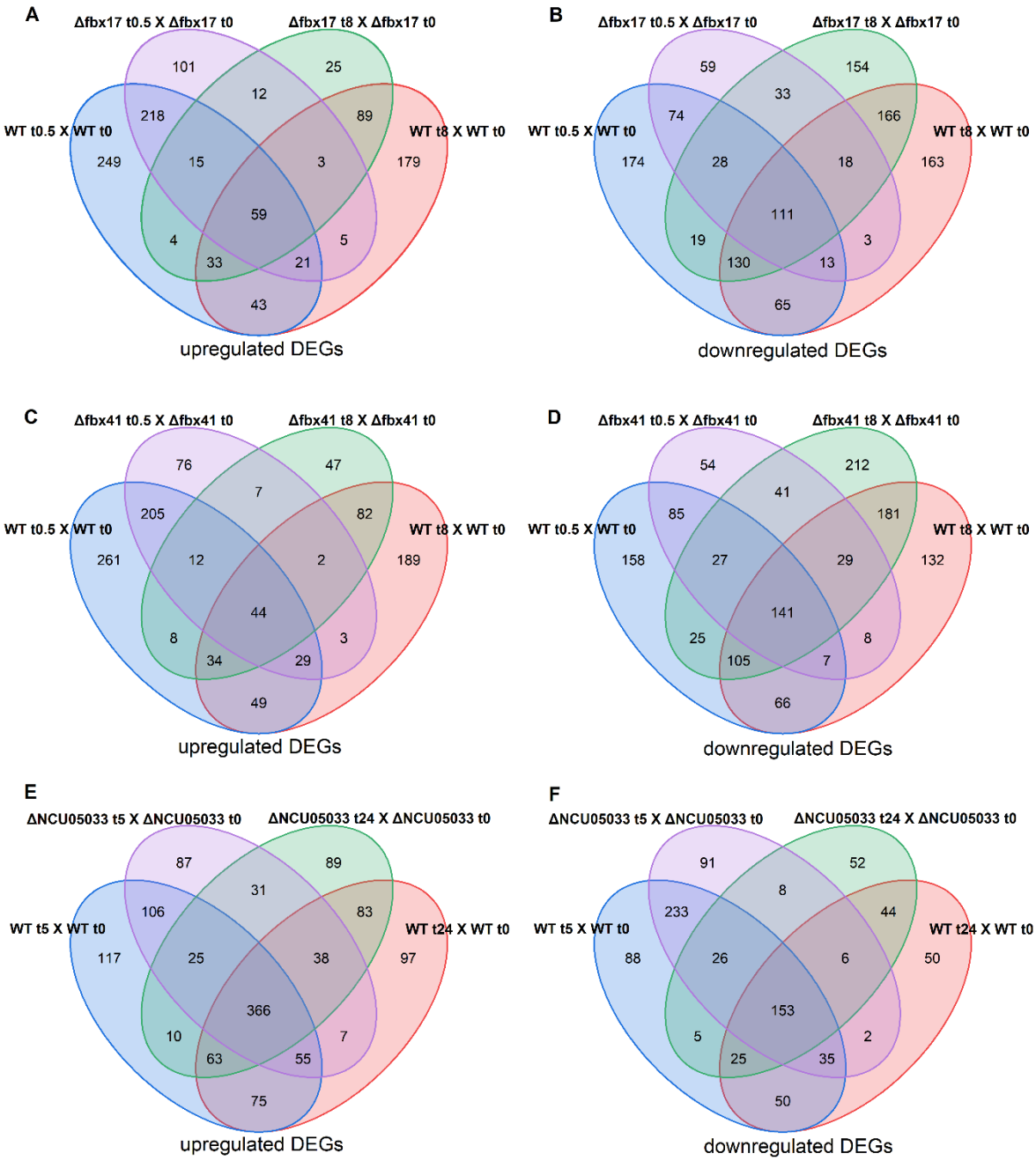

Figure 2-15: Venn diagrams of significant DEGs within each strain at different time points. DEGs across different time points of Δ*fbx17* (A, B), Δ*fbx41* (C, D) and ΔNCU05033 (E, F) were compared to the WT strain. (A to D) Strains were switched from CC-derepressing to CC-repressing condition. (E, F) Strains were switched from CC-repressing to CC-derepressing condition. DEG = log2 fold-change >2 and $P < 0.05$.

A gene ontology (GO) enrichment analysis revealed that the majority of the 59 genes which were significantly upregulated in both WT and Δ*fbx17* at all time point comparisons (Figure 2-15, A), were associated with amino acid transmembrane transport (GO:0003333). Also the 44 genes which were significantly upregulated in both WT and Δ*fbx41* at all time points (Figure 2-15, C) were found to be enriched for the same class.

The 111 genes, which were differentially downregulated in both WT and Δ*fbx17* within all time point comparisons (Figure 2-15, B), were significantly enriched in the GO terms carbohydrate catabolic process (GO:0016052) and cellular component organization or biogenesis (GO:0071840). The 141 differentially downregulated genes in both WT and Δ*fbx41* at all time point comparisons (Figure 2-15, D) were significantly enriched for galactose catabolic process (GO:0033499), disaccharide metabolic process (GO:0005984), glucose metabolic process (GO:0006006), secondary metabolic process (GO:0019748), proton transmembrane transport (GO:1902600), biological regulation (GO:0065007), cellular component biogenesis (GO:0044085), organelle organization (GO:0006996) and gene expression (GO:0010467). Comparing differentially downregulated genes of the WT with both Δ*fbx17/41* deletion strains, differentially downregulated genes across all time points were significantly enriched for carbohydrate metabolic process (GO:0005975), cellular component organization or biogenesis (GO:0071840), macromolecule metabolic process (GO:0043170), carbohydrate transmembrane transport (GO:0034219), carbohydrate catabolic process (GO:0016052) and carbohydrate transport (GO:0008643).

In total, 471 genes were exclusively upregulated in the WT strain compared to Δ*fbx17* either after 30 minutes, eight hours or in both time points (Figure 2-15, A). These genes were significantly enriched in some of the following GO terms of biological processes: in biosynthetic processes of: alpha amino acid (GO:1901607), nucleotide (GO:0009165), ribonucleoside monophosphate (GO:0009156), ribose phosphate (GO:0046390); tRNA methylation (GO:0030488), and maturation of SSU-rRNA from tricistronic rRNA transcript (GO:0000462). Comparing the WT to Δ*fbx41*, a total of 499 genes were exclusively upregulated in the WT strain either after 30 minutes, eight hours or in both time points (Figure 2-15, C). These genes were significantly enriched in the following GO terms: arginine biosynthetic process (GO:0006526), IMP biosynthetic process (GO:0006188), pyrimidine nucleobase metabolic process (GO:0006206), aspartate family amino acid biosynthetic process (GO:0009067) and RNA methylation (GO:0001510). Comparing upregulated genes of the WT to both Δ*fbx17/41* the following GO terms were significantly enriched in the WT strain either after 30 minutes, eight hours or in both time points: biosynthetic processes of: folic acid (GO:0046656), aromatic amino acid (GO:0009073) and

nucleobase (GO:0046112); in glutamine metabolic process (GO:0006541), protein modification process (GO:0036211) and vesicle-mediated transport (GO:0016192).

In total, 138 genes were exclusively upregulated in the Δ*fbx17* strain either after 30 minutes, eight hours or in both time points (Figure 2-15, A). However, these genes were not significantly enriched in GO terms of any biological processes. In the Δ*fbx41* strain, 130 genes were exclusively upregulated either after 30 minutes, eight hours or in both time points (Figure 2-15, C). These genes were also not significantly enriched in GO terms of biological processes.

When compared to Δ*fbx17,* 402 genes were exclusively downregulated in the WT strain either after 30 minutes, eight hours or in both time points (Figure 2-15, B). These genes were significantly enriched in some of the following GO terms of biological processes: branched-chain amino acid (GO:0009083), regulation of cellular process (GO:0050794) and cellular component biogenesis (GO:0044085). Comparing the WT to Δ*fbx41*, a total of 356 genes were exclusively downregulated in the WT strain either after 30 minutes, eight hours or in both time points (Figure 2-15, D). These genes were significantly enriched in the following GO terms: amino acid catabolic process (GO:0009063), monocarboxylic acid metabolic process (GO:0032787), regulation of nucleobase-containing compound metabolic process and macromolecule biosynthetic process (GO:0019219, GO:0010556). Comparing downregulated genes of the WT to both Δ*fbx17/41* the following GO terms were significantly enriched in the WT strain either after 30 minutes, eight hours or in both time points: alpha-amino acid catabolic process (GO:1901606), cellular component organization (GO:0016043), regulation of gene expression (GO:0010468) and RNA processing (GO:0006396).

In total, 246 genes were exclusively downregulated in the Δ*fbx17* strain either after 30 minutes, eight hours or in both time points (Figure 2-15, B). These genes were significantly enriched in some of the following GO classes of biological processes: cellular component organization and biogenesis (GO:0016043, GO:0044085), nucleic acid metabolic process (GO:0090304), gene expression (GO:0010467) and establishment of protein localization (GO:0045184). In the Δ*fbx41* strain, 307 genes were exclusively downregulated either after 30 minutes, eight hours or in both time points (Figure 2-15, D). A significant enrichment of these genes was found regarding: protein metabolic process (GO:0019538), organonitrogen compound biosynthetic process (GO:1901566), cellular localization (GO:0051641), cellular nitrogen compound biosynthetic process (GO:0044271), macromolecule biosynthetic process (GO:0009059), RNA processing (GO:0006396), macromolecule localization (GO:0033036), ellular component assembly (GO:0022607) and negative regulation of biological process (GO:0048519).

A GO enrichment analysis of the switch from glucose to cellulose (Avicel) revealed that the 366 genes that were significantly upregulated in both WT and ΔNCU05033 within all time point comparisons (Figure 2-15, E), were significantly enriched in maltose and glucose metabolic and xylan and cellulose catabolic processes (GO:0000023, GO:0006006, GO:0045493, GO:0030245), carbohydrate and proton transmembrane transport (GO:0034219, GO:1902600), translation (GO:0006412) and some other classes related to protein synthesis and expression. The 153 downregulated DEGs in both WT and ΔNCU05033 within all time point comparisons (Figure 2-15, F), were significantly enriched for the following GO classes: biosynthetic processes of pyridoxine, adenine, pyridoxal phosphate, threonine, chorismate, arginine, 'de novo' IMP, lysine, histidine, isoleucine, valine, aromatic amino acid family, methionine, ergosterol and serine family amino acid (GO:0008615, GO:0046084, GO:0042823, GO:0009088, GO:0009423, GO:0006526, GO:0006189, GO:0019878, GO:0000105, GO:0009097, GO:0009099, GO:0009073, GO:0009086, GO:0006696, GO:0009070). Additionally, genes were significantly enriched within some different metabolic processes: glycolytic process (GO:0006096), carboxylic acid transport (GO:0046942) and spermidine transmembrane transport (GO:1903711).
Two-hundred eighty-nine DEGs, which were exclusively upregulated within the WT strain across all time points during the switch from glucose to cellulose (Avicel) (Figure 2-15, E), were significantly enriched for organonitrogen and nucleobase-containing compound metabolic process (GO:1901564, GO:0006139), organelle organization (GO:0006996), gene expression (GO:0010467) and establishment of localization in cell (GO:0051649).
In contrast, 207 DEGs, which were exclusively upregulated within the ΔNCU05033 deletion strain across all time points during the switch from glucose to cellulose (Avicel) (Figure 2-15, E), were significantly enriched within macromolecule metabolic process (GO:0043170) and cellular nitrogen compound biosynthetic process (GO:0044271).
One-hundred eighty-eight DEGs, which were exclusively downregulated within the WT strain across all time points during the switch from glucose to cellulose (Avicel) (Figure 2-15, F), were significantly enriched for translation (GO:0006412) and amino acid metabolic process (GO:0006520). 151 DEGs, which were exclusively downregulated within the ΔNCU05033 deletion strain across all time points during the switch from glucose to cellulose (Avicel) (Figure 2-15, F) were significantly enriched for maturation of SSU-rRNA from tricistronic rRNA transcript and maturation of 5.8S rRNA (GO:0000462, GO:0000460), organonitrogen compound biosynthetic process (GO:1901566) and small molecule metabolic process (GO:0044281).

Comparing DEGs (Figure 2-15, A to D) with a focus on some selected genes encoding e.g. kinases, enzymes, transporters and transcription factors (TFs) between the WT strain and

both Δ*fbx17/41* strains 30 minutes and eight hours after the switch from Avicel to glucose, the following differences were noticeable:

NCU03238, encoding the G protein-coupled receptor (GPCR) GPR-9, was significantly upregulated within the WT and Δ*fbx17* strain 30 minutes after switch to glucose, but not in Δ*fbx41*. NCU00306 (*mdr-10*, a MFS multidrug transporter) and NCU04528, a laccase, were significantly upregulated within the WT and Δ*fbx17* strain eight hours after switch to glucose, but not in Δ*fbx41*. The TFs NCU07900 (*sgr-26*) and NCU01386 (*ada-10*) were upregulated 30 minutes after switch from Avicel to glucose in the WT and additionally eight hours after medium switch in Δ*fbx17*, but not in Δ*fbx41*. After 30 minutes in glucose, the TF NCU05285 and the GPR-17, NCU04106, were significantly upregulated within the WT and Δ*fbx41* strain, but not in Δ*fbx17*. Moreover, NCU04987, encoding GPR-10, NCU05089 and NCU08425, both encoding transporters, were significantly upregulated in the WT and Δ*fbx41* strain eight hours after switch to glucose, but not in Δ*fbx17*.

Two CAZymes: NCU00061, encoding GH16-13 (a putative endo-1,3(4)-beta-glucanase or concanavalin A-like lectin/glucanase), and NCU01517, encoding the glucoamylase GLA-1, were found to be downregulated within the WT and Δ*fbx41* eight hours after switch to glucose, but not in Δ*fbx17*. The major myo-inositol transporter, NCU07199, was downregulated in WT and Δ*fbx17* but not in Δ*fbx41* eight hours after switch to glucose. The transcription factor NCU04866 (*ada-6*) was downregulated at both time points after switch in the WT and after 30 minutes in Δ*fbx17*, but not differentially expressed in Δ*fbx41*. The C6 zinc finger regulator fluffy (NCU08726) was downregulated at both time points in the WT after switch to glucose and additionally after eight hours in Δ*fbx41*.

Some transcription factors showed differences in expression between the WT and Δ*fbx17/41* after switch from Avicel to glucose: For instance, eight hours after the switch the TF NCU00808 (*znf-48*) was downregulated in the WT only. The TFs *xlr-1* (NCU06971) and *ara-1* (NCU05414) were downregulated at both time points in the WT, but only after eight hours (and therefore delayed) in both deletion strains. The TF *clr-2* was downregulated at all time points within all strains, except 30 minutes after switch to glucose in Δ*fbx17*. Also, some TFs were only upregulated in the WT 30 minutes after medium switch and not in the mutants, including: NCU00155 (*znf-44*), NCU00945 (*col-20*), NCU01640 (*rpn-4*), NCU04827 (*vad-10*), NCU06411 (*vad-4*), NCU08634 (*vsd-1*) and NCU09549 (*znf-51*); and eight hours after medium switch: NCU02142, NCU05257; and at both time points NCU00144. NCU02724, *res-2*, which is known to affect lignocellulase gene expression and potentially regulate secretory pathways [Fan et al. 2015] was downregulated 30 minutes after switch to glucose in the WT but not in the deletion strains.

The *creB* ortholog NCU08378 (*uth-11*) was upregulated 30 minutes after switch to glucose in all strains, and the *creD* ortholog NCU03887 (*cre-3*) was upregulated within all time points and strains.

Next, DEGs were compared between the WT strain and ΔNCU05033 five hours and 24 hours after the switch from glucose to cellulose (Avicel) (Figure 2-15, E, F), also with a focus on genes encoding for kinases, enzymes, transporters and TFs: Five hours after switch from glucose to cellulose (Avicel), *cre-1* (NCU08807) expression was downregulated in both WT and ΔNCU05033. Five and 24 hours after switch to cellulose, the *creD* ortholog NCU03887 (*cre-3*) was downregulated in both strains, while the *creC* ortholog NCU03965 (*cre-2*) was upregulated five hours after switch only in the WT. As expected, within both strains the expression of some transcription factors, cell wall hydrolases and transporters was upregulated after the switch from glucose to Avicel. For instance, both major cellulases of *N. crassa cbh-1* and *-2* (NCU07340, NCU09680), the cellodextrin transporters *cdt-1* and *-2* (NCU00801, NCU08114) and the TFs/transcriptional regulators *clr-1, -2 and -3* (NCU07705, NCU08042, NCU05846) were upregulated five and 24 hours after switch to Avicel in the WT and ΔNCU05033. Also in both, WT and ΔNCU05033 the cellulase repressor *rca-1* (NCU01312) was upregulated 24 hours after switch to Avicel. Interestingly, *stk-12* (NCU07378) and *rco-3* (NCU02582) were upregulated after 24 hours only in ΔNCU05033. TFs which were only downregulated in ΔNCU05033 were for instance NCU05285 (*znf-34*), NCU03073 (*pole-4*), NCU04050 (*cpc-1*) and NCU06919.

Differentially expressed genes of both medium switches, glucose to Avicel and *vice versa*, were compared. Significantly upregulated in all strains (WT, Δ*fbx17/41*) was e.g. *glt-1* (NCU01633), a low-affinity glucose transporter [Wang et al. 2017], after the switch from Avicel to glucose. It was significantly downregulated after switch from glucose to Avicel for WT and ΔNCU05033 after 24 h and ΔNCU05033 already after 5 h. Opposite to that, *hgt-1*/*-2* (NCU10021 and NCU04963), two high-affinity transporters [Wang et al. 2017], were both upregulated at all time points after switch to Avicel within WT and ΔNCU05033. Within WT, Δ*fbx17* and Δ*fbx41*, *hgt-1*/*-2* were both significant downregulated 8 h after switch from Avicel to glucose.

The normalized expression levels of the deletion strains were compared to the WT at the same harvesting time points and condition within scatter plots (Figure 2-16).

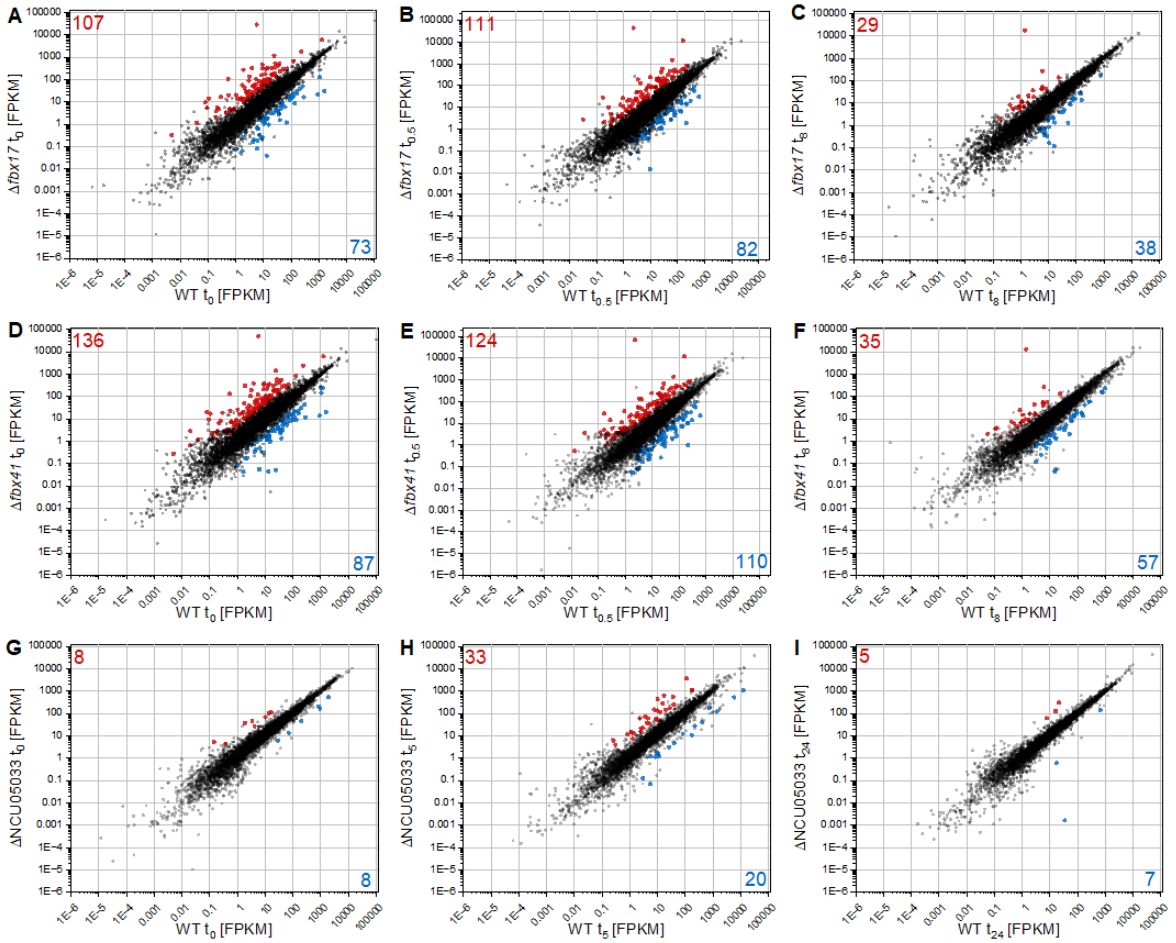

Figure 2-16: Comparison of expression levels of RNA-seq data.
Comparison of expression levels between WT and *fbx* deletion strains at three different harvesting time points per condition. Normalized expression levels are given in FPKM (Fragments Per Kilobase of transcript per Million mapped reads). WT expression levels were compared to those of Δ*fbx17* (A to C) and Δ*fbx41* (D to F) after 24 h in 1% Avicel (t_0, A, D), 30 min after switch from 1% Avicel to 2% glucose ($t_{0.5}$, B, E) and 8 h (t_8, C, F) after switch from 1% Avicel to 2% glucose. WT expression levels were compared to those of ΔNCU05033 (G to I) after 24 h in 2% glucose (t_0, G), 5 h after switch from 2% glucose to 1% Avicel (t_5, H) and 24 h (t_{24}, I) after switch from 2% glucose to 1% Avicel. Significantly upregulated DEGs are coloured in red and downregulated in blue. Number of DEGs are given in the corresponding colour within the scatter plots. Linear fit, R^2: (A) 0.67, (B) 0.90, (C) 0.93, (D) 0.76, (E) 0.84, (F) 0.92, (G) 0.94, (H) 0.94, (I) 0.95.

Overall, the data points within the scatter plots of Δ*fbx17* and Δ*fbx41* are more spread out compared to the WT, indicating less similar expression levels. In contrast, the data points of ΔNCU05033 compared to the WT run more diagonal, indicating highly similar expression patterns across all genes in the investigated conditions. This impression is confirmed by the coefficient of determination. Within a linear fit, the coefficient of determination (R^2) of ΔNCU05033 compared to the WT was closest to one.

Within a GO enrichment analysis, DEGs were analysed for significant enrichment within a GO class of biological processes. Additionally, a Functional Catalogue (FunCat) [Ruepp et al. 2004] enrichment analysis of *N. crassa* genes was performed using a customized database that included expanded categories for cell wall degradation-related genes [Thieme et al. 2017]. For significant enrichment, a threshold *P* value of 0.005 was set. The given rich factor in percent is the ratio of DEGs annotated in a FunCat category to the total number of genes assorted to the corresponding category.

Comparing upregulated genes of Δ*fbx17* to WT at t_0, DEGs were significantly enriched for the GO terms cellular component organization or biogenesis (GO:0071840), regulation of cellular process (GO:0050794) and nucleic acid metabolic process (GO:0090304) (Figure 2-16, A). Upregulated genes were significantly enriched within nineteen FunCat categories. The category with the highest rich factor of 9.5% was degradation/ modification of foreign (exogenous) polysaccharides (*P* $9.13*10^{-4}$), followed by extracellular polysaccharide degradation (5%, *P* $1.44*10^{-3}$), extracellular metabolism (4.14%, $1.69*10^{-3}$) and polysaccharide metabolism (3%, $1.18*10^{-3}$). The seventy-three downregulated genes were not significantly enriched for any GO term, but in sixteen FunCat categories. The highest rich factor of 15.8% was found for the category degradation of tyrosine (*P* $3.17*10^{-4}$). Some other significant categories were, e. g. transcription (*P* $9.24*10^{-5}$), nucleotide/nucleoside/nucleobase binding (*P* $4.34*10^{-4}$) and RNA synthesis (*P* $6.48*10^{-4}$).

Comparing DEGs of Δ*fbx17* to WT at $t_{0.5}$, Figure 2-16 B, upregulated genes were significantly enriched in polysaccharide catabolic process (GO:0000272) and nucleobase-containing compound metabolic process (GO:0006139) as well as within forty-four FunCat categories. The fifteen categories with the highest rich factor were: extracellular pectin specific degradation (42.9%, $4.37*10^{-5}$), extracellular homogalacturonan degradation (40.0%, *P* $1.17*10^{-3}$), homogalacturonan catabolism (22.2%, *P* $4.02*10^{-3}$), specific pectin catabolism (21.4%, *P* $4.22*10^{-4}$), arabinan catabolism (20.0%, *P* $4.97*10^{-3}$), hemicellulose/rhamnogalacturonan catabolism (17.6%, *P* $7.63*10^{-4}$), extracellular hemicellulose/pectin degradation (16.3%, *P* $3.63*10^{-7}$), degradation/ modification of foreign (exogenous) polysaccharides (14.3%, *P* $5.64*10^{-6}$), xylan catabolism (12.0%, *P* 2.37*10-3), hemicellulose/pectin metabolism (11.8%, *P* $2.57*10^{-8}$), hemicellulose/pectin catabolism (11.8%, *P* $2.57*10^{-8}$), extracellular polysaccharide degradation (10.0%, *P* $6.32*10^{-9}$), specific hemicellulose catabolism (10.0%, *P* $3.96*10^{-3}$), extracellular metabolism (7.1%, *P* $2.79*10^{-7}$) and sugar transport (7.0%, *P* $9.75*10^{-6}$).

Comparing DEGs of Δ*fbx17* to WT at $t_{0.5}$, Figure 2-16 B, downregulated genes were not significantly enriched in GO terms, but in fifteen FunCat categories. The categories with the

highest rich factors were peroxidase reaction (16.7%, *P* 3.99*10^{-3}) and vacuolar protein degradation (9.4%, *P* 2.06*10^{-3}).

Comparing DEGs of Δ*fbx17* to WT at t_8, Figure 2-16 C, upregulated genes were not significantly enriched in GO terms, but in one FunCat category, which was cell wall (1.3%, *P* 5.8*10^{-4}). Downregulated genes were also significantly enriched in one category, named protein with binding function or cofactor requirement (0.1%, *P* 3.55*10^{-3}).

Comparing upregulated genes of Δ*fbx41* to WT at t_0, DEGs were significantly enriched for the GO terms cellular component organization (GO:0016043), regulation of biological process (GO:0050789), and nucleic acid metabolic process (GO:0090304) (Figure 2-16 D). Within a total of thirty-five enriched FunCat categories, the highest rich factors were found in degradation/ modification of foreign (exogenous) polysaccharides (11.9%, *P* 2.19*10^{-4}), extracellular polysaccharide degradation (5.8%, *P* 9.65*10^{-4}), extracellular metabolism (5.32%, *P* 3.69*10^{-4}), degradation/ modification of foreign (exogenous) compounds (5.3%, *P* 3.4*10^{-3}) and polysaccharide metabolism (3.5%, *P* 8.72E-4).

Downregulated genes at t_0 (Figure 2-16 D), comparing Δ*fbx41* to WT, were not significantly enriched within the GO analysis. Interestingly, the same FunCat category (degradation of tyrosine; 15.7%, *P* 5.28*10^{-4}) as in the comparison of Δ*fbx17* to WT had the highest rich factor at the same time point.

Comparing DEGs of Δ*fbx41* to WT at $t_{0.5}$ (Figure 2-16 E), upregulated genes were significantly enriched in nitrogen compound metabolic process (GO:0006807), cellular metabolic process (GO:0044237) and cellular component organization or biogenesis (GO:0071840). Forty-two FunCat categories showed significant enrichment of the upregulated genes. The fifteen categories with the highest rich factors were extracellular pectin specific degradation (28.6%, *P* 2.97*10^{-3}), hemicellulose/rhamnogalacturonan catabolism (17.6%, *P* 1.05*10^{-3}), xylan catabolism (12.0%, *P* 3.21*10^{-3}), degradation/ modification of foreign (exogenous) polysaccharides (11.9 %, *P* 1.43*10^{-4}), extracellular hemicellulose/pectin degradation (11.6%, *P* 1.60*10^{-4}), hemicellulose/pectin metabolism (9.4%, *P* 8.28*10^{-6}), hemicellulose/pectin catabolism (9.4%, *P* 8.28*10^{-6}), extracellular polysaccharide degradation (8.3%, *P* 1.83*10^{-6}), metabolism of melanins (7.3%, *P* 4.05*10^{-3}), extracellular metabolism (7.1%, *P* 9.15*10^{-7}), sugar transport (7.0%, *P* 2.34*10^{-5}), proton driven symporter (5.7%, *P* 3.63*10^{-3}), degradation/ modification of foreign (exogenous) compounds (5.3%, *P* 2.20*10^{-3}), symporter (5.2%, *P* 2.49*10^{-3}) and polysaccharide metabolism (4.7%, *P* 1.69*10^{-6}).

Downregulated DEGs of Δ*fbx41* to WT at $t_{0.5}$ were significantly enriched in seventeen FunCat categories, whereas the greatest rich factor was found in vacuolar protein degradation (9.4%, *P* $4.62*10^{-3}$).

At t_8, thirty-five genes were upregulated comparing Δ*fbx41* to WT (Figure 2-16 F). The genes were neither significantly enriched in GO terms nor in the FunCat categories. Significant enrichment was found within the downregulated genes (Figure 2-16 F) for the categories protein with binding function or cofactor requirement (0.25%, *P* $4.11*10^{-4}$) and stress response (0.08%, *P* $4.59*10^{-3}$).

Comparing gene expression of the WT to ΔNCU05033, eight genes were differentially upregulated at t_0 (Figure 2-16, G). These genes were not significantly enriched in a GO term. Additionally, none of the eight upregulated genes were assorted to be significant enriched in a FunCat category. Also, eight genes were downregulated at t_0. No GO term was significantly enriched, but FunCats for extracellular polysaccharide degradation (1.7%, *P* $2.79*10^{-3}$). Some of the thirty-three upregulated DEGs at t_5 (Figure 2-16, H) were assigned to multiple FunCat categories: protein with binding function or cofactor requirement (0.1%, *P* $1.55*10^{-3}$), protein binding (0.04%, *P* $1.64*10^{-3}$), xylan catabolism (8%, *P* $2.91*10^{-3}$) and specific hemicellulose catabolism (6.7%, *P* $4.16*10^{-3}$). Significant enrichment of the GO term glucan catabolic process (GO:0009251) was found in the set of twenty downregulated DEGs at t_5 (Figure 2-16, H). Within this set of genes, significant enrichment was found in the following FunCat categories: cellulose metabolism (11.1%, *P* $2.07*10^{-8}$), cellulose catabolism (11.1%, *P* $2.07*10^{-8}$), extracellular cellulose degradation (16%, *P* $1.39*10^{-7}$), extracellular ester compound degradation (12.5%, *P* $3.90*10^{-7}$), extracellular polysaccharide degradation (4.1%, *P* $2.89*10^{-6}$), extracellular metabolism (2.9%, *P* $1.52*10^{-5}$), polysaccharide metabolism (1.6%, *P* $5.01*10^{-5}$), degradation/ modification of foreign (exogenous) polysaccharides (7.1%, *P* $7.21*10^{-5}$), polysaccharide binding (5.2%, *P* $1.79*10^{-4}$), degradation/ modification of foreign (exogenous) compounds (2.7%, *P* $1.30*10^{-3}$), peptide transport (5.1%, *P* $2.60*10^{-3}$), sugar, glucoside, polyol and carboxylate catabolism (1.3%, *P* $2.88*10^{-3}$) and heavy metal ion transport (1.9%, *P* $3.26*10^{-3}$). After 24 in Avicel, none of the differentially expressed genes were significantly enriched for any GO term or FunCat categories (Figure 2-16, I).

To further analyse causes for the phenotypes observed in chapter 2.2.2 and 2.2.3 on a transcriptional level, gene expression profiles were hierarchically clustered.

Transcriptomal data of N. crassa Δfbx17 deletion strain – Hierarchical clustering analysis

The gene expression profiles of Δ*fbx17* and the WT were hierarchically clustered. Only genes which were expressed at more than 10 FPKMs were considered within the hierarchical clustering analysis. The analysis of Δ*fbx17* and the WT strain of the switch from CC-derepressing (Avicel) to CC-repressing (glucose) condition revealed thirteen clusters (Figure 2-17).

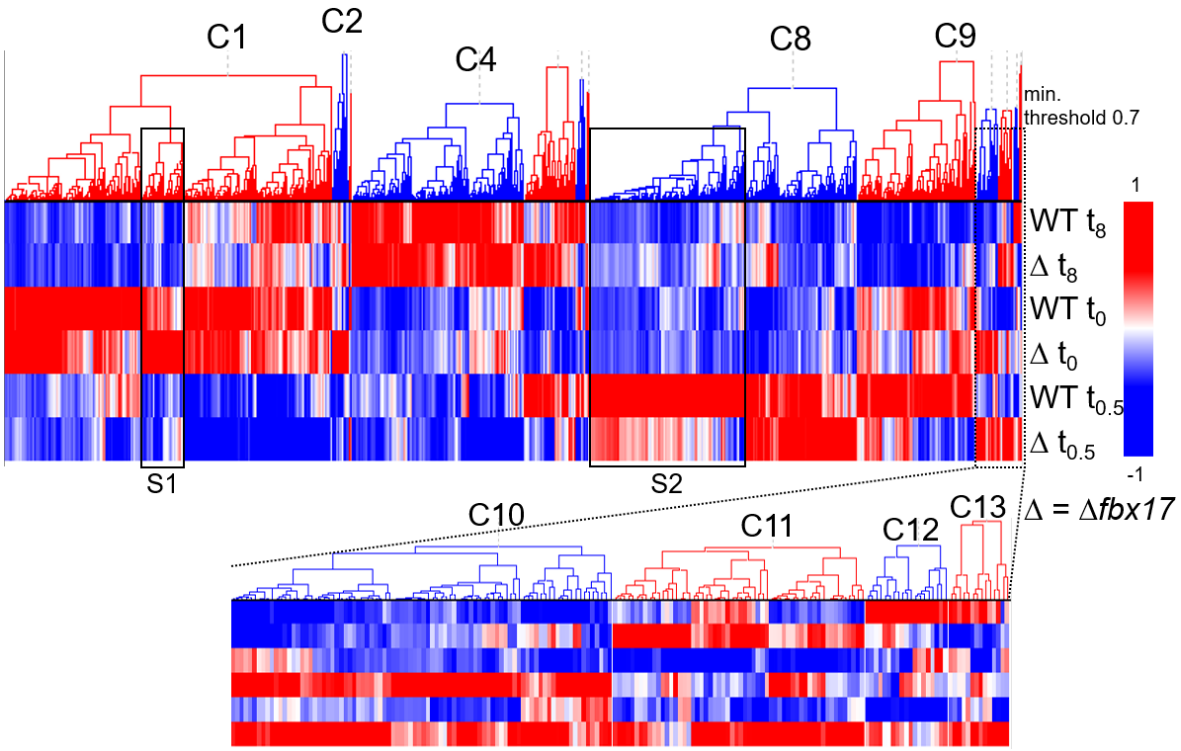

Figure 2-17: Hierarchical clustering analysis of RNA-sequencing data from *N. crassa* Δ*fbx17* and WT strains.
Strains were switched from CC-derepressing (Avicel) to CC-repressing condition. Time point t_0 is after 24 hours in Avicel, directly before medium switch to glucose. $t_{0.5}$ and t_8 indicate 0.5 hours and 8 hours in glucose after medium switch. Genes with a minimum expression level of 10 FPKM were clustered. Rows and columns were clustered. C = cluster. S = subcluster.

Regarding conditions, the same time points clustered together, indicating a generally high similarity of the response over time. At t_0, the strains were grown for 24 h in Avicel, at $t_{0.5}$ and t_8 the cultures were switched for 0.5 and 8 hours into glucose medium. Cluster 1 contains at least 68 CAZymes and 27 transporters. Enriched within C1 were GO terms related to intracellular transport and localization (GO:0032365, GO:0051649), vacuolar processes (GO:0007035, GO:0006623), proteasomal ubiquitin-independent and ubiquitin-dependent processes (GO:0010499, GO:0030433), proteasome assembly (GO:0043248) and protein catabolic process (GO:0010499), to name a few examples. Categories with the highest rich factor in cluster 1 were glycogen catabolism (83.3%, *P* $2.7*10^{-4}$) and

extracellular cellulose degradation (76%, *P* $3.59*10^{-12}$). Both major cellulases of *N. crassa* *cbh-1* and *-2* (NCU07340, NCU09680), the cellodextrin transporter *cdt-2* (NCU08114), one of two high-affinity transporters *hgt-2* (NCU04963) and *clr-1* (NCU07705) were found in cluster 1. Within subcluster 1 (S1, contains 86 genes in total), genes of Δ*fbx17* are more highly expressed at t_0 and $t_{0.5}$, indicating these genes were not downregulated as fast as in the WT. Genes within this subcluster were significantly enriched in carbohydrate metabolic process (GO:0005975). A FunCat enrichment analysis of subcluster 1 revealed twenty-seven significantly enriched categories. The majority of these categories were related to carbon source utilization, like cellulose metabolism and catabolism (15.6%, *P* $8.71*10^{-8}$), sugar transport (7.8%, *P* $1.11*10^{-7}$) and extracellular cellulose degradation (16.0%, *P* $5.29*10^{-5}$). These findings indicate that cluster 1 harbors the genes needed for cellulose degradation and perception. Since some genes were more strongly expressed in Δ*fbx17* compared to the WT at t_0 and $t_{0.5}$, this might partly explain the derepressed phenotype of Δ*fbx17*. The repression of genes needed for cellulase utilization seems to happen more slowly in the deletion mutant compared to the WT.

Half an hour after the switch from Avicel to glucose, the genes in cluster 8 were induced in comparison to t_0. The deletion strain Δ*fbx17* showed lower expressions at $t_{0.5}$ in cluster 8 compared to the WT, especially in subcluster 2 (Figure 2-17). Genes within cluster 8 were significantly enriched in 169 categories, e.g. in RNA processing (26.1%, *P* $2.74*10^{-31}$), and protein synthesis (24.6%, *P* $9.1*10^{-27}$), ribosome biogenesis (27.6%, *P* $3.27*10^{-25}$) and transcription (8.69%, *P* $9.1*10^{-24}$). *cre-1* (NCU08807), the *creD* ortholog NCU00866 (*cre-3*), and the *creB* ortholog NCU08378 (*uth-11*) are located here, while *cre-1* is even part of subcluster 2 (Figure 2-17). Genes in subcluster 2 were significantly enriched within 136 categories, e.g. RNA processing (21.9%, $4.67*10^{-46}$), rRNA processing (29.5%, $5.65*10^{-43}$), transcription (14.4%, $1.38*10^{-39}$), protein synthesis (19.8%, $3.35*10^{-37}$) and ribosome biogenesis (22.8%, $2.18*10^{-34}$), suggesting deficiencies of Δ*fbx17* with transcriptional and translational processes.

Genes of cluster 9 are also generally induced in the WT between t_0 and $t_{0.5}$, but fail for the most part to display this induction in the Δ*fbx17* deletion strain. These genes were enriched in 121 categories. The most significant ones were subcategories of cell cycle and DNA processing (9.4%, *P* $2.57*10^{-17}$). Within cluster 9, one of two high-affinity transporters, *hgt-1* (NCU10021) was found. Also some kinases were clustered together in cluster 9, e.g. kinases of the MAP kinase pathway including MAP kinase kinase kinase SskB *os-4* (NCU03071), MAPKKK *mik-1* (NCU02234), *mek-1* (NCU06419), the serine/threonine protein kinase *stk-13* (NCU00108) and the casein kinase *ckb-1* (NCU05485). The transcription factor *res-1* (NCU03699) was found in cluster 9, as well as *rcm-1* (NCU06842)

and *rco-1* (NCU06205), the two orthologs of yeast Tup1-Ssn6, which are Mig1/CRE-1 corepressors.

Eight hours after switch to glucose, genes within cluster 4, 5, 6 and 7 were induced in the WT and Δ*fbx17*. Genes of cluster 4 were significantly enriched in 126 categories. The most significant ones were all subcategories of protein synthesis (18.2%, $1.61*10^{-25}$), metabolism and energy. The low-affinity glucose transporter *glt-1* (NCU01633) is found in cluster 4, showing its highest expression at t_8 in both strains. Also *vib-1* (NCU03725), which is important for e.g. carbon scouting and cellulose utilization, is located in cluster 4. Genes within cluster 5 were significantly enriched in forty categories. The most significant ones were mitochondrion (14.2%, *P* $9.75*10^{-22}$), ribosomal proteins (13.1%, *P* $7.11*10^{-17}$), ribosome biogenesis (7.5%, *P* $5.06*10^{-12}$), protein synthesis (6.2%, *P* $9.05*10^{-12}$), translation (6.1%, $3.53*10^{-7}$) and respiration (6.2%, $3.10*10^{-6}$). Within cluster 6 and 7, no category was significantly enriched.

Clusters 10 to 13 are also interesting, since the WT and Δ*fbx17* show mainly opposite expression patterns with genes being generally more highly expressed in the deletion strain compared to the WT. Cluster 10 contains in total 88 genes, of which 32 were differentially expressed. Genes of cluster 10 were significantly enriched in ten subcategories of the category metabolism, whereas the subcategory extracellular polysaccharide degradation (7.5%, *P* $8.5*10^{-7}$) was the most significant one. Other significantly enriched categories were nucleic acid binding (0.2%, *P* $1.94*10^{-3}$), perception of nutrients and nutritional adaptation (3.1%, *P* $2.72*10^{-3}$), mitotic cell cycle and cell cycle control (0.2%, *P* $3.17*10^{-3}$) and sugar transport (3.9%, *P* $4.32*10^{-3}$). The DEGs were significantly enriched in the categories extracellular polysaccharide degradation (3.3%, *P* $4.99*10^{-4}$), virulence, disease factors (1.8%, *P* $1.51*10^{-3}$), extracellular metabolism (2.4%, *P* $1.73*10^{-3}$), C-compound and carbohydrate transport (1.5%, *P* $3.2*10^{-3}$) and polysaccharide metabolism (1.4%, *P* $4.54*10^{-3}$). Within cluster 10 are e.g. *clr-3* (NCU05846), *cdt-1* (NCU01233), some CAZymes and transporters as well as at least three G-protein coupled receptors, *gpr-31/-32/-39* (NCU08429, NCU08431, NCU09823), which were all DEGs upregulated at t_0 and *gpr-31/-32* also at $t_{0.5}$ in Δ*fbx17* compared to WT.

58 genes were clustered together in cluster 11, of which 18 were DEGs and upregulated at different time points in Δ*fbx17* compared to WT. The genes of cluster 11 were significantly enriched in protein binding (0.2%, *P* $7.85*10^{-4}$). Generally striking was that many DEGs were located in cluster 10 and 11 and all of the DEGs were upregulated. Genes within cluster 12 and 13 were not significantly enriched in GO terms or FunCat categories.

Transcriptomal data of N. crassa Δfbx41 deletion strain – Hierarchical clustering analysis

The hierarchical clustering of Δ*fbx41* and the WT strain of the expression profiles of a switch from CC-derepressing (Avicel) to CC-repressing (glucose) condition revealed eighteen clusters (Figure 2-18).

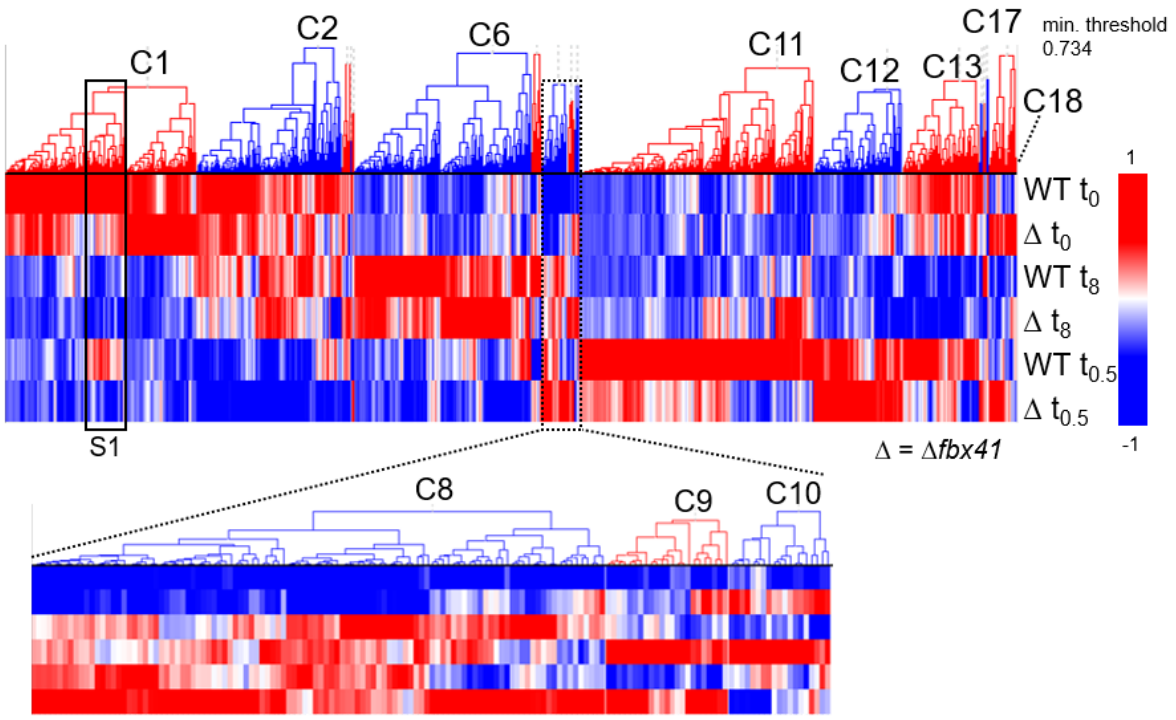

Figure 2-18: Hierarchical clustering analysis of RNA-sequencing data from *N. crassa* Δ*fbx41* and WT strains.
Strains were switched from CC-derepressing (Avicel) to CC-repressing condition. Time point t_0 is after 24 hours in Avicel, directly before medium switch to glucose. $t_{0.5}$ and t_8 indicate 0.5 hours and 8 hours in glucose after medium switch. Genes with a minimum expression level of 10 FPKM were clustered. Rows and columns were clustered. C = cluster. S = subcluster.

Within the hierarchical clustering analysis, the same time points of the WT strain and Δ*fbx41* clustered together, exactly like the clustering results of Δ*fbx17* and the WT strain. This indicates higher similarities between the strains at the same time points and main differences through altered conditions at the other time points.

After 24 h in Avicel (t_0), WT genes within clusters 1 to 5 were more strongly expressed compared to the two other time points (after switch to glucose) (Figure 2-18).

Cluster 1 contained at least 59 CAZymes and 25 transporters. In total 137 FunCat categories were significantly enriched with a *P* value of ≤ 0.005. The most significant categories were C-compound and carbohydrate metabolism (14.7%, *P* $1.91*10^{-23}$), sugar transport (38.3%, *P* $1.62*10^{-21}$), polysaccharide metabolism (22.3%, *P* $1.42*10^{-17}$), cellulose metabolism (57.8%, *P* $1.86*10^{-17}$) and cellulose catabolism (57.8%, *P* $1.86*10^{-17}$).

As in cluster 1 of the analysis Δ*fbx17 vs.* WT (Figure 2-17), also within cluster 1 of Δ*fbx41 vs*. WT (Figure 2-18) genes important for Avicel utilization were clustered, such as both major cellulases of *N. crassa cbh-1* and *-2* (NCU07340, NCU09680), the cellodextrin transporter *cdt-2* (NCU08114), one of two high-affinity transporters (*hgt-2;* NCU04963), and the TF *clr-1* (NCU07705). Especially at t_0 and $t_{0.5}$, genes within subcluster 1 of cluster 1 (in total 168 genes) displayed weaker expression in Δ*fbx41* compared to the WT. The genes within subcluster 1 were significantly enriched in 99 FunCat categories. The most significantly enriched ones were protein fate (3.4%, *P* $1.86*10^{-9}$), modification by phosphorylation, dephosphorylation, autophosphorylation (6.4%, *P* $2.63*10^{-9}$), regulation by modification (7.4%, *P* $3.23*10^{-9}$), cell cycle checkpoints (8.7%, *P* $2.04*10^{-8}$), mitotic cell cycle and cell cycle control (4.0%, *P* $2.91*10^{-8}$) and protein kinase (6.5%, *P* $3.48*10^{-8}$).
Within cluster 2, genes were significantly enriched within 92 FunCat categories related to protein fate (11.2%, *P* $4.6*10^{-20}$) and associated subcategories, cellular transport, transport facilitation and routes (9.2%, *P* $3.25*10^{-10}$). Genes within cluster 3 were significant enriched in nine FunCat categories. Significant enrichment was found in subcategories of cellular transport, protein with binding function, protein fate and metabolism. Cluster 4 and 5 contained only two genes each and were not significantly enriched in any category.

At $t_{0.5}$, genes in clusters 11 to 13 were induced in the WT, while in Δ*fbx41* some genes seemed to be misexpressed. Among others, the *creD* ortholog NCU00866 (*cre-3*) is part of cluster 11 and the *creB* ortholog NCU08378 (*uth-11*) and NCU08807 (*cre-1*) part of cluster 12. Genes within C11 were significantly enriched within 149 FunCat categories, for instance in protein synthesis (27.8%, *P* $2.74*10^{-47}$), transcription (18%, *P* $4.82*10^{-30}$) and protein with binding function or cofactor requirement (14.2%, *P* $3.12*10^{-25}$). Cluster 12 comprises genes that were significantly enriched in 75 FunCat categories and cluster 13 genes significantly enriched in 76 categories. The three most significant categories of cluster 12 were cell fate (6.6%, *P* $2.91*10^{-7}$), second messenger mediated signal transduction (10.1%, *P* $3.58*10^{-7}$) and calcium ion mediated signal transduction (13.6%, *P* $3.44*10^{-6}$). The three most significant categories of cluster 13 were cell cycle and DNA processing (6.2%, *P* $3.37*10^{-12}$), and the subcategories DNA processing (6.6%, *P* $7.89*10^{-10}$) and cell cycle (6.2%, *P* $3.57*10^{-9}$).

At t_8, genes within clusters 6 and 7 were most strongly expressed with some exceptions in Δ*fbx41*. Within cluster 6, genes were significantly enriched in 135 FunCat categories. The most significant ones were ribosomal proteins (36.9%, *P* $6.88*10^{-40}$) and translation (26.5%, *P* $3.44*10^{-37}$). Some CAZymes and *vib-1* (NCU03725) were also located in cluster 6.

Within cluster 8, but especially in clusters 9 and 10, many genes were expressed oppositely in the WT and Δ*fbx41*. No significantly enriched categories were found for genes in clusters

7, 8 and 10, while in cluster 9 the category protein with binding function or cofactor requirement (*P* 4.26*10^{-4}) showed significant enrichment.

Within clusters 14 and 16, genes were neither significantly enriched in FunCat categories, nor differentially expressed. Within cluster 15, significant enrichment was found for heat shock response (1.6%, *P* 3.92*10^{-3}) but none of the genes was found to be differentially expressed.

Within cluster 17, a total of 43 genes was, at least at one time point, significantly differentially upregulated in comparison to the WT, including some CAZymes and transporters. Genes of cluster 17 were significantly enriched in twenty-two FunCat categories, which were related to extracellular polysaccharide degradation (8.3%, *P* 9.24*10^{-7}), transcription (0.5%, *P* 1.48*10^{-3}), or extracellular cellulose degradation (12%, *P* 2.61*10^{-3}), to name a few examples.

Transcriptomal data of N. crassa ΔNCU05033 deletion strain – Hierarchical clustering analysis

The hierarchical clustering of ΔNCU05033 and the WT strain of the expression profiles of a switch from CC-repressing (glucose) to CC-derepressing (Avicel) condition revealed forty-six clusters (Figure 2-19).

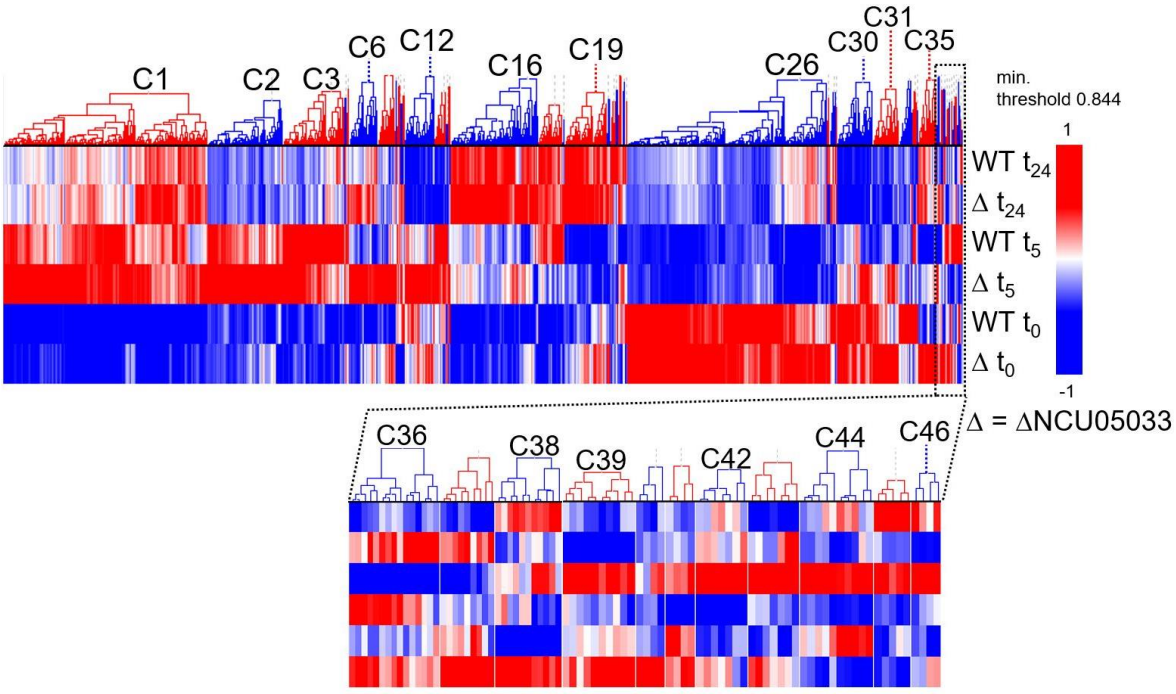

Figure 2-19: Hierarchical clustering analysis of RNA-sequencing data from *N. crassa* ΔNCU05033 and WT strains.

Strains were switched from CC-repressing (glucose) to CC-derepressing (Avicel) condition. Time point t_0 is after 24 hours in glucose, directly before medium switch to Avicel. t_5 and t_{24} indicate 5 hours and 24 hours in Avicel after medium switch. Genes with a minimum expression level of 10 FPKM were clustered. Rows and columns were clustered. C = cluster.

As in the previous clusterings, the WT and ΔNCU05033 deletion strain both clustered together at the same time points (Figure 2-19).

At t_0, which was after 24 h in glucose prior to the switch to Avicel, especially genes within clusters 26 to 34 were most strongly expressed. Genes within cluster 26 were significantly enriched in 177 categories. The most significant ones were related to protein translational processes, metabolism and energy.

Genes within clusters 27, 29, 33 and 34 were not significantly enriched in FunCat categories. Cluster 28 contained genes enriched in one category: energy generation (e.g. ATP synthase) (5.4%, *P* $4.54*10^{-3}$). Genes within cluster 30 were significantly enriched in twenty-seven categories, the most significant being accessory proteins of electron transport and membrane-associated energy conservation (11.7%, *P* $9.78*10^{-8}$), electron transport and membrane-associated energy conservation (6.9%, *P* $1.08*10^{-6}$), cytoplasmic and nuclear protein degradation (5.7%, *P* $1.36*10^{-6}$), proteasomal degradation (ubiquitin/proteasomal pathway) (6.2%, *P* $2.84*10^{-6}$) and protein/peptide degradation (4.9%, *P* $4.85*10^{-6}$). Genes within cluster 31 were generally higher expressed in ΔNCU05033 in glucose (t_0) and 5 h after medium switch to Avicel. Genes within this cluster were significantly enriched in twenty-seven categories, e.g. protein/peptide degradation (3.5%, *P* $1.24*10^{-4}$), cellular signaling (2.8%, *P* $4.75*10^{-4}$) and stress response (2.6%, *P* $5.63*10^{-4}$). For genes within cluster 32 significant enrichment in the subcategory urea catabolism (not urea cycle) (13.3%, *P* $4.58*10^{-3}$) was found.

Five hours after the switch from glucose to Avicel, especially the genes within clusters 1 to 5 were generally induced. Genes in cluster 1 were significantly enriched in 119 FunCat categories. The most significant one was sugar transport (44.5%, *P* $8.47*10^{-23}$), followed by protein synthesis (4%, *P* $1.68*10^{-12}$) and its subcategories, and transmembrane signal transduction (18.8%, *P* $1.29*10^{-9}$). The cluster contains several transcription factors, at least 34 CAZymes, 33 transporters and several kinases. In cluster 2, 90 significantly enriched categories were found, mainly subcategories related to energy (8.5%, *P* $3.53*10^{-10}$) and metabolism (5.4%, *P* $1.98*10^{-5}$).

At t_{24}, genes within clusters 16 to 25 were generally induced when compared to the other time points. Genes within cluster 16 were significantly enriched in seventeen FunCat categories, most significant were bud/growth tip (17.5%, *P* $3.20*10^{-5}$), nuclear and chromosomal cycle (10.4%, *P* $8.07*10^{-5}$), cell cycle (6.8%, *P* $6.47*10^{-4}$) and cellular sensing and response to external stimulus (7.4%, *P* $6.90*10^{-4}$).

Cluster 17 contains genes that generally failed to be upregulated at t_5 in ΔNCU05033 compared to the WT. Overall, 31 categories related e.g. to extracellular polysaccharide degradation (25%, *P* $2.85*10^{-30}$), extracellular metabolism (17.8%, *P* $1.64*10^{-25}$), and

cellulose metabolism (40%, *P* $1.15*10^{-22}$) were overrepresented. For example, the major cellulase *cbh-1* (NCU07340) and the exoglucanase 3 (NCU07190) were both significantly differentially expressed and downregulated at t_5. Additionally, *cbh-2* (NCU09680) was approximately 21-fold lower expressed at t_5 in ΔNCU05033 compared to the WT.

Clusters 35 to 46 showed mostly opposite expression patterns of both strains at the same time points. For instance, genes in cluster 38 show higher expression at t_0 (after twenty-four hours in glucose) in ΔNCU05033, but fail to be expressed after the switch to Avicel and are more strongly expressed in the WT than ΔNCU05033.

Interestingly, some genes in cluster 6 were more strongly expressed in ΔNCU05033 compared to the WT at t_0 and t_{24}, but especially at t_5. Thirteen genes were significantly differentially upregulated at least at t_5. The majority of these genes is described as hypothetical proteins. This could indicate that NCU05033 has an influence on unkown proteins or pathways, which have not been described yet. In total, genes within cluster 6 were significantly enriched in 21 FunCat categories, like sugar transport (6.3%, *P* $8.4*10^{-4}$), second messenger mediated signal transduction (4.2%, *P* $9*10^{-4}$) and actin cytoskeleton (4.4%, *P* $1.11*10^{-3}$).

The gene expression pattern within cluster 7 was also interesting, since genes were expressed more strongly in ΔNCU05033 especially at t_0 and t_5. The most significantly enriched FunCat categories, out of eleven, were vesicular transport (2.7%, *P* $2.54*10^{-4}$) and peptide binding (8.5%, *P* $8.98*10^{-4}$).

Transcriptomal data of N. crassa deletion strains – Hierarchical clustering analysis of CAZymes and sugar transporters

All deletion strains investigated within this transcriptomal approach showed aberrant cellulase activity compared to the WT (chapter 2.2.2). Therefore, the expression of CAZymes and sugar transporters was analysed in more detail.

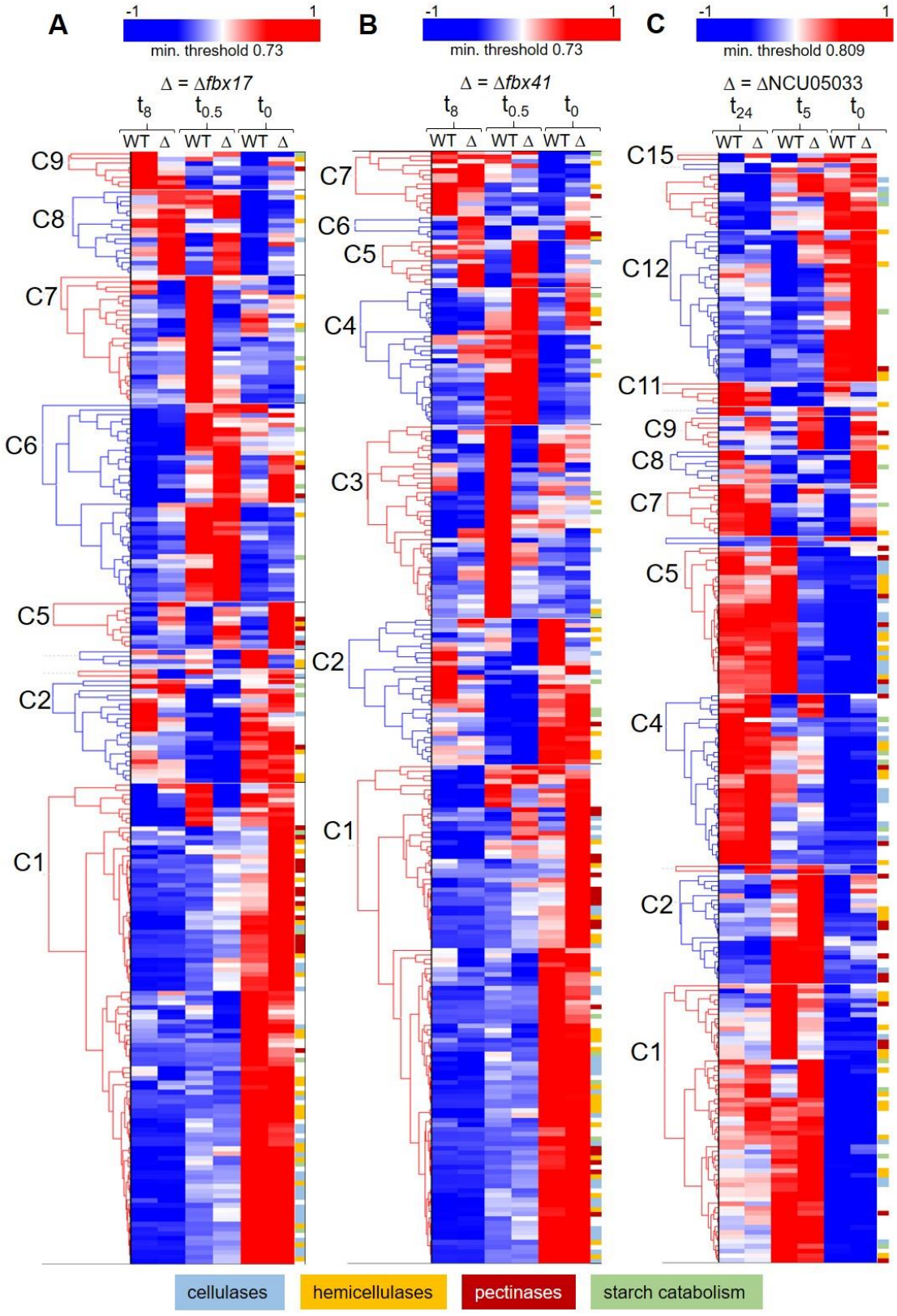

Figure 2-20: Hierarchical clustering of CAZymes.
Hierarchical clustering of 236 CAZyme-encoding genes of the *N. crassa* WT compared to the three *fbx* deletion strains (A) Δ*fbx17*, (B) Δ*fbx41* and (C) ΔNCU05033. Strains were switched from (A, B) CC-derepressing to CC-repressing condition and (C) *vice versa* prior to the RNA-sequencing analysis. The applied minimum similarity threshold is indicated above each hierarchical clustering. Color-coding at the right side of each cluster indicates CAZyme types and is explained below.

After growth of the WT and Δ*fbx17*/*41* in Avicel (t_0), genes clustered within cluster 1 and 2 were most strongly expressed (Figure 2-20 A, B). In total, 124 genes are in C1 and C2 of Δ*fbx17* and 137 in C1 and C2 of Δ*fbx41*, of which 118 genes are identical. Half an hour after switch to glucose ($t_{0.5}$), genes in C6 of Δ*fbx17* and in C4 of Δ*fbx41* showed increased expression. Both clusters show an overlap of 25 identical genes. Very noticeable is the pattern in C7 of Δ*fbx17* (27 genes) and in C3 of Δ*fbx41* (41 genes) at $t_{0.5}$. These clusters contain genes with lower expression in both mutants. Interestingly 26 genes are the same in both C7 of Δ*fbx17* and in C3 of Δ*fbx41*.

During growth of *N. crassa* WT and ΔNCU05033 in glucose (t_0), genes in C12 to C15 are most strongly expressed (Figure 2-20 C). It is striking that genes clustered in C7 to C9 showed an increased expression in the mutant compared to the WT, but none of these genes were DEGs.
After switch to Avicel (t_5), genes clustered in C1 and C2 showed increased expression in both WT and ΔNCU05033 compared to growth in glucose (t_0) (Figure 2-20 C). Interestingly, five hours after switch from glucose to Avicel, genes in C5 were induced in the WT but not in ΔNCU05033. This cluster contains e.g. the two major cellulases *cbh-1* (NCU07340) and *cbh-2* (NCU09680), as well as *gh5-1* (NCU00762), *cdt-1* (NCU00206) and *gh6-3* (NCU07190). After 24 h in Avicel, the expression levels between WT and ΔNCU05033 were overall quite similar.

Since the increased or decreased cellulase activity of all deletion strain compared to the WT (chapter 2.2.2) might be caused by misregulated transporters followed by aberrant inducer uptake, the expression of transporters was investigated within a separate hierarchical clustering (Figure 2-21).

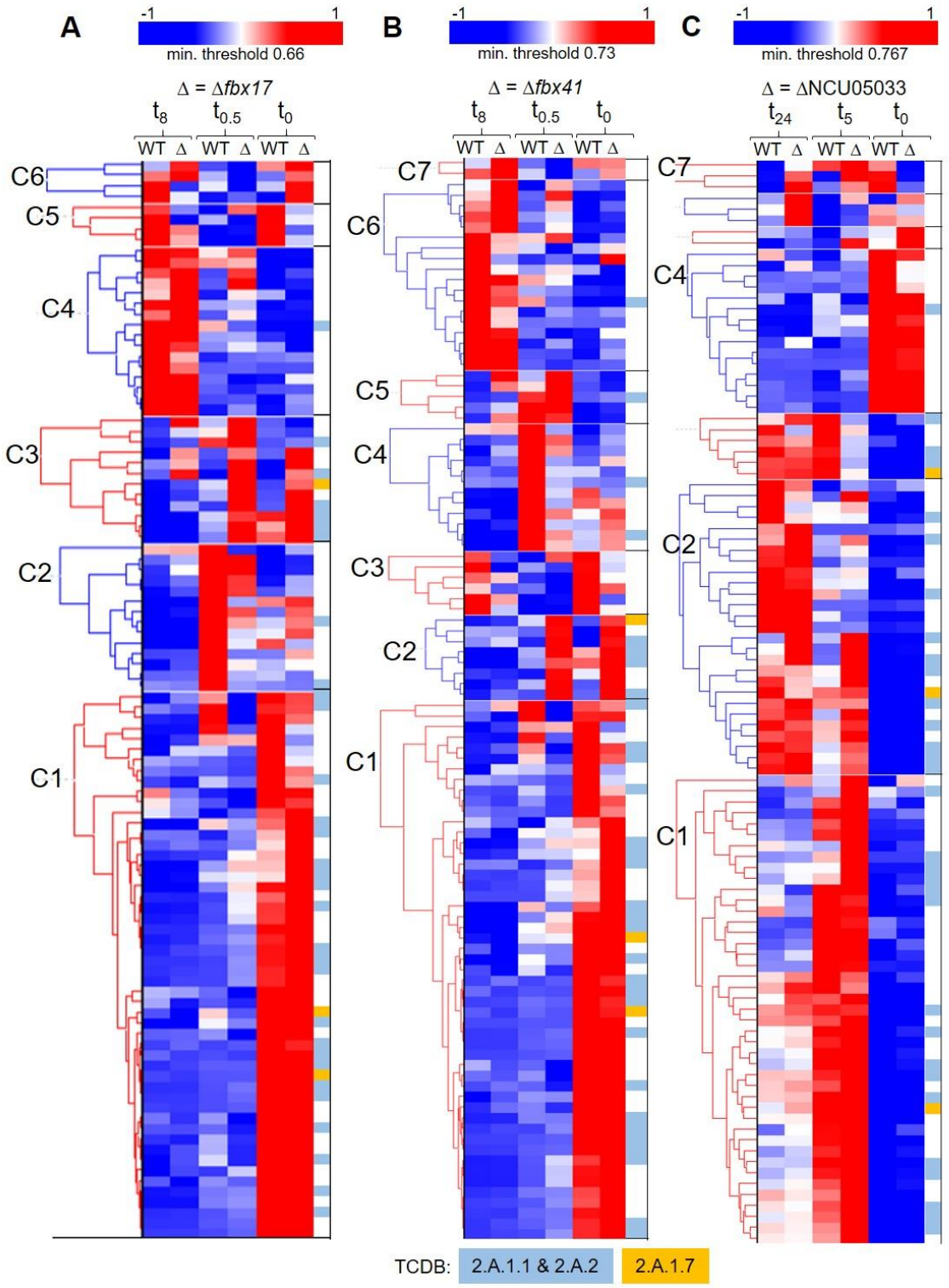

Figure 2-21: Hierarchical clustering of sugar transporter genes.
Hierarchical clustering of 102 sugar transporter-encoding genes of *N. crassa* WT compared to the three *fbx* deletion strains (A) Δ*fbx17*, (B) Δ*fbx41* and (C) ΔNCU05033. Strains were switched from (A, B) CC-derepressing to CC-repressing condition and (C) *vice versa* prior to the RNA-sequencing analysis. The applied minimum similarity threshold is indicated above each hierarchical clustering. Color-coding at the right side of each cluster indicates the transporter classification database (TCDB) class and is explained below the clusters.

Strains which were switched from CC-derepressing to CC-repressing condition showed high expression levels on cellulose in cluster 1 (Figure 2-21, A and B at t_0). Cluster 1 is comprised of 52 genes for Δ*fbx17* and 51 genes for Δ*fbx41*, while a total of 49 genes are shared. Two hypothetical proteins NCU05350 and NCU08292 were found in C1 of Δ*fbx41* but not in Δ*fbx17.* NCU01411, encoding a MFS multidrug resistance transporter, NCU07985, encoding a MFS transporter, and a hypothetical protein, NCU09410, were only found in C1 of Δ*fbx17*.

The hierarchical clustering of ΔNCU05033 and the WT switched from CC-repressing to CC-derepressing condition showed increased expression after 5 h in cellulose in cluster 1 and partly C2, as well as within C3, albeit mainly for the WT, and in C7, but here mainly for the deletion strain (Figure 2-21, C). Comparing C1 of all three *fbx* deletion strains, an overlap of 30 genes was found, including also *cdt-2* (NCU08114). After 24 hours in cellulose, genes clustered within C2 and C3 showed increased expression. In contrast to the WT, genes within C6 and C7 showed increased expression levels in ΔNCU05033 after switch to cellulose. In Δ*fbx17*, genes in C5 and C6 show aberrant expression patterns in cellulose compared to the WT. Half an hour after the switch from cellulose to glucose, increased expression levels were visible in C2 for the WT and in C3 for Δ*fbx17* (Figure 2-21, A). For instance, C2 contains *hgt-1* and C3 contains *cdt-1*, *sut-28* and *xyt-1*. Half an hour after the switch from cellulose to glucose, increased expression levels were visible in C4 and C5 for the WT and C2 and C5 for Δ*fbx41* (Figure 2-21, B). For instance, C5 contains *xyt-1*, C4 *hgt-1*, and C2 *cdt-1* and *sut-28*. Eight hours after the switch from cellulose to glucose, increased expression levels were observed in C4 to C6 for the WT and Δ*fbx17*, and in C3, C6 and C7 for the WT and Δ*fbx41*. Cluster 4, Figure 2-21 A, contains *glt-1*. Cluster 6, Figure 2-21 B, also contains *glt-1*.

In glucose, mainly the transporters clustered within C4 to C7 showed increased expression, for instance *glt-1* clustered within C4 (Figure 2-21 C).

2.4. Identification of F-box interaction partners

This chapter deals with the identification of putative interaction partners of the selected Fbx proteins via immunoprecipitations followed by mass spectrometry analysis, including a complementation analysis as a pre-test for the functionality of the constructs and verification of the specificity of the observed phenotypes.

2.4.1. Complementation of selected F-box candidates and analysis of functionality of the constructs

To determine if the phenotypes of the *fbx* mutants observed in chapter 2.2 were indeed caused by the lack of the corresponding *fbx* gene, complementation studies were performed with the deletion mutants of the six final selected F-box candidates.

To complement the *N. crassa* deletion strains Δ*fbx17* (ΔNCU07521), ΔNCU05033, Δ*fbx22* (ΔNCU05939), Δ*fbx23* (ΔNCU04540), Δ*fbx41* (ΔNCU00471) and Δ*fbx40* (ΔNCU03462) with the corresponding *gfp*-tagged gene, the *Neurospora* expression vector pCCG::C-Gly::GFP was utilized (Figure S 6-24). Additionally, the *N. crassa* Δ*cre-1* (ΔNCU08807) strain was complemented by the same procedure.

Because pCCG::C-Gly::GFP is a *his-3*-targeting vector, the deletion strains listed above were initially all crossed with a WT *his-* strain to receive the *fbx* deletion in a histidine auxotrophic background (Table S 6-3). These strains were transformed with the corresponding plasmid harboring the *gfp*-tagged coding sequence of the corresponding deleted gene (Table 5-8). Additionally, FGSC #6103 (*his-3*$^{-}$) was transformed using the plasmid pCCG::C-Gly::GFP, to generate a strain expressing unbound GFP.

The transformed strains were genotyped and assayed for WT-like phenotypes and observed using fluorescence microscopy (Figure S 6-6 and Figure S 6-7). Complemented *fbx* deletion strains that showed a repressed phenotype and significantly lower cellulase activity in the previous screen (Figure 2-6) were assayed for cellulase activity 80 h after medium switch (Figure 2-22).

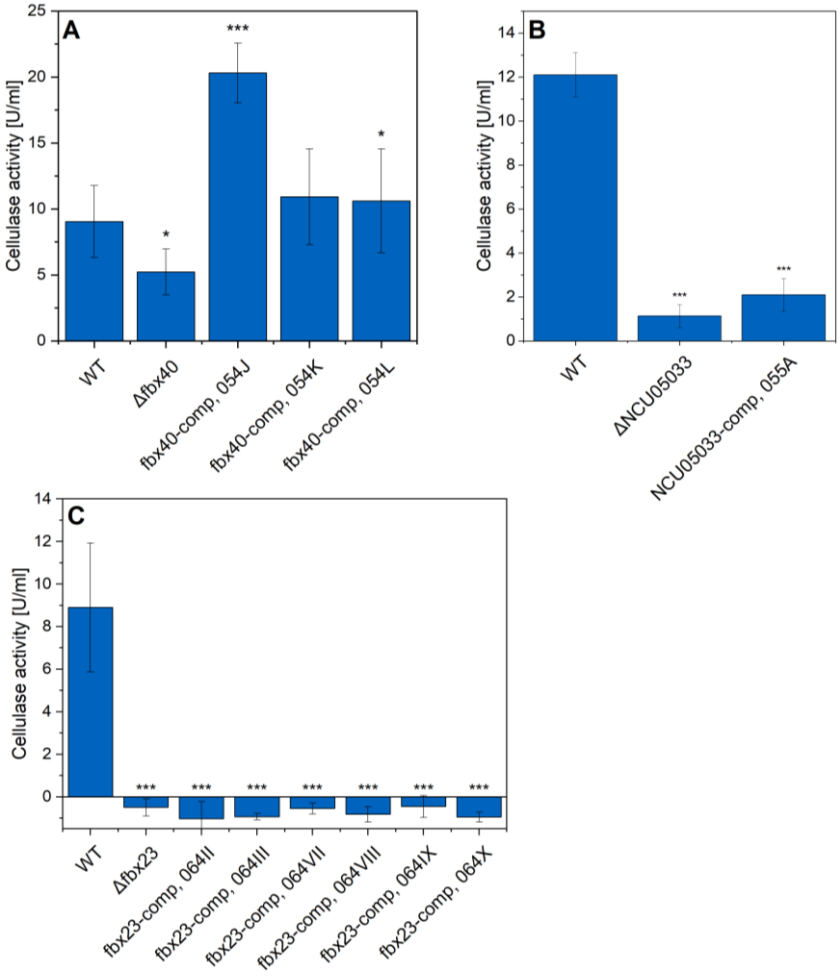

Figure 2-22: Cellulase activity of complemented strains grown in 1% Avicel supplemented with 0.5% glucose.
Pre-cultured complemented *N. crassa fbx* deletion strains were switched into liquid medium containing cellulose supplemented with glucose. The enzymatic activity was determined 80 h after the medium switch. *N. crassa* glycerol stock number nLK# of Professorship of Fungal Biotechnology in Wood Science is given behind the complemented gene. Cellulase activity of (A) *fbx40*, (B) NCU05033 and (C) *fbx23* complemented strains compared to WT and the corresponding deletion mutant. Significance levels were determined using a paired t test. *, $P < 0.05$; **, $P < 0.01$; ***, $P < 0.001$.

Out of three tested complementation strains for Δ*fbx40*, *fbx40*-comp nLK054K showed the most WT-like phenotype (Figure 2-22, A). Therefore, this strain was selected for further investigations.

For ΔNCU05033, only one transformed strain contained the complementation cassette according to genotyping, but the partial complementation did not result in a WT-like phenotype (Figure 2-22, B). The strain (055A) was selected for MS analysis nevertheless, because the full size fusion protein NCU05033::GFP was detectable in a western blot and in fluorescence microscopy (Figure S 6-13, Figure S 6-7).

Several different complementation strains of Δ*fbx23* could not restore WT phenotype. Since the fusion protein was also not detectable in fluorescence microscopy, none of the complementation strains for *fbx23* were chosen.

The complemented strains of the deletion strains that showed a derepressed phenotype, Δ*fbx17*, Δ*fbx22* and Δ*fbx41* (and additionally Δ*cre-1*), were assayed for their biomass formation in the presence of allyl alcohol compared to the WT (Figure 2-23).

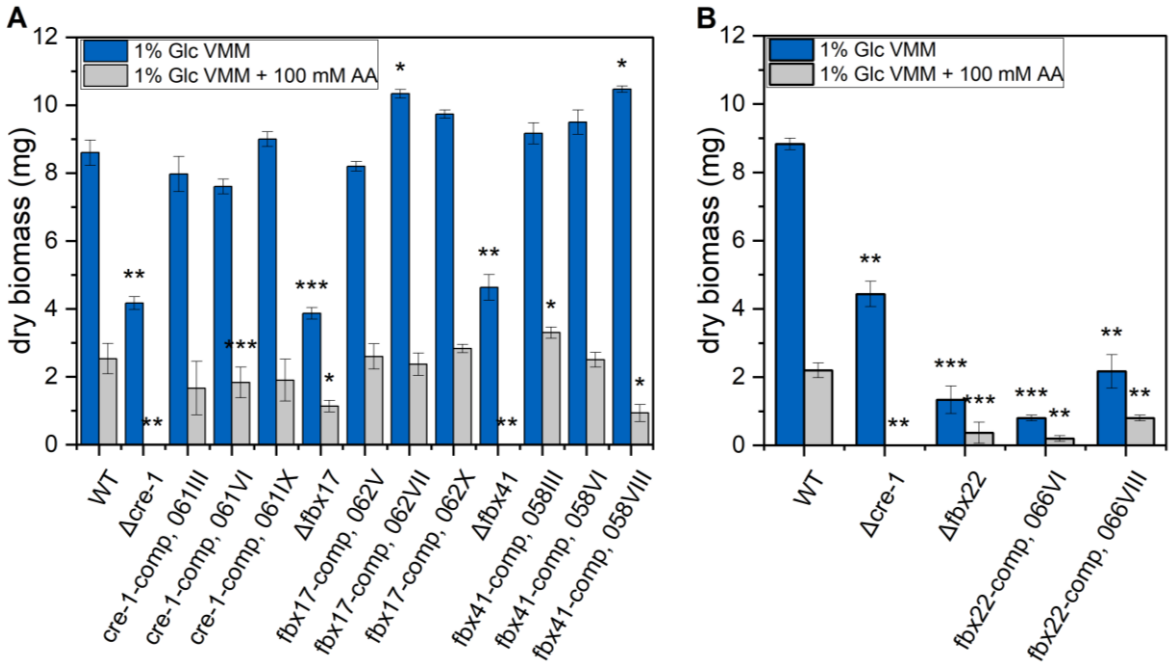

Figure 2-23: Biomass formation of *N. crassa* complemented strains in presence of allyl alcohol.
Complemented *fbx* gene deletion strains were grown on glucose medium supplemented with allyl alcohol before the dry biomass was determined of the strains under all conditions and statistically compared to the WT strain data of the same condition. Dry biomass formation is depicted in mg of (A) *cre-1*, *fbx17*, *fbx41* and (B) *fbx22* complemented strains compared to WT and the corresponding deletion mutant. Significance levels were determined using a paired t test. *, $P < 0.05$; **, $P < 0.01$; ***, $P < 0.001$.

The complementation with the corresponding *gfp*-tagged gene resulted in WT-like phenotypes for all complementation strains of Δ*fbx17*, Δ*fbx41* and Δ*cre-1* (Figure 2-23 A). Figure 2-23 B shows the biomass formation of two exemplary *fbx22*-comp strains. For all *fbx22*-comp strains tested, the WT phenotype could not be restored.

In total, complemented strains were selected for *cre-1*, *fbx17*, *fbx40*, *fbx41*, and NCU05033 for immunoprecipitation experiments followed by mass spectrometry to identify putative interaction partners.

2.4.2. Identification of putative F-box interaction partners via immunoprecipitation and mass spectrometry

To probe protein-protein interactions of F-box proteins, an immunoprecipitation (IP) protocol was established and performed using strains actively expressing GFP-tagged proteins. The exact strains used for the immunoprecipitations are listed in Table S 6-4.

Each strain was grown in six replicates for 24 hours in a main culture containing 1% Avicel in VMM, from now on referred to as "*derepressed condition*". To three of these replicates 2% glucose were supplemented and incubated for an additional four hours, from now on referred to as "*repressed condition*" (see chapter 5.2.3: Culturing procedure prior to immunoprecipitation experiment). Total protein was extracted of the harvested mycelia and immunoprecipitated using GFP-trap agarose beads. To ensure the presence of each bait protein after the immunoprecipitation experiment, the eluates and the crude protein lysates, which were used for the IP, were investigated with anti-GFP western blots (Figure S 6-8 to Figure S 6-15). Within all eluate samples, the corresponding bait protein could be detected successfully. Coomassie stained SDS-PAGE-gels of the samples were used to verify the concentration of total protein through the IP.

The mass spectrometry (MS) data were analyzed quantitatively to detect protein–protein interactions (PPI). The proteins that were co-immunoprecipitated with the corresponding bait protein can be found in the volcano plots within the positive values of the x-axis (Figure 2-24, Figure 2-25 and Figure S 6-16 to Figure S 6-18). The negative values show all proteins with unspecific binding to the GFP control.

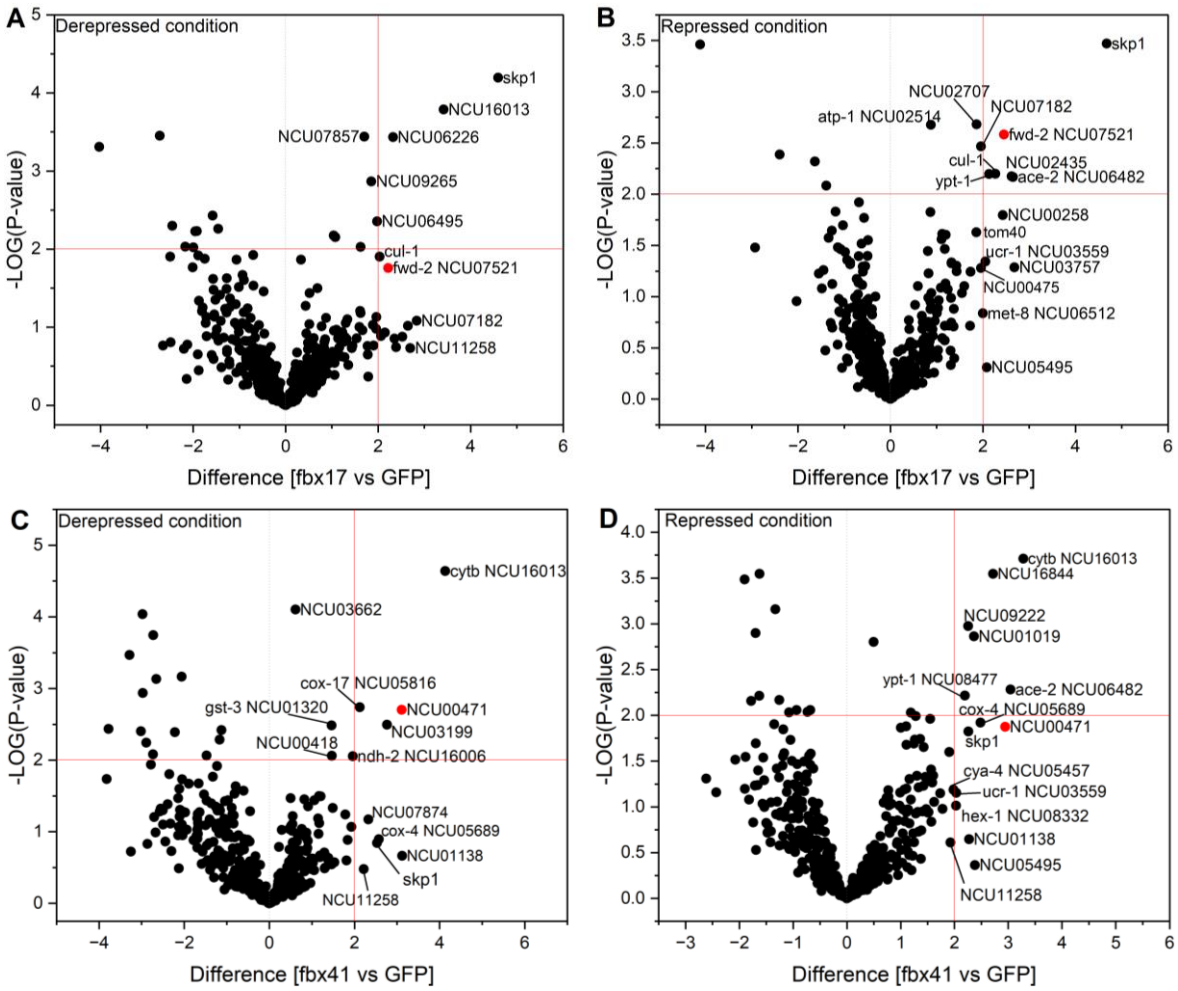

Figure 2-24: Volcano plot of F-box::GFP bait proteins for Fbx17 and Fbx41 (derepressed phenotype).

The F-box::GFP bait MS data is shown against unbound GFP control strain grown in equal culturing conditions. (A) Fbx17::GFP in derepressed culturing and (B) repressed culturing conditions. (C) Fbx41::GFP in derepressed culturing and (D) repressed culturing conditions. Upper right red square frames proteins with significant and highly different abundance. Positive values of x-axis show co-immunoprecipitated proteins with the corresponding bait protein (red dot). Negative values of x-axis show proteins with unspecific binding to the GFP control.

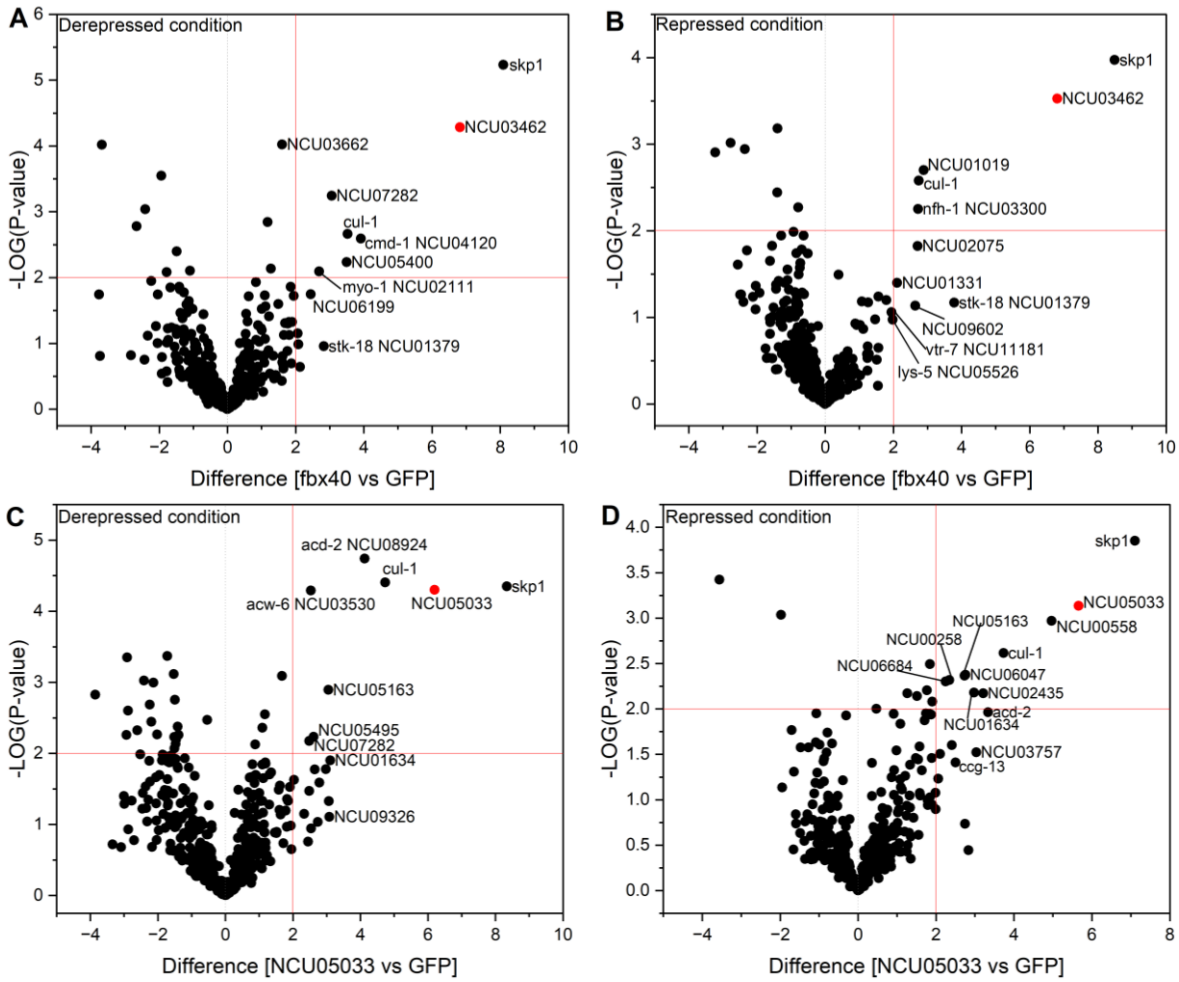

Figure 2-25: Volcano plot of F-box::GFP bait proteins for Fbx40 and NCU05033 (repressed phenotype).

The F-box::GFP bait MS data is shown against unbound GFP control strain grown in equal culturing conditions. (A) Fbx40::GFP in derepressed culturing and (B) repressed culturing conditions. (C) NCU05033::GFP in derepressed culturing and (D) repressed culturing conditions. Upper right red square frames proteins with significant and highly different abundance. Positive values of x-axis show co-immunoprecipitated proteins with the corresponding bait protein (red dot). Negative values of x-axis show proteins with unspecific binding to the GFP control.

Within all Fbx::GFP pulldowns SCON-3 (NCU08991), an orthologue of SKP1 in *Saccharomyces cerevisiae*, was identified as interactor. Additionally, Cullin 1 (cul-1) was identified in the pulldowns and MS analysis of Fbx17::GFP, Fbx40::GFP and NCU05033::GFP, suggesting their participation in the formation of a classical SCF complex. All interactors found in a stringent search of the quantitative analysis data are listed in Table S 6-6 and Table S 6-7.

For NCU05033, 15 putative interactors could be identified in the stringent search. Interestingly, peptides of the Acyl-CoA dehydrogenase (ACD-2, NCU08924) were exclusively found in the NCU05033::GFP samples. The stringent search resulted in 16

putative interactors for NCU07521 (Fbx17), 8 putative interactors for NCU03462 (Fbx40) and 18 putative interactors for NCU00471 (Fbx41), see Table S 6-7.

The MS data were additionally analysed qualitatively by subtracting the interactors found in the GFP and WT control from the Fbx::GFP samples. All interactors found in this way in the repressed condition were compared to interactors found in the derepressed condition (Figure 2-26).

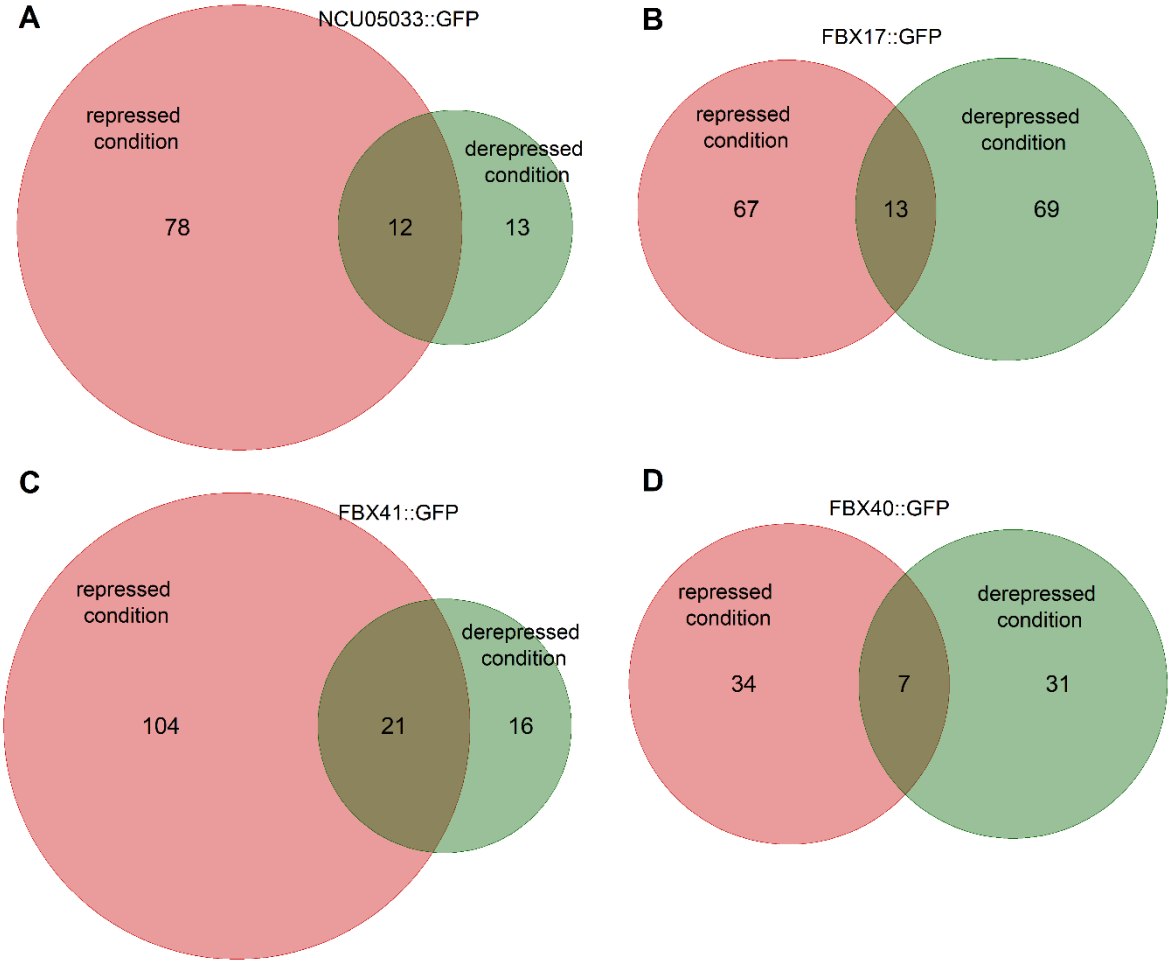

Figure 2-26: Venn diagram of qualitative analysis of MS data.
Number of putative interactors found in both conditions in the (A) NCU05033::GFP, (B) Fbx17::GFP, (C) Fbx41::GFP and (D) Fbx40::GFP samples.

The putative interactors identified via a qualitative analysis in different conditions are listed for NCU05033::GFP in Table S 6-8, for Fbx17::GFP in Table S 6-9, for Fbx40::GFP in Table S 6-10, for Fbx41::GFP in Table S 6-11, and for CRE-1::GFP in Table S 6-12.

Putative interactors identified via qualitative analysis were associated to gene ontology (GO) classes [Ashburner et al. 2000] for NCU05033 and Fbx40 (Figure 2-27), Fbx17 and Fbx41 (Figure 2-28).

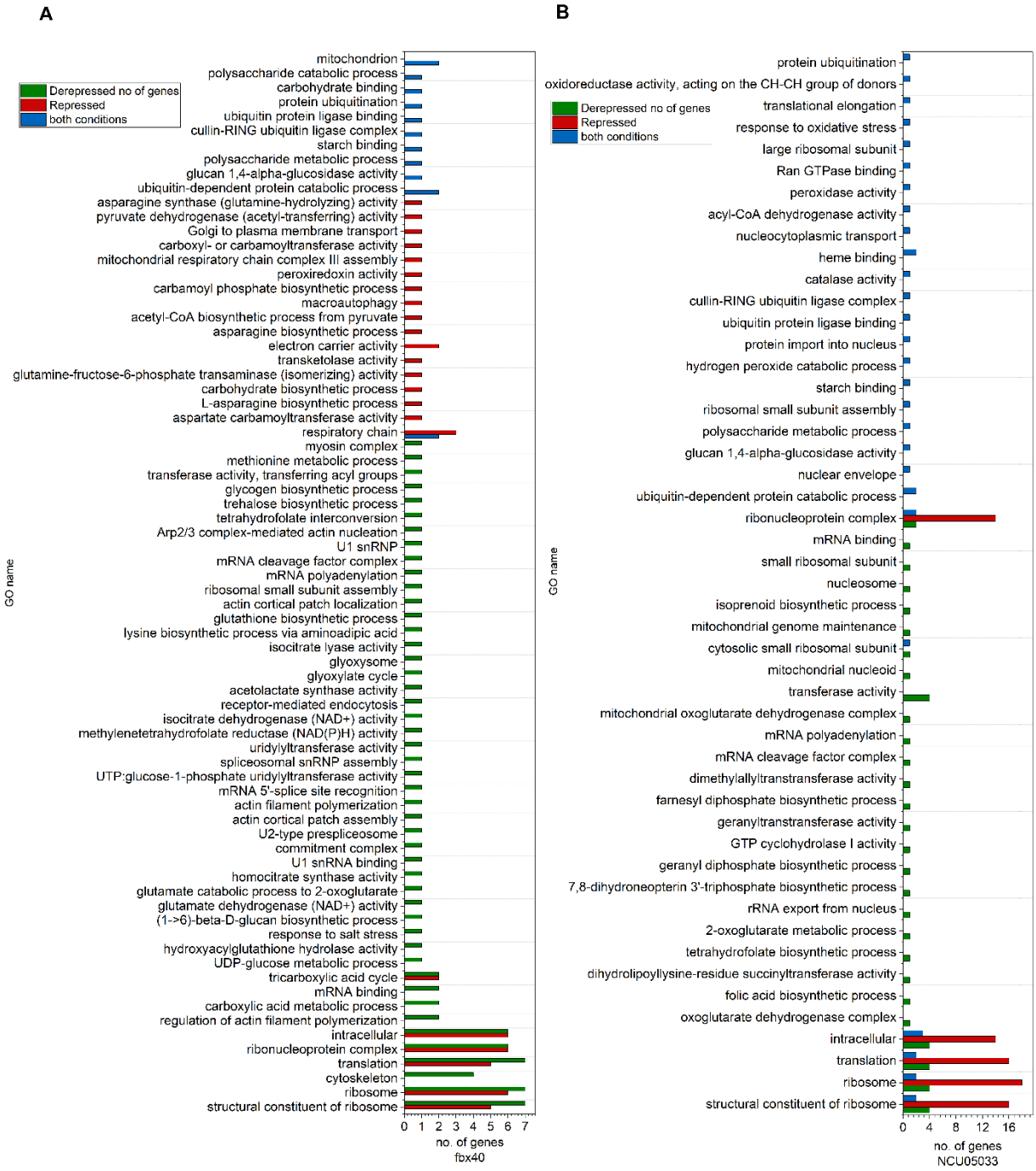

Figure 2-27: GO analysis of putative interactors of Fbx40 and NCU05033.
Number of putative interactors associated with corresponding GO classes of *N. crassa* (A) Fbx40 and (B) NCU05033 identified via qualitative analysis of MS data.

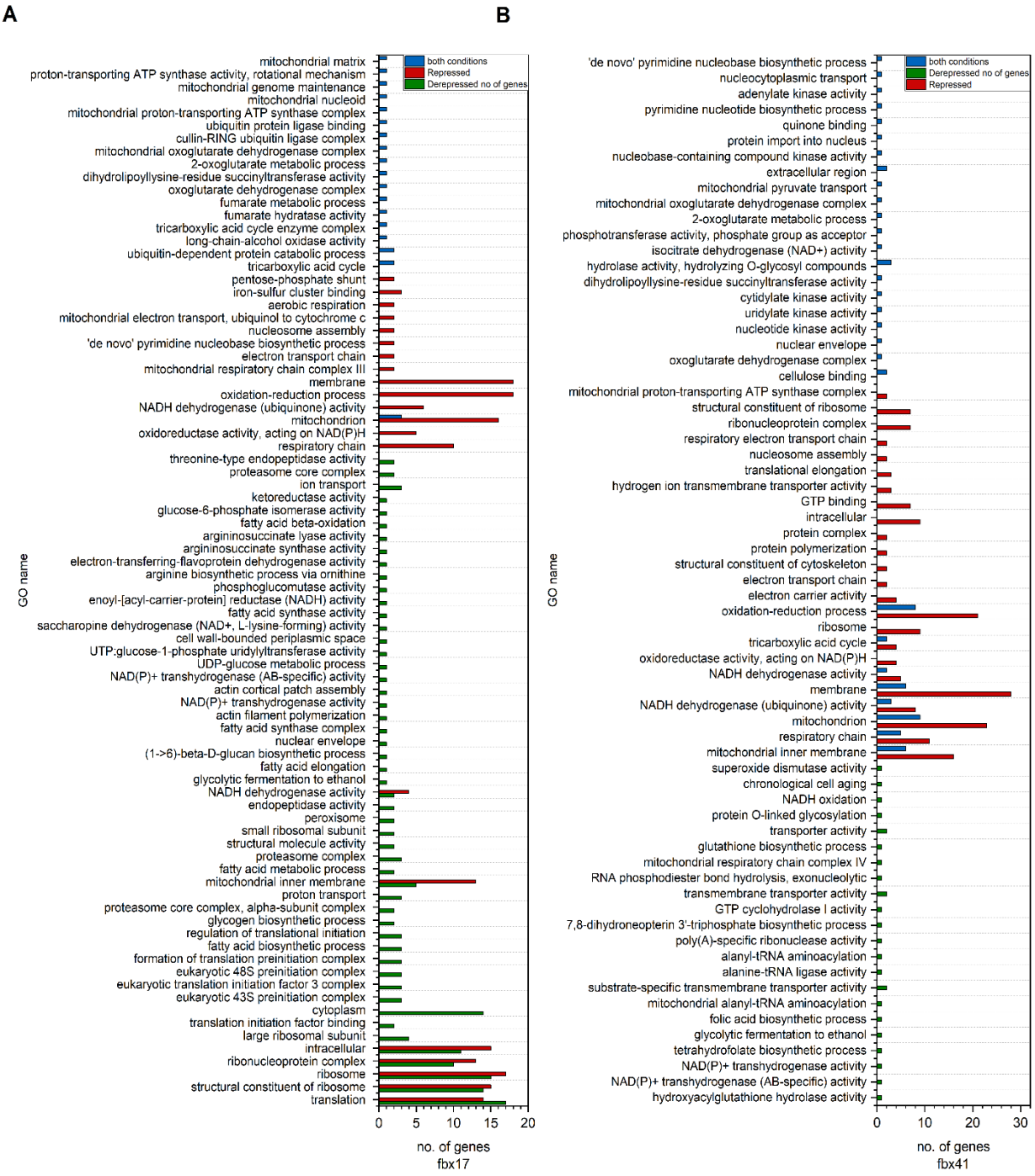

Figure 2-28: GO analysis of putative interactors of Fbx17 and Fbx41.
Number of putative interactors associated with corresponding GO classes of *N. crassa* (A) Fbx17 and (B) Fbx41 identified via qualitative analysis of MS data.

Putative interactors of Fbx40 found in both, derepressed and repressed condition, were associated e.g. to the GO-term ubiquitin-dependent protein catabolic process (GO:0006511) (Figure 2-27, A). These were CUL-1 (NCU05204) and SCON-3 (NCU08991), needed for the formation of a SCF complex, which confirms the result of the quantitative data analysis (Figure 2-27 and Figure 2-28).

Also proteins associated to GO:0030246 (carbohydrate binding) or GO:0000272 (polysaccharide catabolic process) were identified within both conditions (Figure 2-27, A). The highest numbers of genes identified in either derepressed or repressed condition were associated to GO:0005622 (intracellular) or GO:0006412 (translational processes).

In repressed condition, putative interactors of NCU05033 were associated with ribosomal, intracellular or translational processes (Figure 2-27, B). Putative interactors identified for NCU05033 in the derepressed condition were associated with 28 GO-terms.

While the most putative interactors found for Fbx17 were associated with translation, ribosomal and intracellular processes in either derepressed or repressed condition, a higher number was also associated with respiratory chain, mitochondria or oxidation-reduction process in the repressed condition (Figure 2-28, A). For Fbx41, putative interactors found in the derepressed condition were e.g. associated with transporter activity, cellulose binding and biosynthetic processes. In the repressed condition, higher numbers of putative interactors were classified to the respiratory chain, membrane, oxidation-reduction process or GTP binding.

The putative interactors identified in this qualitative analysis were compared across all bait protein samples. Shared interactors were identified for the four investigated F-box proteins (Figure S 6-19, Table S 6-13) and with CRE-1 (Figure S 6-20, Table S 6-14). These included proteins playing a role in protein degradation and formation of the SCF complex (Figure S 6-19). Also ribosomal subunits were identified, proteins involved in chromatin assembly or disassembly, cell wall organization, nuclear or lipid transport and the respiratory chain. In terms of Fbx-specific interactors, for NCU05033 20 exclusive putative interactors were identified, for Fbx40 a total of 13 interactors, for Fbx41 45 interactors and for Fbx17 49 putative interactors (Figure S 6-19, Table S 6-13).

Overall, the most interesting interactors were proteins involved in carbon utilization or proteins of regulatory importance, like kinases or transcription factors. A list of putative interactors of interest can be found in Table 2-3.

Table 2-3: List of putative F-box protein interactors involved in carbon utilization and regulation.

C = condition in which the interactor was identified. D = derepressed condition. R = repressed condition. B = both conditions. The last column in contains brief information concerning the function of the putative interactor or the reason for being of interest for further analysis. Comments include information from FungiDB and Uniprot if not stated otherwise.

bait	C	Putative interactor	comment
Fbx40	D	NCU04120	Calmodulin (CaM): mediates the control of a large number of enzymes, ion channels and other proteins. Enzymes to be stimulated: protein kinases and phosphatases, like NCU09123, camk-1.; found in both analysis methods.

bait	C	Putative interactor	comment
	D	NCU07238	Hyphal anastamosis-14 protein (ham-14): Binds MAP kinase cascade members [Jonkers et al. 2016].
	D	NCU06598	C2H2-type domain-containing protein, could be putative transcription factor
	R	NCU01328	transketolase, involved in pentose phosphate pathway
Fbx41	B	NCU08755	Beta-glucosidase: involved in catabolic processes
	D	NCU00801	MFS lactose permease (cdt-1), involved in hemicellulose perception [Galazka et al. 2010]
	D	NCU08114	Hexose transporter (cdt-2), involved in hemicellulose perception [Galazka et al. 2010]
	R	NCU08823	Protein ras-1: GTP-binding and involved in signal transduction
Fbx41	R	NCU08907	BYS1 domain-containing protein: involved in cell growth and morphogenesis
	R	NCU03893	Short-chain dehydrogenase/reductase SDR: involved in carbohydrate metabolic processes; found in both analysis methods.
	R	NCU06701	Cephalosporin C regulator 1: was identified as RFX transcription factor type [Wu et al. 2020]
Fbx17	D	NCU02208	Eukaryotic translation initiation factor 3 subunit B (eIF3b): part of key regulator of translation initiation
	D	NCU07831	Eukaryotic translation initiation factor 3 subunit C (eIF3c): part of key regulator of translation initiation
	D	NCU01021	Eukaryotic translation initiation factor 3 subunit F (eIF3f): part of key regulator of translation initiation
	D	NCU07281	Glucose-6-phosphate isomerase (gpi-1): involved in glycolysis and gluconeogenesis
	D	NCU10058	Ragged-1 (rg-1): A phosphoglucomutase, involved in metabolic processes
	R	NCU03100	6-phosphogluconate dehydrogenase (ppm-2): involved in carbohydrate degradation
NCU05033	B	NCU08924	Acyl-CoA dehydrogenase (acd-2); found in both analysis methods. Peptides were exclusively identified in NCU05033-comp samples.
	B	NCU00355	Catalase-3 (cat-1): involved in stress response; found in both analysis methods.
	R	NCU05137	Non-anchored cell wall protein 1 (ncw-1): found to be coregulated with cre-1 and important for modulation of extracellular cellulose degrading capacity [Schmoll et al. 2012]
	R	NCU09209	Galactose oxidase-1 (gao-1): involved in carbohydrate metabolic processes
	R	NCU09269	GTP-binding nuclear protein GSP1/Ran (ran): involved, among others, in nucleocytoplasmic transport
	R	NCU08330	hypothetical protein: contains a DJ-1_PfpI domain which can be found in transcriptional regulators; promoter region bound, among others, by CRE-1 [Wu et al. 2020]
	R	NCU00558	hypothetical protein containing transcription factor domain; identified in quantitative analysis with high significance and difference (Figure 2-25, D)

2.4.3. Investigation of putative interaction partners and screening for CCR-phenotypes

Some of the most interesting putative interaction partners of the four *N. crassa* F-box proteins NCU07521 (Fbx17), NCU03462 (Fbx40), NCU00471 (Fbx41) and NCU05033 (2.4.2), as listed in Table 2-3, were further investigated. To this end, the corresponding deletion strains of the putative interactors were analyzed in the same way as the original Fbx-screen (2.2.2 and 2.2.3).

For all putative interactors listed in Table 2-3, at least heterokaryotic deletion strains were available, except for the putative transcription factor NCU06598, which was supposed to interact with Fbx40. Two putative interactors of Fbx41 also needed to be excluded from further investigations: For NCU08823 a heterokaryotic deletion strain was available, which however did not form conidia at all. NCU03893 was also excluded from the investigation for experimental reasons concerning the implementation of the sample.

ΔNCU07281 and ΔNCU10058 showed growth deficits in slants similar to Δ*fbx17* (Figure S 6-21). NCU07281 encodes a glucose-6-phosphate isomerase (GPI-1) and NCU10058 encodes a phosphoglucomutase (RG-1). ΔNCU07281 was not able to form biomass in liquid cultures; therefore, this putative interactor of Fbx17 was also excluded.

Biomass formation of putative interactor deletion strains in presence of allyl alcohol

To determine CCR-related defects of the putative interactors of *N. crassa* F-box proteins, deletion mutants of the interactors were screened for their ability to form biomass in presence of glucose and allyl alcohol (AA). The deletion strains were grown using the same conditions and settings as in chapter 2.2.3 (Figure 2-29). Since AA is known to be converted by alcohol dehydrogenases to the toxic compound acrolein, impaired CCR would lead to a higher sensitivity of the strain to AA (CCR-derepressed phenotype), while functional CCR would result in insensitivity of the strain to AA (CCR-repressed phenotype).

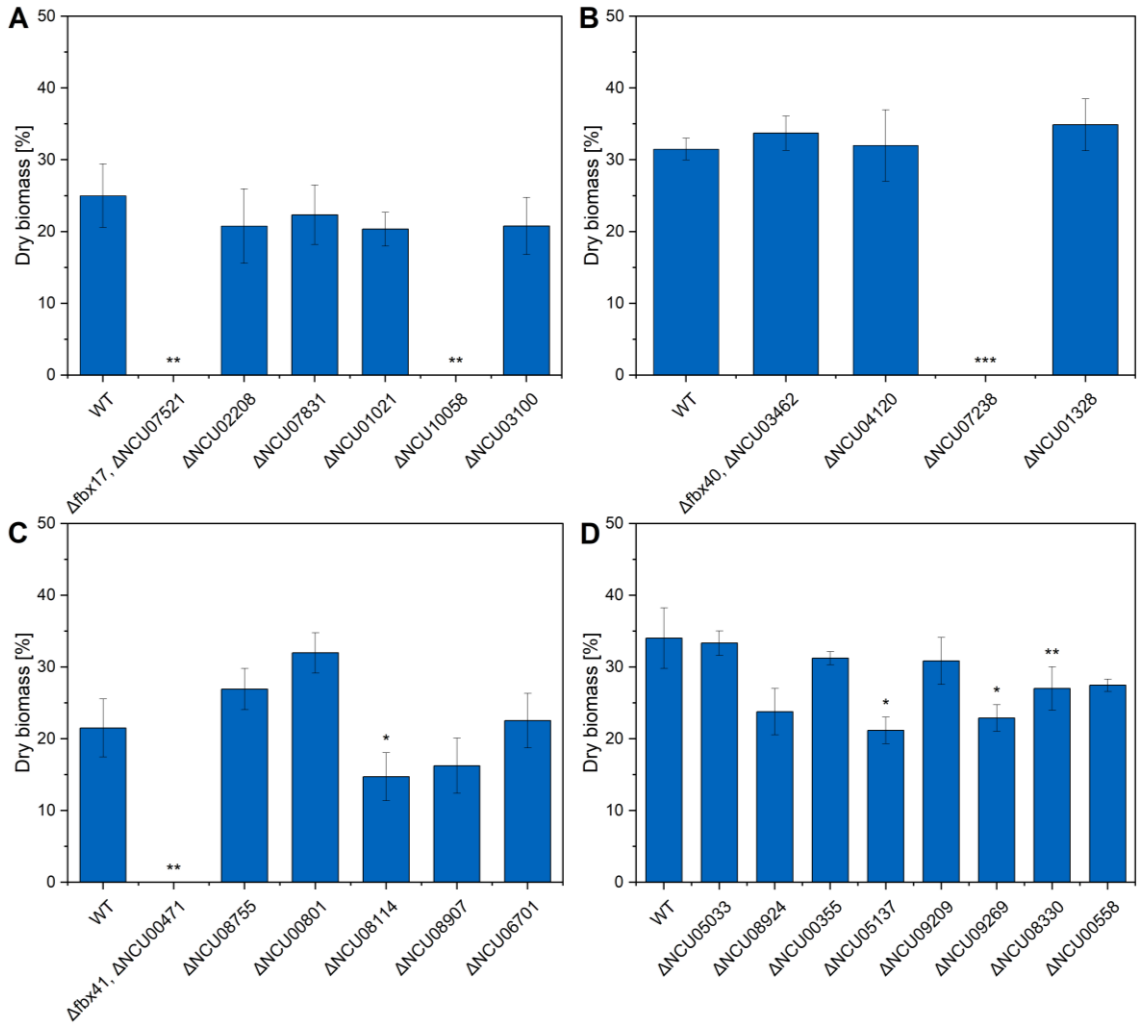

Figure 2-29: Biomass formation of putative interactor deletion strains in presence of allyl alcohol.
Deletion strains of putative interactors of (A) Fbx17, (B) Fbx40, (C) Fbx41 and (D) NCU05033 were grown on glucose medium supplemented with allyl alcohol before the dry biomass was determined of the strains under all conditions, normalized with the control condition and statistically compared to the WT strain data. Significance levels were determined using a paired t-test. *, $P < 0.05$; **, $P < 0.01$; ***, $P < 0.001$.

The deletion strain of the putative Fbx17 interactor NCU10058 showed the same phenotype as the *fbx17* deletion strain (Figure 2-29, A), while the other deletion strains did not show significant difference compared to the *N. crassa* WT.

NCU07238, encoding HAM-14, an Fbx40 interactor, showed significantly higher sensitivity to AA compared to the WT (Figure 2-29, B).

The deletion mutant of the hexose transporter *cdt-2* (ΔNCU08114; interactor of Fbx41) showed a significantly higher sensitivity to AA (Figure 2-29, C), as well as ΔNCU05137, ΔNCU09269 and ΔNCU08330 (Figure 2-29, D), as interactors of NCU05033. In total therefore, six deletion strains of putative interactors showed a significantly higher sensitivity to AA.

Cellulolytic response of putative interactor deletion strains in presence of cellulose and glucose

To identify aberrant phenotypes related to CCR of the putative interactors of *N. crassa* F-box proteins, deletion mutants of the interactors were also screened for their cellulolytic response in presence of cellulose (Avicel) and glucose. Derepressed phenotypes were expected to show higher cellulase activity at an earlier time point, while repressed strains were expected to show lower cellulase activities, compared to the WT. The same culturing conditions were applied as described in 2.2.2. Cellulase activity was determined in the culture supernatant 80 h after medium switch (Figure 2-30), as well as the total protein amount (Figure S 6-22). Protein secretion profiles of culture supernatant were obtained by silver staining of SDS-PAGEs (Figure S 6-23).

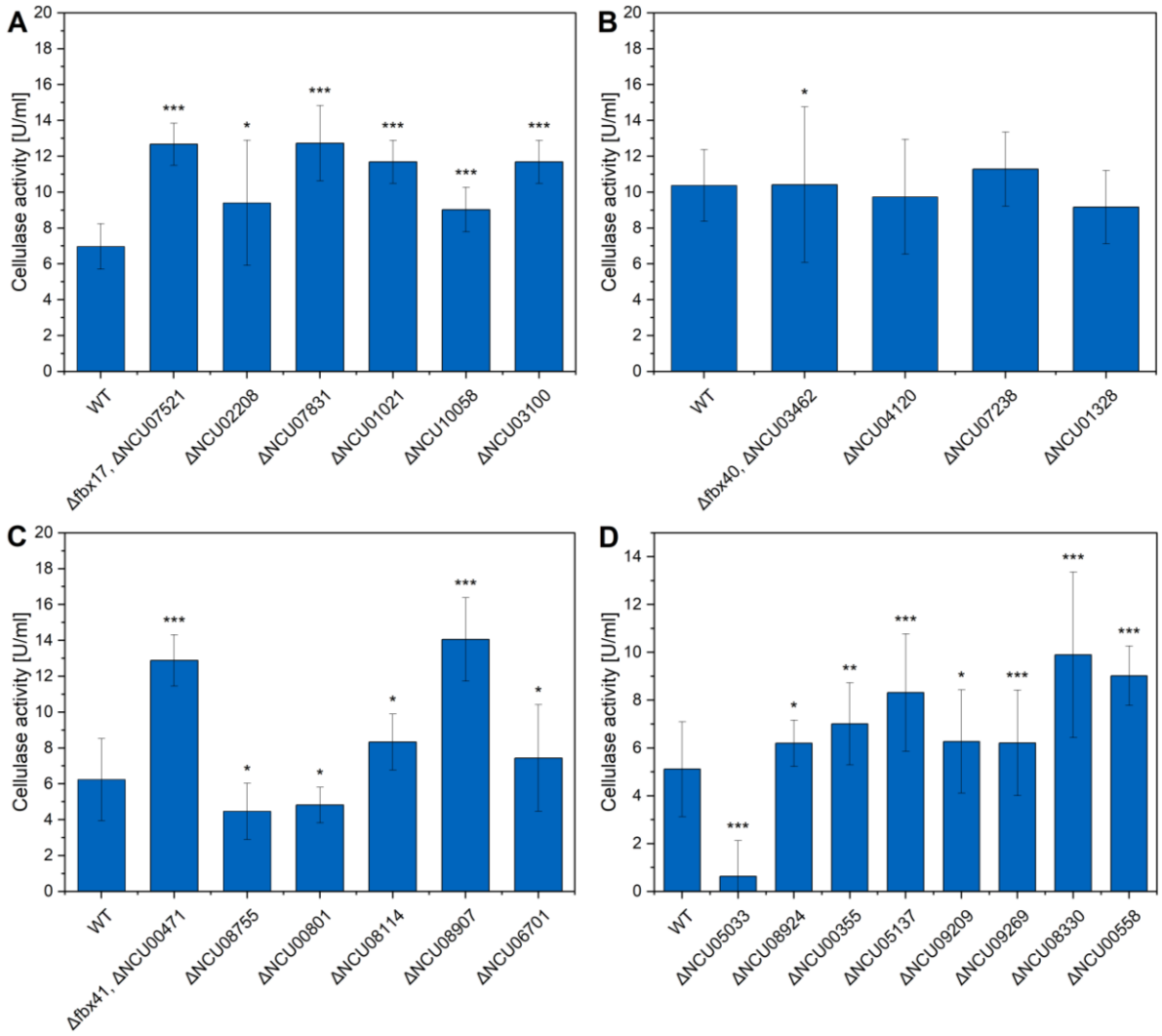

Figure 2-30: Cellulase activity of putative interactor deletion strains grown in 1% Avicel supplemented with 0.5% glucose.

Pre-cultured *N. crassa* deletion strains were switched into liquid medium containing cellulose supplemented with glucose. The enzymatic activity was determined 80 h after the medium switch. Cellulase activity of (A) Fbx17 (*P* 6.402*10^{-8}), (B) Fbx40 (*P* 0.025), (C) Fbx41 (*P* 7.964*10^{-7}) and

(D) NCU05033 (*P* 2.939*10^{-5}) deletion strain and the deletion strains of their putative interactors were compared to the WT. Significance levels were determined using a paired t test. *, $P < 0.05$; **, $P < 0.01$; ***, $P < 0.001$.

After 80 h in 1% Avicel VMM supplemented with 0.5 % glucose, all deletion strains of putative interactors of Fbx17 showed a significantly higher cellulase activity compared to the WT, while none of the deletion strains of interactors of Fbx40 showed a significant difference (Figure 2-30, A and B). The deletion strains ΔNCU08755 and ΔNCU00801 had a significantly lower and ΔNCU08114, ΔNCU08907 and ΔNCU06701 a significant higher cellulase activity compared to the WT (Figure 2-30, C). Also, all seven deletion strains of putative interactors of NCU05033 showed a significant increase of cellulase activity (Figure 2-30, D).

In summary, for all Fbx proteins, some deletion strains of interacting proteins showed a significantly different phenotype in both the biomass formation in presence of AA (Figure 2-29) and cellulase activity (Figure 2-30). An exception were the the deletion strains of Fbx40 interactors, which did not show aberrant cellulase activity. Interestingly, Fbx17 interactors, which showed significant difference to the WT, did show a derepressed phenotype in both assays, like Δ*fbx17*. The opposite was observed for NCU05033 interactors, which showed a derepressed phenotype, while ΔNCU05033 showed a repressed phenotype.

3. Discussion

3.1. Putative F-box proteins of *Neurospora crassa*

F-box proteins are essential for targeted protein degradation and the regulation of various cellular processes. They are responsible for the substrate recognition, which determines the specificity in the ubiquitin system. [Craig and Tyers 1999] Within the genome of *N. crassa* approximately 42 putative F-box proteins were predicted [Horta et al. 2019]. Studies of *N. crassa* F-box proteins have so far focused on the functions of a few individual F-box proteins (see 1.6). The major challenge to securely identify F-box proteins relies within the lack of a strict consensus sequence [Kipreos and Pagano 2000]. The identification of F-box proteins can be made through certain regions of identity and protein domains, especially through the F-box domain itself, but the lack of a strict consensus sequence makes the identification of the F-box motif itself challenging [Kipreos and Pagano 2000]. In studies about F-box proteins, different *in silico* and *in vitro* methods were utilized to identify F-box proteins. For instance, the combination of DNA database search and a yeast two-hybrid approach using Skp1 as bait protein led to the identification of twenty-six novel human F-box proteins [Cenciarelli et al. 1999]. In 2008, seventy *A. nidulans* F-box proteins were identified *in silico*, where the authors pointed out the low general conservation of F-box proteins, leading to a low detection rate [Draht et al. 2008]. Nevertheless, consensus sequences of the F-box motif have been described or reviewed within several studies, in which also highly conserved amino acids have been described, such as e.g. a conserved proline [Kumar and Paietta 1998; Kipreos and Pagano 2000; Jonkers and Rep 2009; Schmidt et al. 2009]. In case of the lack of a canonical F-box domain, F-box proteins were described in literature as “low scoring F-box proteins” [Draht et al. 2008; Sarikaya Bayram et al. 2022].

Whithin this work, a total of forty-nine putative *N. crassa* F-box proteins were identified through database search for relevant domains and an ortholog search to known *A. nidulans* F-box proteins (see chapter 2.1.1). This analysis therefore revealed the presence of seven additional *N. crassa* F-box proteins compared to previous publications [Horta et al. 2019]. Fbx37/40/41/58/65/NCU00488 were found to harbor only a partially conserved F-box domain. For Fbx13/74/NCU07746, the probable location of the F-box motif could not be identified (Figure 2-1). Nevertheless, a lacking F-box domain does not completely exclude a protein interaction with other SCF subunits or excercising the function of a F-box protein. *N. crassa* Fbx74 (NCU01658) is an ortholog to *S. cerevisiae* Rav1p (YJR033C), which was not described as *bona fide* F-box protein, but harbors potential F-box motifs in its sequence. Rav1p participates in the formation of the RAVE complex and is thought to act within a non-

SCF complex. [Hermand 2006] Interestingly, while NCU07746 was named “F-box domain-containing protein” in databases like UniProt or FungiDB, the location or sequence of the F-box domain itself was not annotated. However, the protein contains a tetratricopeptide repeat domain, which is known to be important for the assembly of protein complexes and protein-protein interactions [Perez-Riba and Itzhaki 2019].
Sarikaya Bayram *et al.* demonstrated that Fbx15 in *A. nidulans*, which does not harbor an F-box domain, interacts with other subunits of the SCF complex. Additionally, the conventional hypothesis that only the interaction of the interchangeable F-box protein with SkpA/1 provides diversity of the SCF complexes was questioned and expanded to include other domains within the F-box protein to be important for the assembly of the SCF complex or interaction with different single subunits of this complex. [Sarikaya Bayram et al. 2022] This suggests that the F-box domain itself is not strictly mandatory for the protein function and makes it even more challenging to securely identify proteins holding the function according to the F-box hypothesis.

F-box proteins were found to play a role in *A. nidulans* CreA regulation and to be important for CCR [Assis et al. 2018]. Also in yeast, F-box proteins are known to regulate transcriptional induction of e.g. glucose transporter genes and thus contribute to metabolic switches [Craig and Tyers 1999]. The transcriptome data of the “Fungal Nutritional ENCODE project” [Glass 2012] were used to visualize the transcriptomal responses of *fbx* genes of *N. crassa* to different plant biomass and carbon sources (see chapter 2.1.2). Thirty-five carbon sources were selected due to their ability to cause CCR and carbon starvation stress response (CSSR) [Thieme 2019].
Overall, *fbx* genes were found to be rather constitutively expressed across the tested carbon sources, on a rather low expression level. This substantiates the fact that the regulation of *fbx* genes in *N. crassa* seems to happen rather through other mechanisms or on protein level, like localization or complex assembly. In general, only little information can be found on how F-box protein abundance may be regulated on transcriptional level.
F-box proteins participating within Cullin-RING ligases (CRL) are mainly regulated through limited availability of cullins. Reitsma *et al.* presented two outputs from their study that were not expected. The F-box proteins showed huge binding efficiency variations to cullin, leading to a disequilibrium in the permanent repertoire of SCF ubiquitin ligases. Furthermore, the assembly of F-box proteins to cullin was inefficient, leading to less than ten percent assembly into SCF complexes for more than half of all F-box proteins. The scenario Reitsma *et al.* observed was caused by the four-fold molar excess of Skp1 over cullin and additionally the occupation of cullin by Cand1. This mechanism is important to provide adaptability to different physiological states by interchanging the SCF complexes. [Reitsma et al. 2017]

3.2. Screening for F-box proteins involved in the regulation of sugar metabolism

3.2.1. Altering glucose levels affect *Neurospra crassa* cellulolytic response

Through the secretion of CAZymes, saphrophytic filamentous fungi are able to deconstruct carbohydrate polymers of the plant cell wall. Repression of these enzymes is known to occur in presence of favored energy sources, like glucose. To what extent CCR occurs and in response to which carbon source is species-dependent. [Huberman et al. 2016; Adnan et al. 2017]

Within this work, *N. crassa* WT was cultivated in presence of the microcrystalline cellulose, Avicel, supplemented with different glucose levels to determine cellulase activity within the supernatant samples. As expected, at early time points, nearly no cellulase activity was detectable. Cellulolytic activity increased over time, while culture supernatants from cultures with higher glucose levels displayed a later increase of cellulase activity (Figure 2-5). The cellulase activity in the culture supernatant was expected to increase over time due to the induction of cellulase expression in presence of cellulose [Tian et al. 2009; Znameroski et al. 2014]. After cleavage of cellulose to cellodextrins, like cellobiose, the production of cellulase is induced in *N. crassa*. Xiong *et al.* showed the cellulolytic induction through Avicel in *N. crassa* on protein and transcriptional level. [Xiong et al. 2014] Additionally, growth of *N. crassa* WT in presence of cellobiose and 2-deoxy-glucose, a glucose analogue which can not be metabolized, demonstrated that *N. crassa* favours glucose consumption over cellobiose [Xiong et al. 2014]. Within this work, at least two different effects could be observed: Firstly, *N. crassa* WT consumed glucose first, which led to a delayed increase of cellulase activity due to CCR (Figure 2-5). Secondly, a growth effect was observed in cultures with higher glucose supplementations. The higher the glucose level was at the beginning of the cultivation, the more biomass could be generated by consuming glucose first. More biomass provides a higher capacity for the production and secretion of cellulases. To detect mutants with derepressed and repressed CCR phenotypes in later experiments, three different sampling time points were chosen covering low to moderate to higher cellulase activity during CC-derepression, after glucose was consumed in the WT strain. These data provided a basis to examine screening conditions to detect glucose-induced repression of cellulases of F-box protein deletion strains.

3.2.2. F-box deletion affects the cellulolytic response in *Neurospora crassa* and leads to CCR-related defects

In *A. nidulans* some F-box proteins are known to have an influence on CCR and carbon utilization [Assis et al. 2018]. Also for *N. crassa* F-box proteins, the potential of influencing carbon utilization and signaling had been suggested in a previous study [Horta et al. 2019]. Nevertheless, this thesis work is, so far, the first time putative *N. crassa fbx* deletion strains were compared to the *N. crassa* WT strain for altered cellulolytic responses in cellulose supplemented with glucose and for biomass formation in presence of allyl alcohol on this scale. By combination of these two screening experiments, several deletion strains were found to display significant CCR-repressed or derepressed phenotypes (2.2.2 and 2.2.3). A total of ten *fbx* deletion strains showed significantly higher cellulase activity compared to the WT (Figure 2-6). This suggests that these strains were not able to favor glucose either as a direct or indirect consequence of the *fbx* deletion. Additionally, three of these ten *fbx* deletion strains, *fbx17*/*22*/*41*, were significantly more sensitive to AA compared to the WT (Figure 2-9) and thus display the same phenotype as Δ*cre-1*. The observed phenotype of Δ*cre-1* is in accordance with the data published by Sun and Glass in 2011, where Δ*cre-1* was described to have an increased cellulolytic activity due to increased expression of cellulolytic genes [Sun and Glass 2011].

Repressed strains on the other hand had problems to release CCR, resulting in significantly lower cellulase activity for nine deletion strains compared to the WT (Figure 2-6). Four of these strains, *fbx23*/*30* and NCU05033/09899, also had significantly increased resistance to AA compared to the WT (Figure 2-9). Strains showing aberrant phenotypes with significant difference to the WT in both screens were considered to be highly likely impaired in the regulation of CCR.

Possible reasons for all observed phenotypes can be direct or indirect effects of the *fbx* deletion. For instance, sensing and signaling or enzymatic secretion could be impaired, as well as growth and developmental issues could lead to lower enzyme activity. The yeast F-box protein Cdc4, the ortholog of *N. crassa fbx22*, for example, was shown to control the cell division cycle, morphogenesis, calcium signaling and also nutrient sensing, highlighting the broad potential of an F-box protein to influence various processes [Jonkers and Rep 2009]. Impaired protein secretion due to *fbx* deletion has been suggested for Δ*fbx23* in *A. nidulans* [Assis et al. 2018]. In *N. crassa*, Δ*fbx23* showed a similarly reduced protein secretion (Figure 2-7) as *A. nidulans* Δ*fbx23* [Assis et al. 2018]. These findings lead to the conclusion that Fbx23 of *N. crassa* might also be involved in the secretion of extracellular proteins and could suggest functional similarities of the Fbx23 orthologs in both fungi.

A total of 40 *N. crassa* deletion strains with deletions of genes with putative F-box protein function were screened to identify aberrant phenotypes related to CCR, while significant differences compared to the WT were rated with scores (see chapter 2.2.4).

To further investigate F-box proteins involved in the switch between CCR and lignocellulose utilization, three de-repressed and three repressed F-box candidates were selected based on the observed phenotypes and interesting expression patterns (Figure 2-4). The four candidates with the highest scores (Table 2-2) were each two candidates whose deletion strains showed a significantly derepressed (Fbx17/22) or repressed (Fbx23 and NCU05033) phenotype in both screens (2.2.2, 2.2.3), respectively.

About NCU05033, no previous studies or publications were found, which indicates that it has not yet been investigated. Fbx23 (NCU04540) and Fbx17 (NCU07521) are named FWD1 and FWD2 (F-box and WD40 repeat-containing protein) and share both high similarity with the *Drosophila* Slimb protein and the mammalian β-TRCP proteins [He et al. 2003]. It is known that FWD1/Fbx23 is involved in the degradation of FREQUENCY (FRQ) and FWD2/Fbx17 could potentially mediate the ubiquitylation of FRQ when FWD1/Fbx23 is absent [He et al. 2003]. The orthologs of Fbx17 and Fbx23 in *A. nidulans* were found to be required for light-dependent development [Sarikaya Bayram et al. 2022]. The data of both screens (2.2.2 and 2.2.3) suggest an additional role of those two proteins in carbon utilization and CCR. Moreover, *fbx23* of *A. nidulans* was found to be important for CCR [Assis et al. 2018]. Interestingly, Horta *et al.* identified four different phosphopeptides for Fbx23, seven for Fbx22 and three for Fbx17 on different conditions, suggesting a connection to carbon utilization [Horta et al. 2019]. Additionally, the deletion of *fbx22* in *N. crassa* was found to create a defect of CCR control [Horta et al. 2019], which made it an interesting choice for further investigations.

The next candidate on the score list was *fbx30* (Table 2-2). However, this candidate was not chosen, due to the impaired growth of the deletion strain. The deletion of *fbx30* is known to lead to altered mitochondrial morphology, instability of the mitochondrial DNA and senescence [Kato et al. 2010].

Instead, the last two candidates, which were chosen for further investigations, were *fbx41* (NCU00471) and *fbx40* (ΔNCU03462). The deletion strain Δ*fbx41* showed a Δ*cre-1*-like phenotype within all assays, while Δ*fbx40* showed a slightly repressed phenotype (2.2.2 and 2.2.3). Interestingly, the orthologs in *A. nidulans* showed both a significantly increased AA sensitivity [Assis et al. 2018].

Further interesting phenotypes and observations were that Fbx58 (NCU06688) harbours at least thirteen identified phospho-peptides, which was the highest number identified among the F-box proteins [Horta et al. 2019]. Within this work, the deletion strain Δ*fbx58* showed a significantly increased cellulase activity in the cellulose perception screen (Figure 2-6),

but a WT-like phenotype in presence of allyl alcohol (Figure 2-9). In *A. nidulans,* Fbx58 showed enhanced resilience to cellular stressors [Sarikaya Bayram et al. 2022].

Another interesting observation was that the ΔNCU09899 (Δ*exo-1*) deletion strain showed a CCR-repressed phenotype in the cellulose perception screen, due to a significantly lower cellulase activity (Figure 2-6), but in contrast the determined protein amount in the supernatant was slightly higher than in the WT (Figure S 6-1). These results are in accordance with findings described in a previous study. Gabriel *et al.* identified both Δ*exo-1* and a *N. crassa* strain carring a missense mutation within the *exo-1* gene, as hypersecretion strains [Gabriel et al. 2021], which might explain the increased protein amount within the supernatant. Gabriel *et al.* performed a transcriptional analysis via RNA-sequencing and described a reduced CAZyme expression of Δ*exo-1* on Avicel and a WT-like repression in glucose under CCR [Gabriel et al. 2021]. This observation explains the decreased cellulase activity in the culture supernatant of Δ*exo-1* grown in Avicel supplemented with glucose (Figure 2-6).

Taken together, the deletion of some *fbx* genes caused aberrant phenotypes compared to the WT with regard to cellulose perception and biomass formation in presence of both allyl alcohol and glucose. Remarkably, in the two different screenings the WT ranked intermediate and was consistently flanked in both directions by *fbx* deletion strains. To receive deeper insights into how F-box proteins influence carbon utilization and which role they might play, three candidates which showed a repressed and three which showed a derepressed phenotype were selected for further investigations.

3.3. Characterization of selected F-box candidates

3.3.1. Global transcriptional response to carbon source switches by *N. crassa fbx* deletion strains results in altered gene enrichment

To obtain a more global overview of the consequences and the impact of the *fbx* deletions on gene expression level, a transcriptomic analysis was performed of Δ*fbx17*, Δ*fbx41* and ΔNCU05033 in comparison to the WT (chapter 2.3.2). The transcriptomic changes in the corresponding *fbx* gene deletion strains during the switch from repressed to de-repressed states and *vice versa*, were assayed by RNA-sequencing to identify their regulatory influence on carbon utilization.

The preceding qPCR revealed that the derepression during switches from the repressed (glucose) to the depressed condition (Avicel) appeared to require more time than the other way around (Figure 2-14). A possible reason could be that it results in the expression of many enzymes and transporters, compared to the relatively simple repression of genes encoding e.g. cellulases. This assumption can be confirmed by the interpretations of

Coradetti *et al.* of a shift from sucrose to either Avicel or no carbon conditions. Coradetti *et al.* suggested that CCR is released about one hour after medium shift within a derepression phase. At a later time point, the real induction phase event takes place as a consequence of the cellulosic signal. [Coradetti et al. 2012] In the future, a time series could be performed with other qPCR target genes that appear to be interesting due to the following RNA-sequencing results, to obtain a more precise chronological sequence of CCR events.

The *fbx* deletion strains which showed a derepressed phenotype, Δ*fbx17*/*41*, were switched from a derepressed condition (Avicel, at t_0) to a repressed condition (glucose, at $t_{0.5}$ and t_8) prior to the RNA-sequencing analysis. ΔNCU05033, on the other hand, with a repressed phenotype, was cultivated in a repressing condition (glucose, at t_0) prior to the switch into the derepressing condition (Avicel at t_5 and t_{24}). Within both culturing procedures a *N. crassa* WT strain was added.

The differential gene expression analysis revealed (Figure 2-15) that more genes shared by the WT and both derepressed strains were downregulated. For the repressed *fbx* deletion strain, which was cultivated *vice versa*, a higher amount of DEGs shared with the WT were upregulated.

Remarkable was that DEGs exclusively upregulated in the WT, after switch from derepressed to repressed condition, were significantly enriched in different GO terms. In contrast, exclusively upregulated DEGs for Δ*fbx17*/*41* were not significantly enriched in GO terms of biological processes. This suggests an influence of the *fbx* deletions on various biological processes and different genes that can not be grouped within individual GO classes.

For both, WT and Δ*fbx17,* within all time point comparisons, differentially downregulated genes were significantly enriched in GO:0016052, a term containing genes important for carbohydrate breakdown. This makes sense, since glucose was available instead of cellulose, which is known to trigger CCR and the repression of cellulolytic genes [Sun and Glass 2011; Ries et al. 2016].

Performing a switch from a repressing to derepressing condition, ΔNCU05033 and the WT shared 366 significantly upregulated genes (Figure 2-15, E), which were connected to translation, cellulose catabolic processes and some other classes related to protein synthesis and expression. Differentially downregulated within both strains were, among others, genes related to biosynthetic processes of various amino acids. Coradetti *et al.* published 212 genes specifically induced by Avicel [Coradetti et al. 2012]. A total of 94 of these genes were significantly differentially upregulated in the WT and ΔNCU05033 at both time points after switch into Avicel. These findings indicate the adaptation of the strains to the derepressed condition.

The expression pattern of *cre-1* (NCU08807), as central transcriptional regulator of CCR, was of special interest. However, no significant differences could be detected compared all deletion strains and conditions to the WT. The only exception was five hours after switch from glucose to cellulose, where *cre-1* was significantly downregulated within both the WT and ΔNCU05033. This result is consistent with the data of a quantitative RT-PCR, where the expression level of *cre-1* was decreased in the presence of Avicel [Sun and Glass 2011]. Gene expression of *cre-3* (NCU03887), the ortholog to *A. nidulans creD*, was significantly upregulated in WT and Δ*fbx17/41* at all time points in glucose compared to cellulose (Figure 2-15). After the switch from glucose to cellulose, *cre-3* was found to be significantly downregulated in both WT and ΔNCU05033. This suggests the importance of *cre-3* being present in the repressing condition (glucose) and rather absent in the derepressing condition (Avicel). Sen *et al.* investigated CDT-1 and CDT-2 in yeast, suggesting a role of *cre-3* as regulator for the endocytic removal of the cellodextrin transporters [Sen et al. 2016]. This might explain the expression pattern observed for *cre-3* during carbon source switches (chapter 2.3.2). The *creB* ortholog *uth-11* (NCU08378) was upregulated 30 minutes after the switch from cellulose to glucose in WT and Δ*fbx17/41*. This is in accordance with the fact that CreB was found to be present in CC-repressing conditions, resulting in active CreA [Lockington and Kelly 2002]. The expression of *cre-2* (NCU03965), which is orthologous to *creC*, differed comparing the WT strain to ΔNCU05033. Five hours after switching the strains from glucose to cellulose, *cre-2* was found to be significant upregulated only within the WT, but not in ΔNCU05033 (Figure 2-15).

Apart from known carbon catabolite regulators, genes encoding e.g. kinases, enzymes, transporters and TFs were analysed in further detail. For instance, NCU04106, encoding GPR-17, was significantly upregulated within the WT and Δ*fbx41* strain 30 minutes after switch to glucose, but not in Δ*fbx17*. Additionally, NCU04987, encoding GPR-10, was significantly upregulated within the WT and Δ*fbx41* strain 8 h after switch to glucose, but not in Δ*fbx17*. G protein-coupled receptors are known to be responsible for diverse cell functions, including growth and development. Both GPR-10 and GPR-17 have been identified harboring growth, developmental, chemical sensitivity or nutrition phenotypes within an investigation of kockout mutants lacking GPCR encoding genes. [Cabrera et al. 2015] Within that study, Cabrera *et al.* investigated RNA-seq data, where strains were grown on Avicel and sucrose, published by Coradetti *et al.* in 2012. This RNA-seq analysis revealed that most GPCR genes were more strongly expressed on Avicel compared to sucrose. In contrast, both *gpr-10* and *gpr-17* showed higher mRNA levels on sucrose compared to Avicel, with *gpr-10* expression being strongest. [Coradetti et al. 2012; Cabrera et al. 2015] These findings were in accordance with the expression patterns observed within

this work. In both the WT and Δ*fbx41* expression levels of *gpr-10* and *gpr-17* significantly increased over time after switch from Avicel to glucose, but not in Δ*fbx17* (Figure 2-15). The aberrant expression patterns of *gpr-10* and *gpr-17* could therefore have an influence on the derepressed phenotype and the developmental phenotype of Δ*fbx17* (chapter 2.3.1).
For the deletion strain ΔNCU05033, the expression of *stk-12* (NCU07378) increased 2.2-fold, and for *rco-3* (NCU02582) 2-fold, 24 h after the switch from glucose to cellulose, wherease the gene expression level of *stk-2* increased 1.8-fold and of *rco-3* ~1.9-fold within the WT across the same time points. Loss of *stk-12* is known to cause a “hyper-production phenotype” of cellulase production [Lin et al. 2019]. Additonally, STK-12 was found to directly target IGO-1 to affect the cellulase production [Lin et al. 2019]. In contrast, RCO-3 is known to function as a carbon sensor and regulate, in conjunction with COL-26, the glucose dual-affinity transport system [Li and Borkovich 2006; Li et al. 2021].

Investigating DEGs of both medium switches, glucose to Avicel and *vice versa*, in deeper detail (Figure 2-16) revealed that the conditions and time points selected for ΔNCU05033 led to higher similiarity of the gene expression pattern compared to the WT, than for Δ*fbx17* and Δ*fbx41*. Both Δ*fbx17* and Δ*fbx41* exhibited a more spread scatter plot comparing gene expression patterns to the WT. The lowest coefficient of determination was found after 24 h in Avicel (t_0), indicating greatest difference in these conditions (Figure 2-16 A, D).
After the switch from Avicel to glucose, for instance the low-affinity glucose transporter *glt-1* (NCU01633), was significantly upregulated, and in contrast significantly downregulated after switch from glucose to Avicel for WT (t_{24}) and ΔNCU05033 (t_5, t_{24}). The two high-affinity transporters *hgt-1*/*-2* (NCU10021 and NCU04963) were expressed in exactly the opposite way. The transporters were both upregulated at all time points after switch to Avicel in WT and ΔNCU05033. Within WT, Δ*fbx17* and Δ*fbx41*, *hgt-1*/*-2* were both significantly downregulated 8 h after switch from Avicel to glucose. These observations are in accordance with previous studies: At high glucose levels, low-affinity glucose transporters are induced, while starvation or glucose-limiting conditions lead to increased expression of high-affinity transporters [Wang et al. 2017].
A GO enrichment analysis and a FunCat enrichment analysis of upregulated DEGs confirmed the derepressed phenotype of Δ*fbx17* and Δ*fbx41* after 24 hours in cellulose (Figure 2-16 A, D), since categories associated with cellulose and polysaccharide degradation were enriched. After the switch to glucose, upregulated DEGs (Figure 2-16 B, E) were connected to catabolism, polysaccharide degradation and similar categories for both deletion strains, indicating that a deregulation of these genes could be (at least partially) responsible for the de-repressed phenotype. In contrast, downregulated DEGs in ΔNCU05033 (Figure 2-16, H) were associated with categories important for cellulose

catabolism and degradation. Even though only 20 genes were significantly downregulated compared to the WT, enrichment was found in e.g. cellulose catabolism (11.1%, *P* $2.07*10^{-8}$) and extracellular cellulose degradation (16%, *P* $1.39*10^{-7}$).

The enrichment analysis revealed that DEGs of the mutants compared to the WT were mainly enriched in categories important for carbon utilization. This transcriptional footprint demonstrates that the *fbx* deletions indeed cause global misregulations of genes within these categories.

3.3.2. Comparative analysis of transcriptomes between *N. crassa* WT, Δ*fbx17/41* and ΔNCU05033 mutants distinguishes clusters of genes co-regulated in response to carbon source switches

Fungal utilization of complex carbon sources, like lignocellulosic biomass, has been investigated and described in several studies. The specific transcriptional response induced via complex carbon sources was originally analyzed in *A. niger*, *T. reesei* and *N. crassa* using RNA-seq and microarray approaches. These studies revealed that different fungi utilize different sets of enzymes to degrade complex carbon sources. Even though overlaps can be found, a specific adaptation of the species is detectable. [Tian et al. 2009; Delmas et al. 2012; Ries et al. 2013] For *N. crassa,* a conservative Avicel regulon has been identified by Coradetti *et al.* comprising 212 genes, showing increased expression on Avicel compared to starvation and sucrose as sole carbon source [Coradetti et al. 2012].

Investigating the RNA-seq data within a hierarchical clustering analysis (Figure 2-17, Figure 2-18, Figure 2-19) revealed that the deletion strains showed still higher similarities at the same time points compared to the WT and main differences through altered conditions at the other time points. Nevertheless, the expression of some genes differs when comparing the WT and the mutant. For instance, comparing the WT and Δ*fbx17*, within cluster 1 (Figure 2-17), a total of 74 genes were found which were also described to be part of the Avicel regulon by Coradetti *et al.*. Genes which were clustered in C1 showed increased expression after growth in Avicel (Figure 2-17, t_0). In total, 108 genes of the published conservative Avicel regulon [Coradetti et al. 2012] were expressed higher than ten FPKM and were considered within the hierarchical clustering analysis of Δ*fbx17*.

Thirty minutes after switching the strains from Avicel to glucose medium, genes clustered within C8 were higher expressed, whereas especially genes within subcluster 2 showed an impaired expression pattern in Δ*fbx17* compared to the WT. This could indicate that the genes in cluster 8 are essential to adapt to the new environmental condition after the switch from Avicel to glucose. Genes with a connection to repression, like the *A. nidulans creD* ortholog NCU00866 (*cre-3*), the *creB* ortholog NCU08378 (*uth-11*) and *cre*-1 itself

(NCU08807) were located in C8. Additionally, genes of C8 were significantly enriched in categories connected to transcription and protein synthesis, in line with the cellular adaptation to the new environmental condition. As genes in subcluster 2 were significantly enriched for categories connected to RNA processing, transcription and protein synthesis, this suggests deficiencies of Δ*fbx17* with transcriptional and translational processes.

The glucose dual-affinity transport system of *N. crassa* has been extensively investigated [Wang et al. 2017]. It is comprised of GLT-1, a low-affinity glucose transport system (system I) and of HGT-1 and -2, the high-affinity system (system II). High glucose levels induce system I, while system II is known to be induced at low carbon conditions, especially low glucose conditions [Wang et al. 2017]. Wang *et al.* grew *N. crassa* mycelia in a glucose gradient from 0% to 10% for one or two hours for later RNA-sequencing. Since transcriptomic responses to 0.5%, 2% and 10% were similar within the study of Wang *et al.*, they suggested a glucose threshold of 0.5% to be sufficient to promote vegetative growth. [Wang et al. 2017] Within this work, *hgt-2* (NCU04963) was expressed in Avicel on its highest expression level of the conditions tested. Expression decreased after the switch to glucose (Figure 2-17, C1). *Hgt-1* (NCU10021) showed a slight increase of expression after the switch to glucose and decreased 8 h after the switch. In contrast, *glt-1* (NCU01633) showed the highest expression eight hours after the switch to glucose, whereas the expression after half an hour in glucose was also increased, and its lowest expression on Avicel. These data are in accordance with the findings of Wang *et al.* since a higher glucose level induced system I. [Wang et al. 2017]

The fungal-specific transcription factor *col-22* (NCU04390), was found in cluster 1 within the hierarchical clustering analysis of Δ*fbx17* compared to the WT, and to be 1.3-fold upregulated in Avicel in Δ*fbx17* compared to the WT (Figure 2-17). Additionally, *col-22* was differentially expressed (upregulated) in the WT strain 24 h after switch from glucose to Avicel, compared to the expression level after growth in glucose. This might indicate that *col-22* could play a role in cellulose perception, since its expression increased in the WT after switch from glucose to Avicel and an increased expression was detected in the derepressed strain Δ*fbx17* compared to the WT in Avicel.

Overall, the repression of genes needed for cellulase utilization seems to happen more slowly in the deletion mutant Δ*fbx17* compared to the WT.

Szőke *et al.* investigated to what extent the molecular clock is influenced by constant glucose deficiency. Within their work, they discovered the severe impact of the white collar complex (WCC) on nutrient-dependent expression. The core clock component displayed altered expression after glucose deprivation, however they stated that short deprivation of glucose does not lead to an effect on the expression of the core components. [Szőke et al. 2023] As Fbx17 was found to play a role within the circadian clock [He et al. 2003],

expression patterns of core clock genes were reviewed. However, none of the core clock genes (f*rq* NCU02265, *wc-1* NCU02356, *wc-2* NCU00902), as well as none of the other genes relevant for the clock function (*frh* NCU03363, *ck1a* NCU00685, *pp2a* NCU00488) showed significantly altered gene expression when comparing Δ*fbx17* to the WT (chapter 2.3.2).

When comparing the expression levels of the Δ*fbx41* deletion strain to the WT, most interesting was the expression pattern observed within subcluster 1 (Figure 2-18). These genes showed lower expression within the deletion strain in comparison the WT after growth on Avicel and especially half an hour after the switch to glucose. Genes in subcluster 1 were significantly enriched in FunCat categories related to protein fate, phosphorylation, dephosphorylation, autophosphorylation and protein kinase. Genes identified within subcluster 1 were for instance *stk-13* (NCU00108), *mik-1* (NCU02234), the adenylate cyclase *cr-1* (NCU08377), *stk-10* (NCU03200), *tor2* (NCU05608) and *wc-2* (NCU00902). Alongside PKA, TOR2 is one of the major kinases influencing cell growth as consequence to nutritional changes and STK-10 was found to execute the most modifications upon detection of cellobiose [Horta et al. 2019]. The slightly aberrant expression of the genes in subcluster 1 could indicate problems with signal transduction and cell cycle regulations within Δ*fbx41*.

Alcohol dehydrogenases (ADH) are key enzymes for the utilization of alcohols and for instance also convert allyl alcohol to the toxic compound acrolein [Park et al. 2007; Xiong et al. 2014]. Interestingly, *adh-1* (NCU01754) was significantly differentially expressed and more than 3-fold upregulated in both Δ*fbx17*/*41* compared to the WT half an hour after the switch to glucose (Figure 2-17 C10; Figure 2-18 C17). This might explain the significant increased sensitivity of both deletion strains in the presence of allyl alcohol (chapter 2.2.3). The genes clustered within C17 (Figure 2-18) were more connected to extracellular polysaccharide degradation, transcription or extracellular cellulose degradation and showed aberrant expression patterns comparing Δ*fbx41* to the WT - especially in Avicel and also half an hour after the switch to glucose. Within C17, *clr-3* (NCU05846) was identified. Half an hour after the switch to glucose, *clr-3* showed a 1.7-fold higher expression in the deletion strain compared to the WT.

The hierarchical clustering of CAZymes (Figure 2-20) furthermore revealed an interesting gene expression pattern in C7 of Δ*fbx17* (27 genes) and in C3 of Δ*fbx41* (41 genes) at $t_{0.5}$. Interestingly, 26 genes were shared between C7 of Δ*fbx17* and C3 of Δ*fbx41*. Since the analyses demonstrated a lower expression within both mutants, this suggests that they may (directly or indirectly) affect the same genes. Probably however, both proteins (Fbx17/41) intervene at different points in the regulation of these genes.

Comparing the transcriptome of ΔNCU05033 to the WT, after 24 h in glucose, prior to the switch to Avicel, especially genes within clusters 26 to 34 were found to be upregulated (Figure 2-19). Generally, genes which were upregulated in glucose (chapter 2.3.2) were significantly enriched in categories related to translation, transcription and protein synthesis across all strains tested. These data are consistent with the fact that during glucose consumption metabolic pathways are being ramped up as consequence of available energy [Benz et al. 2014; Li et al. 2014]. Comparing the most glucose-specific clusters of all three mutant strains, which were C8 of Δ*fbx17* (Figure 2-17, 1142 genes), C11 of Δ*fbx41* (Figure 2-18, 1013 genes) and C26 of ΔNCU05033 (Figure 2-19, 1168 genes) revealed an overlap of 361 genes. This indicates the importance of these genes in presence of glucose.

Five hours after the switch from Avicel to glucose, genes clustered within C17 (Figure 2-19) were more upregulated in the WT than in ΔNCU05033. Severe alterations of the expression patterns of especially *cbh-1*, exoglucanase 3 (*gh6-3*) and *cbh-2* were detected within this cluster and these genes showed significant downregulation within the ΔNCU05033 strain. The drastically decreased expression level of the major cellulases could be causative for the observed repressed phenotype of ΔNCU05033 (chapter 2.2.2). In cellulose-inducing conditions, CBH-1, CBH-2, GH5-1, and GH3-4 account for 65 % of the entire secretome in *N. crassa* [Glass et al. 2013]. All of them were clustered in C17, except *gh3-4,* which was clustered in C16 (Figure 2-19). Among other genes, Xiong *et al.* identified NCU09235/*con-8* within a transcriptomal analysis in a cluster containing 173 genes, which was generally declared to contain genes that play a role in response to carbon starvation [Xiong et al. 2014]. Intriguingly, this gene was significantly upregulated in ΔNCU05033 in Avicel (Figure 2-19, C1). In total, 39 genes identified by Xiong *et al.* to be related to starvation [Xiong et al. 2014] were identified within cluster 1 where increased expression on Avicel was detectable (Figure 2-19). Znameroski *et al.* identified genes significantly induced in WT *N. crassa* in response to Avicel [Znameroski et al. 2012]. In total, 35 of these genes were found in cluster 1. These findings suggest genes clustered within cluster 1 are Avicel-specific and are partwise also connected to starvation.

Overall, the transcriptional analysis clearly verified the repressed phenotype of ΔNCU05033 on transcriptional level. Interestingly, many misregulated genes are described as “hypothetical”, just as NCU05033 itself. This indicates that the deletion of NCU05033 has an influence on many unkown proteins or pathways which have not been described (sufficiently) yet.

3.4. Identification of F-box interaction partners

Four candidate F-box proteins with a strong potential for regulatory importance in lignocellulose signaling pathways were subjected to GFP pull-down experiments to elucidate potential interaction partners and downstream targets.

3.4.1. Localization events could cause functional consequences of complemented strains

In a study by Sarikaya Bayram *et al.,* F-box proteins were GFP-fused under control of their native promoter to execute localization studies and MS analysis, similar to this study. Finally, utilizing the native promoter failed to show both localization patterns and identify F-box proteins via MS. Therefore, Sarikaya Bayram *et al.* utilized the constitutive promoter of *gdpA* to overexpress the Fbx-GFP fusion proteins. [Sarikaya Bayram et al. 2022] In accordance with these findings, the overexpression promoter *ccg-1* was utilized within this study (chapter 6.4). Unfortunately however, the complementation was not successful for all constructs (chapter 2.4.1).

The ortholog of *N. crassa fbx22* in yeast, Cdc4, was found to be exclusively located in the cell nucleus. Blondel *et al.* described strains carring cytoplasmic Cdc4 were not able to complement growth defects and that the nuclear localization of Cdc4 is essential for its function *in vivo*. [Blondel et al. 2000] For *N. crassa* Δ*fbx22* growth defects were observed as well (chapter 2.2, 2.3.1) and a defect especially in high glucose concentrations has been described in literature [Horta et al. 2019]. The complementation of Δ*fbx22* was not successful, leading to strains still showing a growth defect as the deletion strain (Figure 2-23). Since nuclear localization is known to be essential for Cdc4 in yeast, this suggests that overexpression might have interfered with this in the setup used within this work. Further investigations to examine the localization of Fbx22-GFP would be a first step adressing this hypothesis.

3.4.2. Three F-box candidates assemble within the SCF complex – one might functions in a SCF-independent manner

First described in *S. cerevisiae*, one kind of Cullin-based E3 ubiquitin ligases is known to consist of the tetrameric Skp1-Cullin-F-Box (SCF) complex [Bai et al. 1996]. The identification of SCON-3 (NCU08991), an orthologue of SKP1 in *S. cerevisiae*, and Cullin 1 in the pulldowns and MS analyses of Fbx17::GFP, Fbx40::GFP and NCU05033::GFP suggests the ability of these F-box proteins to participate in the SCF complex. In the pull-down of Fbx41::GFP, SCON-3 was found but no cullin was identified, suggesting potentially

an independent function for this F-box protein from the SCF complex. Within other studies, non SCF F-box protein-SkpI complexes have been described, but compared with the widely studied SCF complex the function of SCF independent F-box proteins is largely unexplored [Hermand 2006; Liu et al. 2011]. In yeast, cullin-independent roles of Skp1 have been described. For instance, Skp1 regulates vesicle trafficking through its association with the F-box protein Rcy1 (Reviewed within [Willems et al. 2004]). The F-box protein Rcy1 itself is able to interact with Skp1, but does not associate in a complex with Cullin and Rbx1 [Liu et al. 2011].

Generally, protein-protein interactions of F-box proteins and their targets can be weak and transient, which may lead to low target protein abundancies within the MS analysis and therefore not all targets may be identified.

Nevertheless, for all investigated Fbx::GFP fusion proteins exclusive putative interactors were identified.

3.4.3. Fbx40 might influence anastomosis through HAM-14

Hyphal anastomosis-14 protein (HAM-14) was found to physically interact with MAP kinase cascade members, MAK-2, MEK-2 and HAM-5. It has been stated that HAM-14 might play a role in the MAK-2 recruitment, having an impact on the downstream signaling mediating chemotropic interactions and cell fusion. Deletion strains lacking *ham-14* showed deficient fusion, which might be caused by their inability to recruit MAK-2. [Jonkers et al. 2016]

MAK-2 is thought to be involved in the phosphatase acquisition pathway and influences hyphal growth, protein phosphorylation, the regulation of the growth rate, and more [Gras et al. 2013]. The impact of *N. crassa* morphology on enzyme expression was shown by Lin *et al.* in 2018. The deletion of *gul-1*, which affects the cell wall structure and mycelial morphology, for example, resulted in an increased secretion of enzymes. [Lin et al. 2018]

Since HAM-14 has been identified as a putative interaction partner of Fbx40, the abundance of HAM-14 might be misregulated in the Δ*fbx40* strain on protein level. Therefore, Fbx40 might influence anastomosis, which could indirectly have an impact on the enzyme secretion rates. While Δ*fbx40* showed a slightly repressed phenotype, the Δ*ham-14* strain (ΔNCU07238) showed high sensitivity to allyl alcohol in presence of glucose, suggesting a de-repressed phenotype.

3.4.4. Putative transcriptional regulator targeted by NCU05033 is part of the CRE-1 regulon

In *N. crassa*, Sun and Glass investigated the CRE-1 regulon and identified genes which are directly regulated by CRE-1 by performing chromatin-immunoprecipitation (ChIP) [Sun and Glass 2011]. These findings were completed by the study of Wu *et al.* in which they proposed that CRE-1 either directly regulates transcription factors required for the activation of plant biomass-degrading enzymes or that CRE-1 is responsible for the repression of genes that activate the transcription factors. Among other genes, Wu *et al.* identified CRE-1 to bind the promoter region of NCU08330. [Wu et al. 2020] NCU08330 encodes a hypothetical protein containing a DJ-1_PfpI domain, which can be found in transcriptional regulators. In the immunoprecipitation approach of NCU05033::GFP, NCU08330 was identified as putative interaction partner. In presence of allyl alcohol, ΔNCU08330 showed significant sentitivity and growth deficiency. Moreover, the cellulase activity of ΔNCU08330 was significantly increased, indicating a derepressed phenotype. These finding suggest that NCU08330 encodes a transcriptional regulator influencing carbon utilization and CCR, which is regulated on transcriptional level through CRE-1 and on post-translational level through NCU05033.

3.4.5. NCW-1 protein levels might contribute to the repressed phenotype of ΔNCU05033

The non-anchored cell wall protein 1 (NCW-1, NCU05137) was identified as potential interactor of the F-box protein NCU05033 (Table 2-3). Schmoll *et al.* found *ncw-1* to be coregulated with *cre-1* and *cpc-1* and to be “important for modulation of extracellular cellulose-degrading capacity” [Schmoll et al. 2012]. Within a study of Tian *et al.*, NCU05137 was identified to be highly upregulated in presence of cellulose and a *ncw-1* deletion to be causative for increased cellulolytic activity, including upregulation of *cbh-1* and *gh6-2* (*cbh-2*). [Tian et al. 2009] This observation is in line with the data from this work, where ΔNCU05137 showed significantly increased cellulase activity compared to the WT (Figure 2-30, D). The deletion of the ortholog of NCU05137 in *Penicillium oxalicum* resulted in a similarly increased production of cellulases and transporter gene expression, suggesting a conserved function of this protein across some fungal species [Li et al. 2015]. The transciptomal analysis of the F-box deletion strain ΔNCU05033 revealed significantly lower expression of *cbh-1* (NCU07340) and exoglucanase 3 (NCU07190, *gh6-3*) five hours after switch from glucose to Avicel compared to the WT, as well as approximately 21-fold lower expression of *cbh-2* (NCU09680) in ΔNCU05033 compared to the WT 5 h after medium switch (Figure 2-19, Figure 2-20, C). Lin *et al.* demonstrated an increased cellobiose uptake

in Δ*ncw-1* as the cause for an increased cellulase production in a *cre-1* independent manner [Lin et al. 2017]. Employing a quadruple mutant having the three major β-glucosidases (NCU00130, NCU04952, NCU08755) and *ncw-1* deleted, the Δ3βGΔ*ncw-1* mutant showed significantly increased expression of three cellulase genes (NCU07340, NCU09680, NCU00762), the cellobiose dehydrogenase (*cdh-1*, NCU00206), three hemicelluase genes (NCU02855, NCU05955, NCU07326) and four lytic polysaccharide monooxygenase genes (NCU08760, NCU02916, NCU02240, NCU01050) [Lin et al. 2017]. Comparing these data with the transcriptomal analysis of this work, all genes listed above were clustered together in cluster 5 within the hierarchical clustering of CAZyme genes (Figure 2-20, C). In cluster 5, all genes were only approximately 0.1-fold expressed in ΔNCU05033 with respect to the WT (fold change of expression levels of mutant/WT), at 5 h post switch from glucose to Avicel. In the Δ3βGΔ*ncw-1* mutant, *cdt-1* and *cdt-2* were upregulated [Lin et al. 2017], while *cdt-2* was expressed WT-like in ΔNCU05033 (cluster 1, Figure 2-21, C) and *cdt-1* was only 0.4-fold expressed five hours after medium switch in ΔNCU05033 compared to the WT (cluster 3, Figure 2-21, C). Lin *et al.* also reported misregulation of transcription factors related to cellulose and hemicellulose consumption in the Δ3βGΔ*ncw-1* mutant [Lin et al. 2017]. These severe misregulations of the transcription factors could not be observed within the transcriptomal data of ΔNCU05033 of this work. The most significantly misregulated transcription factor was *vad-12* (NCU05035), which is associated with cellular response to oxidative stress. As *vad-12* seems to be located close to NCU05033 this could be an artifact. The transcription factor *ada-6* (NCU04866) was downregulated 51-fold in the Δ3βGΔ*ncw-1* mutant [Lin et al. 2017], while it was 2.4-fold upregulated in ΔNCU05033. *Clr-2* was approximately 19-fold upregulated in the Δ3βGΔ*ncw-1* mutant [Lin et al. 2017], while *clr-2* was only 0.4-fold expressed in ΔNCU05033 compared to the WT five hours after the switch (cluster 17, Figure 2-19). Moreover, the cross-pathway control protein 1 (*cpc-1*, NCU04050) was significantly differentially downregulated only in ΔNCU05033 comparing t_0 to t_5 within this strain (Figure 2-15).

The F-box protein NCU05033 was found to interact with NCW-1 after growth in glucose within this work (Table 2-3). After growth in both Avicel and *Miscanthus*, NCW-1 was identified in the secretome [Tian et al. 2009], suggesting its importance for lignocellulosic biomass consumption. Additionally, NCW-1 was found to have a regulatory influence on cellulolytic capacities [Tian et al. 2009; Schmoll et al. 2012; Lin et al. 2017]. Taken together, the results of the analyses of the transcriptomal data (chapter 2.3.2) and the mass spectrometry data of the immunoprecipitated proteins interacting physically (chapter 2.4.2), as well as the findings published in literature provide a connection of the F-box protein encoded by NCU05033, NCW-1 and altered cellulolytic capacities (Figure 3-1).

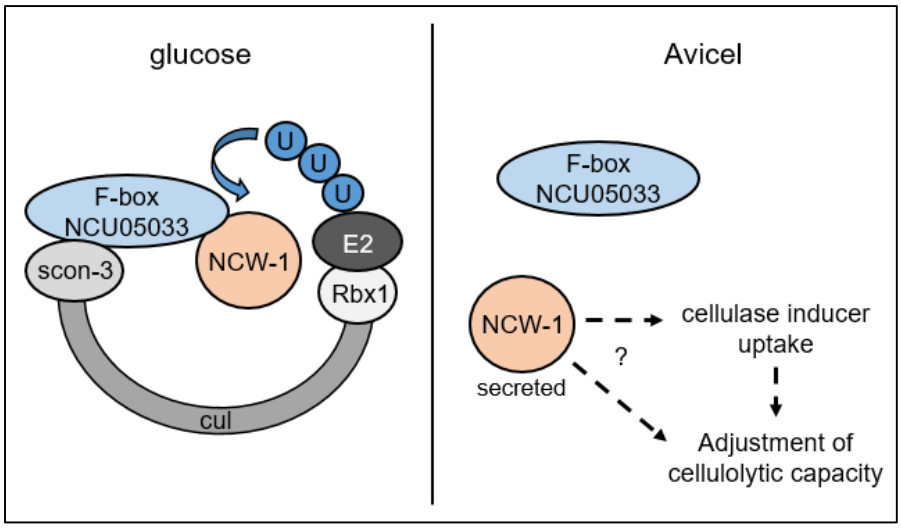

Figure 3-1: Model of F-box protein NCU05033 indirectly influencing the cellulolytic capacity in *Neurospora crassa*.
In glucose (left), NCW-1 interacts with $SCF^{NCU05033}$. In Avicel (right), NCW-1 is secreted and has either a direct or indirect influence on the adjustment of the cellulolytic capacity. The indirect influence probably occurs through the regulation of the uptake of cellulase inducers.

The misregulation of NCW-1 levels in the ΔNCU05033 strain might therefore contribute to or potentially cause its repressed phenotype (Figure 2-6, Figure 2-9) through lower expression levels of the major cellulases at early time points after the switch from glucose to Avicel. The physical interaction of NCU05033 and NCW-1 remains to be confirmed with alternative methods suitable for identification of protein-protein interactions on different carbon sources.

3.4.6. Fbx41 might indirectly influence the concentration of cellulose signaling molecules

The two *N. crassa* cellodextrin transporters CDT-1 and CDT-2 were the first ones described in filamentous fungi and are nowadays known to be important for sensing and transportation of cellodextrins at low amounts of extracellular cellobiose [Cai et al. 2014; Sen et al. 2016]. Both play a critical role in cellulose degradation and are important for *N. crassa* growth on cellulose. Significant growth deficiencies of Δ*cdt-2* were observed within a study of Galazka *et al*. [Galazka et al. 2010]. Within this work, a significant growth defiency of Δ*cdt-2* could be confirmed on cellulose and both Δ*cdt-1/-2* deletion strains showed increased sensitivity in presence of allyl alcohol (chapter 2.4.3). Additionally, Sen *et al.* suggested a role of *cre-3* as regulator for the endocytic removal of the heterologously expressed cellodextrin transporters in yeast [Sen et al. 2016]. This hypothesis highlights the potential importance of these cellodextrin transporters for CCR.

Both cellodextrin transporters were identified in the pull down experiment with F-box protein Fbx41. Fbx41 was shown to interact with SCON-3 in both glucose and cellulose (chapter 2.4.2). In *A. nidulans* Fbx41 was shown to interact with SkpA during vegetative stage and stress, additionally the interaction with CulA was identified through pull down experiments [Sarikaya Bayram et al. 2022].

The transcriptomal analysis of Δ*fbx41* compared to the WT revealed that *cdt-1* expression showed a fold change of 1.6 in Δ*fbx41* with respect to the WT at t_0. Half an hour after switch from cellulose to glucose the fold change was 2.4, and 0.8 after eight hours in Δ*fbx41* with respect to the WT (Figure 2-21 B, cluster 2). Similar was observed for *cdt-2*, which was 1.6-fold lower expressed in Δ*fbx41* with respect to the WT at t_0. Half an hour after switch from cellulose to glucose the fold change was 3.1, and 2.1 after eight hours in Δ*fbx41* with respect to the WT (Figure 2-21 B, cluster 1). Over time, both *cdt 1/-2* were downregulated within the WT and Δ*fbx41*.

The β-glucosidase 1 (*gh3-3*, NCU08755), which is involved in catabolic processes, was also identified in the Fbx41 pull-down approach. The Δ*gh3-3* deletion strain displayed a significantly decreased cellulase activity (chapter 2.4.3). A similar observation was made before, where the deletion strain ΔNCU08755, also named Δ*bgl6*, showed the slowest rate of cellobiose utilization of all tested deletion strains [Wu et al. 2013]. Within the transcriptional analysis of Δ*fbx41*, *gh3-3* was found to be downregulated over time within both the WT and the deletion strain. The fold change expression of *gh3-3* in cellulose was 0.6, after half an hour in glucose 1.0 and eight hours in glucose 1.3 in the deletion strain with respect to the WT (Figure 2-20 B, cluster 1).

Mis-expression or aberrant protein abundance of β-glucosidases is thought to have an effect on regulation. A possible reason could be their impact on inducer molecules available for the organism. [Znameroski et al. 2012; Zhang et al. 2024] Addionally, Zhang *et al.* provided insights into the interplay of β-glucosidases and CDT-1/-2, demonstrating the importance of the main cellodextrin transporters for cellobiose utilization in absence of the three major β-glucosidases [Zhang et al. 2024].

Overall, Fbx41 seems to interact with several proteins that affect the concentration of cellulose signaling molecules in the cell and therefore might play an important role in the regulation of the ratio between cellulolytic inducer (cellobiose) and repressor (glucose) availability. Further investigations would be necessary to verify this hypothesis.

3.4.7. Fbx17 could indirectly influence glucose-6-phosphate levels

Glucose-6-phosphat (G6P) serves as an important metabolite produced from glucose and is utilized in different pathways. NCU03100, encoding a 6-phosphogluconate dehydrogenase (PPM-2), is involved in the pentose phosphate pathway, which serves for instance as a primary source of NADPH and the synthesis of precursors for nucleotide synthesis. NCU07281, encoding a glucose-6-phosphate isomerase (GPI-1), catalyzes the conversion of G6P to fructose-6-phosphate, the second step in glycolysis, and the reverse reaction during gluconeogenesis. [Radford 2004; Masi et al. 2021]

NCU10058 encodes ragged-1 (RG-1), a phosphoglucomutase that can convert G6P to α-glucose-1-phosphate and *vice versa*. RG-1 was found to potentially interact with GNA-3 [Kim 2011], one of three Gα subunit of heterotrimeric G-proteins in *N. crassa* [Collier et al. 2020]. Moreover, GNA-3 was shown to regulate levels of the adenylyl cyclase CR-1, and to be important during growth on Avicel by regulating cellulase activity in a positive manner via cAMP signaling [Kays et al. 2000; Collier et al. 2020]. In *T. reesei,* CR-1, PKA and the RAS GTPase Ras2, which are crucial components of the cAMP pathway, regulate cellulase gene expression through cAMP levels. Moreover, the promoter region of *cr-1* was shown to be bound by CLR-4. [Liu et al. 2019] Prior to cellulase synthesis, in *T. reesei* an increase of cAMP levels was detected within the cell and in parallel, a decrease of the intracellular G6P levels [Tisch and Schmoll 2010].

PPM-2, GPI-1 and RG-1 were identified within the pull down approach of Fbx17, suggesting these three proteins to be interactors of Fbx17 (Table 2-3). In Δ*fbx17* NCU03100 (*ppm-2*) (Figure 2-17, C4) and NCU10058 (*rg-1*) (Figure 2-17, C1) were expressed in a WT-like manner. However, comparing Δ*fbx17* to the WT, NCU07281 (*gpi-1*) was expressed 0.5-fold higher in the deletion strain in cellulose, 1.8-fold higher after half an hour in glucose and 0.6-fold lower after eight hours in glucose. Both Δ*rg-1* and Δ*ppm-2* showed significantly increased cellulase activity. Additionally, Δ*rg-1* was very sensitive to allyl alcohol and showed a similar phenotype as Δ*fbx17* (chapter 2.4.3). Since Δ*gpi-1* showed severe growth defects and was not able to form biomass in liquid cultures, no further investigations could be performed with this deletion strain (Figure S 6-21).

Nevertheless, in summary, Fbx17 appears to interact with several components that influence the concentration of G6P in the cell, suggesting an impact on G6P levels and therefore on a crucial CCR inducer molecule. Further investigations will be necessary. For instance, detection of intracellular G6P levels of Δ*fbx17* compared to the WT on CC-derepressing and CC-repressing conditions may provide insights into how G6P levels are impacted as consequence of the deletion of this F-box protein. However, first of all, the physical protein interaction of the F-box protein and its putative targets should be verified.

4. Concluding remarks and outlook

In summary, all available deletion strains of *N. crassa* F-box proteins were screened for their performance on different carbon sources, which can be considered one of the most extensive screens performed for this protein family so far. Doing so, several F-box proteins were identified, whose deletions were affecting cellulase production and carbon utilization. While some seem to affect CRR positively (repressed phenotype), some had a negative influence (derepressed phenotype). Of both phenotypes candidate genes were selected and investigated for both transcriptional response during carbon source switches and for putative interactors on protein level.

In the following, the first transcriptome analysis of *N. crassa fbx* deletion strains under carbon source switch conditions was conducted. These data provided insights into altered gene expression patterns caused by the *fbx* gene deletion. Moreover, these data were used to partially explain the observed phenotypes by displaying the genetic footprint of the mutations. This data set therefore also offered the potential to deepen the understanding of the *N. crassa* WT itself during carbon switches.

Identification of F-box interaction partners by combining immunoprecipitation and mass spectrometry revealed that three of the F-box candidates: NCU05033, Fbx17 and Fbx40, are associated with the SCF complex within the conditions tested. For Fbx41, only an interaction with SCON-3 could be detected, suggesting either a possible SCF independent function, only assembling with SCON-3 in the conditions tested, or a less strong assembly with the SCF-complex, at least in the tested conditions.

Investigation of Fbx-specific interactions revealed that the interaction partners were found to be involved in transport, transcription, signaling and carbon utilization. The F-box proteins Fbx17/41 and NCU05033 impact carbon utilization through different mechanisms. For instance, Fbx17 could influence glucose-6-phosphat levels through interactions with relevant proteins regulating G6P levels. Furthermore, Fbx40 might influence anastomosis through physical interaction with HAM-14 and thus might intervene MAP kinase cascades indirectly. For Fbx41, an influence on the concentration of cellulose signaling molecules through the interaction with cellodextrin transporters and the β-glucosidase GH3-3 appears likely.

Moreover, this work provided first insights into possible functions and effects of the hypothetical proteins NCU05033 and NCU00471 for which barely no data or detailed studies are available. Also, the majority of the DEGs of the transcriptomal analysis of NCU05033 were hypothetical proteins, which demonstrates that there is still a lot of work to be done to unravel all pathways and mechanism affected by this F-box protein. NCU05033 might interact with a transcriptional regulator (NCU08330) which is part of the CRE-regulon.

ΔNCU08330 was shown to lead to CC-defects, indicating its importance for carbon utilization and CCR. Additionally, the MS data generated within this work revealed that NCU05033 might interact with NCW-1, which is co-regulated with *cre-1* and *cpc-1* and relevant for the extracellular capacity of enzymes needed to degrade cellulose [Schmoll et al. 2012].

Looking forward, it is recommended to provide supporting evidence for the hypotheses and functional proposals developed in this work. Further experiments are needed to provide additional evidence for the physical interactions of the F-box proteins and the specific putative interactors. A split luciferase system, for instance, could be used to demonstrate this [Bardiya et al. 2008]. Determining the protein abundances of the putative interactors of the F-box proteins within the *fbx* deletion strains and *fbx* overexpressing strains compared to the WT would be also interesting, since F-box proteins are known to harbor SCF- and ubiquitination-independent functions [Hermand 2006].
Overall, the data generated in this work and the analyses performed deepen our understanding of F-box proteins in filamentous fungi, especially with regard to carbon utilization. The deepened knowledge can contribute to improvements of rational and targeted strain modifications, leading to improved enzyme-producing strains of high interest for the industry.

5. Materials and methods

5.1. Equipment, chemicals and strains

5.1.1. Software and instruments

Table 5-1: List of used software and online tools for data processing and analysis.

name	Purpose of use	Manufacturer/ reference
Basic Local Alignment Search Tool (BLAST)	sequence retrieval, sequence alignments	National Center for Biotechnology Information (NCBI) (Bethesda MD, USA)
Benchling	*in silico* cloning, primer design, alignments, plasmid map visualizations	Benchling [Biology Software]. (2019- 2023). Retrieved from https://benchling.com
Carbohydrate-Active enZYmes (CAZY) Database	classification of catalytic and carbohydrate-binding modules of enzymes that degrade glycosidic bonds	Université d'Aix-Marseille, architecture et function des macromolecules biologiques (Marseille, France)
Clustal Omega	Sequence alignments	The European Bioinformatics Institute (EMBL-EBI) (Cambridgeshire, United Kingdom) [Sievers et al. 2011]
Dataset of “The Fungal Nutritional ENCODE project”	Investigation of expression strength of *N. crassa* genes across different carbon sources	Glass, N. Louise, USDOE Joint Genome Institute (JGI) (Berkeley, CA, United States) https://doi.org/10.25585/1488072
FunCat	Functional Catalogue (FunCat) of *N. crassa* were determined using a customized macro based excel dataset	Professorship of Fungal Biotechnology in Wood Science at TUM (Freising, Germany) [Ruepp et al. 2004; Thieme et al. 2017]
fungal and oomycete genomics resources (FungiDB)	nucleotide and protein sequence retrieval, orthology searches, domain annotations, data set: *Neurospora crassa* gene co-expression network	National Institute of Allergy and Infectious Diseases (NIAID) (Maryland, USA) and University of California, Riverside (Riverside, USA)
Fungal Genetics Stock Center (FGSC)	collection of *N. crassa* strain information, navigation for the *N. crassa* deletion strain stock collection	Kansas State University, Department of Plant Pathology (Manhattan KS, USA)
FungiFun 2.2.8 BETA	Gene to category association for Gene Ontology classification [Ashburner et al. 2000], default settings	[Priebe et al. 2015]
Galaxy Server	Analyzation of RNA-Seq data	Pennsylvania State University, Center for Computational Biology and Bioinformatics (CCBB) (Pennsylvania, USA), John Hopkins University (Baltimore, USA) and Oregon

name	Purpose of use	Manufacturer/ reference
		Health & Science University, Computational Biology (Portland OR, USA)
Gene Ontology webpage	Gene ontology enrichment analysis for biological processes in *N. crassa*	© 1999–2023 Gene Ontology Consortium http://geneontology.org/ [Ashburner et al. 2000; Thomas et al. 2022; Aleksander et al. 2023]
Hierarchical Clustering Explorer V3.5	hierarchical clustering of gene expression data	University of Michigan (Ann Arbor, USA)
Interactive Tree Of Life (iTOL)	creation of phylogenetic tree and phylogenetic analysis	(https://itol.embl.de) [Letunic and Bork 2021]
InterPro	Protein domain search	The European Bioinformatics Institute (EMBL-EBI) (Cambridgeshire, United Kingdom) [Paysan-Lafosse et al. 2023]
LAS AF	microscopy figure preparation	Leica Microsystems (Wetzlar, Germany)
MaxQuant version 2.1.3.0	mass spectrometry data processing	[Cox and Mann 2008]
Microsoft Office 2016	statistical analysis, manuscript preparation	Microsoft (Redmond, USA)
NCBI Conserved Domains	prediction of conserved domains on nucleotide and amino acid sequences	National Center for Biotechnology Information (NCBI) (Bethesda MD, USA)
NLS mapper	Prediction of importin α-dependent nuclear localization signals	Shunichi Kosugi, https://nls-mapper.iab.keio.ac.jp/cgi-bin/NLS_Mapper_form.cgi [Kosugi et al. 2009]
OriginPro, version 2021b	data visualization, statistical analysis	OriginLab Corporation (Northampton, MA, USA)
Perseus version 1.6.15.0	quantitative analysis of mass spectrometry data	[Tyanova et al. 2016]
Pfam	annotations	The European Bioinformatics Institute (EMBL-EBI) (Cambridgeshire, United Kingdom)
PlaNet	co-expressed genes (accessed in 2020, now available on FungiDB)	Max Planck Society for the Advancement of Science e.V. (Munich, Germany)
SMART (Simple Modular Architecture Research Tool)	Protein domain determination	[Letunic and Bork 2018; Letunic et al. 2021]
Transporter Classification Database (TCDB)	classification of transporters	University of California San Diego, Division of Biological Sciences (San Diego, USA)
UniProt Database	amino acid sequence retrieval, domain architecture and putative	The European Bioinformatics Institute (EMBL-EBI)

name	Purpose of use	Manufacturer/ reference
	function of proteins, proteome retrieval	(Cambridgeshire, United Kingdom), Swiss Institute of Bioinformatics (SIB) (Lausanne, Switzerland) and Protein Information Resource (Delaware, USA) [The UniProt Consortium 2023]

Table 5-2: List of used instruments.

name	model	manufacturer
autoclave	Varioklav 135 S	Thermo Fisher Scientific (Waltham, USA)
autoclave	Systec VX-150	Systec (Linden, Germany)
Büchner funnel	XX44.1	Carl Roth (Karlsruhe, Germany)
electroporator	Eporator	Eppendorf (Hamburg, Germany)
fine balance	Mettler Model TLE 104	ZEFA Laborservice (Harthausen, Germany)
gel imaging system	Fusion solo S	Vilber Lourmat (Eberhardzell, Germany)
heating block	ThermoMixer C	Eppendorf (Hamburg, Germany)
Incubator 30 °C	Heratherm IGS100	Thermo Fisher Scientific (Waltham, USA)
Incubator 37 °C	IR 1500	Flow Laboratories (Inglewood, USA)
incubator shaking	Excella 24	New Brunswick Scientific (Edison, USA)
laboratory bead mill	BeadBug 24 D1030	Süd-Laborbedarf Gauting (Gauting, Germany)
large scale centrifuge	Megafuge 40R	Heraeus (Hanau, Germany)
light Incubator 25 °C	BK 5060 EL	Heraeus (Hanau, Germany)
light incubator shaking	Innova 42	New Brunswick Scientific (Edison, USA)
MIC Magnetic Induction Cycler, 2-Channel	68MIC-2	Biozym (Hessisch Oldendorf, Germany)
Mini Trans-Blot Module	1703935EDU	Bio-Rad Laboratories GmbH (Feldkirchen, Neuried, Germany)
Mini-PROTEAN Tetra Vertical Electrophoresis Cell	1658001FC	Bio-Rad Laboratories GmbH (Feldkirchen, Neuried, Germany)
oven	Jouan	Thermo Fisher Scientific (Waltham, USA)
pH-meter	SevenEasy	Mettler Toledo (Columbus, USA)
plate reader	Infinite 200 PRO NanoQuant reader	Tecan (Männedorf, Switzerland)
precision balance	Kern Model PLJ 3000-2CM	ZEFA Laborservice (Harthausen, Germany)
rocking machine	RT 26	Analytik Jena (Jena, Germany)
stereo microscope	S8AP0	Leica Microsystems (Wetzlar, Germany)
sterile bench	BDK-S	BDK Luft- und Reinraumtechnik (Sonnenbühl-Genkingen, Germany)
tabletop centrifuge	Centrifuge 5424	Eppendorf (Hamburg, Germany)
tabletop centrifuge (cooled)	Centrifuge 5427 R	Eppendorf (Hamburg, Germany)
thermocycler	ProfessionalTRIO	Analytik Jena (Jena, Germany)
thermocycler gradient	peqStar 2x Gradient	VWR (Radnor, USA)

name	model	manufacturer
tube revolver	Rotator	Analytik Jena (Jena, Germany)
water purifier	mini-UP+	Berrytec (Grünwald, Germany)

5.1.2. Chemicals and consumables

Table 5-3: List of used chemicals and carbon sources.

name	order number	manufacturer
2-mercaptoethanol	M3148	Sigma-Aldrich Chemie GmbH (Taufkirchen, Germany)
2-propanol	6752	Carl Roth (Karlsruhe, Germany)
acetic acid 100%	3738	Carl Roth (Karlsruhe, Germany)
Acrylamide/Bis-acrylamide (37.5:1)	10688.02	SERVA Electrophoresis GmbH (Heidelberg, Germany)
agar-agar, Kobe I	5210	Carl Roth (Karlsruhe, Germany)
agarose	AG02	Nippon Genetics Europe (Dueren, Germany)
allyl alcohol	240532-100ML	Merck (Darmstadt, Germany)
ammonium iron(II) sulfate hexahydrate	P728	Carl Roth (Karlsruhe, Germany)
ammonium nitrate	K299	Carl Roth (Karlsruhe, Germany)
ammonium peroxydisulphate	9592.3	Carl Roth (Karlsruhe, Germany)
Ampicillin sodium salt	HP62	Carl Roth (Karlsruhe, Germany)
benzamidine	12072	Merck (Darmstadt, Germany)
boric acid	6943	Carl Roth (Karlsruhe, Germany)
bovine serum albumin (BSA) fraction V	8076	Carl Roth (Karlsruhe, Germany)
Bromophenol Blue	B0126	Merck (Darmstadt, Germany)
calcium chloride dihydrate	5239	Carl Roth (Karlsruhe, Germany)
chloroform	3313.1	Carl Roth (Karlsruhe, Germany)
citric acid monohydrate	20276	VWR (Radnor, USA)
cOmplete™, EDTA-free Protease Inhibitor Cocktail	4693132001	Merck (Darmstadt, Germany)
Coomassie Brilliant Blue R 250	17525.01	SERVA Electrophoresis GmbH (Heidelberg, Germany)
copper (II) sulfate pentahydrate	23174	VWR (Radnor, USA)
D-biotin	3822	Carl Roth (Karlsruhe, Germany)
D-fructose	4981	Carl Roth (Karlsruhe, Germany)
di-potassium phosphate	P749	Carl Roth (Karlsruhe, Germany)
DL-Dithiothreitol	43819	Merck (Darmstadt, Germany)
D-sorbitol	S6021	Merck (Darmstadt, Germany)
ethanol >96%	T171	Carl Roth (Karlsruhe, Germany)
ethanol >99%	9065	Carl Roth (Karlsruhe, Germany)
ethylenediaminetetraacetic acid (EDTA)	CN06.2	Carl Roth (Karlsruhe, Germany)
Ficoll 400	F2637	Merck (Darmstadt, Germany)
formaldehyde solution	4979.1	Carl Roth (Karlsruhe, Germany)

name	order number	manufacturer
glucose	X997	Carl Roth (Karlsruhe, Germany)
glycerol	3783	Carl Roth (Karlsruhe, Germany)
glycine	3187.3	Carl Roth (Karlsruhe, Germany)
hydrochloric acid	4625	Carl Roth (Karlsruhe, Germany)
Hygromycin B Gold	ant-hg-1	InvivoGen (Toulouse, France)
L-histidine	H5659	Merck (Darmstadt, Germany)
L-sorbose	4028	Carl Roth (Karlsruhe, Germany)
magnesium chloride hexahydrate	M2670	Merck (Darmstadt, Germany)
magnesium sulfate heptahydrate	P027	Carl Roth (Karlsruhe, Germany)
manganese (II) sulfate monohydrate	25303	VWR (Radnor, USA)
methanol	HN41.2	Carl Roth (Karlsruhe, Germany)
milk powder	T145.1	Carl Roth (Karlsruhe, Germany)
Nonidet P 40 substitute (NP-40)	11754599001	Merck (Darmstadt, Germany)
phenylmethylsulfonyl fluoride (PMSF)	6367.1	Carl Roth (Karlsruhe, Germany)
PhosSTOP™	PHOSS-RO	Merck (Darmstadt, Germany)
potassium chloride	P9333	Merck (Darmstadt, Germany)
potassium dihydrogen phosphate	3904	Carl Roth (Karlsruhe, Germany)
potassium nitrate	P021.1	Carl Roth (Karlsruhe, Germany)
Roti-phenol/chloroform/isoamyl-mix	A156	Carl Roth (Karlsruhe, Germany)
Roti-Quant 5x	K015	Carl Roth (Karlsruhe, Germany)
silver nitrate	9370.4	Carl Roth (Karlsruhe, Germany)
sodium acetate anhydrous	6773	Carl Roth (Karlsruhe, Germany)
sodium carbonate	A135.1	Carl Roth (Karlsruhe, Germany)
sodium chloride	3957	Carl Roth (Karlsruhe, Germany)
sodium dodecyl sulphate (SDS)	2326.4	Carl Roth (Karlsruhe, Germany)
sodium hydroxide	6771.1	Carl Roth (Karlsruhe, Germany)
sodium molybdate dihydrate	0274	Carl Roth (Karlsruhe, Germany)
sodium thiosulfate anhydrous	APPCA6830	VWR (Radnor, USA)
sucrose	S7903	Merck (Darmstadt, Germany)
tetramethylethylenediamine (TEMED)	2367.3	Carl Roth (Karlsruhe, Germany)
Tris(hydroxymethyl)-aminomethane	4855.3	Carl Roth (Karlsruhe, Germany)
trisodium citrate dihydrate	3580	Carl Roth (Karlsruhe, Germany)
Triton X-100	T8787	Merck (Darmstadt, Germany)
tryptone/peptone from casein	8952	Carl Roth (Karlsruhe, Germany)
Tween 20	P9416	Merck (Darmstadt, Germany)
Xylene Cyanol FF	X4126	Merck (Darmstadt, Germany)
yeast extract	2363	Carl Roth (Karlsruhe, Germany)
zinc sulfate heptahydrate	29253236	VWR (Radnor, USA)

Table 5-4: List of used consumables and kits.

name	order number	manufacturer
100 bp Quick-Load DNA ladder	N0467	New England Biolabs (Ipswich, USA)
24 deep well plate	742926	Biozym (Hessisch Oldendorf, Germany)
96-well plates, flat bottom, transparent	82.1581.001	Sarstedt (Nümbrecht, Germany)
Anti-GFP from mouse IgG1κ	11814460001	Merck (Darmstadt, Germany)
Azo-CM-Cellulose (Powder)	S-ACMC	Megazyme Ltd. (Bray, Ireland)
BlueStar Prestained Protein Marker; Tris-Glycine 4~20%	MWP03	NIPPON Genetics EUROPE GmbH (Düren, Germany)
breathable membrane	Z380059-1PAK	Merck (Darmstadt, Germany)
ChromoTek GFP-Trap® Agarose	gta	Proteintech Group, Inc. (Rosemont, USA)
Competent Cells TG1 Mix & Go!	T3017	zymo research (Freiburg, Germany)
DNA ladder 1 kb	N3232	New England Biolabs (Ipswich, USA)
DNase I (RNase-Free)	M0303	New England Biolabs (Ipswich, USA)
FastGene Scriptase Basic cDNA Kit	LS62	NIPPON Genetics EUROPE GmbH (Düren, Germany)
Filtropur BT 50, 0.2 µm filter	83.1823.101	Sarstedt (Nümbrecht, Germany)
Gel Loading Dye, Purple (6x)	B7025S	New England Biolabs (Ipswich, USA)
GeneJet RNA Purification Kit	K0731	Thermo Fisher Scientific (Waltham, USA)
Goat anti-Mouse IgG (H+L) Secondary Antibody, HRP	31430	Thermo Fisher Scientific (Waltham, USA)
Hi Yield® Gel/PCR DNA Fragment Extraction Kit	HYDF100	Süd-Laborbedarf (Gauting, Germany)
Hi-Yield Plasmid Mini Prep DNA isolation kit	30 HYPD300	Süd-Laborbedarf Gauting (Gauting, Germany)
MIC Tubes and Caps	68MIC-60653	Biozym (Hessisch Oldendorf, Germany)
Midori Green Advance	MG04	Nippon Genetics Europe (Dueren, Germany)
Nuclease-free water	W4502	Merck (Darmstadt, Germany)
NuPage™ 4-12% Bis-Tris gel, 1.5 mm x 10 wells	NP0335BOX	Thermo Fisher Scientific (Waltham, USA)
PacI restriction enzyme	R0547	New England Biolabs (Ipswich, USA)
Phusion High-Fidelity DNA-Polymerase	M0530	New England Biolabs (Ipswich, USA)
Protein-LoBind reaction tube, 1.5 ml	72,706,600	Sarstedt (Nümbrecht, Germany)
Protein-LoBind reaction tube, 2 ml	72,706,600	Sarstedt (Nümbrecht, Germany)
PVDF membrane, 0.45 µm	88518	Thermo Fisher Scientific (Waltham, USA)
qPCRBIO SyGreen Mix Separate-ROX	PB20. 14	NIPPON Genetics EUROPE GmbH (Düren, Germany)

name	order number	manufacturer
RNase Away	038186	Kisker Biotech (Steinfurt, Germany)
RNA-Solv® reagent	R6830-02	VWR (Radnor, USA)
SuperSignal™ West Pico PLUS Chemiluminescent Substrate	34577	Thermo Fisher Scientific (Waltham, USA)
syringe filter 0.2 µm Filtropur S	83.1826.001	Sarstedt (Nümbrecht, Germany)
T4 DNA Ligase	M0202	New England Biolabs (Ipswich, USA)
Trypsin Sequencing Grade, modified from porcine pancreas	37283.01	SERVA Electrophoresis GmbH (Heidelberg, Germany)
Whatman™ filter paper	1003-917	GE Healthcare UK Limited (Buckinghamshire, UK)
XbaI restriction enzyme	R0145	New England Biolabs (Ipswich, USA)
Zirconium beads (Ø = 0.5 mm)	24 D1132-05	Süd-Laborbedarf Gauting (Gauting, Germany)

5.1.3. Buffers and media

Substances used in media and solutions were dissolved in double distilled water (ddH_2O) if not stated otherwise.

Table 5-5: List of buffers and media.

name	substances	concentration
D-biotin stock solution	D-biotin	0.1 mg/ml
	filter sterilize	
trace elements stock solution	citric acid monohydrate	1.2 mM
	zinc sulfate heptahydrate	0.87 mM
	ammonium iron(II) sulfate hexahydrate	0.13 mM
	copper (II) sulfate pentahydrate	50 µM
	manganese (II) sulfate monohydrate	15 µM
	boric acid	40 µM
	sodium molybdate dihydrate	10.3 µM
	filter sterilize	
50x Vogel's solution [Vogel 1956]	trisodium citrate dihydrate	0.43 M
	potassium dihydrogen phosphate	1.84 M
	ammonium nitrate	1.25 M
	magnesium sulfate heptahydrate	40.0 mM
	calcium chloride dihydrate (pre-dissolve in water)	34.0 mM
	D-biotin stock solution (0.1 mg/ml)	0.25% (v/v)
	trace elements stock solution	0.50% (v/v)
	filter sterilize	
Vogel's Minimal Medium (VMM)	sucrose	2.0% (w/v)
	50x Vogel's solution	2.0% (v/v)
	agar-agar (only solid medium)	1.5% (w/v)
10x FIGS solution	L-sorbose	20.0% (w/v)
	D-fructose	0.5% (w/v)
	D-glucose	0.5% (w/v)
	filter sterilize	
bottom agar	50x Vogel's solution	2.0% (v/v)
	agar-agar	1.5% (w/v)
	autoclave, add 10x FIGS solution afterwards	10.0% (v/v)
top agar	50x Vogel's solution	2.0% (v/v)
	agar-agar	1.0% (w/v)
	autoclave, add 10x FIGS solution afterwards	10.0% (v/v)
2x Westergaard's solution [Westergaard and Mitchell 1947]	potassium nitrate	0.2% (w/v)
	di-potassium phosphate	0.14% (w/v)
	potassium dihydrogen phosphate	0.1% (w/v)
	magnesium sulfate heptahydrate	0.1% (w/v)
	sodium chloride	0.02% (w/v)

name	substances	concentration
	calcium chloride dihydrate (pre-dissolve in water)	0.02% (w/v)
	D-biotin stock solution (0.1 mg/ml)	0.01% (v/v)
	trace elements stock solution	0.02% (v/v)
	filter sterilize	
Westergaard's medium (WGM)	2x Westergaard's solution	50.0% (v/v)
	sucrose	1.5% (w/v)
	agar-agar	2.0% (w/v)
Lysogeny Broth (LB) Medium [Bertani 1951]	yeast extract	0.5% (w/v)
	tryptone/peptone	1.0% (w/v)
	sodium chloride	1.0% (w/v)
	agar-agar (only solid medium)	1.5% (w/v)
	pH was set to 7.5 prior autoclaving	
5x KCM for *E. coli* TG-1 transformation	potassium chloride	0.5 M
	calcium chloride	0.15 M
	magnesium chloride	0.25 M
	filter sterilize	
5x Taq buffer	Tris HCl pH 8.5	0.25 M
	sodium chloride	0.1 M
	magnesium chloride hexahydrate	10.0 mM
	Ficoll 400	12.5% (w/v)
	BSA	0.25% (w/v)
	Xylene Cyanol FF	0.1% (w/v)
50x Tris Acetate EDTA (TAE) stock solution	Tris	2 M
	acetic acid 100%	1 M
	EDTA	50 mM
gDNA extraction lysis buffer	sodium hydroxide	50 mM
	EDTA	1 mM
	Triton X-100	1% (v/v)
Precipitant solution (Megazyme kit S-ACMC)	Sodium acetate trihydrate	40 g/l
	zinc acetate	4 g/l
	Set pH to 5.0 using hydrogen chloride	5 M
	ethanol (95%)	800 ml/l
4x Laemmli buffer	Tris-HCl, pH 6.8	62.5 mM
	Glycerol	10% (w/v)
	SDS	1% (w/v)
	Bromophenol Blue	0.005% (w/v)
	2-mercaptoethanol	100 µl/ 900µl of ingredients above
10x running buffer (SDS-PAGE)	Tris base	30 g/l
	glycine	144 g/l
	SDS	10 g/l
	pH 8.3 (without adjustment)	
Fix solution (silver staining)	ethanol	30% (v/v)
	acetic acid	10% (v/v)

name	substances	concentration
Wash solution (silver staining)	ethanol	30% (v/v)
Background solution (silver staining)	sodium thiosulfate	2.5 mM
Silver solution (silver staining)	silver nitrate	0.2% (w/v)
	formaldehyde solution	80 µl/ 100 ml
Revelation solution (silver staining)	sodium carbonate	3% (w/v)
	formaldehyde solution	50 µl/ 100 ml
	2.5 mM sodium thiosulfate	800 µl/ 100 ml
Coomassie staining solution	Coomassie Blue	0.1% (w/v)
	ethanol	40% (v/v)
	acetic acid	10% (v/v)
Coomassie destaining solution	ethanol	10% (v/v)
	acetic acid	7.5% (v/v)
B250 lysis buffer [Assis et al. 2020]	sodium chloride	250 mM
	Tris-HCl, pH 7.5	100 mM
	glycerol	10% (v/v)
	EDTA	1 mM
	Nonidet P 40 substitute (NP-40), optional	0.1% (v/v)
	Set pH at 4 °C to 7.5	
	Supplements to be added fresh prior to usage:	
	1 M DTT, optional	1.5 ml/l
	Complete-mini Protease Inhibitor Cocktail EDTA-free	1pill/10 ml buffer
	0.5 M benzamidine	3 ml/l
	phosphoSTOP phosphatase inhibitor	1pill/ 10ml buffer
	100 mM phenylmethylsulfonyl fluoride (PMSF)	10 ml/l
2x SDS elution buffer	Tris/Cl pH 6.8	120 mM
	glycerol	20% (v/v)
	SDS	4% (w/v)
	bromphenol blue	0.04% (w/v)
	2-mercaptoethanol	10% (v/v)
Transfer buffer (western blot)	Glycine	14.4 g/l
	Tris base	3.03 g/l
	methanol	15% (v/v)
	SDS	0.1% (w/v)
10x Tris-buffered saline (TBS) buffer (western blot)	Tris-HCl, pH 7.5	500 mM
	Sodium chloride	1.5 mM
Tris-buffered saline with Tween 20 (TBST) buffer (western blot)	10x TBS buffer	1x
	Tween 20	0.1% (v/v)
Blocking buffer (western blot)	milk powder	5% (w/v)
	Dissolved in TBST buffer	

Table 5-6: List of antibiotics and supplements.

name	substances	Work concentration
1000x Ampicillin stock solution, 100 mg/ml	Ampicillin sodium salt	1.2 x
100x histidine stock solution, 20 mg/ml	L-histidine	1 x
Hygromycin B stock solution, 100 mg/ml	Hygromycin B Gold	150 µg/ml

5.1.4. Primers and plasmids

Table 5-7: List of used primers.
The first column contains the laboratory internal primer number, the second the name of the primer. Primer types are given in the third column: G = genotyping, S = sequencing, C = cloning, Q = qPCR. The melt temperature (Tm) is listed in column five. The oligonucleotides were customized from Eurofins Genomics in Ebersberg, Germany.

#	Name	Type	Sequence (5´to 3´)	Tm (°C)
1	Tail-hph3	G	CGACAGACGTCGCGGTGAGTTCAG	64
oJPB 757	NCU00488-wt_fw	G	CCAAGGTTATGGCTATGGGTGCC	63
oJPB 756	NCU00488-3´flank_rv	G	cgctgctctgttggctcattgatgg	65
oJPB 759	NCU05316-wt_fw	G	GAGATGGCATACGAGGGTGGCTC	65
oJPB 758	NCU05316-3´flank_rv	G	CGTCCCATTACCAGATCCCATAGTTGCAC	65
oJPB 761	NCU06483-wt_fw	G	GAAGTGCGTTGCGATGGCACTG	65
oJPB 760	NCU06483-3´flank_rv	G	CGACTTTCGCCAACCAATGCGC	65
oJPB 763	NCU07521-wt_fw	G	GCGTATTGTCAGCTCCGGACAGGATC	66
oJPB 762	NCU07521-3´flank_rv	G	gcaaagcaaacagtgcccaagttacccag	67
oJPB 765	NCU08563-wt_fw	G	GGAAGCGGAAGCCCCTCC	65
oJPB 764	NCU08563-3´flank_rv	G	cgaggacgctgataggtgaagatggc	66
oJPB 767	NCU08991-wt_fw	G	CGTGTTGTTGCCGAGCGATCCC	67
oJPB 766	NCU08991-3´flank_rv	G	ggcgttgcaaagtgacttgacgtgg	66
oJPB 923	pFW_PCR_XbaI-fbx17-NCU07521	C	cttttctagaATGGAGGCACACGCTC	59
oJPB 924	pRV_fbx17-NCU07521_PCR_PacI	C	GACCTTAATTAAAAAATACCCGCCCGGC	59
oJPB 925	pFW_PCR_XbaI-fbx22-NCU05939	C	GTTGtctagaATGCCTTTCGAATTTGATGG	56
oJPB 926	pRV_fbx22-NCU05939_PCR_PacI	C	GTCAGttaattaaTTCGCCTTCTGCAAGC	57
oJPB 927	pFW_PCR_XbaI-fbx23-NCU04540	C	GCTAGCtctagaATGGCCGGCTTTCCTC	59
oJPB 928	pRV_fbx23-NCU04540_PCR_PacI	C	GACGTAttaattaaCTGCACAGTGTCAAAGAACC	59
oJPB 929	pFW_PCR_XbaI-fbx40-NCU03462	C	CAAGTCtctagaATGGTCATCTTGCATCACC	57
oJPB 930	pRV_fbx40-NCU03462_PCR_PacI	C	CTTAACttaattaaGAGCTTGCGCCCAAAC	58

#	Name	Type	Sequence (5´to 3´)	Tm (°C)
oJPB 931	pFW_PCR_XbaI-fbx41-NCU00471	C	GTTCtctagaATGACCTTCCCGGGC	57
oJPB 932	pRV_fbx41-NCU00471_PCR_PacI	C	CCATAttaattaaGTACTCTTCTCCGTCGGAATC	59
oJPB 933	pFW_PCR_XbaI-NCU05033	C	CGAAtctagaATGAGCGAACCACAAGGAC	60
oJPB 934	pRV_NCU05033_PCR_PacI	C	CACTttaattaaGTCCAACCAGTCTCCCG	59
226	226_ccg1_fwd	S	ccatcatcagccaacaaagcaatcacatc	60.9
435	435_gfp_check_R	S	gatgaacttcagggtcagc	52.2
oJPB 1037	seq&colonyPCR-pLK052-NCU07521-fbx17_rev	S	CGATGTGCTTGTCATCGAAGACAAG	60
oJPB 1038	seq&colonyPCR-pLK053-NCU05939-fbx22_rev	S	CGAACAGTTCCTTCCAACCTGTCTC	62
oJPB 1043	seq-pLK053-NCU05939-fbx22_rev	S	GAAGGCGCCAAACGCG	61
oJPB 1039	seq&colonyPCR-pLK054-NCU04540-fbx23-rev	S	GAATCTGCACTGCATTGACAGCC	61
oJPB 1044	seq-pLK054-NCU04540-fbx23-fwd	S	CTGTAATACCGCCGTGGACC	61
oJPB 1040	seq&colonyPCR-pLK055-NCU03462-fbx40-rev	S	GATCGGCCAATAGCCAGTTCC	61
oJPB 1041	seq&colonyPCR-pLK056-NCU00471-fbx41-rev	S	CAACTGACATCAGGGTGAGAGACTTAAG	61
oJPB 1042	seq&colonyPCR-pLK057-NCU05033-rev	S	CTGACCACAAAGTCCGTCAACTC	60
625	NCU05939_F	G	CAGCGACATAACGCCAGAC	59
626	NCU05939_R	G	GATTGATGTGCGATATTCCGC	56
oJPB 1050	NCU04540-wt_fw	G	CCAGGGTGTTCAAGTTGCAGTAC	61
oJPB 1049	NCU04540-3´flank_rv	G	GTTGAAGCTGAGGGAGGGTATGC	63
oJPB 1048	NCU03462-wt_fw	G	GATGGATGGTGCGACAGAAGTC	60
oJPB 1047	NCU03462-3´flank_rv	G	gtctgtctctcgcctcctgttc	62
oJPB 1046	NCU00471-wt_fw	G	CGGAAGAGTATCTCTCGGTCGCAG	64
oJPB 1045	NCU00471-3´flank_rv	G	GATATAGGCATGCAAAGCGTACCTGTAAGC	63
oJPB 1052	NCU05033-wt_fw	G	GTCGCGGGAGAACATGGAG	61
oJPB 1051	NCU05033-3´flank_rv	G	cgcttattGGTTGCTGAGCATATTGTG	61
oJPB 1094	pFW_PCR_XbaI-cre-1-NCU08807	C	CGAAtctagaATGCAACGCGTACAGTCAG	60

#	Name	Type	Sequence (5´to 3´)	Tm (°C)
oJPB 1095	pRV_PCR_cre-1-NCU08807-PacI	C	GTCAGttaattaaCAACCGGTC CATCATCTCC	60
oJPB 1096	hphF primer-FGSC	G	GTCGGAGACAGAAGATGAT ATTGAAGGAGC	62
oJPB 1097	hphR primer-FGSC	G	GTTGGAGATTTCAGTAACGT TAAGTGGAT	58
oJPB 1098	seq&colonyPCR-pLK058-NCU08807-cre-1-rev	S	GCTGTCGAGTTGGGCGAGT TG	64
oJPB 1119	seq-pLK054-NCU04540-fbx23-fwd2	S	CTCTGTCTTCAGTTCGACTC TAGC	62
oJPB 1140	GFP-check-FWD	G	cagctcgccgaccactac	61
oJPB 1141	His-3_WT_locus_FWD	G	CCCGAACTATCATGATGCA GTACCTA	63
oJPB 1155	seq-pLK052-NCU07521-fbx17_fwd	S	GGCTTCTGCTTCCCTCGTC	61
133	133_cre1_end_fwd	G	GCCCAACTCGACAGCACCT TC	60.1
134	134_cre1_3'flank_rev	G	GCTGTGCCAACTGTCCGAT TTC	58.8
oJPB 544	qPCR primer cbh-1 redesign 61 FW	Q	GTGCTTACCGTGGCGAGTG	61
oJPB 545	qPCR primer cbh-1 re-design 61 RV	Q	GAAGGGTTGGAAGGAGGG GT	61
oJPB 325	qRTPCRprimer_actin reference gene-NCU04173_FW	Q	GTCTCTCCGACCGTATGCA G	60
oJPB 320	qRTPCRprimer_actin reference gene-NCU04173_RV	Q	GCGAGAATGGAACCACCGA T	60

Table 5-8: List of plasmids used in this study.

name	characteristics	plasmid map	reference
pCCG::C-Gly::GFP	5' and 3' flank of *N. crassa his-3* gene, *ccg-1* promoter of *N. crassa*, MCS, *gfp*, *adh-1* terminator and Ampicillin resistance to *E. coli*	Figure S 6-24	[Honda and Selker 2009]
pLK052, pCCG::NCU07521::C-Gly::GFP	5' and 3' flank of *N. crassa his-3* gene, *ccg-1* promoter of *N. crassa*, coding sequence NCU07521, *gfp*, *adh-1* terminator and Ampicillin resistance to *E. coli*	Figure S 6-25	this study
pLK053, pCCG::NCU05939::C-Gly::GFP	5' and 3' flank of *N. crassa his-3* gene, *ccg-1* promoter of *N. crassa*, coding sequence NCU05939, *gfp*, *adh-1* terminator and Ampicillin resistance to *E. coli*	Figure S 6-26	this study

name	characteristics	plasmid map	reference
pLK054, pCCG::NCU04540::Gly-GFP	5’ and 3’ flank of *N. crassa his-3* gene, *ccg-1* promoter of *N. crassa*, coding sequence NCU04540, *gfp*, *adh-1* terminator and Ampicillin resistance to *E. coli*	Figure S 6-27	this study
pLK055, pCCG::NCU03462::Gly-GFP	5’ and 3’ flank of *N. crassa his-3* gene, *ccg-1* promoter of *N. crassa*, coding sequence NCU03462, *gfp*, *adh-1* terminator and Ampicillin resistance to *E. coli*	Figure S 6-28	this study
pLK056, pCCG::NCU00471::C-Gly::GFP	5’ and 3’ flank of *N. crassa his-3* gene, *ccg-1* promoter of *N. crassa*, coding sequence NCU00471, *gfp*, *adh-1* terminator and Ampicillin resistance to *E. coli*	Figure S 6-29	this study
pLK057, pCCG::NCU05033::C-Gly::GFP	5’ and 3’ flank of *N. crassa his-3* gene, *ccg-1* promoter of *N. crassa*, coding sequence NCU05033, *gfp*, *adh-1* terminator and Ampicillin resistance to *E. coli*	Figure S 6-30	this study
pLK058, pCCG::NCU08807::Gly-GFP	5’ and 3’ flank of *N. crassa his-3* gene, *ccg-1* promoter of *N. crassa*, coding sequence NCU08807, *gfp*, *adh-1* terminator and Ampicillin resistance to *E. coli*	Figure S 6-31	this study

5.1.5. Utilized organisms and strains

The utilized *Neurospora crassa* wildtype (WT) reference strain was OR74A [Mylyk et al. 1974]. The used *N. crassa* deletion strains were obtained from the Fungal Genetics Stock Center (FGSC) [Colot et al. 2006].

Table 5-9: List of used organisms and strains.
p = promoter of gene, comp = complemented

#[a]	name	genotype	origin
1	*N. crassa* WT	oak ridge (OR) 74, mat A	FGSC #2489
2	*N. crassa* WT	oak ridge (OR) 74, mat a	FGSC #988
16	Δ*pdr-1*, *his*$^{-}$	ΔNCU09033::hph, his3^{-}, mat a	EBI[b]
22	WT, *his*$^{-}$	his-3^{-}, mat A	FGSC #6103
47	Δfluffy a	ΔNCU08726::hph	FGSC #11044
48	Δfluffy A	ΔNCU08726::hph	[Thieme 2019]
124	*pdr-1-GFP*	his-3:: pNCU03753-NCU09033::GFP, mat A	[Thieme 2019]
130	Δ*cre-1*	ΔNCU08807::hph, mat a	FGSC #18633
230	WT, *his*$^{-}$	his-3^{-}, mat a	this study
232	unbound GFP	his-3::pNCU03753-GFP, mat A	this study
nLK033	Δ*fbx1*	ΔNCU03146::hph, mat a	FGSC #19761
nLK031	Δ*fbx3*	ΔNCU07257::hph, mat a	FGSC #17642
nLK040	Δ*fbx7*	ΔNCU03022::hph, mat a	FGSC #18740
nLK041	Δ*fbx9*	ΔNCU03658::hph, mat A	FGSC #21255
nLK002	Δ*fbx10*	ΔNCU04785::hph, mat A	FGSC #17862
nLK038	Δ*fbx11*	ΔNCU07996::hph, mat a	FGSC #20259
nLK019	Δ*fbx15*	ΔNCU04576::hph, mat a	FGSC #14639
nLK024III	Δ*fbx17*	ΔNCU07521::hph, mat a	FGSC #13527[c]
nLK036	Δ*fbx18*	ΔNCU07425::hph, mat a	FGSC #18092
nLK003	Δ*fbx19*	ΔNCU08642::hph, mat a	FGSC #15478
nLK005	Δ*fbx20*	ΔNCU06250::hph, mat A	FGSC #15629
nLK006	Δ*fbx22*	ΔNCU05939::hph, mat a	FGSC #13190
nLK028	Δ*fbx23*	ΔNCU04540::hph, mat A	FGSC #15872
nLK022III	Δ*fbx24*	ΔNCU06483::hph, mat a	FGSC #11497[c]
nLK042	Δ*fbx27*	ΔNCU10476::hph, mat a	FGSC #21574
nLK021	Δ*fbx29*	ΔNCU07419::hph, mat a	FGSC #14810
nLK013	Δ*fbx30*	ΔNCU02379::hph, mat A	FGSC #16886
nLK032	Δ*fbx37*	ΔNCU07359::hph, mat a	FGSC #15407
nLK007	Δ*fbx40*	ΔNCU03462::hph, mat a	FGSC #20477
nLK009	Δ*fbx41*	ΔNCU00471::hph, mat a	FGSC #12780
nLK014	Δ*fbx50*	ΔNCU01216::hph, mat a	FGSC #14510
nLK043	Δ*fbx58*	ΔNCU06688::hph, mat a	FGSC #22093
nLK030	Δ*fbx65*	ΔNCU06056::hph, mat a	FGSC #14975
nLK016	ΔNCU01081	ΔNCU01081::hph, mat A	FGSC #17169
nLK012	ΔNCU01865	ΔNCU01865::hph, mat a	FGSC #13862
nLK011	ΔNCU01926	ΔNCU01926::hph, mat a	FGSC #13886
nLK017	ΔNCU02346	ΔNCU02346::hph, mat a	FGSC #17281

#[a]	name	genotype	origin
nLK018	ΔNCU03881	ΔNCU03881::hph, mat A	FGSC #17231
nLK029	ΔNCU04383	ΔNCU04383::hph, mat a	FGSC #17334
nLK020	ΔNCU05033	ΔNCU05033::hph, mat a	FGSC #14738
nLK015	ΔNCU05243	ΔNCU05243::hph, mat a	FGSC #14579
nLK045	ΔNCU05393	ΔNCU05393::hph, mat a	FGSC #22628
nLK048	ΔNCU07110	ΔNCU07110::hph, mat a	FGSC #23816
nLK039	ΔNCU08348	ΔNCU08348::hph, mat a	FGSC #19335
nLK046	ΔNCU08403	ΔNCU08403::hph, mat a	FGSC #23477
nLK044	ΔNCU08717	ΔNCU08717::hph, mat A	FGSC #22298
nLK037	ΔNCU08842	ΔNCU08842::hph, mat a	FGSC #18199
nLK035	ΔNCU09807	ΔNCU09807::hph, mat a	FGSC #19960
nLK034	ΔNCU09899	ΔNCU09899::hph, mat a	FGSC #19860
nLK047	ΔNCU12130	ΔNCU12130::hph, mat A	FGSC #23399
nLK051 I	Δ*fbx40*, *his-*	ΔNCU03462::hph, his-3^{-}	this study
nLK053 III	ΔNCU05033 *his-*	ΔNCU05033::hph, his-3^{-}	this study
nLK051 B	Δ*fbx41*, *his-*	ΔNCU00471::hph, his-3^{-}	this study
nLK056 VII	Δf*bx17*, *his-*	ΔNCU07521::hph, his-3^{-}	this study
nLK057 I	Δ*cre-1*, *his-*	ΔNCU08807::hph, his-3^{-}	this study
nLK059 I	Δ*fbx22*, *his-*	ΔNCU05939::hph, his-3^{-}	this study
nLK060 V	Δ*fbx23*, *his-*	ΔNCU04540::hph, his-3^{-}	this study
nLK054J	*fbx40*-comp	ΔNCU03462::hph, his-3::pNCU03753-NCU03462::GFP	this study
nLK054K	*fbx40*-comp	ΔNCU03462::hph, his-3::pNCU03753-NCU03462::GFP	this study
nLK054L	*fbx40*-comp	ΔNCU03462::hph, his-3::pNCU03753-NCU03462::GFP	this study
nLK055A	NCU05033-comp	ΔNCU05033::hph, his-3::pNCU03753-NCU05033::GFP	this study
nLK058 III	*fbx41*-comp	ΔNCU00471::hph, his-3::pNCU03753-NCU00471::GFP	this study
nLK058 VI	*fbx41*-comp	ΔNCU00471::hph, his-3::pNCU03753-NCU00471::GFP	this study
nLK058 VIII	*fbx41*-comp	ΔNCU00471::hph, his-3::pNCU03753-NCU00471::GFP	this study
nLK061 III	*cre-1*-comp	ΔNCU08807::hph, his-3::pNCU03753-NCU08807::GFP	this study
nLK061 VI	*cre-1*-comp	ΔNCU08807::hph, his-3::pNCU03753-NCU08807::GFP	this study
nLK061 IX	*cre-1*-comp	ΔNCU08807::hph, his-3::pNCU03753-NCU08807::GFP	this study
nLK062 V	*fbx17*-comp	ΔNCU07521::hph, his-3::pNCU03753-NCU07521::GFP	this study
nLK062 VII	*fbx17*-comp	ΔNCU07521::hph, his-3::pNCU03753-NCU07521::GFP	this study
nLK062 X	*fbx17*-comp	ΔNCU07521::hph, his-3::pNCU03753-NCU07521::GFP	this study

#[a]	name	genotype	origin
nLK064 II	*fbx23*-comp	ΔNCU04540::hph, his-3::pNCU03753-NCU04540::GFP	this study
nLK064 III	*fbx23*-comp	ΔNCU04540::hph, his-3::pNCU03753-NCU04540::GFP	this study
nLK064 VII	*fbx23*-comp	ΔNCU04540::hph, his-3::pNCU03753-NCU04540::GFP	this study
nLK064 VIII	*fbx23*-comp	ΔNCU04540::hph, his-3::pNCU03753-NCU04540::GFP	this study
nLK064 IX	*fbx23*-comp	ΔNCU04540::hph, his-3::pNCU03753-NCU04540::GFP	this study
nLK064 X	*fbx23*-comp	ΔNCU04540::hph, his-3::pNCU03753-NCU04540::GFP	this study
nLK066 VI	*fbx22*-comp	ΔNCU05939::hph, his-3::pNCU03753-NCU05939::GFP	this study
nLK066 VIII	*fbx22*-comp	ΔNCU05939::hph, his-3::pNCU03753-NCU05939::GFP	this study
nLK075	ΔNCU08924	ΔNCU08924::hph, heterokaryon mat a	FGSC #14526
nLK076	ΔNCU00355	ΔNCU00355::hph, mat a	FGSC #11201
nLK077	ΔNCU05163	ΔNCU05163::hph, mat A	FGSC #14789
nLK078	ΔNCU05137	ΔNCU05137::hph, mat a	FGSC #11681
nLK079	ΔNCU09209	ΔNCU09209::hph, mat a	FGSC #14415
nLK080	ΔNCU09269	ΔNCU09269::hph, heterokaryon	FGSC #12980
nLK081	ΔNCU08330	ΔNCU08330::hph, mat A	FGSC #17982
nLK082	ΔNCU08755	ΔNCU08755::hph, mat a	FGSC #18387
nLK084	ΔNCU00801	ΔNCU00801::hph, mat a	FGSC #16575
nLK085	ΔNCU08114	ΔNCU08114::hph, mat a	FGSC #17868
nLK088	ΔNCU08907	ΔNCU08907::hph, mat a	FGSC #18422
nLK090	ΔNCU06701	ΔNCU06701::hph, mat A	FGSC #15895
nLK091	ΔNCU04120	ΔNCU04120::hph, heterokaryon	FGSC #11618
nLK092	ΔNCU07238	ΔNCU07238::hph, mat a	FGSC #14336
nLK093	ΔNCU01328	ΔNCU01328::hph, heterokaryon, mat a	FGSC #18825
nLK094	ΔNCU02208	ΔNCU02208::hph, mat a	FGSC #20904
nLK095	ΔNCU07831	ΔNCU07831::hph, heterokaryon, mat a	FGSC #20914
nLK096	ΔNCU01021	ΔNCU01021::hph, heterokaryon, mat a	FGSC #16510
nLK098	ΔNCU10058	ΔNCU10058::hph, mat A	FGSC #18976
nLK099	ΔNCU03100	ΔNCU03100::hph, heterokaryon, mat a	FGSC #16484
nLK100	ΔNCU00558	ΔNCU00558::hph, mat a	FGSC #16762

[a] *N. crassa* glycerol stock number of Professorship of Fungal Biotechnology in Wood Science (TUM); [b] Energy Biosciences Institute, Berkeley, USA; [c] FGSC strain was homokaryonized via microconidiation;

5.2. Physiological methods

In general, handling with organisms was performed under sterile conditions with the usage of personal protective equipment. Spore producing fungi were always kept in a sterile bench, when culture flasks had to be opened. If not stated otherwise, experiments were performed with triplicates.

5.2.1. Propagation of *N. crassa*

Agar slants containing 2 ml of solid 2 % sucrose Vogel´s minimal medium [Vogel 1956] were inoculated with spores from glycerol stocks using a sterile wooden applicator. The inoculated slants were incubated at 30 °C for two days in the dark, then at 25 °C in a light:dark cycle (12:12). Seven to ten day old conidia were harvested by adding 1 ml sterile ddH_2O into the slant, vortexing it and transferring the spore suspension into a 1.5 ml reaction tube. Conidia were separated from residual hyphae via centrifugation at 1,000 rpm for 1 min. The supernatant was discarded and the conidia pellet was dissolved in 500 µl ddH_2O. The spores were used for glycerol stocks, DNA extraction or the inoculation of assays.

5.2.2. Glycerol stocks

To preserve living organisms, spore suspensions or bacterial liquid cultures were supplemented with a final concentration of 30 % sterile glycerol and frozen at -80 °C.

5.2.3. *N. crassa* growth assays

Inoculation of liquid cultures

Ten day old conidia were harvested as described in 5.2.1 from slants. The conidia were inoculated in a concentration of $1*10^6$ conidia/ml. The concentration of the conidia suspension was determined using a Tecan plate reader by measuring the optical density at a wavelength of 600 nm. A standardized formula was used to calculate the needed volume of the conidia suspension ($V_{conidia\ suspension}$):

$$V_{conidia\ suspension} = \frac{0.0123 * V_{final}}{(OD_{600} * dilution\ factor)}$$

The constant 0.0123 was previous determined for the used Tecan reader by cell counting with a hemocytometer of a dilution series of a conidia suspension and corresponding OD_{600} measurements of the counted dilutions. V_{final} is the volume of the medium, which was inoculated. In 96-well plates a final volume of 200 µl/well was used, in 24-deep well plates 3 ml/well, in 100 ml Erlenmeyer flasks 50 ml medium and in 250 ml Erlenmeyer flasks

100 ml medium. If not stated otherwise, medium consisted of 1x Vogel´s salt solution [Vogel 1956] supplemented with 2% (w/v) carbon source.

Pre-cultures followed by medium switch

As pre-culture vessels 24-deep well plates were used containing 2% fructose VMM, if not stated otherwise. Medium was inoculated as described above. The plates were covered with a breathable membrane and incubated at 25 °C, constant light and shaking at 200 rpm. Medium switches were performed as follows. Mycelium was transferred using tweezers into 50 ml 1x Vogel´s salt solutions in a 50 ml falcon tube and centrifuged at 2,000 rpm for 5 min. This washing step was repeated two times maximum. The mycelium was transferred into the main culture medium and incubated at the same conditions. Main culture medium was 100 ml 1% Avicel VMM supplemented with 0.5% glucose in 250 ml plastic Erlenmeyer flasks, if not stated otherwise.

Allyl alcohol growth assay

As cultivation vessel 24-deep well plates were used. Each well contained 3 ml Vogel´s minimal medium supplemented with 1% glucose as control condition or 1% glucose and 100 mM allyl alcohol as test condition. The medium was inoculated with fresh harvested conidia as described in “Inoculation of liquid cultures”. If not stated otherwise each strain was inoculated in both condition using triplicates. The 24-deep well plates were sealed with a sterile breathable membrane and incubated at 25 °C, 200 rpm, constant light for 24 h.
After the incubation, the mycelium was harvested and dry weight was determined as described in 5.2.4. The mycelial dry weight of each strain grown in the test condition was normalized by the control condition, and statistically compared to the WT strain data.

Culturing procedure prior to immunoprecipitation experiment

N. crassa strains listed in Table S 6-4 were inoculated from fresh conidia (as described in “Inoculation of liquid cultures”) into a first pre-culture. The cultivation of the first pre-culture was in a 24-deep well plate format with 3 ml 2% fructose VMM per well. Of each strain six replicates were inoculated and incubated for 16 h at 30 °C and 200 rpm and constant light. Afterwards, the grown mycelium of each strain was transferred into a second pre-culture consisting of 50 ml 2% fructose VMM per 250 ml glass Erlenmeyer flask. The second pre-culture was incubated at the same conditions. After 24 h growth in the second pre-culture, the mycelia were washed in conical tubes containing 50 ml 1x Vogel´s salt solution and centrifuged at 2,000 rpm for 5 min. The washed mycelia were transferred into the main culture consisting of 100 ml 1% Avicel VMM in 250 ml plastic Erlenmeyer flasks, which corresponds to the “derepressing condition”. The main culture was incubated for 24 h again

at 30°C, 200 rpm and constant light. Afterwards, three replicates of each strain were supplemented with a final concentration of 2% glucose and incubated for additional 4 h at the same settings and were harvested afterwards. This corresponds to the “repressing condition”. The remaining three replicates per strain were harvested after 24 h in the main culture. The mycelia were harvested using a Büchner funnel and directly transferred into 15 ml conical tubes and immediately frozen with liquid nitrogen. The tubes were stored at -80 °C. The mycelia were used for protein extraction followed by immunoprecipitation as described in 5.4.6.

Culturing procedure prior to qPCR and RNA-sequencing experiment

Inoculated slants were incubated at 30 °C for two days in the dark, then at 25 °C in constant light to avoid the influence of the circadian rhythm on gene expression levels. Ten day old conidia were used to inoculate liquid cultures as described in “Inoculation of liquid cultures”. The culturing was performed as described in Table 5-10 and Table 5-11. For all culturing steps 24-deep well plates were utilized as cultivation vessels containing 3 ml medium per well. For qPCR experiments each strain was grown in duplicates per time point and condition. For the RNA sequencing experiment strains were grown in triplicates per time point and condition. Strains used in this experimental setup were *N. crassa* WT (FGSC #2489), Δ*fbx17* (nLK024III), Δ*fbx41* (nLK009) and ΔNCU05033 (nLK020).

Table 5-10: Culturing procedure and time points for first qPCR experiment.
D = derepressing condition. R = repressing condition. Between each medium switch, mycelia were washed in petri dishes containing 1x Vogel´s three times for each 5 min.

	Day 1	**Day 2**	**Day 3/ Day 4**
Switch from D to R	pre-culture: 2% Fructose VMM	De-repressing cond.: 1% Avicel VMM	Repressing cond.: 2% glucose VMM
Cultivation period and harvesting time points	16 h	24 h	t_0 harvest directly from D t_4, t_8, t_{24} = harvest after h as indicated
Switch from R to D	Repressing cond.: 2% glucose VMM	De-repressing cond.: 1% Avicel VMM	
Cultivation period and harvesting time points	16 h	t_0 harvest directly from R t_4, t_8 = harvest after h as indicated	t_{24} = harvest after h as indicated

Since Δ*fbx17* and Δ*fbx41* did not form comparable biomass amounts than the WT and ΔNCU05033, the cultivation time points were improved, see Table 5-11.

Table 5-11: Culturing procedure and time points for second qPCR and RNA-seq experiment. D = derepressing condition. R = repressing condition. Between each medium switch, mycelia were washed in petri dishes containing 1x Vogel´s three times for each 15 min (45 min washing in total).

	Day 1	**Day 2**	**Day 3**
Switch from D to R	pre-culture: 2% Fructose VMM	De-repressing cond.: 1% Avicel VMM	Repressing cond.: 2% glucose VMM
Cultivation period and harvesting time points	24 h	24 h	**qPCR:** t_0 harvest directly from D t_1, t_2, t_4 = harvest after h as indicated **RNA-seq:** t_0 harvest directly from D $t_{0.5}$, t_8 = harvest after h as indicated
Switch from R to D	Repressing cond.: 2% glucose VMM	De-repressing cond.: 1% Avicel VMM	
Cultivation period and harvesting time points	24 h	**qPCR:** t_0 harvest directly from R t_6, t_8 = harvest after h as indicated **RNA-seq:** t_0 harvest directly from R t_5 = harvest after h as indicated	**RNA-seq:** t_{24} = harvest after h as indicated

The harvesting procedure was done as follows. The mycelia were quickly dried on a tissue and each subsequently transferred into a tube containing 0.25 to 0.30 g Zirconium beads. The tubes were directly frozen using liquid nitrogen and stored at -80 °C until RNA was extracted as described in 5.3.10.

5.2.4. Determination of mycelial dry weight

To determine mycelial dry weight, the mycelium grown in a liquid culture was harvested using tweezers (after cultivation in 24-deep well plates) or a Büchner funnel covered with filter paper (after cultivation in larger volumes than 3 ml).

The mycelium was transferred into pre-weighted and numbered aluminum pans and dried overnight or over the weekend at 80 °C in an oven. Then, the aluminum pans with the dry biomass were weighed and the weight of the aluminum pans was subtracted to receive the weight of the dry biomass.

5.2.5. Homokaryotization of *N. crassa* via microconidia isolation

To receive the predominantly uninucleate *N. crassa* microconidia, the corresponding strain was inoculated on 2% water agar and incubated in a humidity chamber at 30 °C in the dark for three days. Afterwards, the plate was incubated for four days at room temperature

exposed to a day:night cycle. Then, 2 ml sterile water were added onto the plate to wash and collect the microconidia. The microconidia suspension was added into a sterile syringe and filtered through a filter with 5 µm pore size into a sterile 1.5 ml tube. The microconidia suspension was centrifuged for 7.5 min at full speed and 8 °C. Except 100 µl, the supernatant was discarded. The pellet was resuspended in the remaining 100 µl and spread dropwise onto a VMM agar plate and distributed using a Drigalski spatula. The plate was incubated at 30 °C overnight in the dark.
Germinating microconidia were picked under the stereo microscope and transferred into agar slants containing VMM. After one week, conidia were harvested and preserved as described in 5.2.2 and genomic DNA was extracted for genotyping as described in 5.3.9.

5.2.6. Crossing of *N. crassa* strains

To perform *Neurospora crassa* crossings, one mating type, either mat A or mat a, was inoculated as female strain on a Westergaard´s agar plate. The opposite mating type was inoculated on an agar slant containing Vogel´s minimal medium. Both strains were incubated in the dark at 30 °C for two to three days. Afterwards both strains were incubated in a day:night cycle (12:12 h) at room temperature for five to seven days, until the strain growing on the Westergaard´s agar plate developed protoperithecia. To perform the mating, conidia were harvested from the slant by adding 1 ml sterile ddH_2O into the slant, vortexing it and transferring the spore suspension into a 1.5 ml reaction tube. Conidia were separated from residual hyphae via centrifugation at 1,000 rpm for 1 min. The supernatant was discarded and the conidia pellet was dissolved in 500 µl ddH_2O. The conidia suspension was added dropwise onto the Westergaard´s plate containing the opposite mating type.
The agar plate was incubated at room temperature in a closed chamber for seven days until the perithecia fully developed.
Ascospores were harvested from the lid of the petri dish by adding 100 µl to 1 ml sterile ddH_2O onto the lid. Ascospores were collected via pipetting and transferred into a sterile 1.5 ml reaction tube. The spores were centrifuged at 4,000 rpm for 1 min and supernatant was discarded. Ascospores were resuspended in 500 µl sterile ddH_2O and stored at 4 °C.

Plating ascospores

To retrieve a strain of one ascospore a 1:10 dilution of harvested ascospores was prepared using sterile water. 100 µl of the dilution were heat shocked at 60 °C for 30 minutes. The heat shocked dilution was added dropwise onto a Vogel´s minimal medium (VMM) agar plate containing the corresponding supplements for auxotrophic strains or hygromycin for deletion strains. The plate was incubated at room temperature overnight. On the next day,

single germinating ascospores were picked under the stereo microscope and transferred into agar slants containing VMM with the corresponding supplements. The strains were propagated as described in 5.2.1. The genotype was confirmed as described in 5.3.2 of gDNA extracted as described in 5.3.9. Strains originating from crossings are listed in Table S 6-3. To determine unknown mating type of strains, both *N. crassa fluffy* mutants were used as female crossing partners.

5.2.7. Race tube assay

The race tube assay was performed using biological duplicates. Sterile 25 ml serological pipettes were filled with 13 ml of 2% sucrose VMM containing agar and used as race tubes. The pipette tip was removed once the agar was solid. Open ends were closed using sterilized lids. At the 3 ml line of each race tube 2 µl of conidia suspension with an OD_{600} of 0.0123, which corresponds with approximately 2,000 conidia, were added to inoculate the race tube. The race tubes were incubated at 25 °C in constant darkness for 24 h. Afterwards, the tubes were transferred to constant light at 25 °C. The hyphal growth front was labeled and served as time point 0 h. The growth front was measured using a ruler throughout three days from the labeled darkness-to-light transition line.

5.3. Molecular biological methods

5.3.1. PCR for cloning using Phusion polymerase

The Phusion polymerase was used to amplify DNA fragments for cloning experiments. The PCR reaction pipetting scheme and the thermocycler program can be found in Table 5-12 and

Table 5-13. To proceed with cloning after the PCR reaction, the PCR products were separated by size (5.3.3) and purified from the agarose gel (5.3.4).

Table 5-12: Phusion polymerase PCR amplification reaction master mix.

component	volume (µl)
ddH_2O	35.4 (33.6 with DMSO)
5x Phusion HF Buffer	10
10 mM dNTPs	1
DMSO (optional)	1.5
Phusion DNA polymerase	0.5
Forward primer (10 µM)	2.5
Reverse primer (10 µM)	2.5
DNA template	1 (plasmid) or 2.5 (gDNA)

Table 5-13: Thermocycler protocol for Phusion polymerase PCR amplification.

cycles	step	temperature (°C)	time (m:s)
	initial denaturation	98	05:00
30- 35	denaturation	98	00:10
	annealing	60[a]	00:30
	elongation	72	00:30[b]
	final elongation	72	10:00
	hold	16	infinite

[a] annealing temperature was dependent from the used primer pair.
[b] 30 seconds elongation time was set per 1 kb PCR fragment size.

5.3.2. Genotyping PCR using Taq polymerase

With Taq DNA Polymerase all genotyping or colony PCRs were performed. The recipe of the 5x Taq buffer is in Table 5-5, the PCR reaction master mix in Table 5-14 and the used thermocycler protocol in Table 5-15. All PCR reactions were prepared on ice. DMSO was used optional as troubleshooting. Custom DNA oligos were received from Eurofins Genomics in tubes. For colony PCRs the corresponding *E. coli* colony was picked with a pipette tip and added directly into the PCR reaction tube.

Table 5-14: Taq polymerase PCR amplification reaction master mix.

component	volume (µl)
ddH_2O	8.2 (7.9 with DMSO)
5x Taq buffer	3
10 mM dNTPs	0.3
DMSO (optional)	0.3
Taq DNA polymerase	0.5
Forward primer (1:10 dilution)	1
Reverse primer (1:10 dilution)	1
gDNA (optional)	1.5

Table 5-15: Thermocycler protocol for Taq polymerase PCR amplification.

cycles	step	temperature (°C)	time (m:s)
	initial denaturation	95	05:00
35	denaturation	95	00:30
	annealing	60[a]	00:30
	elongation	72	01:00[b]
	final elongation	72	00:30
	hold	16	infinite

[a] annealing temperature was dependent from the used primer pair.
[b] 1 min elongation time was set per 1 kb PCR fragment size.

5.3.3. Agarose gel electrophoresis

Gloves were worn while working with the DNA staining component Midori Green. For the separation of nucleic acids by size a 1% agarose gel was prepared. The agarose was dissolved in 1x TAE buffer by heating (see recipe for 50x stock solution in Table 5-5). Midori Green was added to the liquid 1% agarose in TAE. The gel was poured into a chamber with combs. The solidified gel was placed in an electrophoresis chamber filled with 1x TAE buffer. Samples were mixed with 6x purple loading dye (1x final concentration). A suitable DNA ladder (NEB) was added into one well of the gel, as well as the samples containing loading dye. The electrophoresis was performed at 130 V and 500 mA for about 30 min.
Qualitative PCR results were documented using a gel imaging system. For cloning, the corresponding gel bands were cut out the gel and extracted as described in 5.3.4.

5.3.4. DNA gel extraction and purification

To extract PCR products or DNA fragments for cloning from agarose gels, the targeted DNA band was cut out from the gel and transferred into a 1.5 ml reaction tube. The manufacturer instruction was followed from the Hi Yield® Gel/PCR DNA Fragment Extraction Kit (SLG). DNA was finally dissolved in water and DNA concentration was determined using the Infinite 200 PRO NanoQuant reader.

5.3.5. Restriction digest and ligation cloning of *N. crassa* expression cassettes

For cloning, PCR products from Phusion PCR approaches (5.3.1) were used. The plasmid pCCG::C-Gly::GFP (Figure S 6-24) served as vector backbone for *gfp*-tagged constructs.

The restriction digest of both insert and vector was prepared as described in Table 5-16.

Table 5-16: Composition of restriction digest approach.

component	Volume (µl) or amout
DNA	1 µg
CutSmart buffer (NEB)	5
Restriction enzyme XbaI (20 units/µl)	0.5
Restriction enzyme PacI (10 units/µl)	1
water	50 µl (deducting volume of DNA)

The restriction digest approaches were incubated for 1 hour at 37 °C and separated by size in a gel electrophoresis as described in 5.3.3 and cut out from the gel and purified as described in 5.3.4.

For the T4 ligation approach a molar ratio of 3:1 of the insert:vector was used and 100 ng vector backbone were used for the cloning approach. The required insert DNA mass per ligation approach was calculated according to the following formula: required mass insert (g) = desired insert/vector molar ratio x mass of vector (g) x ratio of insert to vector lengths. The used mass of each insert per ligation approach is listed in Table 5-17.

Table 5-17: Required insert DNA mass per T4 ligation approach.

Used primers for fragment amplification	Fragment length (bp)	Final plasmid name	Amount of insert per ligation approach (ng)
oJPB923 + oJPB924	2339	pLK052	82.73
oJPB925 + oJPB926	3230	pLK053	114.2
oJPB927 + oJPB928	3056	pLK054	108.1
oJPB929 + oJPB930	2092	pLK055	73.99
oJPB931 + oJPB932	1906	pLK056	67.41
oJPB933 + oJPB934	1788	pLK057	63.24
oJPB1094 + oJPB1095	1313	pLK058	46.44

For each ligation approach the following components were combined.

Table 5-18: T4 ligation assembly approach.

component	amount
T4 DNA ligase buffer (10x)	2 µl
vector DNA	100 ng
insert DNA	see Table 5-17, last column
Nuclease-free water	up to 20 µl final volume
T4 DNA ligase	1 µl

Each assembly approach was gently mixed and incubated for 10 min at room temperature, then heat inactivated at 65 °C for 10 min. The assembly approach was stored on ice prior to transformation into competent *E. coli* cells as described in 5.3.6.

5.3.6. *Escherichia coli* transformation

To verify and amplify plasmids E. coli TG-1 cells (Table 5-4) were heat shock transformed as follows. TG-1 cells were thawed on ice for 10 min. Then, 50 µl of ice-cold 5x KCM (Table 5-5) were added into the tube containing the cells and carefully mixed by pipetting. 50 µl from this cell suspension were used per transformation approach and transferred into a fresh reaction tube. 4 µl of the assembled plasmid (approximately 100 ng/µl) were added to the cells and incubated for 5 min on ice. Afterwards, the cells were heat shocked at 42 °C

for 90 sec. Before 150 µl LB medium (Table 5-5) were added, the cells were placed on ice for 2 min.
The transformation approach was incubated at 37 °C for 45 min and plated afterwards on LB agar plates containing Ampicillin. The plate was incubated at 37 °C overnight.

5.3.7. *E. coli* plasmid miniprep and sequencing

To extract plasmids from *E. coli*, the Hi-Yield Plasmid Mini Prep DNA isolation kit (SLG) was used according to the manufacturer instructions. Plasmid concentrations were determined using the Infinite 200 PRO NanoQuant reader.
To sequence plasmids after cloning, the Mix2Seq Kit (Eurofins Genomics, Ebersberg, Germany) was used following the manufacturer protocol and with customized sequencing primers (Table 5-7). DNA samples were stored at -20 °C.

5.3.8. *N. crassa* transformation by electroporation

For the transformation of *N. crassa* histidine auxotrophic strains were used. The strains were pre-grown in 250 ml Erlenmeyer flasks containing solid VMM supplemented with histidine. 10 day old conidia were harvested by pouring 50 ml ice-cold 1 M sorbitol into the flask, vortexing it and pouring the conidia suspension through sterile gauze into a sterile 50 ml conical tube. The tube was centrifuged first at 2,000 rpm for 5 min at 4 °C, then the supernatant was discarded and fresh ice-cold 1 M sorbitol was filled into the tube and vortexed. After centrifugation at 1,500 rpm for 5 min at 4 °C, the supernatant was discarded again and the tube was filled with fresh ice-cold 1 M sorbitol. This step was repeated two more times. After the last centrifugation step, the conidia pellet was resuspended in 5 ml ice-cold sorbitol. This suspension was measured for optical density at 600 nm using the Infinite 200 PRO NanoQuant reader. An OD_{600} of 0.0123 corresponds with a concentration of $1*10^6$ conidia/ml. The volume of sorbitol was calculated which needs to be added to the conidia pellet to reach a concentration of $2.5*10^9$ conidia/ml. The conidia suspension was centrifuged at 2,000 rpm for 5 min at 4 °C, the supernatant was discarded and the pellet was resuspended in the calculated amount of sorbitol.
Up to 5 µl, 1 to 2 µg total DNA, of the corresponding *his-3*-targeting plasmid which should be transformed were added into a sterile 1.5 ml reaction tube. For each transformation approach and strain, one negative control was added containing 5 µl sterile water. In total, 40 µl conidia suspension were added per tube containing either DNA or the negative control. After an incubation of 30 min on ice, the conidia-DNA mixture was transferred into an ice-cold 1 mm gap cell cuvette. To conduct the electroporation, the cuvette was added into an Eppendorf Eporator® setting the voltage to 1,500 V.

Subsequently after the electroporation 950 µl ice-cold sorbitol were added into to cuvette. The electroporated conidia were transferred into a 15 ml conical tube containing 2 ml liquid VMM and incubated at 30 °C for one hour. Afterwards, the conidia were centrifuged at 1,500 rpm for 2 min. 2 ml of the supernatant were discarded and the pellet was resuspended in the remaining supernatant. Two additional 15 ml tubes were filled with 10 ml warm, liquidated top agar (Table 5-5). Into one tube 250 ml conidia suspension were added and mixed through inversion and 750 µl were added into the other. Each tube was distributed onto a petri dish containing bottom agar (Table 5-5).
The plates were incubated for three days in the dark at 30 °C. Then, growing *N. crassa* colonies were picked and transferred into slants and grown as described in 5.2.1.

5.3.9. gDNA extraction from *N. crassa* conidia

To extract gDNA from *N. crassa* conidia, the conidia suspension, harvested as described in 5.2.1, was transferred into a tube containing 0.25 to 0.30 g Zirconium beads. 400 µl lysis buffer were added to the tube containing the conidia and the beads. The tube was beat-beaten using a laboratory bead mill for 1 min at maximum speed (400) and incubated afterwards for 30 min at 65 °C. Then 80 µl of 1 M Tris-HCl (pH 7.5) were added. The mixture was centrifuged at 14,000 rpm for 1 min. The supernatant was transferred into a 1.5 ml reaction tube and an equal volume of phenol:chloroform:isoamylalcohol (25:24:1) was added and mixed by vortexing. The tube was centrifuged at 14,000 rpm for 10 min. Afterwards, the aqueous phase was transferred into a fresh 1.5 ml reaction tube and 600 µl of -20 °C cold ethanol (95%) were added and mixed by inverting the tube.
The tube was incubated at room temperature for 10 min and centrifuged at 14,000 rpm for 15 min. Supernatant was discarded and the DNA pellet was washed with 500 µl ice-cold ethanol (70%) and centrifuged at 14,000 rpm for 5 min. The supernatant was discarded and residual ethanol was collected through a quick spin of the tube in the centrifuge and also discarded. In the sterile bench the DNA pellet was air dried for 10 min. In 50 µl ddH_2O the DNA pellet was resuspended and incubated at 37 °C to dissolve the DNA. Storage of gDNA occurred at -20 °C.

5.3.10. RNA extraction from *N. crassa* biomass

While working with RNA, fresh gloves were worn at all times. The utilized equipment and all surfaces were first cleaned with 70 % ethanol and treated with RNase Away (Kisker). Only RNase-free low-binding reaction tubes were used as well as clean pipette tips. Work with RNA was always performed on ice if not stated otherwise. Handling of toxic substances was only done in fume hoods.

The tubes suitable for beat-beating, which contained *N. crassa* mycelium and beads (see "Culturing procedure prior to qPCR and RNA-sequencing experiment"), were placed on ice and 1 ml RNA-Solv® reagent (VWR) were added per tube. Each tube was beat-beaten using a laboratory bead mill three times for 30 sec at maximum speed (400) and afterwards gently shook at room temperature for 10 min on a flat shaker. 200 µl chloroform were added per tube and vortexed. On a shaker, the tubes were incubated at room temperature for additional 10 min. Then the tubes were centrifuged for 15 min at 12,000 x g and 4 °C. Avoiding debris layer, approximately 400 µl of the aqueous phase were transferred into a fresh nuclease-free reaction tube. RNA was precipitated by adding 500 µl 2-propanol per tube, mixing it well immediately and incubating it at room temperature for 10 min. Then, tubes were centrifuged for 10 min at maximum speed and 4 °C. Supernatant was carefully discarded. RNA pellet was washed by adding 1 ml 75% ethanol, briefly vortexing and centrifugation at 7,500 x g for 5 min at 4 °C. The supernatant was discarded and the tubes were shortly centrifuged to remove remaining supernatant. The RNA pellet was dried for 5 to 10 min in a sterile bench. To dissolve the RNA, 90 µl RNase-free water were added per tube and the tubes were incubated for 5 to 10 min at 60 °C.
RNA concentrations were determined using the Infinite 200 PRO NanoQuant reader.
The half of each RNA sample, 45 µl, were transferred into a new RNase-free reaction tube. One tube of each RNA sample was stored at -80 °C as backup, into the other tube 5 µl DNase buffer were added and 1 µl DNase I. The tube was incubated at 37 °C for 30 min. Then, 0.5 µl DNase I were added again into the tube which was incubated for additional 30 min at 37 °C.
The DNase I treated RNA samples were purified by using the GeneJET RNA purification kit (Thermo Fisher Scientific) according to the manufacturer instructions for "RNA cleanup after DNase I digestion". The final step of RNA purification diverged from of the manufacturers protocol. The RNA samples were eluted two times in 35 µl RNase-free water. RNA concentrations were determined using the Infinite 200 PRO NanoQuant reader.
The RNA samples were stored at -80 °C. To check the quality of RNA samples for RNA sequencing, an agarose gel was prepared as described in 5.3.11. For qPCR experiments, RNA was transcribed into cDNA (see 5.3.12).

5.3.11. Quality control of RNA samples

For quality control of RNA samples prior to RNA sequencing, the samples were checked in an agarose gel containing bleach. A 2% agarose gel in TAE buffer was prepared containing 2.5 ml bleach 6% per 50 ml gel. After adding the bleach, the liquidized gel was incubated for 5 min at room temperature. 2 to 8 µl RNA sample were mixed with purple loading dye

and pipetted into the wells of the solidified gel. One well was filled with a ladder. The samples were run at 135 V, 500 mA for 0.6 h. For total RNA extracts, two bands were expected at a size of 1 kb and between 1.5 to 2 kb. RNA samples which showed two expected bands were send for RNA sequencing as described in 5.5.1.

5.3.12. cDNA synthesis and quantitative PCR

For the synthesis of cDNA, 1 µg RNA (see 5.3.10) was diluted to a final volume of 10 µl in nuclease-free water. Buffers and solutions of the FastGene Scriptase Basic cDNA kit (Nippon Genetics) were used. To each tube containing RNA, 1 µl oligo dT primer were added for cDNA synthesis starting at the 3´ end, and incubated at 42 °C for 5 min.
Then, 2 µl 10x FastGene® Scriptase basic buffer, 1 µl FastGene® Scriptase basic (200 units/µl), 2 µl dNTP mixture, 2 µl oligo dT primer, 0.5 µl RNase inhibitor and 1.5 µl nuclease-free water were added into the tube containing RNA to achieve a final volume of 20 µl.
This mixture was incubated at 42 °C for 60 min, then for 5 min at 90 °C. cDNA was stored on ice for short term storage and at -20 °C for long term storage.
To perform a quantitative PCR (qPCR) the following steps were performed.
First the primer mixture was prepared. 30 µl of a 1:10 dilution of oJPB325 and 30 µl of a 1:10 dilution of oJPB320 were mixed together with 127.5 µl nuclease-free water in one tube. This primer pair was used to quantify the housekeeping gene actin, *act* (NCU04173). Then, 30 µl of a 1:10 dilution of oJPB544 and 30 µl of a 1:10 dilution of oJPB545 were mixed together with 127.5 µl nuclease-free water in one tube. This primer pair was used to quantify the gene of interest exoglucanase 1, *cbh-1* (NCU07340).
For each sample and technical replicate 5 µl SyGreen mix (qPCRBIO SyGreen Mix Separate-ROX, Nippon Genetics) were used without adding the ROX additive. 2 µl nuclease-free water and 0.5 µl template cDNA were added. For the no template control (NTC) 0.5 µl nuclease-free water were added instead of cDNA. 7.5 µl of this mixture were added per MIC qPCR tube. Into each tube 2.5 µl of the corresponding primer mixture were added. If not stated otherwise, technical triplicates were done for each biological replicate.
The tubes were closed using the provided caps and added into the MIC Magnetic Induction Cycler (Biozym). The Magnetic Induction Cycler was used according to manufacturer instructions.

5.4. Biochemical methods

If not stated otherwise, all experiments including *N. crassa* strains or culture supernatants were performed in triplicates.

5.4.1. Protein quantification assay according to Bradford

The quantify total protein amounts, the Bradford assay was performed using the Bradford solution of Carl Roth. The assay was performed according to the manufacturer instructions chapter “D. Protein assay in 96-well culture plates”. The calibration standard was prepared differently according to the pipetting schedule in Table 5-19.

Table 5-19: Pipetting schedule for BSA calibration standard for Bradford assay.

BSA [µg/ml]	µl BSA solution	ddH_2O
500.0	500 µl out of 1 mg/ml	500 µl
250.0	500 µl out of 0.5 mg/ml	500 µl
125.0	500 µl out of 0.25 mg/ml	500 µl
62.5	500 µl out of 0.125 mg/ml	500 µl
31.3	500 µl out of 0.0625 mg/ml	500 µl
15.6	500 µl out of 0.03125 mg/ml	500 µl
7.8	500 µl out of 0.015625 mg/ml	500 µl
0	0	1000 µl

Protein samples were first measured undiluted and only measured diluted, if the resulted OD_{595} value was out of the linear range of the standard curve. To determine the total protein amount in µg/ml, the following formula was applied on the standard curve.

$$\text{protein amount } \left(\frac{\mu g}{ml}\right) = \frac{\left(\left(OD_{sample} - OD_{average\ blank}\right) \pm b\right)}{m}$$

Within the linear equation above, b is the y-intercept and m is the slope.

5.4.2. Determination of enzymatic activity of *endo*-1.4-β-D-glucanase (cellulase)

To determine the enzymatic activity of cellulases, a modified procedure of the manufacturers protocol using Azo-CM-Cellulose (Megazyme) was followed. The substrate dissolution was performed according to instructions of the manufacturer. One-fold master mix for the assay procedure consisted of 80 µl Azo-CMC-substrate, 20 µl 1 M sodium acetate at pH 5 and 50 µl ddH_2O. Per reaction, 150 µl master mix were added into a 1.5 ml reaction tube. Each sample was measured in technical duplicates. 10 µl sample or water blank were added into the lid of the reaction tube. The lids were closed carefully and all

reactions from one run were centrifuged simultaneous in a quick spin up to 7,000 rpm in a tabletop centrifuge. The tubes were immediately incubated at 37 °C on a heating block for 10 min. 400 µl precipitant solution (Table 5-5) were added into each tube. The tubes were vortexed and centrifuged at 4,000 rpm for 2 min. Two times 200 µl supernatant per tube were transferred into a transparent 96-well plate. The optical density was measured at 590 nm using a plate reader. To convert absorbance to Units of activity, the following modified formula was used.

$$\text{activity}\left(\frac{\text{U}}{\text{ml}}\right) = (412.5 * (\text{OD}_{590}\,\text{of sample} - \text{blank}) - 6) * 100 * (\frac{1}{1000})$$

The factor 100 is the conversion from 0.01 ml (10 µl supernatant per assay) to 1 ml. 1/1000 is the conversion from milliUnits to Units. 6 is the y-intercept and 412.5 the slope of the formula provided by the manufacturer.

5.4.3. Sodium dodecyl sulfate polyacrylamide gel electrophoresis (SDS-PAGE)

Sample preparation

Three parts of each protein sample was diluted with one part of 4x Laemmli buffer (Table 5-5), vortexed and boiled at 95 °C for 5 minutes and immediately transferred on ice.

SDS-PAGE gel preparation and electrophoresis

The chamber glasses were assembled according to the manufacturer instructions. A 10% acrylamide separating gel was prepared and poured, if not stated otherwise.

Table 5-20: Composition of acrylamide separating gel for SDS-PAGE.

Ingredients	amount (ml) 8% acrylamide gel	amount (ml) 10% acrylamide gel
Double destilled water	4.6	3.8
Acrylamide/Bis-acrylamide (37.5:1)	2.6	3.4
1.5 M Tris-HCL, pH 8.8	2.6	2.6
10 % (w/v) SDS	0.1	0.1
To be added direclty before pouring the gel:		
10% (w/v) ammonium peroxydisulphate	0.1	0.1
TEMED	0.01	0.01

Immediately after pouring the separating gel, the gel was covered with 2-propanol, to flatten the surface. After solidification of the gel, the 2-propanol was removed and carefully washed with destilled water and dried with whatman paper.

The stacking gel was prepared (Table 5-21) and added on top of the solid separating gel. A comb was added on top of the gel.

Table 5-21: Composition of a stacking gel for SDS-PAGE.

Ingredients	amount (ml)
Double destilled water	2.975
0.5 M Tris-HCL, pH 6.8	1.25
10 % (w/v) SDS	0.05
Acrylamide/Bis-acrylamide (37.5:1)	0.67
To be added direclty before pouring the gel:	
10% (w/v) ammonium peroxydisulphate	0.05
TEMED	0.005

The solidified gel was placed in the running chamber. The 10x running buffer (Table 5-5) was diluted to 1x concentration using ddH_2O. The chamber was filled with 1x running buffer according to manufacturers instructions and the comb was removed. 5 µl BlueStar Prestained Protein Marker (NIPPON Genetics EUROPE GmbH) was added into one well per gel when the gel was silver stained and 3 µl ladder was used if the gel was used for western blotting. If not stated otherwise, 15 µl Laemmli treated protein sample was load per well. The gel was run at 80 V for 20 min. Afterwards for at least 1 h at 120 V.

5.4.4. Silver staining of protein gels

SDS gels were silver stained as follows. The incubation steps were performed at room temperature during gentle shaking. After the electrophoresis, the SDS gel was incubated overnight in fix solution. Afterwards, the gel was washed three times for 5 min with wash solution and rehydrated for 20 min in ddH_2O. Background was decreased by incubating the gel for 1 min in background solution. Then the gel was washed two times for 5 min in ddH_2O and exposed to silver for at least 30 min. For 1 min, the gel was washed in ddH_2O and incubated for 2 to 10 min in revelation solution. When the desired staining grade was achieved, fix solution was added into the revelation solution to stop the reaction. Finally, the gel was washed in water and visualized using the gel imaging system Fusion solo S (Vilber Lourmat) using the conversion screen.

5.4.5. Coomassie Blue staining of protein gels

SDS gels were incubated in Coomassie staining solution at room temperature for approximately 1 h, until staining of the gel was observed. The staining solution was discarded and the gel briefly rinsed in ddH_2O. The gel was incubated in Coomassie destaining solution until the desired decrease of the background was achieved and only the protein bands were still stained blue.

5.4.6. Protein extraction and immunoprecipitation

The frozen mycelium (see also “Culturing procedure prior to immunoprecipitation experiment”) was freeze dried and grounded. 5 ml of B250 lysis buffer containing all supplements (Table 5-5) were added to each conical tube containing the grounded freeze-dried mycelium. After 2.5 h on an end-over-end rotator at speed 10 at 4 °C, the cell lysates were centrifuged at maximum speed for 20 min at 4 °C. The supernatants were transferred into 5 ml reaction tubes. Total protein amount of the supernatants was determined according to Bradford, as described in 5.4.1.

The GFP-trap agarose beads were equilibrated by adding 500 µl B250 buffer to 20 µl bead resin into a 2 ml protein-LoBind reaction tube and incubating it on ice for 10 min.

The beads were sedimented by centrifugation at 2,500 x g for 5 min at 4 °C. The supernatant was discarded and the equilibration strep was repeated by adding again 500 µl B250 lysis buffer and collecting the resin via centrifugation. The supernatant was discarded. A total amount of 10- 15 mg protein extract were added per GFP-trap resin tube. The beads and the lysate were incubated on an end-over-end rotator at 4 °C for 1 h and 40 min.

Afterwards, the beads were collected by centrifugation at 2,500 x g for 5 min at 4 °C. Supernatant was discarded and the beads were resuspended in 500 µl B250 lysis buffer which did not contain NP-40 and DTT.

The beads were collected again by centrifugation at 2,500 x g for 5 min at 4 °C. Supernatant was discarded and the beads were resuspended in 500 µl B250 lysis buffer which did not contain NP-40 and DTT. Again, the beads were collected by centrifugation at 2,500 x g for 5 min at 4 °C. Supernatant was discarded and the beads were resuspended in 500 µl B250 lysis buffer which did not contain NP-40 only. During the last washing step, the beads were transferred into a new 1.5 ml protein-LoBind reaction tube and collected by centrifugation at 2,500 x g for 5 min at 4 °C. The supernatant was discarded.

To eluate the proteins bound to the GFP-trap agarose beads, the beads were resuspended in 80 µl 2x SDS elution buffer (Table 5-5) and boiled at 95 °C for 5 min to dissociate immunocomplexes from beads. The beads were sedimented by centrifugation at 2,500 x g for 2 min at 4 °C. The supernatant was analyzed for quality control in SDS-PAGE and western blot as described in 5.4.3 and 5.4.7. Finally, the supernatant was used for trypsin digestion and mass spectrometry analysis, as described in 5.4.8. All samples used for immunoprecipitation and mass spectrometry analysis are listed in Table S 6-5.

5.4.7. Fusion protein detection by Western Blotting

To detect proteins via western blotting, 8% acrylamide SDS-PAGE gels were used, as described in 5.4.3. Whatman filter paper was cut to the size of the Mini Trans-Blot Module

fiber pads four times. The Whatman filter paper and two fiber pads were pre-soaked in transfer buffer. A PVDF membrane was cut to the size of the SDS gel and soaked for 10 seconds in methanol.

The western blot was assembled as follows. Onto the black side of the gel holder cassette a fiber pad was placed. On top of the fiber pad, two Whatman filter papers, then the SDS gel followed by the PVDF membrane were placed. Finally, two Whatman filter papers and one fiber pad were placed on top of the membrane. The cassette was closed and placed into the chamber according to manufacturer instructions.

A small magnetic stirrer was placed inside the wet transfer chamber and the cassette containing the gel and the membrane. According to manufacturer instructions the transfer buffer was filled into the chamber. During stirring of the transfer buffer, the wet transfer was performed overnight at 4 °C, 30 V and 0.16 A.

On the next day, the PVDF membrane was developed as follows. For 20 min the membrane was incubated in blocking buffer during constant shaking at 4 °C. The blocking buffer was removed and 15 ml fresh blocking buffer containing 15 µl of the first antibody (Anti-GFP from mouse IgG1κ) were added to the membrane and incubated for 1 h at 4 °C during constant shaking. Afterwards, the buffer containing the first antibody was discarded and the membrane was washed three times in TBST buffer for each 5 min at 4 °C, constant shaking. After the last washing step, TBST was discarded and 15 ml blocking buffer containing 2 µl of the second antibody (Goat anti-Mouse IgG, HRP) were added to the membrane and incubated for 1 h at 4 °C during constant shaking. Then, the buffer containing the second antibody was discarded and the membrane was washed three times in TBST buffer for each 5 min at 4 °C, constant shaking. As a last washing step, the membrane was washed in 1x TBS buffer for 5 min. To visualize the antibody bound protein the *SuperSignal™ West Pico PLUS Chemiluminescent Substrate* was used. The membrane was placed on the black tray of the gel imaging system. Of each component from the chemiluminescent substrate, 5 ml were added to a 15 ml conical tube and mixed by inversion. The two mixed components were directly poured onto the membrane on the black tray. After 5 min the membrane was visualized using the gel imaging system and the accumulation settings of the serial mode.

5.4.8. Trypsin in-gel digestion of protein samples after immunoprecipitation

The tryptic in-gel digestion was performed at the Bavarian Center for Biomolecular Mass Spectrometry (BayBioMS) in Weihenstephan, Freising. The procedure was performed as established at the BayBioMS using the buffers available there.

From each immunoprecipitation approach (procedure described in 5.4.6, all samples are listed in Table S 6-5) 30 µl eluate were loaded per well into a NuPageTM 4-12% Bis-Tris

gel (Thermo Fisher Scientific). Every second well was left empty to avoid cross contaminations. The gels were run at 200 V, 500 mA for 6 min, according to the standard protocol of the BayBioMS.

The gels were stained and destained in square petri dishes according to the following procedure. The gels were incubated at room temperature during shaking for 30 min in fixing solution (40% methanol, 20% acetic acid). The solution was discarded and the gels were incubated for 30 min in staining solution (30 ml Coomassie Blue (Roti-Blue 5x Roth), 80 ml methanol, 290 ml ddH_2O). Then, the gels were shortly washed in Pre-destaining solution (5% acetic acid, 25% methanol) and incubated for 15 min in destaining solution (1% acetic acid, 25% ethanol). The destaining solution was continuously replaced until the gels were destained. The gels were stored in storage solution (1% acetic acid) at 4°C until the next day.

On the next day, the gel bands were cut off the gel and each was placed into one well of a 96-well plate with predrilled holes within each well. Using tweezers, the gel bands were cut into small pieces. Then a destaining step was done by adding 100 µl of a solution consisting 50% from 5 mM Triethylammonium bicarbonate buffer (TEAB, Sigma, T7408) and 50% from ethanol. The gel pieces were incubated for 45 min at 55 °C. A collection plate, 96-well format, was placed underneath the plate containing the gel pieces. The plates were centrifuged for 1 min at 1,500 rpm and the collected solution in the lower plate was discarded. The destaining step was repeated one more time. Then, a drying step was done by adding 100 µl ethanol per well and incubating the plate for 10 min at room temperature.

A reduction step was performed by adding 100 µl 10 mM DTT in 5 mM TEAB to each well and incubating for 45 min at 55 °C. The plates were centrifuged for 1 min at 1,500 rpm and the collected solution in the lower plate was discarded. Afterwards, alkylation was done by adding 100 µl 55 mM Chloroacetamide (CAA) in 5 mM TEAB and incubating for 30 min at room temperature. The plates were centrifuged for 1 min at 1,500 rpm and the collected solution in the lower plate was discarded. The gel pieces were washed with 100 µl 5 mM TEAB and incubated for 20 min at room temperature. The plates were centrifuged for 1 min at 1,500 rpm and the collected solution in the lower plate was discarded.

Two times a drying step was performed by incubating the protein samples in 100 µl ethanol for each 10 min at room temperature. After each drying step, the plates were centrifuged for 1 min at 1,500 rpm and the collected solution in the lower plate was discarded.

25 µl of 50 mM acetic acid were added to a trypsin vial (Serva) containing 25 µg lyophilized trypsin. 20 µl of the dissolved trypsin were added to 1,980 µl 5 mM TEAB. 40 µl of this trypsin TEAB solution were added into each well containing protein sample and incubated for 15 min at 4 °C. The plates were centrifuged for 1 min at 1,500 rpm and the collected solution in the lower plate was discarded. A new, V-bottom 96-well plate was placed

underneath the plate with the predrilled holes containing the protein samples. Starting from this point, the flow through was kept. 20 µl digestion buffer (5 mM TEAB) were added per well and incubated overnight at 37 °C.

Acidification was done by adding 5 µl of 5% formic acid (FA) into each well, followed by centrifugation at 1,500 rpm for 1 min. The first extraction was done by adding 20 µl 1% FA per well and incubating the digested protein samples for 30 min at room temperature, followed by centrifugation at 1,500 rpm for 1 min. This step was repeated once.

A third extraction step was performed adding 20 µl from a solution consisting to 60% from acetonitrile (ACN) and to 40% from 0.1% FA. The samples were incubated for 30 min at room temperature und centrifuged afterwards at 1,500 rpm for 1 min. 30 µl ACN were added per well and incubated at room temperature for 15 min followed by centrifugation at 1,500 rpm for 1 min. Then, 20 µl ACN were added per well and incubated at room temperature for 15 min followed by centrifugation at 1,500 rpm for 1 min. This step was repeated one more time.

Finally, the digested peptide samples were transferred from the lower V-bottom plate into 1.5 ml protein-LoBind reaction tubes and dried in a SpeedVac (ThermoFisher) for 3.5 h.

5.4.9. Mass spectrometry

The dried peptide samples (Table S 6-5) which were digested using trypsin, as described in 5.4.8 were send to the *Service Unit LCMS Protein Analytics* at the University of Göttingen. The MS-instrument used in Göttingen for data acquisition was a Exactive HF. The raw data was provided by the Service Unit and downloaded for further analysis as described in 5.6.

5.5. Transcriptome analysis

5.5.1. RNA sequencing

N. crassa liquid cultures were done as described in chapter 5.2.3 “Culturing procedure prior to qPCR and RNA-sequencing experiment”. Total RNA was extracted as described in 5.3.10 and the quality of the samples was checked as described in 5.3.11. The RNA samples (Table 5-22) were send to the chair of Animal Physiology and Immunology (TUM), where Dr. Christine Wurmser prepared the library for RNA sequencing using the Lexogen QuantSeq 3' mRNA kit.

Table 5-22: Metadata of the submitted RNA samples to the chair of Animal Physiology and Immunology (TUM) for performing sequencing.

Sample name: r = RNA. LM = Lisa Meyer. RNA concentrations were determined by Dr. Christine Wurmser using Qubit c1. Third column contains strain number of which the RNA was derived. Fourth column indicates the growth condition and sampling time point as described in Table 5-11.

sample name	RNA conc. (ng/µl)	strain	treatment/condition
rLM01	142	FGSC #2489	Derepr. to repr. t_0
rLM02	148		
rLM03	82.8		
rLM04	400		Derepr. to repr. $t_{0.5}$
rLM05	103		
rLM06	438		
rLM07	270		Derepr. to repr. t_8
rLM08	137		
rLM09	81.6		
rLM10	115	FGSC #13527 [1]	Derepr. to repr. t_0
rLM11	115		
rLM12	107		
rLM13	123		D-repr. to repr. $t_{0.5}$
rLM14	82		
rLM15	71.2		
rLM16	146		Derepr. to repr. t_8
rLM17	111		
rLM18	65		
rLM19	123	FGSC #12780	Derepr. to repr. t_0
rLM20	105		
rLM21	116		
rLM22	81.2		Derepr. to repr. $t_{0.5}$
rLM23	68.2		
rLM24	61		
rLM25	70.6		Derepr. to repr. t_8
rLM26	378		
rLM27	91		
rLM28	179	FGSC #2489	repr. to derepr. t_0
rLM29	254		
rLM30	260		
rLM31	154		repr. to derepr. t_5
rLM32	146		
rLM33	165		
rLM34	127		repr. to derepr. t_{24}
rLM35	157		
rLM36	184		
rLM37	160	FGSC #14738	repr. to derepr. t_0
rLM38	122		
rLM39	104		
rLM40	140		repr. to derepr. t_5
rLM41	147		
rLM42	71.2		
rLM43	89.4		repr. to derepr. t_{24}
rLM44	112		
rLM45	126		

[1]derived heterokaryon was homokaryotized within this study

Sequencing was performed on the Illumina NovaSeq® 6000 Next-Generation Sequencing system with its single-read (SR) chemistry using a 100 cycle run by IMGM Laboratories GmbH (Martinsried, Germany).
The raw data were processed by Dr. Maria Augusta Crivelente Horta on the Galaxy platform as follows. Data trimming was performed using Trimmomatic [Bolger et al. 2014], the alignment using HISAT2 [Kim et al. 2015], StringTie was used to perform counting [Pertea et al. 2015] and the differential expression was performed using DESeq2 [Love et al. 2014].

5.5.2. Hierarchical clustering of transcriptome data

The hierarchical clustering of the average FPKMs of RNA-seq library replicates was performed utilizing the Hierarchical Clustering Explorer 3.5 software. Only samples were included with a minimum threshold of 10 FPKM were taken into account for full transcriptome clusterings. Row-by-row normalization ($\frac{X-m}{\sigma}$) was applied. Columns and rows were clustered via the average linkage (unweighted pair group method with arithmetic mean) method with small node arrangement to the right and similarity distribution according Pearson's correlation.

5.6. Statistical and computational methods

5.6.1. Determination of F-box proteins and protein domains

The ortholog search was conducted with the help of Dr. Maria Augusta Crivelente Horta. Orthologs were identified on the platforms FungiDB and Uniprot (Table 5-1) by searching for relevant domains, GO terms and predicted functions.

Domain architectures of the putative F-box domain proteins from *N. crassa* were searched using the online tools SMART, FungiDB ortholog search, InterPro, ClustalOmega alignments and NLS mapper using a cut-off score of 4.0 (Table 5-1). Visualization of the protein domain structures was done using DOG version 2.0 [Ren et al. 2009] and IBS version 1.0 [Liu et al. 2015].

5.6.2. Statistical methods

Testing for statistical significance of normally distributed data, parametric tests like a t test were performed. Data which was not normally distributed was analysed using non-parametric tests, like a post-hoc test based on Kruskal-Wallis test.

5.6.3. Quantitative analysis of mass spectrometry data using MaxQuant and Perseus

The MS raw data files were received from the *Service Unit LCMS Protein Analytics* at the University of Göttingen (see 5.4.9). MS raw data were processed using MaxQuant operated with the default settings for label-free quantification with trypsin as digestion specific enzyme. In global parameters, the proteome UP000001805 of *N. crassa*, available on UniProt Database, was added as reference sequence. For the identification, *match between runs* was selected. In the section *Label free quantification*, the method iBAQ was selected. After data processing, the text file *proteinGroups.txt* generated in MaxQuant was uploaded using the Perseus software. Using Perseus, the data were processed according to the protocols provided by the *Service Unit LCMS Protein Analytics* at the University of Göttingen. The data were filtered and potential contaminants were removed. Afterwards, the data matrix was log2-fold transformed and filtered for valid values. A *N. crassa* annotation file was added for protein identification. Finally, differentially abundant proteins in F-box samples were quantified against the controls. The retrieved data were visualized using OriginPro software.

5.6.4. Qualitative analysis of mass spectrometry data

To perform a qualitative analysis the mass spectrometry (MS) data were run by Proteome Discoverer Software Version 1.4 (Thermo Fisher). To determine specific F-box interaction partners, proteins found in GFP and WT control samples were subtracted from proteins found only in the F-box sample.

6. Appendix

6.1. Abbreviations

abbreviations	description
µl	microliter
AA	allyl alcohol
ada	All development-altered regulator
adh-1	alcohol dehydrogenase 1
ANOVA	Analysis of Variance
ATP	adenosine triphosphate
bp	base pair
C	cluster
camk-1	Ca/CaM-dependent kinase-1
cAMP	cyclic adenosine monophosphate
CAND1	Cullin-associated and neddylation-dissociated 1 protein
CAZymes	carbohydrate-active enzymes
ccg-1	clock controlled gene 1
CCR	Carbon Catabolite Repression
cDNA	complementary deoxyribonucleic acid
cre-1	carbon catabolite repressor protein 1
CSSR	carbon starvation stress response
ddH_2O	double distilled water
DEG	differentially expressed gene
DNA	deoxyribonucleic acid
dNTP	deoxynucleotide triphosphates
e. g.	exempli gratia / for example
E1	enzyme-1
ENCODE	Encyclopedia of DNA elements
et al.	*et alia* (Latin: and others)
Figure S	supplementary figure
FPKM	reads per kilobase of transcript per million mapped reads/ Fragments Per Kilobase Million
FunCat	Functional Catalogue
G6P	Glucose-6-phosphat
gDNA	genomic deoxyribonucleic acid
GO	gene ontology
GPCR	G protein-coupled receptors
h	hour(s)
HECT E3 ligase	Homologous to E6-AP C-Terminus E3 ligase
his-3	histidine biosynthesis trifunctional protein coding gene
hp	hypothetical protein
ID	identification
IP	immunoprecipitation
kb	kilobase
l	liter

abbreviations	description
log_2	logarithm to the base 2
MCS	multiple cloning site
min	minute(s)
ml	milliliter
mm	Millimeter
MS	mass spectrometry
NADPH	Nicotinamide adenine dinucleotide phosphate
NCU	*Neurospora crassa* unit
nm	nanometer
OD	optical density
P	p-value/ probability value
PCR	polymerase chain reaction
pdr-1	pectin degradation regulator 1
PKA	protein kinase A
PPI	protein–protein interactions
PTMs	Post-translational modifications
qPCR	quantitative polymerase chain reaction
R^2	coefficient of determination
RBR E3 ligase	RING-between-RING E3 ligase
Rbx	RING-box 1 protein
RING E3 ligase	really interesting new gene E3 ligase
RNA	ribonucleic acid
RNA-seq	ribonucleic acid sequencing
RPKM	reads per kilobase per million mapped reads
rpm	revolutions per minute
S	subcluster
SCF complex	Skp1-Cullin-F-box complex
SCON-3	sulfur control-3 protein
SDS-PAGE	sodium dodecyl sulfate polyacrylamide gel electrophoresis
sec	second(s)
Skp1	S-phase kinase-associated protein 1
SUMO	Small Ubiquitin-Related Modifier
Table S	supplementary table
TAE	Tris Acetate EDTA buffer
TCDB	Transporter Classification Database
TEMED	tetramethylethylenediamine
TF	transcription factor
TUM	Technical University of Munich
U	units
V	volt
VMM	Vogel´s Minimal Medium
w/v	weight per volume
WCC	white collar complex
WT	wild type
x g	times gravity/ gravitational acceleration
znf	zinc finger transcription factor

6.2. Supplementary figures

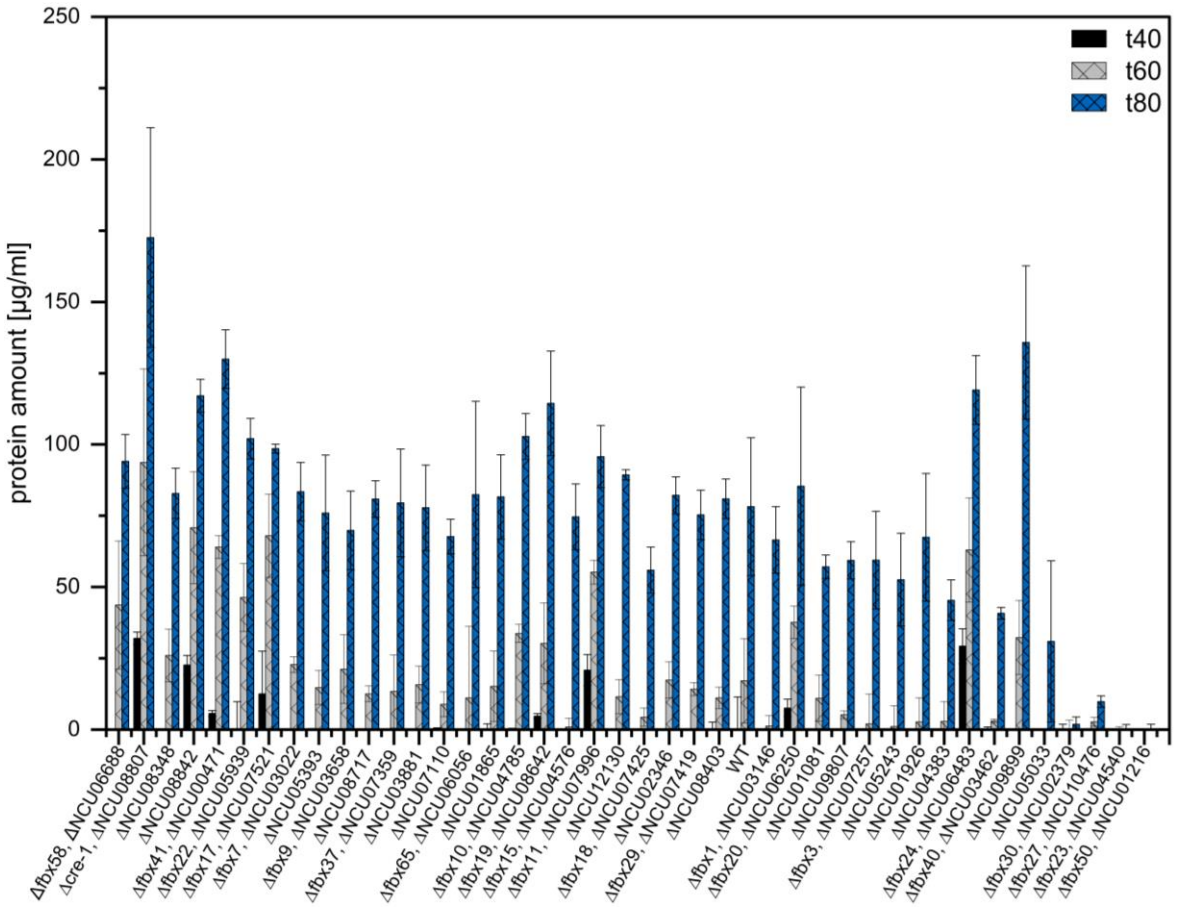

Figure S 6-1: Determined protein amount of culture supernatants.
Protein amount in the supernatant of *N. crassa fbx* deletion strains grown in 1% Avicel supplemented with 0.5% glucose. Pre-cultured *N. crassa fbx* deletion strains were switched into liquid medium containing cellulose supplemented with glucose. The total protein amount was determined 40 h, 60 h and 80 h after the medium switch.

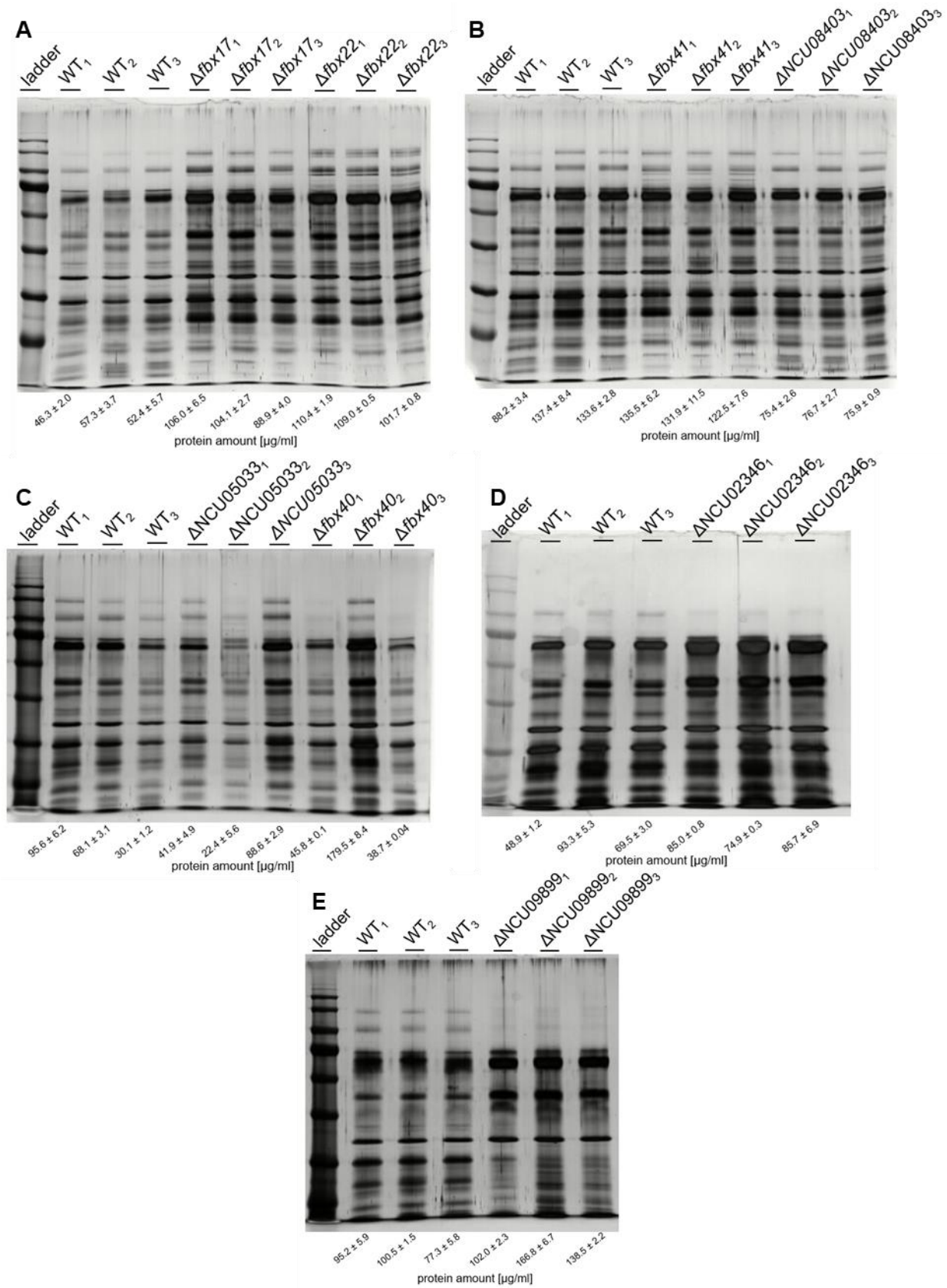

Figure S 6-2: Protein profile of culture supernatants from *N. crassa*.
SDS-PAGE from unconcentrated culture supernatants of *N. crassa* WT and Δ*fbx* deletion strains using same samples as from Figure 2-6, 80 h after medium switch. The number below the strain name is the number of the corresponding replicate. (A) and (B): supernatants of strains which showed a derepressed phenotype in presence of allyl alcohol. (C), (D) and (E): supernatants of strains which

showed a repressed phenotype in presence of allyl alcohol (Figure 2-9). Below the lanes is the determined protein amount and standard deviation in µg/ml of each supernatant sample. The used ladder is BlueStar Prestained Protein Marker (NIPPON Genetics EUROPE GmbH).

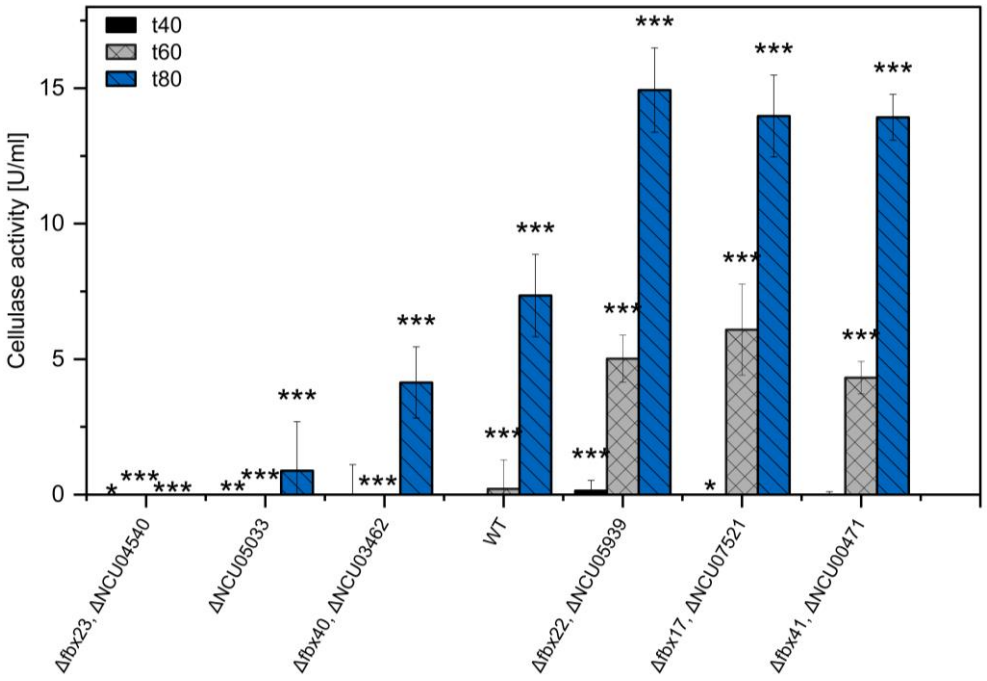

Figure S 6-3: Repetition of enzymatic activity profiles of selected *N. crassa fbx* deletion strains grown in 1% Avicel supplemented with 0.5% glucose.

Pre-cultured *N. crassa fbx* deletion strains were switched into liquid medium containing cellulose supplemented with glucose. The enzymatic activity was determined 40 h, 60 h and 80 h after the medium switch. Significance levels were determined using a t test. *, $P < 0.05$; **, $P < 0.01$; ***, $P < 0.001$.

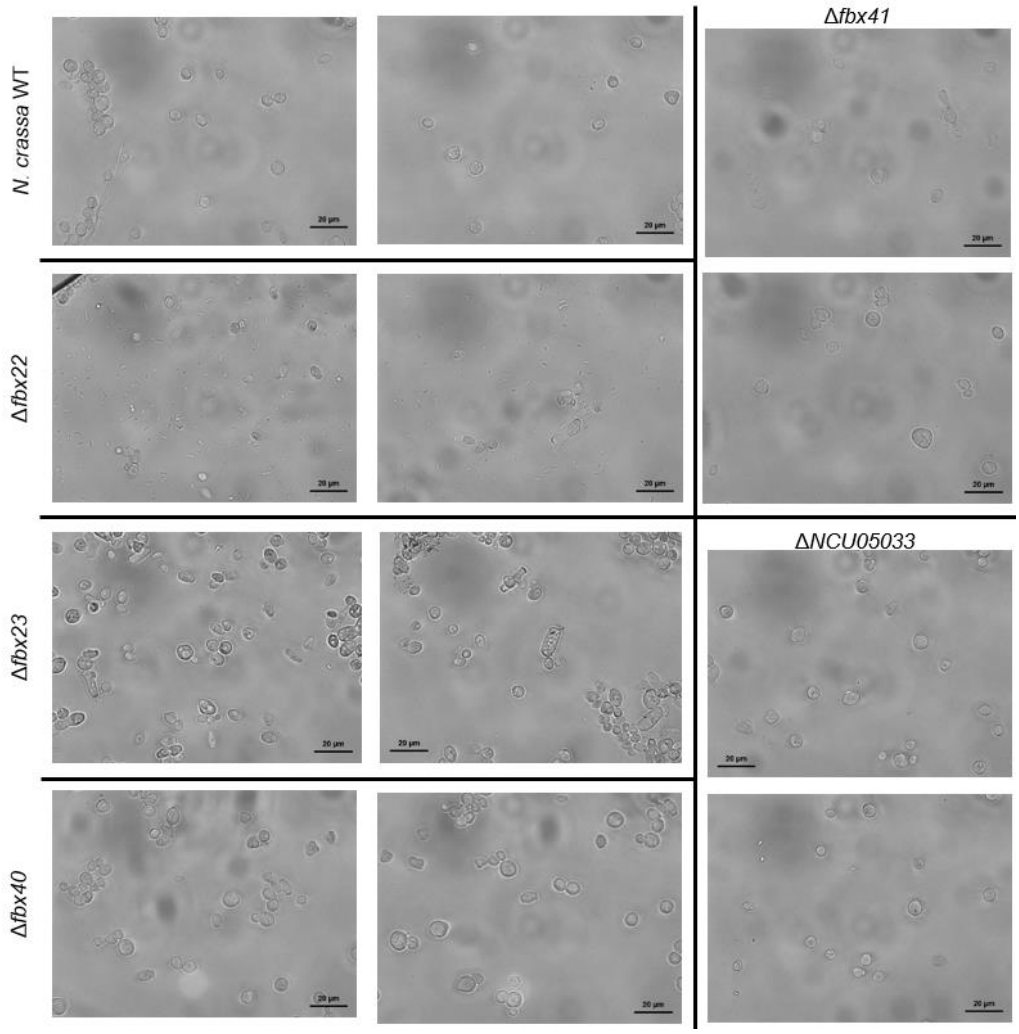

Figure S 6-4: *N. crassa* conidia.
Optical microscopy images of *N. crassa* conidia from WT and selected *fbx* deletion strains (as indicated within the figure). 40x magnification. Ruler indicates 20 µm.

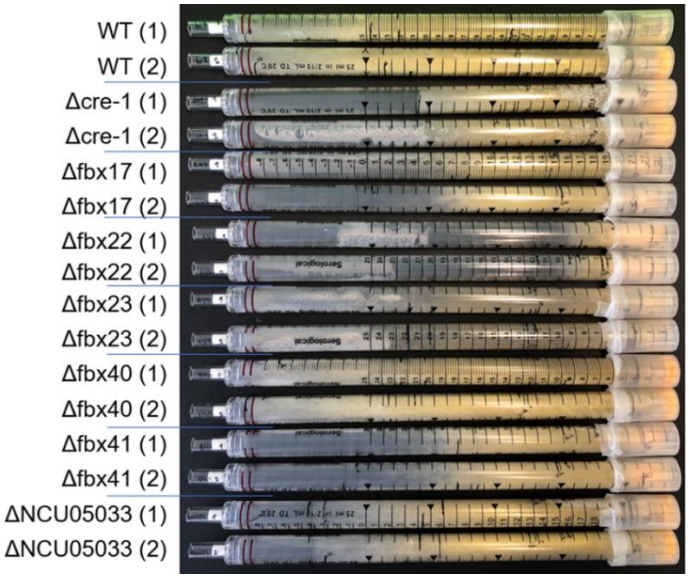

Figure S 6-5: Race tube assay of selected *N. crassa* deletion strains compared to WT and Δ*cre-1*.

Strains were grown on 2% sucrose VMM. The hyphal growth rate was determined through measurements of the hyphal growth front over time.

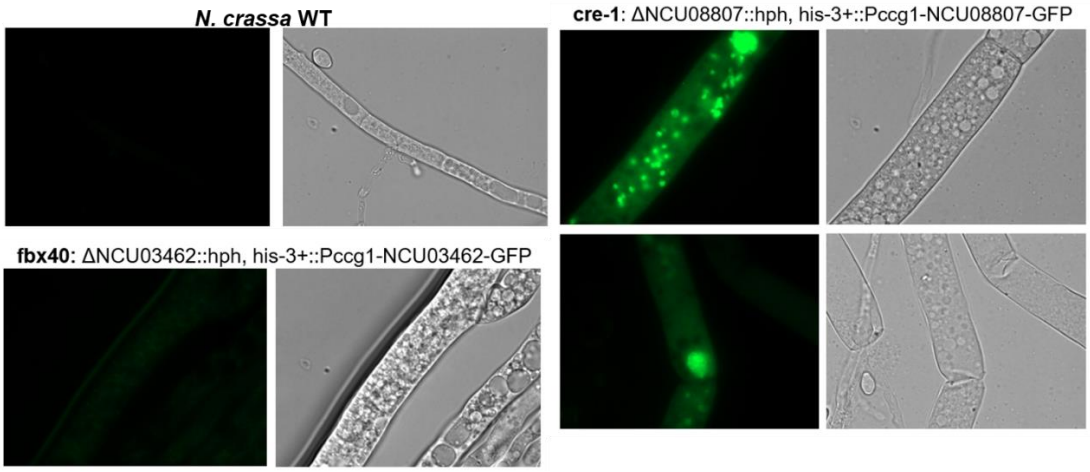

Figure S 6-6: Fluorescent microscopy of *N. crassa* WT, *fbx40*-comp and *cre-1*-comp.
Strains (FGSC #2489; nLK054K; nLK061VI) were grown on 2% fructose VMM agar plates prior to microscopy overnight at room temperature. Hyphae were scratched off the plates and observed in an object carrier. Specimens were covered with a cover glass. Images were taken at 100-fold magnification using immersion oil under an Axioskop optical microscope (Zeiss). Microscope filter settings: GFP 5800 ms, bright 3.81 V intensity. Filters of the images were set to black at 281 and white at 2692.

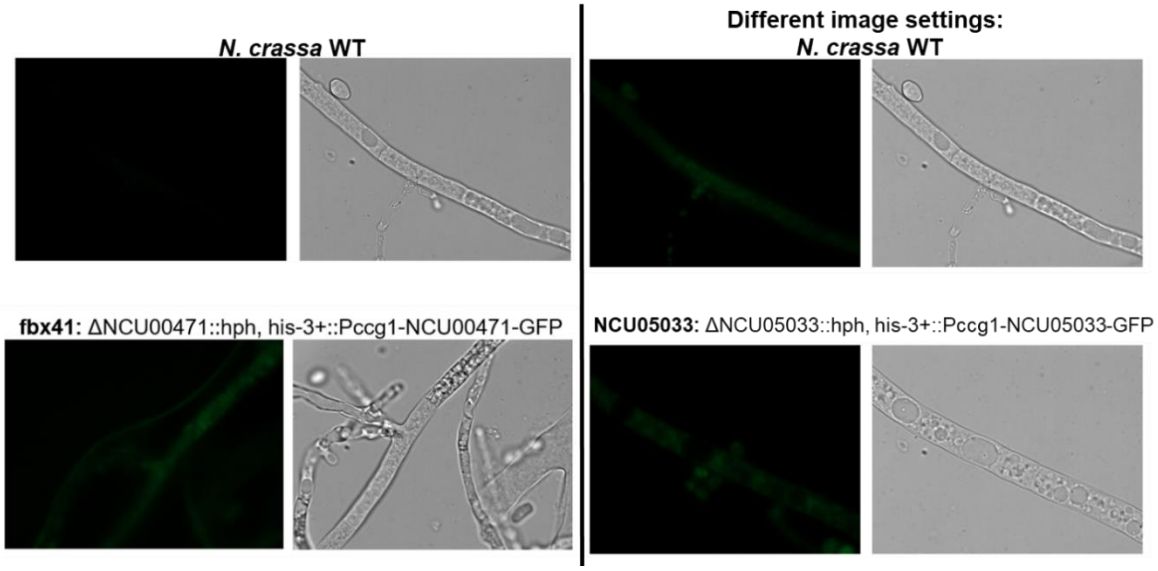

Figure S 6-7: Fluorescent microscopy of *N. crassa* WT, *fbx41*-comp and NCU05033-comp.
Strains (FGSC #2489; nLK058III; nLK055A) were grown on 2% fructose VMM agar plates prior to microscopy overnight at room temperature. Hyphae were scratched off the plates and observed in an object carrier. Specimens were covered with a cover glass. Images were taken at 100-fold magnification using immersion oil under an Axioskop optical microscope (Zeiss). Microscope filter settings: GFP 5800 ms, bright 3.81 V intensity. Filters of the images on the left side were set to black at 281 and white at 2692. For the images on the right side different filter settings were used: black at 254 and white at 900.

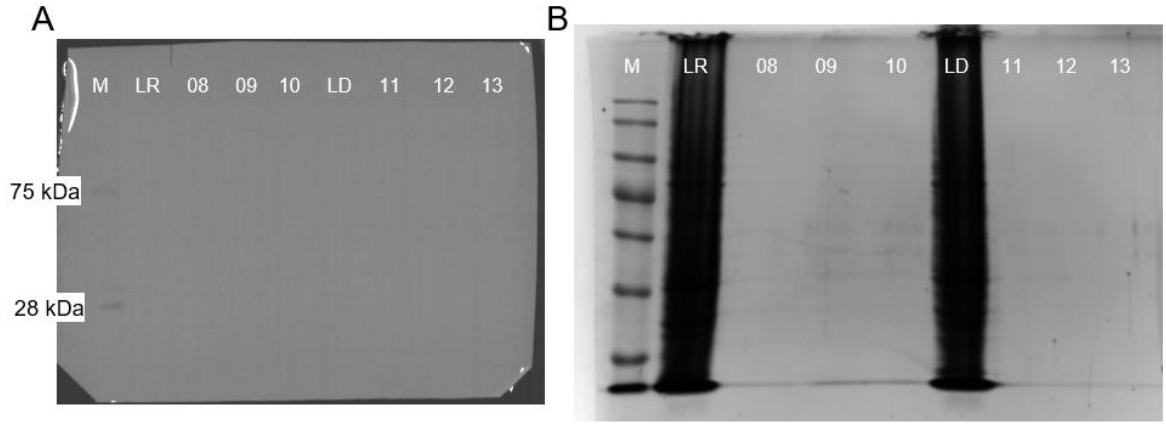

Figure S 6-8: Quality control of *N. crassa* WT samples for IP and MS analysis.
(A) Anti-GFP western blot and (B) Coomassie stained SDS-gel. M is the lane containing the protein ladder used. LR = lysate of repressed condition, LD = lysate of derepressed condition. The numbers above the lanes are the LM## sample numbers listed in Table S 6-5.

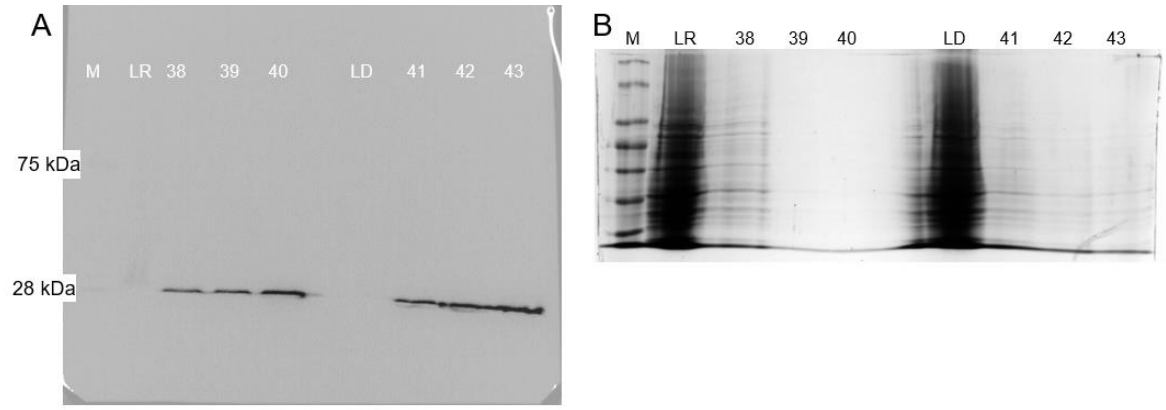

Figure S 6-9: Quality control of *N. crassa* GFP control samples for IP and MS analysis.
(A) Anti-GFP western blot and (B) Coomassie stained SDS-gel. M is the lane containing the protein ladder used. LR = lysate of repressed condition, LD = lysate of derepressed condition. The numbers above the lanes are the LM## sample numbers listed in Table S 6-5. Size of bait protein: 26.98 kDa.

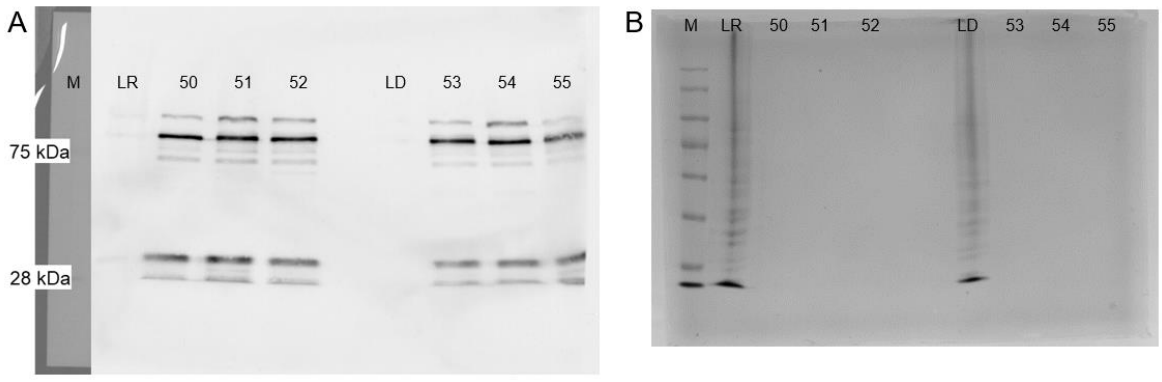

Figure S 6-10: Quality control of *N. crassa fbx17*-comp samples for IP and MS analysis.
(A) Anti-GFP western blot and (B) Coomassie stained SDS-gel. M is the lane containing the protein ladder used. LR = lysate of repressed condition, LD = lysate of derepressed condition. The numbers above the lanes are the LM## sample numbers listed in Table S 6-5. Size of bait protein: 110.8 kDa.

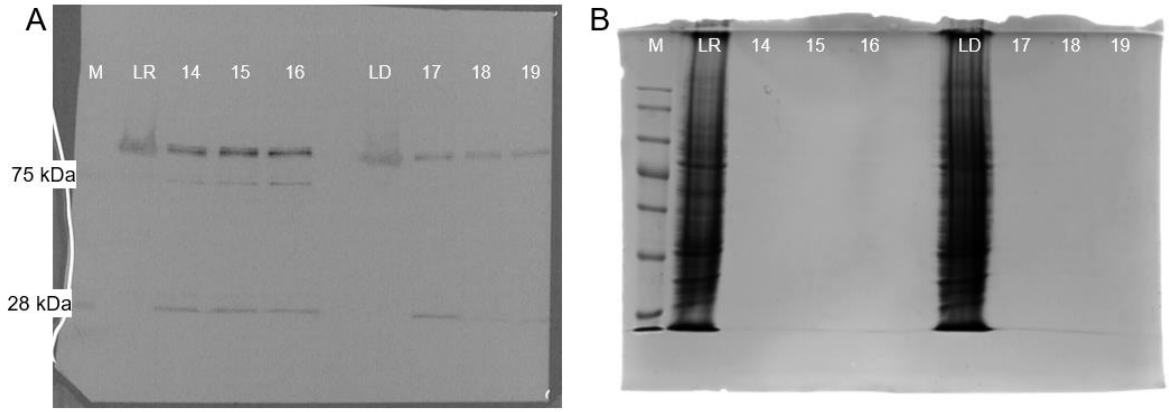

Figure S 6-11: Quality control of *N. crassa fbx40*-comp samples for IP and MS analysis.
(A) Anti-GFP western blot and (B) Coomassie stained SDS-gel. M is the lane containing the protein ladder used. LR = lysate of repressed condition, LD = lysate of derepressed condition. The numbers above the lanes are the LM## sample numbers listed in Table S 6-5. Size of bait protein: 101.8 kDa.

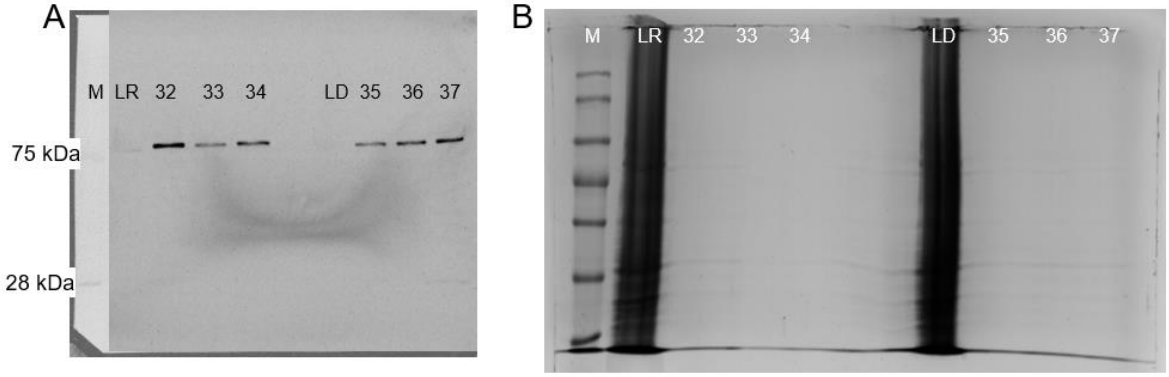

Figure S 6-12: Quality control of *N. crassa fbx41*-comp samples for IP and MS analysis.
(A) Anti-GFP western blot and (B) Coomassie stained SDS-gel. M is the lane containing the protein ladder used. LR = lysate of repressed condition, LD = lysate of derepressed condition. The numbers above the lanes are the LM## sample numbers listed in Table S 6-5. Size of bait protein: 90.02 kDa.

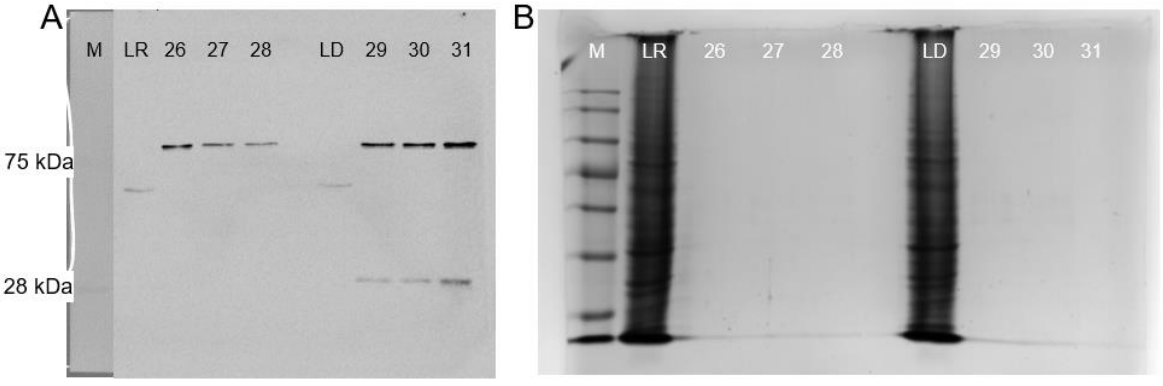

Figure S 6-13: Quality control of *N. crassa* NCU05033-comp samples for IP and MS analysis.
(A) Anti-GFP western blot and (B) Coomassie stained SDS-gel. M is the lane containing the protein ladder used. LR = lysate of repressed condition, LD = lysate of derepressed condition. The numbers above the lanes are the LM## sample numbers listed in Table S 6-5. Size of bait protein: 92.26 kDa.

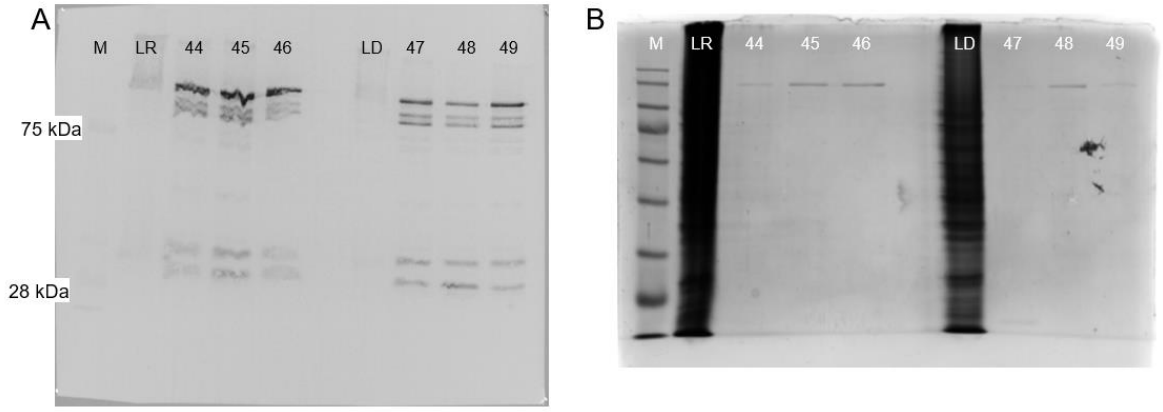

Figure S 6-14: Quality control of *N. crassa pdr-1*-comp samples for IP and MS analysis.
(A) Anti-GFP western blot and (B) Coomassie stained SDS-gel. M is the lane containing the protein ladder used. LR = lysate of repressed condition, LD = lysate of derepressed condition. The numbers above the lanes are the LM## sample numbers listed in Table S 6-5. Size of bait protein: 135.99 kDa.

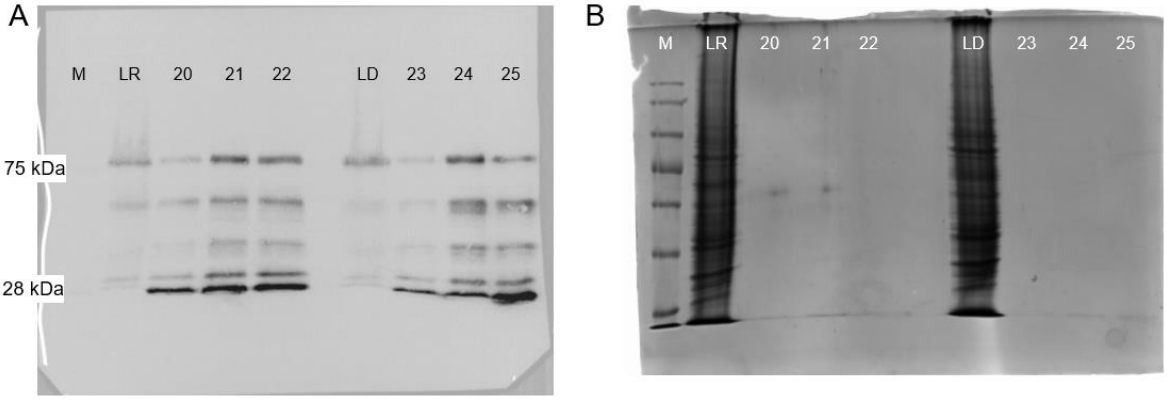

Figure S 6-15: Quality control of *N. crassa cre-1*-comp samples for IP and MS analysis.
(A) Anti-GFP western blot and (B) Coomassie stained SDS-gel. M is the lane containing the protein ladder used. LR = lysate of repressed condition, LD = lysate of derepressed condition. The numbers above the lanes are the LM## sample numbers listed in Table S 6-5. Size of bait protein: 74.8 kDa.

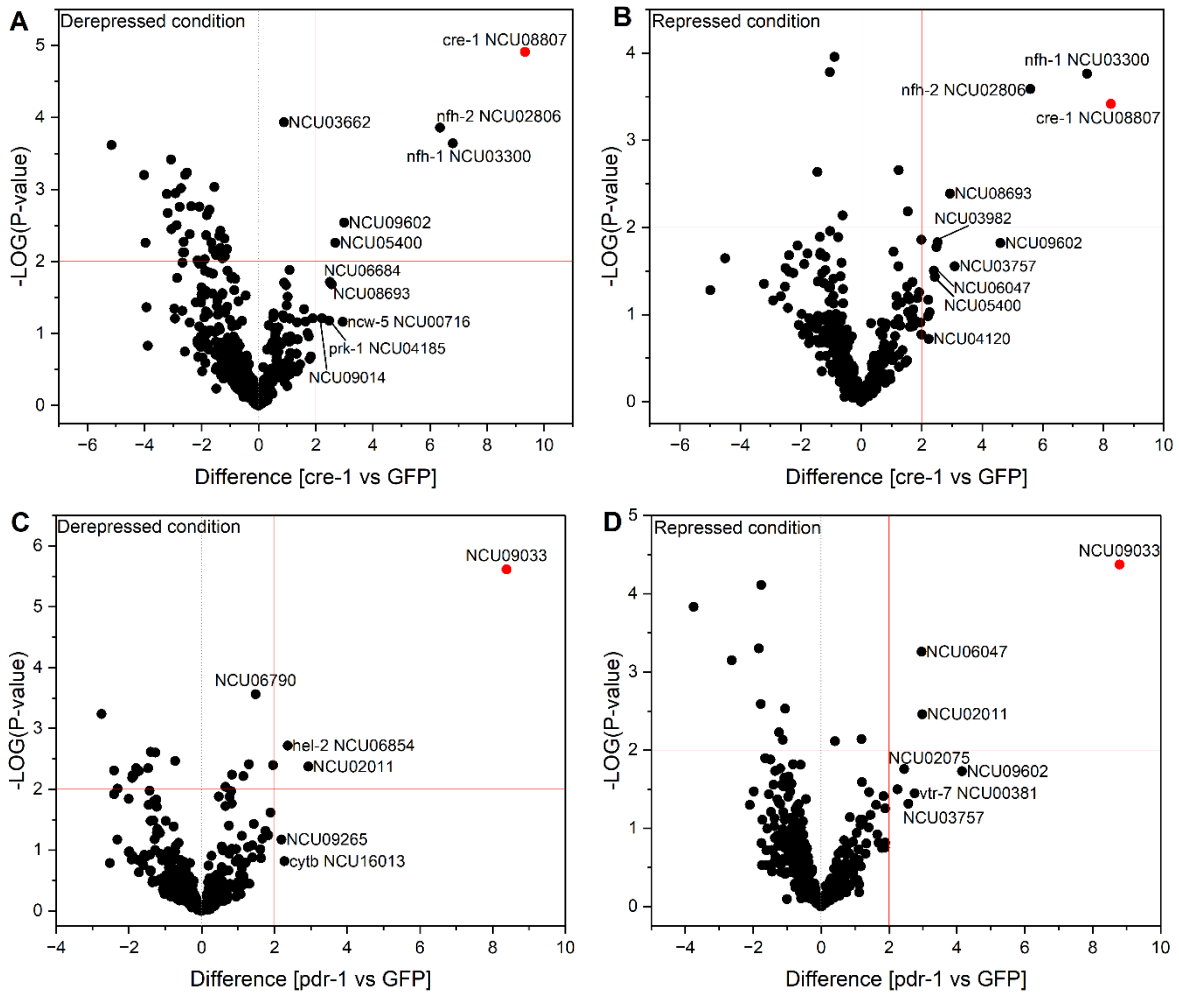

Figure S 6-16: Volcano plot of both transcription factors CRE-1::GFP and PDR-1::GFP.
The GFP-tagged bait MS data is shown against unbound GFP control strain grown in equal culturing conditions. (A) CRE-1::GFP in derepressed culturing and (B) repressed culturing conditions. (C) PDR-1::GFP in derepressed culturing and (D) repressed culturing conditions. Upper right red square frames proteins with significant and highly different abundance. Positive values of x-axis show co-immunoprecipitated proteins with the corresponding bait protein (red dot). Negative values of x-axis show proteins with unspecific binding to the GFP control.

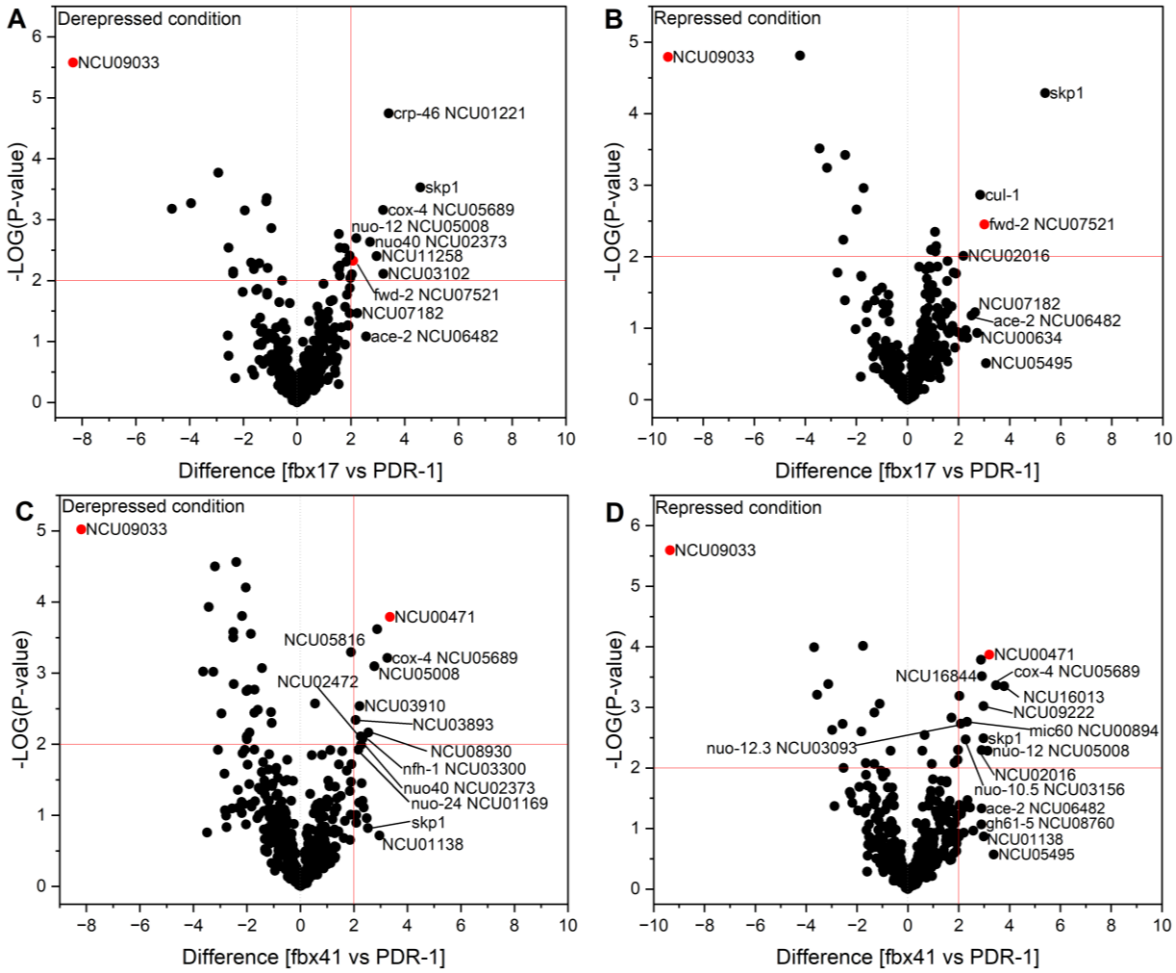

Figure S 6-17: Volcano plot F-box::GFP bait proteins whose deletions showed a derepressed phenotype.

The F-box::GFP bait MS data is shown against PDR-1::GFP strain grown in equal culturing conditions. (A) Fbx17::GFP in derepressed culturing and (B) repressed culturing conditions. (C) Fbx41::GFP in derepressed culturing and (D) repressed culturing conditions. Upper right red square frames proteins with significant and highly different abundance. Positive values of x-axis show co-immunoprecipitated proteins with the corresponding bait protein (red dot). Negative values of x-axis show proteins with binding to PDR-1::GFP (red dot).

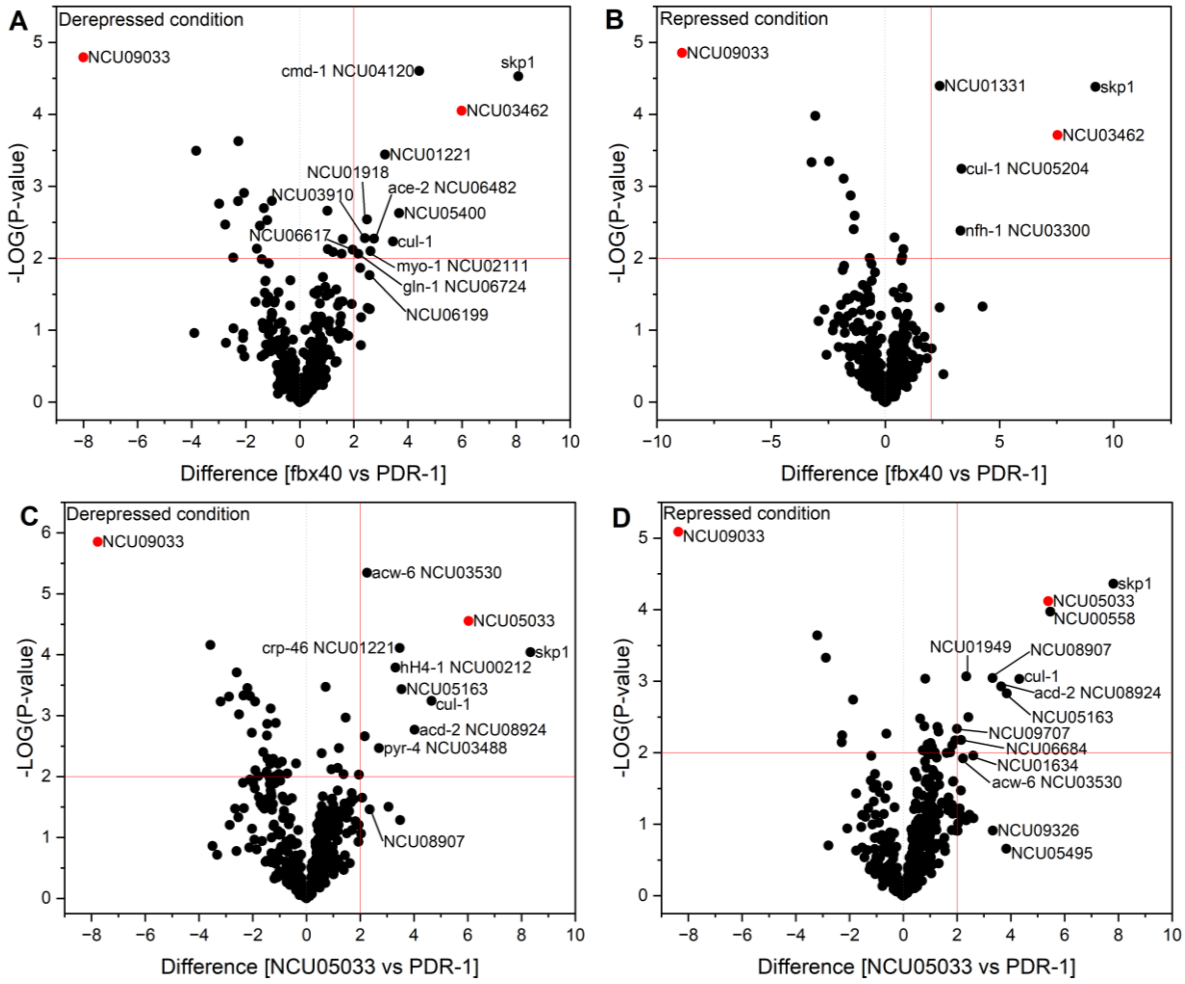

Figure S 6-18: Volcano plot F-box::GFP bait proteins whose deletions showed a repressed phenotype.

The F-box::GFP bait MS data is shown against PDR-1::GFP strain grown in equal culturing conditions. (A) Fbx40::GFP in derepressed culturing and (B) repressed culturing conditions. (C) NCU05033::GFP in derepressed culturing and (D) repressed culturing conditions. Upper right red square frames proteins with significant and highly different abundance. Positive values of x-axis show co-immunoprecipitated proteins with the corresponding bait protein (red dot). Negative values of x-axis show proteins with binding to PDR-1::GFP (red dot).

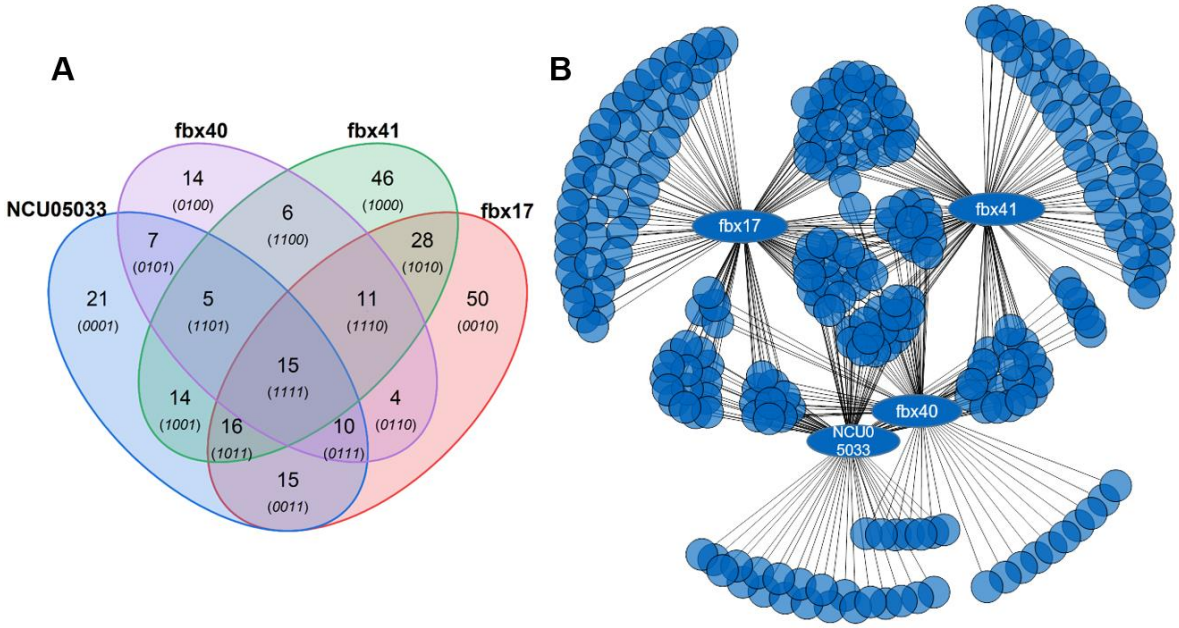

Figure S 6-19: Venn and network diagram of putative interactors identified via qualitative analysis of MS data across all conditions for the investigated F-box proteins.
(A) Venn diagram displays the number of genes identified in the corresponding sample within both conditions. The number in brackets guides to the corresponding gene ID given in NCU numbers in Table S 6-13. (B) Network diagram shows shared and exclusive putative interaction partners as circles within both conditions.

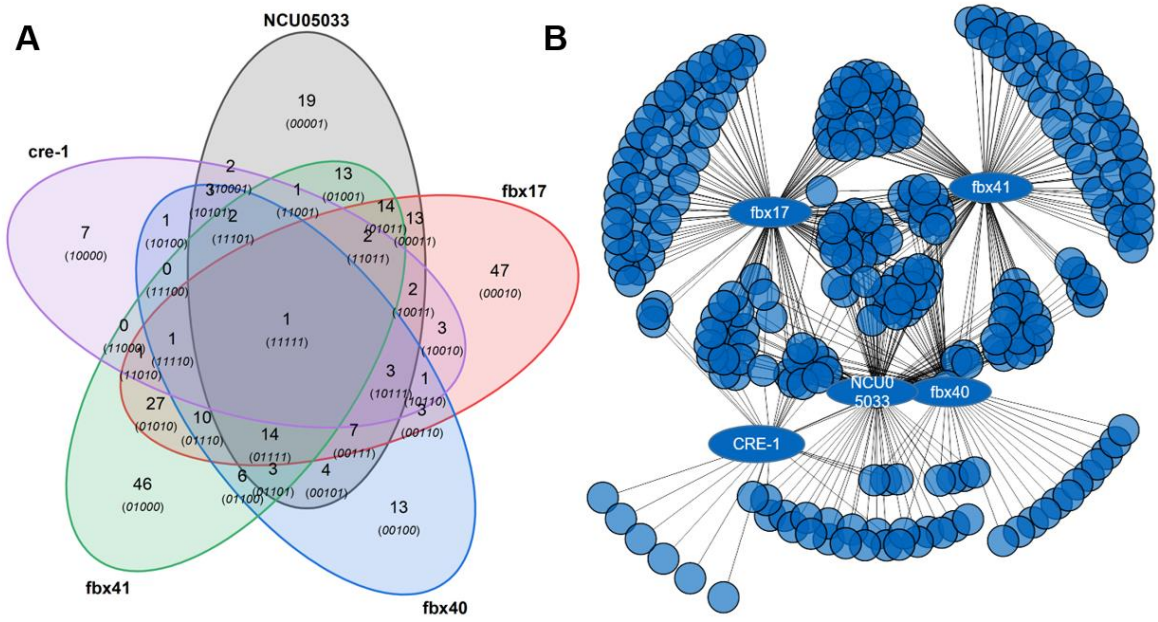

Figure S 6-20: Venn and network diagram of putative interactors identified via qualitative analysis of MS data across all conditions for the investigated F-box proteins and CRE-1.
(A) Venn diagram displays the number of genes identified in the corresponding sample within both conditions. The number in brackets guides to the corresponding gene ID given in NCU numbers in Table S 6-14. (B) Network diagram shows shared and exclusive putative interaction partners as circles within both conditions.

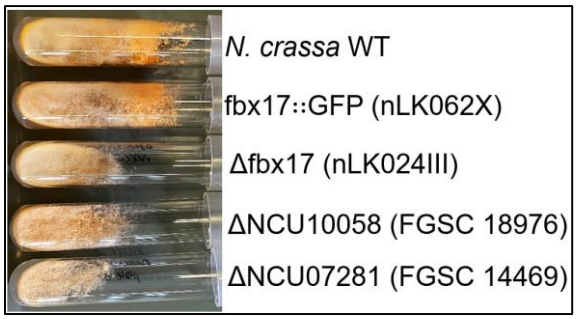

Figure S 6-21: Growth phenotype of deletion strains of putative interactors of Fbx17.
Growth phenotype in slants of *N. crassa* WT, *fbx17*-comp, Δ*fbx17* and two deletion strains of putative interactors. In brackets: internal stock numbers and FGSC numbers.

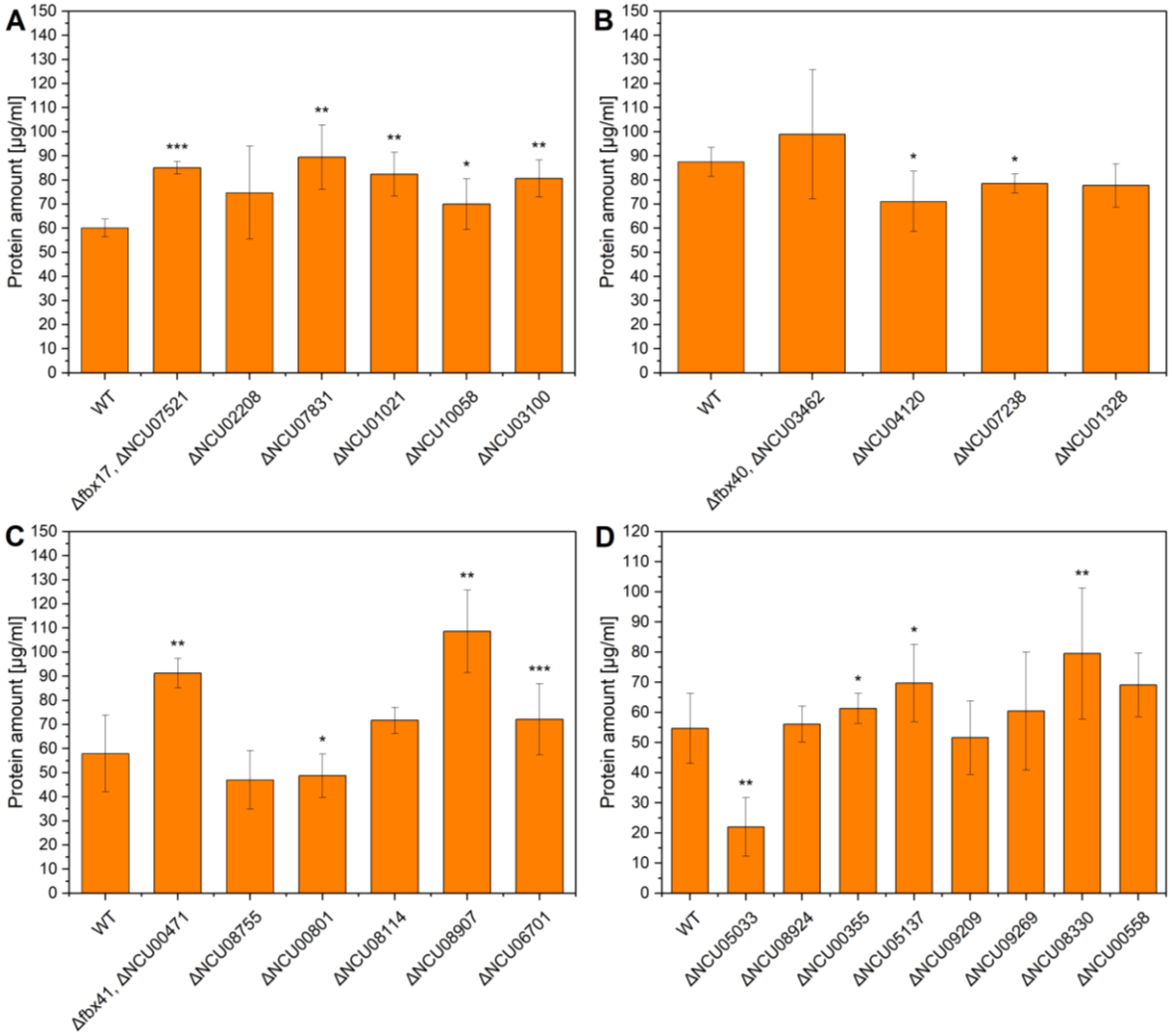

Figure S 6-22: Total protein amount in culture supernatants of putative interactor deletion strains grown in 1% Avicel supplemented with 0.5% glucose.
Pre-cultured *N. crassa* deletion strains were switched into liquid medium containing cellulose supplemented with glucose. The total protein amount in the culture supernatant was determined 80 h after the medium switch. Protein amounts of (A) Fbx17, (B) Fbx40, (C) Fbx41 and (D) NCU05033 deletion strain and the deletion strains of their putative interactors were compared to the WT. Significance levels were determined using a paired t test. *, $P < 0.05$; **, $P < 0.01$; ***, $P < 0.001$.

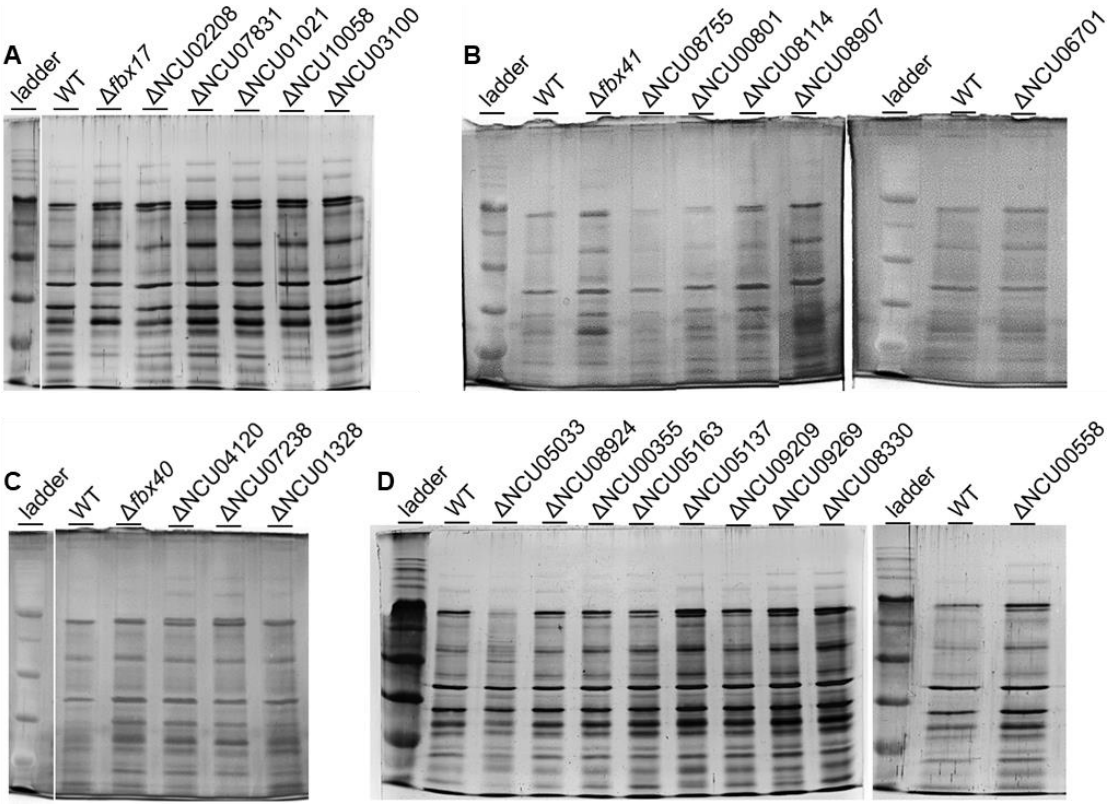

Figure S 6-23: Protein profile of culture supernatants from *N. crassa* Fbx interactor deletion strains.

SDS-PAGE from unconcentrated culture supernatants of *N. crassa* WT, Δ*fbx* and interactor deletion strains using same samples as from Figure 2-30, 80 h after medium switch. Protein profile of (A) Fbx17, (B) Fbx41, (C) Fbx40 and (D) NCU05033 deletion strain and of the deletion strains of their putative interactors. Average protein amounts of the supernatants are shown in Figure S 6-22. The utilized ladder is BlueStar Prestained Protein Marker (NIPPON Genetics EUROPE GmbH).

6.3. Supplementary tables

Table S 6-1: Number of differentially expressed genes of RNA-sequencing analysis (switch from CC-derepressing to CC-repressing condition).

contrasts	DEGs	genes up	genes down
WT $t_{0.5}$ X WT t_0	1256	642	614
WT t_8 X WT t_0	1101	432	669
Δ*fbx17* $t_{0.5}$ X Δ*fbx17* t_0	773	434	339
Δ*fbx17* t_8 X Δ*fbx17* t_0	899	240	659
Δ*fbx41* $t_{0.5}$ X Δ*fbx41* t_0	770	378	392
Δ*fbx41* t_8 X Δ*fbx41* t_0	997	236	761
Δ*fbx17* t_0 X WT t_0	180	107	73
Δ*fbx17* $t_{0.5}$ X WT $t_{0.5}$	193	111	82
Δ*fbx17* t_8 X WT t_8	67	29	38
Δ*fbx41* t_0 X WT t_0	223	136	87
Δ*fbx41* $t_{0.5}$ X WT $t_{0.5}$	234	124	110
Δ*fbx41* t_8 X WT t_8	92	35	57

Table S 6-2: Number of differentially expressed genes from RNA-sequencing analysis (switch from CC-repressing to CC-derepressing condition).

contrasts	DEGs	genes up	genes down
WT t_5 X WT t_0	1432	817	615
WT t_{24} X WT t_0	1149	784	365
ΔNCU05033 t_5 X ΔNCU05033 t_0	1269	715	554
ΔNCU05033 t_{24} X ΔNCU05033 t_0	1024	705	319
ΔNCU05033 t_0 X WT t_0	16	8	8
ΔNCU05033 t_5 X WT t_5	53	33	20
ΔNCU05033 t_{24} X WT t_{24}	12	5	7

Table S 6-3: Generation of histidine auxotrohic *N. crassa* strains through mating.

1st mating partner	2nd mating partner	resulted strain
FGSC #6103, WT, *his-3*$^-$, mat A	#16, Δ*pdr-1*, his-3$^-$, mat a	#230, WT, his-3$^-$, mat a
	FGSC #20477, ΔNCU03462::hph, mat a	#nLK051I, ΔNCU03462::hph, his-3$^-$
	FGSC #14738, ΔNCU05033::hph, mat a	#nLK053III, ΔNCU05033::hph, his-3$^-$
	FGSC #12780, ΔNCU00471::hph, mat a	#nLK051B, ΔNCU00471::hph, his-3$^-$
	FGSC #13527[a], ΔNCU07521::hph, mat a	#nLK056VII, ΔNCU07521::hph, his-3$^-$
	#130, ΔNCU08807::hph, mat a	#nLK057I, ΔNCU08807::hph, his-3$^-$
	FGSC #13190, ΔNCU05939::hph, mat a	# nLK059I, ΔNCU05939::hph, his-3$^-$
#230, WT, his-3$^-$, mat a	FGSC #15872, ΔNCU04540::hph, mat A	#nLK060V, ΔNCU04540::hph, his-3$^-$

[a] FGSC strain was homokaryonized via microconidiation.

Table S 6-4: *N. crassa* strains used for immunoprecipitation experiments (chapter 2.4.2).

Internal stock number	name	genotype
1	*N. crassa* WT	oak ridge (OR) 74, mat A
124	*pdr-1-GFP*	his-3:: pNCU03753-NCU09033::GFP, mat A
232	unbound GFP	his-3::pNCU03753-GFP, mat A
nLK054K	*fbx40*-comp	ΔNCU03462::hph, his-3::pNCU03753-NCU03462::GFP
nLK055A	NCU05033-comp	ΔNCU05033::hph, his-3::pNCU03753-NCU05033::GFP
nLK058 III	*fbx41*-comp	ΔNCU00471::hph, his-3::pNCU03753-NCU00471::GFP
nLK061 IX	*cre-1*-comp	ΔNCU08807::hph, his-3::pNCU03753- NCU08807::GFP
nLK062 X	*fbx17*-comp	ΔNCU07521::hph, his-3::pNCU03753-NCU07521::GFP

Table S 6-5: Samples used for immunoprecipitation and mass spectrometry analysis.
The protein amount used for each immunoprecipitation approach is given in the last column for each replicate. The cultivation procedure is described in 5.2.3 “Culturing procedure prior to immunoprecipitation experiment”.

Sample name	condition	strain	Replicate	Protein (mg)
LM08	repressed (4h Glc)	#1, WT (negative control)	1	15
LM09	repressed (4h Glc)		2	15
LM10	repressed (4h Glc)		3	15
LM11	de-repressed		4	15
LM12	de-repressed		5	15
LM13	de-repressed		6	15
LM14	repressed (4h Glc)	nLK054 K, *fbx40*-comp	1	15
LM15	repressed (4h Glc)		2	15
LM16	repressed (4h Glc)		3	15
LM17	de-repressed		4	15
LM18	de-repressed		5	15
LM19	de-repressed		6	15
LM20	repressed (4h Glc)	nLK061 IX, *cre-1*-comp	1	15
LM21	repressed (4h Glc)		2	15
LM22	repressed (4h Glc)		3	15
LM23	de-repressed		4	15
LM24	de-repressed		5	15
LM25	de-repressed		6	15
LM26	repressed (4h Glc)	nLK055 A, NCU05033-comp	1	10
LM27	repressed (4h Glc)		2	10
LM28	repressed (4h Glc)		3	10
LM29	de-repressed		4	10
LM30	de-repressed		5	10
LM31	de-repressed		6	10
LM32	repressed (4h Glc)	nLK058 III, *fbx41*-comp	1	15
LM33	repressed (4h Glc)		2	15
LM34	repressed (4h Glc)		3	15
LM35	de-repressed		4	15
LM36	de-repressed		5	15

Sample name	condition	strain	Replicate	Protein (mg)
LM37	de-repressed		6	15
LM38	repressed (4h Glc)	nLK065 VIII, unbound GFP (control)	1	15
LM39	repressed (4h Glc)		2	15
LM40	repressed (4h Glc)		3	15
LM41	de-repressed		4	15
LM42	de-repressed		5	15
LM43	de-repressed		6	15
LM44	repressed (4h Glc)	#124, *pdr-1*::GFP (control to have another non-interfering fusion protein)	1	15
LM45	repressed (4h Glc)		2	15
LM46	repressed (4h Glc)		3	15
LM47	de-repressed		4	15
LM48	de-repressed		5	15
LM49	de-repressed		6	15
LM50	repressed (4h Glc)	nLK062 X, *fbx17*-comp	1	15
LM51	repressed (4h Glc)		2	15
LM52	repressed (4h Glc)		3	15
LM53	de-repressed		4	15
LM54	de-repressed		5	15
LM55	de-repressed		6	15

Table S 6-6: List of interactors identified for several bait proteins via quantitative analysis.
= number of bait proteins for which the interactors were identified. Only interactors were taken into account with significance >2 and difference >2 against all controls (stringent search).

#	bait	Uniprot accession	Protein name	Gene Name
4	NCU05033; NCU07521 Fbx17; NCU03462 Fbx40; NCU00471 Fbx41	Q8NK13	E3 ubiquitin ligase complex SCF subunit scon-3	scon-3 NCU08991
		P06810	Cytochrome c oxidase subunit 5	NCU05457
		Q01359	Cytochrome c oxidase subunit 6	NCU06695
3	NCU05033; NCU07521 Fbx17; NCU03462 Fbx40	V5IP38	Cullin 1	cul-1 NCU05204
		Q9P720; V5ILK7	60S ribosomal protein L16	NCU0122
		Q7RVN0	60S ribosomal protein L11	NCU02509
3	NCU07521 Fbx17; NCU03462 Fbx40; NCU00471 Fbx41	P24391	Mitochondrial import receptor subunit tom40	tom40 NCU01179
		Q7RYJ2	Pyruvate dehydrogenase E1 component subunit alpha (EC 1.2.4.1)	ace-2 NCU06482
		P10255	Peptidyl-prolyl cis-trans isomerase	NCU00726
		Q1K756	Translocon-associated protein subunit alpha	NCU01146
		Q7RW96	Heat shock protein 30	NCU07232
3	NCU05033; NCU07521 Fbx17; NCU00471 Fbx41	P11943	Acyl carrier protein, mitochondrial (ACP) (NADH-ubiquinone oxidoreductase 9.6 kDa subunit)	NCU05008

#	bait	Uniprot accession	Protein name	Gene Name
3	NCU05033; NCU03462 Fbx40; NCU00471 Fbx41	V5IRL8	DNA damage checkpoint protein rad24	nfh-1 NCU03300
2	NCU05033; NCU07521 Fbx17	P37210	Histone H2B	hh2b NCU02435
2	NCU07521 Fbx17; NCU00471 Fbx41	P33723	GTP-binding protein ypt1	ypt-1 NCU08477
		V5IPL7; V5IM17	Uncharacterized protein	NCU08949
		Q7SFL6	Uncharacterized protein	NCU02016
		P56525	ATP synthase subunit delta, mitochondrial	atp16 NCU00385
		Q35128	Cytochrome b (EC 7.1.1.8)	cob NCU16013
		P06809	Cytochrome c oxidase subunit 4, mitochondrial	cox-4 NCU05689
		V5IP95	Cytochrome b-c1 complex subunit 10	NCU16844
		P19968	NADH-ubiquinone oxidoreductase 21.3 kDa subunit (EC 7.1.1.2)	NCU08930
		P21976	NADH-ubiquinone oxidoreductase 20.8 kDa subunit	NCU02472
		Q07842	NADH-ubiquinone oxidoreductase 10.5 kDa subunit (Complex I) (CI)	nuo-10.5 NCU03156
2	NCU05033; NCU03462 Fbx40	Q7S985	CUE domain-containing protein	NCU07282
2	NCU03462 Fbx40; NCU00471 Fbx41	Q1K8D1	Uncharacterized protein	NCU01019
		Q9P5L0	Probable cytochrome b5	NCU03910

Table S 6-7: List of interactors identified exclusively for one bait protein via quantitative analysis.

Only interactors were taken into account with significance >2 and difference >2 against all controls (stringent search). C = condition in which the interactor was identified. D = derepressed condition. R = repressed condition. B = both conditions.

bait	C	Uniprot accession	Protein name	Gene Name
NCU03462 Fbx40	B	Q7RWJ3	Leucine Rich Repeat domain-containing protein (bait)	NCU03462
	R	Q1K7U2	Ribonucloprotein (crp-75, snRNP and snoRNP protein)	NCU01331
	D	P61859	Calmodulin (CaM)	cmd-1 NCU04120
	D	Q86ZF9	Glutamine synthetase (GS) (EC 6.3.1.2) (Glutamate--ammonia ligase)	gln-1 NCU06724
	D	Q1K8R9	LsmAD domain-containing protein	NCU05400
	D	Q7SDM3	Myosin-1 (Class I unconventional myosin) (Type I myosin)	myo-1 NCU02111

bait	C	Uniprot accession	Protein name	Gene Name
	D	Q7SH88	Actin-related protein 2/3 complex subunit 4	NCU01918
	D	Q7SBC4	RNA binding protein Jsn1	puf1 NCU06199
	D	Q7S9P8	Myosin regulatory light chain cdc4	cdc4-2 NCU06617
NCU07521 Fbx17	B	Q7S199	F-box/WD-40 domain-containing protein 2 (bait)	fwd-2 NCU07521
	R	Q7S796	Uncharacterized protein	crp-70 NCU08960
	D	A7UWA6	NADH dehydrogenase [ubiquinone] 1 beta subcomplex subunit 9	NCU11258
	D	Q7SFZ2	40S ribosomal protein S11	crp-19 NCU03102
	D	P25284	NADH-ubiquinone oxidoreductase 40 kDa subunit	NCU02373
	D	Q7SE03	40S ribosomal protein S4	NCU02181
	D	Q7SBS9	60S ribosomal protein L25	NCU06226
	D	Q7RW05	Small GTPase RAC	Rac-1 NCU02160
	D	U9W5H2	Uncharacterized protein	NCU08550
	D	P08978	60S ribosomal protein L28	NCU03806
	D	P20080	FK506-binding protein 1A	fkr-2 NCU04140
	D	Q02854	NADH-ubiquinone oxidoreductase 20.9 kDa subunit	NCU01859
	D	Q1K6I4	Thiamine thiazole synthase (EC 2.4.2.60)	NCU06110
	D	Q7RWN7	Endoglucanase II	gh61-5 NCU08760
	D	Q7S156	60S ribosomal protein L33	NCU09109
	D	Q7S9A9	Alpha-1,4 glucan phosphorylase (EC 2.4.1.1)	NCU07027
	D	Q7SGF1	Ribosomal protein S12	NCU00971
NCU05033	B	Q1K6J3	Acyl-CoA dehydrogenase	acd-2 NCU08924
	B	Q7RX55	F-box domain-containing protein (bait)	NCU05033
	B	Q7S8H0	Uncharacterized protein	NCU05163
	B	Q1K5D9	Anchored cell wall protein 6	acw-6 NCU03530
	B	P04914	Histone H4	NCU01634
	R	Q7SF91	Uncharacterized protein	NCU00558
	R	V5ILH6	RNA binding protein (RNA binding protein, variant)	NCU06684
	R	Q7S503	40S ribosomal protein S2	NCU06047
	R	Q1K678	BYS1 domain-containing protein	mkr-1 NCU08907
	R	Q7SDY7	40S ribosomal protein S9	NCU01949
	R	O43105	40S ribosomal protein S7	NCU00258
	D	Q7S6U4	Cyanovirin-N homolog	NCU05495
	D	P05035	Orotidine 5'-phosphate decarboxylase (EC 4.1.1.23)	pyr-4 NCU03488
	D	Q9C169	Catalase-3 (EC 1.11.1.6)	cat-3 NCU00355

bait	C	Uniprot accession	Protein name	Gene Name
	D	Q1K6S6	Clock-controlled gene-15	ccg-15 NCU08936
	D	V5INQ2	40S ribosomal protein S6	NCU08502
NCU00471 Fbx41	B	Q7RXX4	Uncharacterized protein (bait)	NCU00471
	B	Q7SI08	ATP synthase subunit G	ats-3 NCU00644
	B	Q7SDV9	Cytochrome c peroxidase, mitochondrial (CCP) (EC 1.11.1.5)	ccp-1 NCU03297
	B	P23231	Mitochondrial import receptor subunit tom70	tom70 NCU04245
	B	Q7SFD8	MICOS complex subunit mic60 (Mitofilin)	mic60 NCU00894
	R	Q7S3A0	Uncharacterized protein	NCU09222
	R	Q03015	NADH-ubiquinone oxidoreductase 12 kDa subunit, mitochondrial	NCU03093
	R	Q7S7R7	Elongation factor 1-gamma	NCU03826
	R	Q7SDR1	Endoglucanase gh5-1 (EC 3.2.1.4)	gh5-1 NCU00762
	R	Q7SGT7	Cytochrome b-c1 complex subunit 9, mitochondrial	NCU03233
	R	Q7SI16	ATP synthase subunit d, mitochondrial	NCU00636
	D	Q7SGX0	ATP synthase subunit H	NCU03199
	D	Q7RZD4	Short-chain dehydrogenase/reductase SDR	NCU03893
	D	P87252	Woronin body major protein	NCU08332
	D	Q1K761	CipA protein	NCU01138
	D	Q7S5M7	Cytochrome c oxidase subunit 9, mitochondrial	NCU05816
	D	Q7SAS0	Nuclear and cytoplasmic polyadenylated RNA-binding protein pub1	NCU07874
	D	P23710	NADH-ubiquinone oxidoreductase 30.4 kDa subunit, mitochondrial (EC 7.1.1.2)	NCU04074
	D	Q7S2W8	NADH:ubiquinone oxidoreductase 10.6kD subunit	NCU09002

Table S 6-8: Qualitative analysis of NCU05033::GFP MS data.
(B) = gene ID of bait protein.

interactors in repressed condition				interactors in both conditions	interactors in derepressed condition
NCU01438	NCU08434	NCU07110	NCU00775	NCU01517	NCU03806
NCU03559	NCU03305	NCU08960	NCU03118	NCU07014	NCU07774
NCU01634	NCU02260	NCU08964	NCU02707	NCU04759	NCU03530
NCU00212	NCU09269	NCU08963	NCU02905	NCU08924	NCU08909
NCU05995	NCU08340	NCU08287	NCU00644	NCU04232	NCU09014
NCU07830	NCU02160	NCU07027	NCU08471	NCU05033 (B)	NCU05937
NCU02534	NCU03876	NCU08330	NCU01674	NCU05163	NCU06892
NCU03982	NCU01467	NCU05667	NCU06684	NCU07948	NCU02438
NCU03156	NCU04493	NCU06277	NCU03897	NCU08991	NCU05599
NCU03565	NCU07366	NCU08541	NCU07308	NCU00355	NCU06226
NCU05137	NCU09416	NCU09476	NCU06783	NCU03703	NCU02437
NCU03438	NCU09109	NCU00836	NCU02639	NCU05204	NCU01175

interactors in repressed condition				interactors in both conditions	interactors in derepressed condition
NCU07182	NCU09700	NCU02111	NCU08500		NCU01789
NCU04592	NCU07550	NCU01956	NCU08502		
NCU09209	NCU09210	NCU01948	NCU00541		
NCU08956	NCU02240	NCU02181	NCU08389		
NCU08936	NCU02400	NCU02797	NCU03300		
NCU03757	NCU02263	NCU03310	NCU00959		
NCU01331	NCU05804	NCU00716			
NCU01002	NCU04779	NCU02016			

Table S 6-9: Qualitative analysis of Fbx17::GFP MS data.
(B) = gene ID of bait protein.

interactors in repressed condition			interactors in both conditions	interactors in derepressed condition		
NCU06743	NCU03004	NCU09476	NCU02373	NCU03388	NCU08794	NCU02797
NCU01438	NCU16006	NCU05425	NCU06431	NCU01843	NCU11297	NCU02064
NCU03559	NCU08340	NCU01948	NCU07521 (B)	NCU03953	NCU00294	NCU01992
NCU01634	NCU02160	NCU02181	NCU09041	NCU05269	NCU10061	NCU00792
NCU00212	NCU00160	NCU01985	NCU08977	NCU03806	NCU07562	NCU00775
NCU01517	NCU06495	NCU03310	NCU02438	NCU02280	NCU05937	NCU03118
NCU07830	NCU09109	NCU00716	NCU10008	NCU07014	NCU08980	NCU03102
NCU02534	NCU09002	NCU00894	NCU05633	NCU04230	NCU09228	NCU01918
NCU04074	NCU07550	NCU00867	NCU05220	NCU16025	NCU06892	NCU02887
NCU04044	NCU09222	NCU03100	NCU06226	NCU00418	NCU02240	NCU00692
NCU05299	NCU06031	NCU03199	NCU08991	NCU03395	NCU02208	NCU06764
NCU05221	NCU02263	NCU02707	NCU05204	NCU06843	NCU08162	NCU01175
NCU08947	NCU05804	NCU02905	NCU08949	NCU04759	NCU04768	NCU03703
NCU01859	NCU04779	NCU00644		NCU08828	NCU07690	NCU01552
NCU03156	NCU08960	NCU08940		NCU01666	NCU06588	NCU03910
NCU07225	NCU08964	NCU06550		NCU03795	NCU07263	NCU01221
NCU07182	NCU08963	NCU03635		NCU04232	NCU07281	NCU01021
NCU05772	NCU06532	NCU01142		NCU05338	NCU08299	NCU00422
NCU08956	NCU08287	NCU16844		NCU03305	NCU07831	NCU07307
NCU08936	NCU07027	NCU08500		NCU01140	NCU06247	NCU07308
NCU01146	NCU07898	NCU08502		NCU01479	NCU10058	NCU02639
NCU03757	NCU05667	NCU00959		NCU00413	NCU00904	NCU07465
NCU06741				NCU07857	NCU00823	NCU08389

Table S 6-10: Qualitative analysis of Fbx40::GFP MS data.
(B) = gene ID of bait protein.

interactors in repressed condition		interactors in both conditions	interactors in derepressed condition	
NCU01328	NCU06031	NCU01517	NCU00461	NCU06598
NCU03559	NCU02400	NCU02373	NCU03806	NCU06226
NCU05995	NCU05804	NCU03093	NCU07014	NCU02111
NCU02534	NCU08287	NCU03462 (B)	NCU04230	NCU02797
NCU09468	NCU05667	NCU09867	NCU04120	NCU03302
NCU05772	NCU09476	NCU08991	NCU03438	NCU00775
NCU08936	NCU01948	NCU05204	NCU03530	NCU02599
NCU04303	NCU00716		NCU01666	NCU01918
NCU01146	NCU00768		NCU08909	NCU03703
NCU01331	NCU03199		NCU01341	NCU05526
NCU03004	NCU02707		NCU07238	NCU03749
NCU08340	NCU00644		NCU00160	NCU06684
NCU04522	NCU08940		NCU00311	NCU03050
NCU07366	NCU03635		NCU09014	NCU00541
NCU07756	NCU08500		NCU06892	NCU08389
NCU09002	NCU00959		NCU07690	
NCU09222	NCU03300			

Table S 6-11: Qualitative analysis of Fbx41::GFP MS data.
(B) = gene ID of bait protein.

interactors in repressed condition				interactors in both conditions	interactors in derepressed condition
NCU06743	NCU00431	NCU03893	NCU01948	NCU03953	NCU04792
NCU01438	NCU03156	NCU07366	NCU02181	NCU16020	NCU07774
NCU03559	NCU01589	NCU07756	NCU03310	NCU02373	NCU03438
NCU01634	NCU03530	NCU09143	NCU00716	NCU16025	NCU01140
NCU00212	NCU07225	NCU09002	NCU00894	NCU00418	NCU00160
NCU05689	NCU08907	NCU09222	NCU00867	NCU00969	NCU08980
NCU05995	NCU05772	NCU06880	NCU02016	NCU04759	NCU00801
NCU16004	NCU08936	NCU06031	NCU02013	NCU03093	NCU08114
NCU05601	NCU06666	NCU02263	NCU00768	NCU08755	NCU09332
NCU01517	NCU01146	NCU04799	NCU08339	NCU08794	NCU00823
NCU07830	NCU04192	NCU05515	NCU03199	NCU00471 (B)	NCU02566
NCU08930	NCU04232	NCU08960	NCU02707	NCU09416	NCU00137
NCU02472	NCU03737	NCU06701	NCU02905	NCU02438	NCU07842
NCU08823	NCU08434	NCU06532	NCU00644	NCU02240	NCU09560
NCU02534	NCU06741	NCU05163	NCU08940	NCU00904	NCU03749
NCU07732	NCU03004	NCU06588	NCU06550	NCU02812	NCU01962
NCU04074	NCU16013	NCU07027	NCU08471	NCU02064	
NCU05299	NCU16006	NCU07898	NCU01674	NCU00775	
NCU05221	NCU02260	NCU08299	NCU06727	NCU08991	
NCU04230	NCU08340	NCU07874	NCU00326	NCU08949	
NCU09132	NCU02160	NCU05667	NCU01142	NCU07465	
NCU09468	NCU03979	NCU08541	NCU16844		

interactors in repressed condition				interactors in both conditions	interactors in derepressed condition
NCU05274	NCU01467	NCU06245	NCU08500		
NCU03982	NCU04522	NCU09476	NCU06397		
NCU03463	NCU04493	NCU00836	NCU00959		
NCU01859	NCU11348	NCU01956	NCU03300		

Table S 6-12: Qualitative analysis of CRE-1::GFP MS data.
(B) = gene ID of bait protein.

interactors in repressed condition	interactors in both conditions	interactors in derepressed condition
NCU05995	NCU08807 (B)	NCU03806
NCU07830		NCU07014
NCU04074		NCU08294
NCU04120		NCU03395
NCU03982		NCU04232
NCU03922		NCU02400
NCU03757		NCU07948
NCU09269		NCU02495
NCU06464		NCU01552
NCU06031		NCU01021
NCU08964		NCU06684
NCU10337		NCU04185
NCU08287		
NCU02111		
NCU00716		
NCU01918		
NCU03300		

Table S 6-13: List of interactors identified within several F-box samples via qualitative analysis of the MS data.
Numbers of column headers are according to Figure S 6-19. Bait proteins are highlighted in grey.

0001	0010		0011	0100	0101	0110
NCU03565	NCU04044	NCU04768	NCU07182	NCU01328	NCU01331	NCU03635
NCU05137	NCU08947	NCU07263	NCU08956	NCU04303	NCU02400	NCU01666
NCU04592	NCU06495	NCU07281	NCU03757	NCU00461	NCU02111	NCU07690
NCU09209	NCU05425	NCU07831	NCU03305	NCU04120	NCU06684	NCU01918
NCU01002	NCU01985	NCU06247	NCU09109	NCU01341	NCU00541	
NCU09269	NCU03100	NCU10058	NCU07550	NCU07238	NCU08909	
NCU03876	NCU03388	NCU01992	NCU04779	NCU00311	NCU09014	
NCU09700	NCU01843	NCU00792	NCU08964	NCU06598		
NCU09210	NCU05269	NCU03102	NCU08963	NCU03302		
NCU07110	NCU02280	NCU02887	NCU03118	NCU02599		
NCU08330	NCU03395	NCU00692	NCU07308	NCU05526		
NCU06277	NCU06843	NCU06764	NCU02639	NCU03050		
NCU03897	NCU08828	NCU01552	NCU08502	NCU03462		
NCU06783	NCU03795	NCU03910	NCU05937	NCU09867		
NCU05599	NCU05338	NCU01221	NCU01175			
NCU02437	NCU01479	NCU01021				
NCU01789	NCU00413	NCU00422				

NCU08924	NCU07857	NCU07307				
NCU05033	NCU11297	NCU06431				
NCU07948	NCU00294	NCU07521				
NCU00355	NCU10061	NCU09041				
	NCU07562	NCU08977				
	NCU09228	NCU10008				
	NCU02208	NCU05633				
	NCU08162	NCU05220				

0111	**1000**		**1001**	**1010**	**1011**	**1100**
NCU05804	NCU05689	NCU05515	NCU03982	NCU06743	NCU01438	NCU09468
NCU08287	NCU16004	NCU06701	NCU08434	NCU04074	NCU01634	NCU04522
NCU02797	NCU05601	NCU07874	NCU02260	NCU05299	NCU00212	NCU07756
NCU08389	NCU08930	NCU06245	NCU01467	NCU05221	NCU07830	NCU00768
NCU03806	NCU02472	NCU02013	NCU04493	NCU01859	NCU03156	NCU03749
NCU06892	NCU08823	NCU08339	NCU09416	NCU07225	NCU02160	NCU03093
NCU06226	NCU07732	NCU06727	NCU08541	NCU06741	NCU02240	
NCU07014	NCU09132	NCU00326	NCU00836	NCU16006	NCU02263	
NCU03703	NCU05274	NCU06397	NCU01956	NCU06532	NCU08960	
NCU05204	NCU03463	NCU04792	NCU02016	NCU07898	NCU07027	
	NCU00431	NCU00801	NCU08471	NCU00894	NCU02181	
	NCU01589	NCU08114	NCU01674	NCU00867	NCU03310	
	NCU08907	NCU09332	NCU07774	NCU06550	NCU02905	
	NCU06666	NCU02566	NCU05163	NCU01142	NCU02438	
	NCU04192	NCU00137		NCU16844	NCU04759	
	NCU03737	NCU07842		NCU03953	NCU04232	
	NCU16013	NCU09560		NCU16025		
	NCU03979	NCU01962		NCU00418		
	NCU11348	NCU16020		NCU01140		
	NCU03893	NCU00969		NCU08794		
	NCU09143	NCU08755		NCU08980		
	NCU06880	NCU00471		NCU06588		
	NCU04799	NCU02812		NCU08299		
				NCU00904		
				NCU00823		
				NCU02064		
				NCU07465		
				NCU08949		

1101	**1110**	**1111**	
NCU05995	NCU05772	NCU03559	NCU00959
NCU03438	NCU01146	NCU02534	NCU01517
NCU07366	NCU03004	NCU08936	NCU08991
NCU03300	NCU00160	NCU08340	
NCU03530	NCU09002	NCU05667	
	NCU09222	NCU09476	
	NCU06031	NCU01948	
	NCU03199	NCU00716	
	NCU08940	NCU00775	
	NCU04230	NCU02707	
	NCU02373	NCU00644	
		NCU08500	

Table S 6-14: List of interactors identified within several F-box samples and CRE-1 via qualitative analysis of the MS data.
Numbers of column headers are according to Figure S 6-20. Bait proteins are highlighted in grey.

00001	00010		00011	00100	00101	00110
NCU03565	NCU04044	NCU04768	NCU07182	NCU01328	NCU01331	NCU03635
NCU05137	NCU08947	NCU07263	NCU08956	NCU04303	NCU00541	NCU01666
NCU04592	NCU06495	NCU07281	NCU03305	NCU00461	NCU08909	NCU07690
NCU09209	NCU05425	NCU07831	NCU09109	NCU01341	NCU09014	
NCU01002	NCU01985	NCU06247	NCU07550	NCU07238		
NCU03876	NCU03100	NCU10058	NCU04779	NCU00311		
NCU09700	NCU03388	NCU01992	NCU08963	NCU06598		
NCU09210	NCU01843	NCU00792	NCU03118	NCU03302		
NCU07110	NCU05269	NCU03102	NCU07308	NCU02599		
NCU08330	NCU02280	NCU02887	NCU02639	NCU05526		
NCU06277	NCU06843	NCU00692	NCU08502	NCU03050		
NCU03897	NCU08828	NCU06764	NCU05937	NCU03462		
NCU06783	NCU03795	NCU03910	NCU01175	NCU09867		
NCU05599	NCU05338	NCU01221				
NCU02437	NCU01479	NCU00422				
NCU01789	NCU00413	NCU07307				
NCU08924	NCU07857	NCU06431				
NCU05033	NCU11297	NCU07521				
NCU00355	NCU00294	NCU09041				
	NCU10061	NCU08977				
	NCU07562	NCU10008				
	NCU09228	NCU05633				
	NCU02208	NCU05220				
	NCU08162					

00111	01000		01001	01010	01011	01100
NCU05804	NCU05689	NCU05515	NCU08434	NCU06743	NCU01438	NCU09468
NCU02797	NCU16004	NCU06701	NCU02260	NCU05299	NCU01634	NCU04522
NCU08389	NCU05601	NCU07874	NCU01467	NCU05221	NCU00212	NCU07756
NCU06892	NCU08930	NCU06245	NCU04493	NCU01859	NCU03156	NCU00768
NCU06226	NCU02472	NCU02013	NCU09416	NCU07225	NCU02160	NCU03749
NCU03703	NCU08823	NCU08339	NCU08541	NCU06741	NCU02240	NCU03093
NCU05204	NCU07732	NCU06727	NCU00836	NCU16006	NCU02263	
	NCU09132	NCU00326	NCU01956	NCU06532	NCU08960	
	NCU05274	NCU06397	NCU02016	NCU07898	NCU07027	
	NCU03463	NCU04792	NCU08471	NCU00894	NCU02181	
	NCU00431	NCU00801	NCU01674	NCU00867	NCU03310	
	NCU01589	NCU08114	NCU07774	NCU06550	NCU02905	
	NCU08907	NCU09332	NCU05163	NCU01142	NCU02438	
	NCU06666	NCU02566		NCU16844	NCU04759	
	NCU04192	NCU00137		NCU03953		
	NCU03737	NCU07842		NCU16025		
	NCU16013	NCU09560		NCU00418		
	NCU03979	NCU01962		NCU01140		
	NCU11348	NCU16020		NCU08794		
	NCU03893	NCU00969		NCU08980		
	NCU09143	NCU08755		NCU06588		

	NCU06880 NCU04799	NCU00471 NCU02812		NCU08299 NCU00904 NCU00823 NCU02064 NCU07465 NCU08949		

01101	**01110**	**01111**	**10000**	**10001**	**10010**	**10011**
NCU03438 NCU07366 NCU03530	NCU05772 NCU01146 NCU03004 NCU00160 NCU09002 NCU09222 NCU03199 NCU08940 NCU04230 NCU02373	NCU03559 NCU02534 NCU08936 NCU08340 NCU05667 NCU09476 NCU01948 NCU00775 NCU02707 NCU00644 NCU08500 NCU00959 NCU01517 NCU08991	NCU03922 NCU06464 NCU10337 NCU08294 NCU02495 NCU04185 NCU08807	NCU09269 NCU07948	NCU03395 NCU01552 NCU01021	NCU03757 NCU08964

10100	**10101**	**10110**	**10111**	**11001**	**11010**	**11011**
NCU04120	NCU02400 NCU02111 NCU06684	NCU01918	NCU08287 NCU03806 NCU07014	NCU03982	NCU04074	NCU07830 NCU04232

11101	**11110**	**11111**
NCU05995 NCU03300	NCU06031	NCU00716

6.4. Plasmid maps

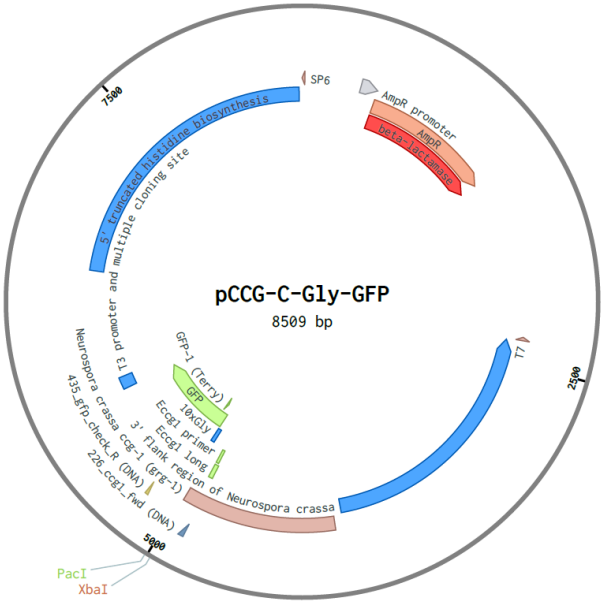

Figure S 6-24: Map of *Neurospora* expression vector pCCG::C-Gly::GFP.
This expression vector targets the *his-3* gene of *N. crassa*. By homologous recombination the *his-3* 5´ and 3´ flanking regions restore histidine auxotrophy from the recipient strain. In-between both flanks, lies the overexpression promoter *ccg-1*, the multiple cloning site (MCS), *gfp* gene and the *adh* terminator. The map was created using Benchling. Cutting sites of the restriction enzymes PacI and XbaI which are flanking the MCS are shown in the figure. Ampicillin resistance to *E. coli* is conveyed by the *β-lactamase* gene.

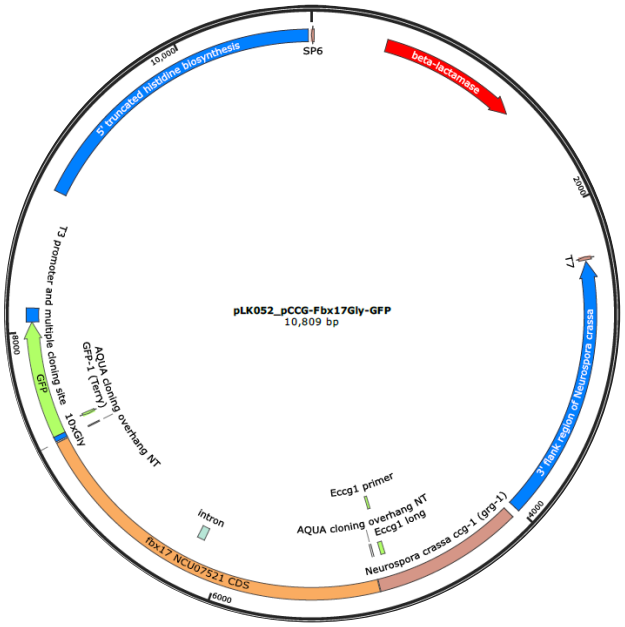

Figure S 6-25: Map of *Neurospora* expression vector pLK052, pCCG::NCU07521::C-Gly::GFP.
This expression vector targets the *his-3* gene of *N. crassa*. By homologous recombination the *his-3* 5´ and 3´ flanking regions restore histidine auxotrophy from the recipient strain. In-between both flanks, lies the overexpression promoter *ccg-1*, the coding sequence of NCU07521, *gfp* gene and the *adh* terminator. The map was visualized using SnapGene. Ampicillin resistance to *E. coli* is conveyed by the *β-lactamase* gene.

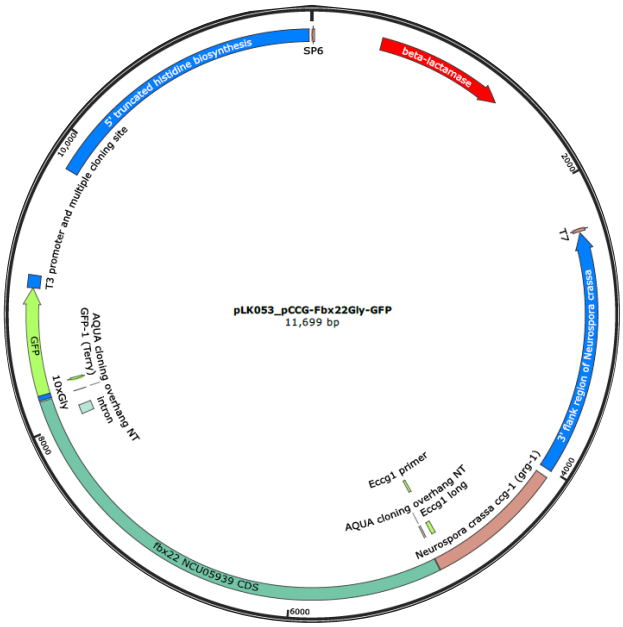

Figure S 6-26: Map of *Neurospora* expression vector pLK053, pCCG::NCU05939::C-Gly::GFP. This expression vector targets the *his-3* gene of *N. crassa*. By homologous recombination the *his-3* 5´ and 3´ flanking regions restore histidine auxotrophy from the recipient strain. In-between both flanks, lies the overexpression promoter *ccg-1*, the coding sequence of NCU05939, *gfp* gene and the *adh* terminator. The map was visualized using SnapGene. Ampicillin resistance to *E. coli* is conveyed by the *β-lactamase* gene.

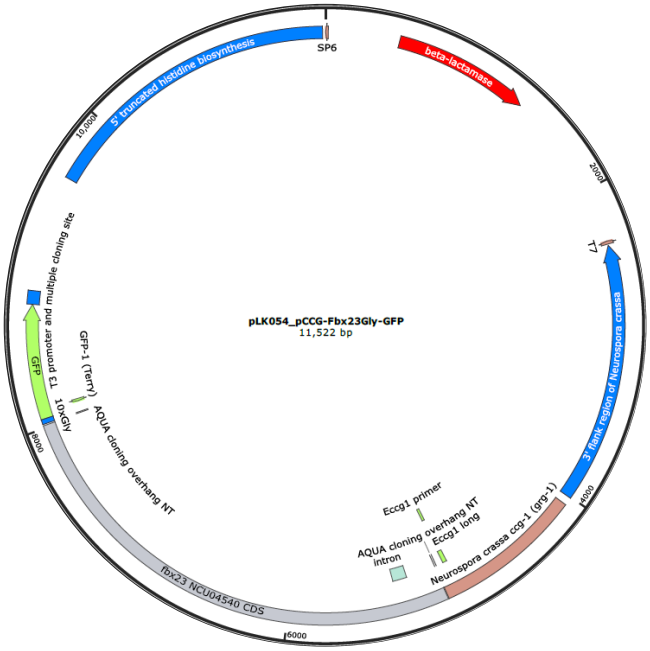

Figure S 6-27: Map of *Neurospora* expression vector pLK054, pCCG::NCU04540::Gly-GFP . This expression vector targets the *his-3* gene of *N. crassa*. By homologous recombination the *his-3* 5´ and 3´ flanking regions restore histidine auxotrophy from the recipient strain. In-between both flanks, lies the overexpression promoter *ccg-1*, the coding sequence of NCU04540, *gfp* gene and the *adh* terminator. The map was visualized using SnapGene. Ampicillin resistance to *E. coli* is conveyed by the *β-lactamase* gene.

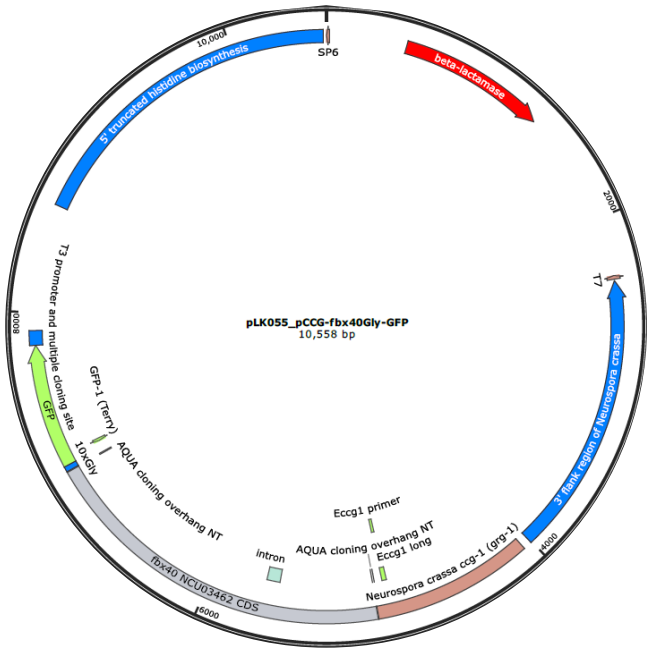

Figure S 6-28: Map of *Neurospora* expression vector pLK055, pCCG::NCU03462::Gly-GFP.
This expression vector targets the *his-3* gene of *N. crassa*. By homologous recombination the *his-3* 5´ and 3´ flanking regions restore histidine auxotrophy from the recipient strain. In-between both flanks, lies the overexpression promoter *ccg-1*, the coding sequence of NCU03462, *gfp* gene and the *adh* terminator. The map was visualized using SnapGene. Ampicillin resistance to *E. coli* is conveyed by the *β-lactamase* gene.

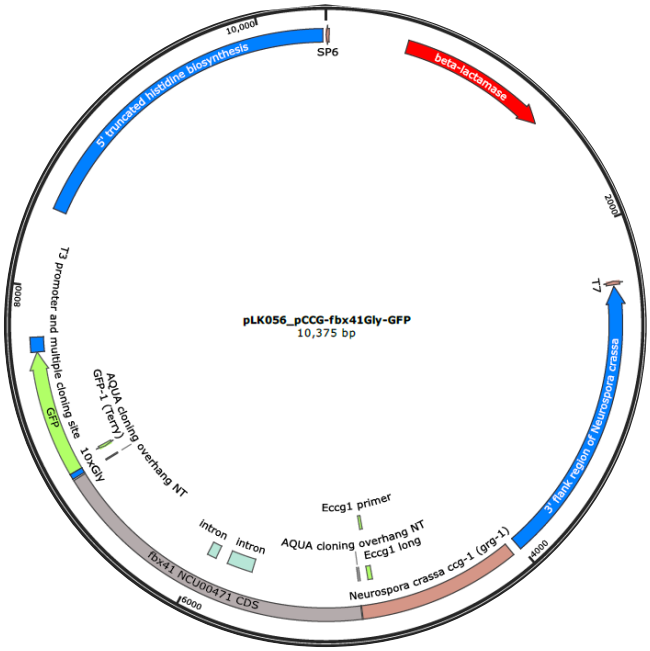

Figure S 6-29: Map of *Neurospora* expression vector pLK056, pCCG::NCU00471::C-Gly::GFP.
This expression vector targets the *his-3* gene of *N. crassa*. By homologous recombination the *his-3* 5´ and 3´ flanking regions restore histidine auxotrophy from the recipient strain. In-between both flanks, lies the overexpression promoter *ccg-1*, the coding sequence of NCU00471, *gfp* gene and the *adh* terminator. The map was visualized using SnapGene. Ampicillin resistance to *E. coli* is conveyed by the *β-lactamase* gene.

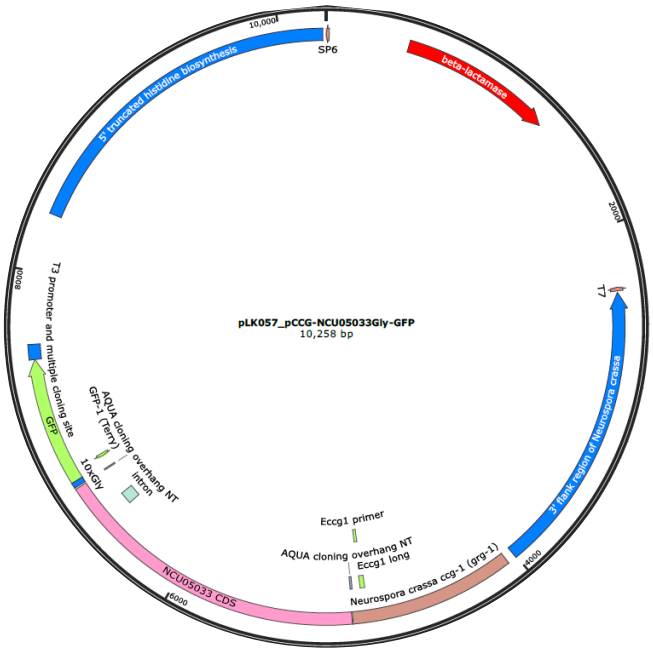

Figure S 6-30: Map of *Neurospora* expression vector pLK057, pCCG::NCU05033::C-Gly::GFP. This expression vector targets the *his-3* gene of *N. crassa*. By homologous recombination the *his-3* 5´ and 3´ flanking regions restore histidine auxotrophy from the recipient strain. In-between both flanks, lies the overexpression promoter *ccg-1*, the coding sequence of NCU05033, *gfp* gene and the *adh* terminator. The map was visualized using SnapGene. Ampicillin resistance to *E. coli* is conveyed by the *β-lactamase* gene.

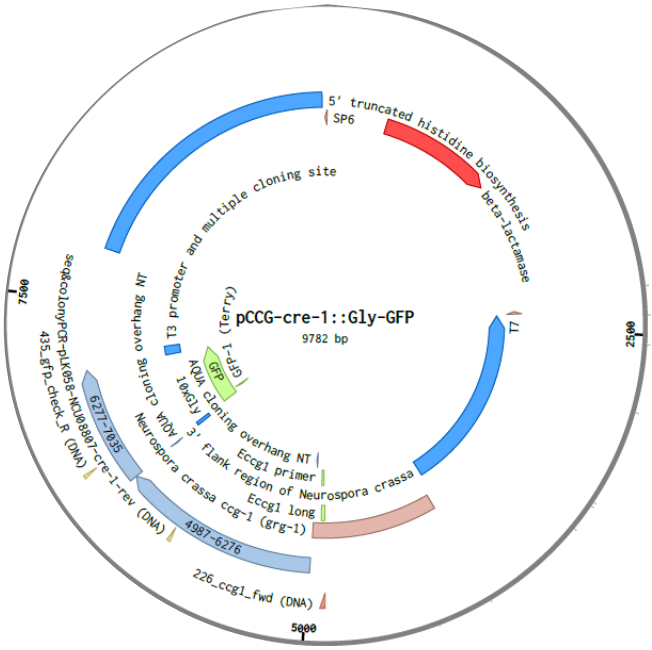

Figure S 6-31: Map of *Neurospora* expression vector pLK058, pCCG::NCU08807::Gly-GFP. This expression vector targets the *his-3* gene of *N. crassa*. By homologous recombination the *his-3* 5´ and 3´ flanking regions restore histidine auxotrophy from the recipient strain. In-between both flanks, lies the overexpression promoter *ccg-1*, the coding sequence of NCU08807, *gfp* gene and the *adh* terminator. The map was visualized using Benchling. Ampicillin resistance to *E. coli* is conveyed by the *β-lactamase* gene.

References

ADNAN, M., ZHENG, W., ISLAM, W., ARIF, M., ABUBAKAR, Y.S., WANG, Z., AND LU, G. 2017. Carbon Catabolite Repression in Filamentous Fungi. *International Journal of Molecular Sciences 19*, 1. https://www.ncbi.nlm.nih.gov/pmc/articles/PMC5795998/.

ALAM, M.A., AND KELLY, J.M. 2017. Proteins interacting with CreA and CreB in the carbon catabolite repression network in *Aspergillus nidulans*. *Curr Genet 63*, 4, 669–683. https://link.springer.com/article/10.1007/s00294-016-0667-2.

ALEKSANDER, S.A., BALHOFF, J., CARBON, S., CHERRY, J.M., DRABKIN, H.J., EBERT, D., FEUERMANN, M., GAUDET, P., HARRIS, N.L., HILL, D.P., LEE, R., MI, H., MOXON, S., MUNGALL, C.J., MURUGANUGAN, A., MUSHAYAHAMA, T., STERNBERG, P.W., THOMAS, P.D., VAN AUKEN, K., RAMSEY, J., SIEGELE, D.A., CHISHOLM, R.L., FEY, P., ASPROMONTE, M.C., NUGNES, M.V., QUAGLIA, F., TOSATTO, S., GIGLIO, M., NADENDLA, S., ANTONAZZO, G., ATTRILL, H., DOS SANTOS, G., MARYGOLD, S., STRELETS, V., TABONE, C.J., THURMOND, J., ZHOU, P., AHMED, S.H., ASANITTHONG, P., LUNA BUITRAGO, D., ERDOL, M.N., GAGE, M.C., ALI KADHUM, M., LI, K.Y.C., LONG, M., MICHALAK, A., PESALA, A., PRITAZAHRA, A., SAVERIMUTTU, S.C.C., SU, R., THURLOW, K.E., LOVERING, R.C., LOGIE, C., OLIFERENKO, S., BLAKE, J., CHRISTIE, K., CORBANI, L., DOLAN, M.E., NI, L., SITNIKOV, D., SMITH, C., CUZICK, A., SEAGER, J., COOPER, L., ELSER, J., JAISWAL, P., GUPTA, P., NAITHANI, S., LERA-RAMIREZ, M., RUTHERFORD, K., WOOD, V., PONS, J.L. DE, DWINELL, M.R., HAYMAN, G.T., KALDUNSKI, M.L., KWITEK, A.E., LAULEDERKIND, S.J.F., TUTAJ, M.A., VEDI, M., WANG, S.-J., D'EUSTACHIO, P., AIMO, L., AXELSEN, K., BRIDGE, A., HYKA-NOUSPIKEL, N., MORGAT, A., ENGEL, S.R., KARRA, K., MIYASATO, S.R., NASH, R.S., SKRZYPEK, M.S., WENG, S., WONG, E.D., BAKKER, E., BERARDINI, T.Z., REISER, L., AUCHINCLOSS, A., ARGOUD-PUY, G., BLATTER, M.-C., BOUTET, E., BREUZA, L., CASALS-CASAS, C., COUDERT, E., ESTREICHER, A., LIVIA FAMIGLIETTI, M., GOS, A., GRUAZ-GUMOWSKI, N., HULO, C., JUNGO, F., LE MERCIER, P., LIEBERHERR, D., MASSON, P., PEDRUZZI, I., POURCEL, L., POUX, S., RIVOIRE, C., SUNDARAM, S., BATEMAN, A., BOWLER-BARNETT, E., BYE-A-JEE, H., DENNY, P., IGNATCHENKO, A., ISHTIAQ, R., LOCK, A., LUSSI, Y., MAGRANE, M., MARTIN, M.J., ORCHARD, S., RAPOSO, P., SPERETTA, E., TYAGI, N., WARNER, K., ZARU, R., DIEHL, A.D., CHAN, J., DIAMANTAKIS, S., RACITI, D., ZAROWIECKI, M., FISHER, M., JAMES-ZORN, C., PONFERRADA, V., ZORN, A., RAMACHANDRAN, S., RUZICKA, L., AND WESTERFIELD, M. 2023. The Gene Ontology knowledgebase in 2023. *Genetics 224*, 1.

ANDLAR, M., REZIĆ, T., MARĐETKO, N., KRACHER, D., LUDWIG, R., AND ŠANTEK, B. 2018. Lignocellulose degradation: An overview of fungi and fungal enzymes involved in lignocellulose degradation. *Engineering in life sciences 18*, 11, 768–778.

ARST, H.N., AND COVE, D.J. 1973. Nitrogen metabolite repression in *Aspergillus nidulans*. *Molecular & general genetics : MGG 126*, 2, 111–141.

ASHBURNER, M., BALL, C.A., BLAKE, J.A., BOTSTEIN, D., BUTLER, H., CHERRY, J.M., DAVIS, A.P., DOLINSKI, K., DWIGHT, S.S., EPPIG, J.T., HARRIS, M.A., HILL, D.P., ISSEL-TARVER, L., KASARSKIS, A., LEWIS, S., MATESE, J.C., RICHARDSON, J.E., RINGWALD, M., RUBIN, G.M., AND SHERLOCK, G. 2000. Gene ontology: tool for the unification of biology. The Gene Ontology Consortium. *Nature genetics 25*, 1, 25–29.

ASSIS, L.J. DE, SILVA, L.P., BAYRAM, O., DOWLING, P., KNIEMEYER, O., KRÜGER, T., BRAKHAGE, A.A., CHEN, Y., DONG, L., TAN, K., WONG, K.H., RIES, L.N.A., AND GOLDMAN, G.H. 2021. Carbon Catabolite Repression in Filamentous Fungi Is Regulated by Phosphorylation of the Transcription Factor CreA. *mBio 12*, 1.

ASSIS, L.J. DE, SILVA, L.P., LIU, L., SCHMITT, K., VALERIUS, O., BRAUS, G.H., RIES, L.N.A., AND GOLDMAN, G.H. 2020. The High Osmolarity Glycerol Mitogen-Activated Protein Kinase regulates glucose catabolite repression in filamentous fungi. *PLOS Genetics 16*, 8, e1008996.

ASSIS, L.J. DE, ULAS, M., RIES, L.N.A., EL RAMLI, N.A.M., SARIKAYA-BAYRAM, O., BRAUS, G.H., BAYRAM, O., AND GOLDMAN, G.H. 2018. Regulation of *Aspergillus nidulans* CreA-Mediated Catabolite Repression by the F-Box Proteins Fbx23 and Fbx47. *mBio 9*, 3.

BAI, C., SEN, P., HOFMANN, K., MA, L., GOEBL, M., HARPER, J.W., AND ELLEDGE, S.J. 1996. SKP1 connects cell cycle regulators to the ubiquitin proteolysis machinery through a novel motif, the F-box. *Cell 86*, 2, 263–274. https://www.sciencedirect.com/science/article/pii/S0092867400800987.

BAILEY, C., AND ARST, H.N. 1975. Carbon catabolite repression in *Aspergillus nidulans*. *European journal of biochemistry 51*, 2, 573–577.

BARDIYA, N., ALEXANDER, W.G., PERDUE, T.D., BARRY, E.G., METZENBERG, R.L., PUKKILA, P.J., AND SHIU, P.K.T. 2008. Characterization of interactions between and among components of the meiotic silencing by unpaired DNA machinery in *Neurospora crassa* using bimolecular fluorescence complementation. *Genetics 178*, 1, 593–596.

BASTAWDE, K.B. 1992. Xylan structure, microbial xylanases, and their mode of action. *World J Microbiol Biotechnol 8*, 4, 353–368. https://link.springer.com/article/10.1007/bf01198746.

BEADLE, G.W., AND TATUM, E.L. 1941. Genetic Control of Biochemical Reactions in *Neurospora*. *Proceedings of the National Academy of Sciences of the United States of America 27*, 11, 499–506.

BENZ, J.P., CHAU, B.H., ZHENG, D., BAUER, S., GLASS, N.L., AND SOMERVILLE, C.R. 2014. A comparative systems analysis of polysaccharide-elicited responses in *Neurospora crassa* reveals carbon source-specific cellular adaptations. *Molecular microbiology 91*, 2, 275–299.

BERNDSEN, C.E., AND WOLBERGER, C. 2014. New insights into ubiquitin E3 ligase mechanism. *Nat Struct Mol Biol 21*, 4, 301–307. https://www.nature.com/articles/nsmb.2780.

BERTANI, G. 1951. Studies on lysogenesis. I. The mode of phage liberation by lysogenic *Escherichia coli*. *Journal of bacteriology 62*, 3, 293–300.

BLONDEL, M., GALAN, J.M., CHI, Y., LAFOURCADE, C., LONGARETTI, C., DESHAIES, R.J., AND PETER, M. 2000. Nuclear-specific degradation of Far1 is controlled by the localization of the F-box protein Cdc4. *The EMBO Journal 19*, 22, 6085–6097.

BOLGER, A.M., LOHSE, M., AND USADEL, B. 2014. Trimmomatic: a flexible trimmer for Illumina sequence data. *Bioinformatics (Oxford, England) 30*, 15, 2114–2120. https://academic.oup.com/bioinformatics/article/30/15/2114/2390096?login=false.

BROWN, N.A., RIES, L.N.A., AND GOLDMAN, G.H. 2014. How nutritional status signalling coordinates metabolism and lignocellulolytic enzyme secretion. *Fungal genetics and biology 72*, 48–63.

CABRERA, I.E., PACENTINE, I.V., LIM, A., GUERRERO, N., KRYSTOFOVA, S., LI, L., MICHKOV, A.V., SERVIN, J.A., AHRENDT, S.R., CARRILLO, A.J., DAVIDSON, L.M., BARSOUM, A.H., CAO, J., CASTILLO, R., CHEN, W.-C., DINKCHIAN, A., KIM, S., KITADA, S.M., LAI, T.H., MACH, A., MALEKYAN, C., MOUA, T.R., TORRES, C.R., YAMAMOTO, A., AND BORKOVICH, K.A. 2015. Global Analysis of Predicted G Protein-Coupled Receptor Genes in the Filamentous Fungus, *Neurospora crassa*. *G3 (Bethesda, Md.) 5*, 12, 2729–2743.

CAI, P., GU, R., WANG, B., LI, J., WAN, L., TIAN, C., AND MA, Y. 2014. Evidence of a critical role for cellodextrin transporte 2 (CDT-2) in both cellulose and hemicellulose degradation and utilization in *Neurospora crassa*. *PLoS ONE 9*, 2, e89330.

CANTAREL, B.L., COUTINHO, P.M., RANCUREL, C., BERNARD, T., LOMBARD, V., AND HENRISSAT, B. 2009. The Carbohydrate-Active EnZymes database (CAZy): an expert resource for Glycogenomics. *Nucleic acids research 37*, Database issue, D233-8.

CENCIARELLI, C., CHIAUR, D.S., GUARDAVACCARO, D., PARKS, W., VIDAL, M., AND PAGANO, M. 1999. Identification of a family of human F-box proteins. *Current biology : CB 9*, 20, 1177–1179.

CLAUSER, N.M., GONZÁLEZ, G., MENDIETA, C.M., KRUYENISKI, J., AREA, M.C., AND VALLEJOS, M.E. 2021. Biomass Waste as Sustainable Raw Material for Energy and Fuels. *Sustainability 13*, 2, 794.

COLLIER, L.A., GHOSH, A., AND BORKOVICH, K.A. 2020. Heterotrimeric G-Protein Signaling Is Required for Cellulose Degradation in *Neurospora crassa*. *mBio 11*, 6.

COLOT, H.V., PARK, G., TURNER, G.E., RINGELBERG, C., CREW, C.M., LITVINKOVA, L., WEISS, R.L., BORKOVICH, K.A., AND DUNLAP, J.C. 2006. A high-throughput gene knockout procedure for *Neurospora* reveals functions for multiple transcription factors. *Proceedings of the National Academy of Sciences of the United States of America 103*, 27, 10352–10357. https://www.pnas.org/doi/10.1073/pnas.0601456103.

CORADETTI, S.T., CRAIG, J.P., XIONG, Y., SHOCK, T., TIAN, C., AND GLASS, N.L. 2012. Conserved and essential transcription factors for cellulase gene expression in ascomycete fungi. *Proceedings of the National Academy of Sciences of the United States of America 109*, 19, 7397–7402.

COX, J., AND MANN, M. 2008. MaxQuant enables high peptide identification rates, individualized p.p.b.-range mass accuracies and proteome-wide protein quantification. *Nat Biotechnol 26*, 12, 1367–1372. https://www.nature.com/articles/nbt.1511.

CRAIG, K.L., AND TYERS, M. 1999. The F-box: a new motif for ubiquitin dependent proteolysis in cell cycle regulation and signal transduction. *Progress in Biophysics and Molecular Biology 72*, 3, 299–328. https://www.sciencedirect.com/science/article/pii/S0079610799000103.

CUPERTINO, F.B., VIRGILIO, S., FREITAS, F.Z., CANDIDO, T.D.S., AND BERTOLINI, M.C. 2015. Regulation of glycogen metabolism by the CRE-1, RCO-1 and RCM-1 proteins in *Neurospora crassa*. The role of CRE-1 as the central transcriptional regulator. *Fungal genetics and biology : FG & B 77*, 82–94.

DALY, P., VAN MUNSTER, J., RAULO, R., AND ARCHER, D.B. 2016. Transcriptional Regulation and Responses in Filamentous Fungi Exposed to Lignocellulose. In *Mycology: Current and Future Developments*. *Fungal Biotechnology for Biofuel Production*, R. N. SILVA, Ed. Bentham Science Publishers, Sharjah, U. A. E., 82–127.

DAVIS, R.H., AND PERKINS, D.D. 2002. Timeline: *Neurospora*: a model of model microbes. *Nat Rev Genet 3*, 5, 397–403. https://www.nature.com/articles/nrg797.

DELMAS, S., PULLAN, S.T., GADDIPATI, S., KOKOLSKI, M., MALLA, S., BLYTHE, M.J., IBBETT, R., CAMPBELL, M., LIDDELL, S., ABOOBAKER, A., TUCKER, G.A., AND ARCHER, D.B. 2012. Uncovering the genome-wide transcriptional responses of the filamentous fungus *Aspergillus niger* to lignocellulose using RNA sequencing. *PLOS Genetics 8*, 8, e1002875.

DEVI, A., BAJAR, S., KOUR, H., KOTHARI, R., PANT, D., AND SINGH, A. 2022. Lignocellulosic Biomass Valorization for Bioethanol Production: a Circular Bioeconomy Approach. *Bioenerg. Res. 15*, 4, 1820–1841. https://link-springer-com.eaccess.tum.edu/article/10.1007/s12155-022-10401-9.

DOGARIS, I., MAMMA, D., AND KEKOS, D. 2013. Biotechnological production of ethanol from renewable resources by *Neurospora crassa*: an alternative to conventional yeast fermentations? *Applied microbiology and biotechnology 97*, 4, 1457–1473.

DRAHT, O.W., BUSCH, S., HOFMANN, K., BRAUS-STROMEYER, S., HELMSTAEDT, K., GOLDMAN, G.H., AND BRAUS, G.H. 2008. Amino Acid Supply of *Aspergillus*. In *The Aspergilli*. *Genomics, medical aspects, biotechnology, and research methods*, S. A. OSMANI AND G. H. GOLDMAN, Eds. CRC Press, Boca Raton, Fla., 143–175.

DUNLAP, J.C., BORKOVICH, K.A., HENN, M.R., TURNER, G.E., SACHS, M.S., GLASS, N.L., MCCLUSKEY, K., PLAMANN, M., GALAGAN, J.E., BIRREN, B.W., WEISS, R.L., TOWNSEND, J.P., LOROS, J.J., NELSON, M.A., LAMBREGHTS, R., COLOT, H.V., PARK, G., COLLOPY, P., RINGELBERG, C., CREW, C., LITVINKOVA, L., DECAPRIO, D., HOOD, H.M., CURILLA, S., SHI, M., CRAWFORD, M., KOERHSEN, M., MONTGOMERY, P., LARSON, L., PEARSON, M., KASUGA, T., TIAN, C., BAŞTÜRKMEN, M., ALTAMIRANO, L., AND XU, J. 2007. Enabling a community to dissect an organism: overview of the *Neurospora* functional genomics project. *Advances in genetics 57*, 49–96.

EBBOLE, D.J. 1998. Carbon catabolite repression of gene expression and conidiation in *Neurospora crassa*. *Fungal genetics and biology : FG & B 25*, 1, 15–21. https://www.sciencedirect.com/science/article/pii/S108718459891088X.

FAN, F., MA, G., LI, J., LIU, Q., BENZ, J.P., TIAN, C., AND MA, Y. 2015. Genome-wide analysis of the endoplasmic reticulum stress response during lignocellulase production in *Neurospora crassa*. *Biotechnol Biofuels 8*, 66.

FREY-WYSSLING, A. 1954. The Fine Structure of Cellulose Microfibrils. *Science (New York, N.Y.) 119*, 3081, 80–82.

GABRIEL, R., THIEME, N., LIU, Q., LI, F., MEYER, L.T., HARTH, S., JECMENICA, M., RAMAMURTHY, M., GORMAN, J., SIMMONS, B.A., MCCLUSKEY, K., BAKER, S.E., TIAN, C., SCHUERG, T., SINGER, S.W., FLEIßNER, A., AND BENZ, J.P. 2021. The F-box protein gene *exo-1* is a target for reverse engineering enzyme hypersecretion in filamentous fungi. *Proceedings of the National Academy of Sciences of the United States of America 118*, 26.

GALAGAN, J.E., CALVO, S.E., BORKOVICH, K.A., SELKER, E.U., READ, N.D., JAFFE, D., FITZHUGH, W., MA, L.-J., SMIRNOV, S., PURCELL, S., REHMAN, B., ELKINS, T., ENGELS, R., WANG, S., NIELSEN, C.B., BUTLER, J., ENDRIZZI, M., QUI, D., IANAKIEV, P., BELL-PEDERSEN, D., NELSON, M.A., WERNER-WASHBURNE, M., SELITRENNIKOFF, C.P., KINSEY, J.A., BRAUN, E.L., ZELTER, A., SCHULTE, U., KOTHE, G.O., JEDD, G., MEWES, W., STABEN, C., MARCOTTE, E., GREENBERG, D., ROY, A., FOLEY, K., NAYLOR, J., STANGE-THOMANN, N., BARRETT, R., GNERRE, S., KAMAL, M., KAMVYSSELIS, M., MAUCELI, E., BIELKE, C., RUDD, S., FRISHMAN, D., KRYSTOFOVA, S., RASMUSSEN, C., METZENBERG, R.L., PERKINS, D.D., KROKEN, S., COGONI, C., MACINO, G., CATCHESIDE, D., LI, W., PRATT, R.J., OSMANI, S.A., DESOUZA, C.P.C., GLASS, L., ORBACH, M.J., BERGLUND, J.A., VOELKER, R., YARDEN, O., PLAMANN, M., SEILER, S., DUNLAP, J., RADFORD, A., ARAMAYO, R., NATVIG, D.O., ALEX, L.A., MANNHAUPT, G., EBBOLE, D.J., FREITAG, M., PAULSEN, I., SACHS, M.S., LANDER, E.S., NUSBAUM, C., AND BIRREN, B. 2003. The genome sequence of the filamentous fungus *Neurospora crassa*. *Nature 422*, 6934, 859–868.

GALAZKA, J.M., TIAN, C., BEESON, W.T., MARTINEZ, B., GLASS, N.L., AND CATE, J.H.D. 2010. Cellodextrin transport in yeast for improved biofuel production. *Science (New York, N.Y.) 330*, 6000, 84–86.

GANOTH, D., BORNSTEIN, G., KO, T.K., LARSEN, B., TYERS, M., PAGANO, M., AND HERSHKO, A. 2001. The cell-cycle regulatory protein Cks1 is required for SCF^{Skp2}-mediated ubiquitinylation of p27. *Nat Cell Biol 3*, 3, 321–324. https://www.nature.com/articles/ncb0301_321.

GARCÍA, I., MATHIEU, M., NIKOLAEV, I., FELENBOK, B., AND SCAZZOCCHIO, C. 2008. Roles of the *Aspergillus nidulans* homologues of Tup1 and Ssn6 in chromatin structure and cell viability. *FEMS microbiology letters 289*, 2, 146–154.

GLASS, N.L. 2012. *The Fungal Nutritional ENCODE project*. United States: N. p., Web.

GLASS, N.L., SCHMOLL, M., CATE, J.H.D., AND CORADETTI, S. 2013. Plant cell wall deconstruction by ascomycete fungi. *Annual review of microbiology 67*, 477–498.

GOH, P.Y., AND SURANA, U. 1999. Cdc4, a protein required for the onset of S phase, serves an essential function during G_2/M transition in *Saccharomyces cerevisiae*. *Molecular and cellular biology 19*, 8, 5512–5522.

GOLDSTEIN, G., SCHEID, M., HAMMERLING, U., SCHLESINGER, D.H., NIALL, H.D., AND BOYSE, E.A. 1975. Isolation of a polypeptide that has lymphocyte-differentiating properties and is probably represented universally in living cells. *Proceedings of the National Academy of Sciences of the United States of America 72*, 1, 11–15. https://www.ncbi.nlm.nih.gov/pmc/articles/PMC432229/.

GRAS, D.E., PERSINOTI, G.F., PERES, N.T.A., MARTINEZ-ROSSI, N.M., TAHIRA, A.C., REIS, E.M., PRADE, R.A., AND ROSSI, A. 2013. Transcriptional profiling of *Neurospora crassa* Δ*mak-2* reveals that mitogen-activated protein kinase MAK-2 participates in the phosphate signaling pathway. *Fungal genetics and biology : FG & B 60*, 140–149. https://www.sciencedirect.com/science/article/pii/S1087184513001011.

GRIFFIN, D.H. 1994. *Fungal physiology*. Wiley-Liss, New York.

GUERRIERO, G., HAUSMAN, J.-F., STRAUSS, J., ERTAN, H., AND SIDDIQUI, K.S. 2015. Destructuring plant biomass: focus on fungal and extremophilic cell wall hydrolases. *Plant science : an international journal of experimental plant biology 234*, 180–193.

HE, Q., CHENG, P., HE, Q., AND LIU, Y. 2005. The COP9 signalosome regulates the *Neurospora* circadian clock by controlling the stability of the SCF^{FWD-1} complex. *Genes & development 19*, 13, 1518–1531.

HE, Q., CHENG, P., YANG, Y., HE, Q., YU, H., AND LIU, Y. 2003. FWD1-mediated degradation of FREQUENCY in *Neurospora* establishes a conserved mechanism for circadian clock regulation. *The EMBO Journal 22*, 17, 4421–4430.

HERMAND, D. 2006. F-box proteins: more than baits for the SCF? *Cell division 1*, 30.

HERSHKO, A., HELLER, H., ELIAS, S., AND CIECHANOVER, A. 1983. Components of ubiquitin-protein ligase system. Resolution, affinity purification, and role in protein breakdown. *Journal of Biological Chemistry 258*, 13, 8206–8214. https://www.sciencedirect.com/science/article/pii/S002192582082050X.

HICKS, J., LOCKINGTON, R.A., STRAUSS, J., DIERINGER, D., KUBICEK, C.P., KELLY, J., AND KELLER, N. 2001. RcoA has pleiotropic effects on *Aspergillus nidulans* cellular development. *Molecular microbiology 39*, 6, 1482–1493.

HONDA, S., AND SELKER, E.U. 2009. Tools for fungal proteomics: multifunctional *Neurospora* vectors for gene replacement, protein expression and protein purification. *Genetics 182*, 1, 11–23.

HORTA, M.A.C., THIEME, N., GAO, Y., BURNUM-JOHNSON, K.E., NICORA, C.D., GRITSENKO, M.A., LIPTON, M.S., MOHANRAJ, K., ASSIS, L.J. DE, LIN, L., TIAN, C., BRAUS, G.H., BORKOVICH, K.A., SCHMOLL, M., LARRONDO, L.F., SAMAL, A., GOLDMAN, G.H., AND BENZ, J.P. 2019. Broad Substrate-Specific Phosphorylation Events Are Associated With the Initial Stage of Plant Cell Wall Recognition in *Neurospora crassa*. *Frontiers in Microbiology 10*, 2317.

HUBERMAN, L.B., CORADETTI, S.T., AND GLASS, N.L. 2017. Network of nutrient-sensing pathways and a conserved kinase cascade integrate osmolarity and carbon sensing in Neurospora crassa. *Proceedings of the National Academy of Sciences of the United States of America 114*, 41, E8665-E8674. https://www.ncbi.nlm.nih.gov/pmc/articles/PMC5642704/.

HUBERMAN, L.B., LIU, J., QIN, L., AND GLASS, N.L. 2016. Regulation of the lignocellulolytic response in filamentous fungi. *Fungal Biology Reviews 30*, 3, 101–111. https://www.sciencedirect.com/science/article/pii/S1749461316300379.

HUIBREGTSE, J.M., SCHEFFNER, M., BEAUDENON, S., AND HOWLEY, P.M. 1995. A family of proteins structurally and functionally related to the E6-AP ubiquitin-protein ligase. *Proceedings of the National Academy of Sciences of the United States of America 92*, 7, 2563–2567.

HYNES, M.J., AND KELLY, J.M. 1977. Pleiotropic mutants of *Aspergillus nidulans* altered in carbon metabolism. *Molecular & general genetics : MGG 150*, 2, 193–204.

IEA. 2023. *CO2 Emissions in 2022*. https://www.iea.org/reports/co2-emissions-in-2022. Accessed 27 June 2023.

JACOBSON, D.J., DETTMAN, J.R., ADAMS, R.I., BOESL, C., SULTANA, S., ROENNEBERG, T., MERROW, M., DUARTE, M., MARQUES, I., USHAKOVA, A., CARNEIRO, P., VIDEIRA, A., NAVARRO-SAMPEDRO, L., OLMEDO, M., CORROCHANO, L.M., AND TAYLOR, J.W. 2006. New findings of *Neurospora* in Europe and comparisons of diversity in temperate climates on continental scales. *Mycologia 98*, 4, 550–559.

JIN, J., CARDOZO, T., LOVERING, R.C., ELLEDGE, S.J., PAGANO, M., AND HARPER, J.W. 2004. Systematic analysis and nomenclature of mammalian F-box proteins. *Genes & development 18*, 21, 2573–2580.

JONKERS, W., FISCHER, M.S., DO, H.P., STARR, T.L., AND GLASS, N.L. 2016. Chemotropism and Cell Fusion in *Neurospora crassa* Relies on the Formation of Distinct Protein Complexes by HAM-5 and a Novel Protein HAM-14. *Genetics 203*, 1, 319–334.

JONKERS, W., AND REP, M. 2009. Lessons from fungal F-box proteins. *Eukaryotic Cell 8*, 5, 677–695. https://www.ncbi.nlm.nih.gov/pmc/articles/PMC2681605/.

KAMADURAI, H.B., SOUPHRON, J., SCOTT, D.C., DUDA, D.M., MILLER, D.J., STRINGER, D., PIPER, R.C., AND SCHULMAN, B.A. 2009. Insights into ubiquitin transfer cascades from a

structure of a UbcH5B approximately ubiquitin-HECT(NEDD4L) complex. *Molecular Cell 36*, 6, 1095–1102. https://www.ncbi.nlm.nih.gov/pmc/articles/PMC2859195/.

KATO, A., KURASHIMA, K., CHAE, M., SAWADA, S., HATAKEYAMA, S., TANAKA, S., AND INOUE, H. 2010. Deletion of a novel F-box protein, MUS-10, in *Neurospora crassa* leads to altered mitochondrial morphology, instability of mtDNA and senescence. *Genetics 185*, 4, 1257–1269.

KAYS, A.M., ROWLEY, P.S., BAASIRI, R.A., AND BORKOVICH, K.A. 2000. Regulation of conidiation and adenylyl cyclase levels by the Galpha protein GNA-3 in *Neurospora crassa*. *Molecular and cellular biology 20*, 20, 7693–7705.

KERKAERT, J.D., AND HUBERMAN, L.B. 2023. Regulation of nutrient utilization in filamentous fungi. *Appl Microbiol Biotechnol*, 1–26. https://link.springer.com/article/10.1007/s00253-023-12680-4.

KIM, D., LANGMEAD, B., AND SALZBERG, S.L. 2015. HISAT: a fast spliced aligner with low memory requirements. *Nat Methods 12*, 4, 357–360. https://www.nature.com/articles/nmeth.3317.

KIM, J.D.-M. 2011. *Elucidation of G-Protein Signal Transduction in Neurospora crassa Using Chemical Genomics, Metabonomics, and Genetics*. Dissertation, University of California.

KIPREOS, E.T., AND PAGANO, M. 2000. The F-box protein family. *Genome Biol 1*, 5, REVIEWS3002. https://link.springer.com/article/10.1186/gb-2000-1-5-reviews3002.

KÕIVOMÄGI, M., VALK, E., VENTA, R., IOFIK, A., LEPIKU, M., BALOG, E.R.M., RUBIN, S.M., MORGAN, D.O., AND LOOG, M. 2011. Cascades of multisite phosphorylation control Sic1 destruction at the onset of S phase. *Nature 480*, 7375, 128–131.

KOSUGI, S., HASEBE, M., TOMITA, M., AND YANAGAWA, H. 2009. Systematic identification of cell cycle-dependent yeast nucleocytoplasmic shuttling proteins by prediction of composite motifs. *Proceedings of the National Academy of Sciences of the United States of America 106*, 25, 10171–10176.

KRIZSÁN, K., ALMÁSI, É., MERÉNYI, Z., SAHU, N., VIRÁGH, M., KÓSZÓ, T., MONDO, S., KISS, B., BÁLINT, B., KÜES, U., BARRY, K., CSEKLYE, J., HEGEDÜS, B., HENRISSAT, B., JOHNSON, J., LIPZEN, A., OHM, R.A., NAGY, I., PANGILINAN, J., YAN, J., XIONG, Y., GRIGORIEV, I.V., HIBBETT, D.S., AND NAGY, L.G. 2019. Transcriptomic atlas of mushroom development reveals conserved genes behind complex multicellularity in fungi. *Proceedings of the National Academy of Sciences of the United States of America 116*, 15, 7409–7418. https://www.pnas.org/doi/10.1073/pnas.1817822116.

KUBICEK, C.P. 2013. *Fungi and lignocellulosic biomass*. Biomass and biofuels series. Wiley-Blackwell, Ames, Iowa.

KUMAR, A., AND PAIETTA, J.V. 1998. An additional role for the F-box motif: gene regulation within the *Neurospora crassa* sulfur control network. *Proceedings of the National Academy of Sciences of the United States of America 95*, 5, 2417–2422.

LETUNIC, I., AND BORK, P. 2018. 20 years of the SMART protein domain annotation resource. *Nucleic acids research 46*, D1, D493-D496.

LETUNIC, I., AND BORK, P. 2021. Interactive Tree Of Life (iTOL) v5: an online tool for phylogenetic tree display and annotation. *Nucleic acids research 49*, W1, W293-W296.

LETUNIC, I., KHEDKAR, S., AND BORK, P. 2021. SMART: recent updates, new developments and status in 2020. *Nucleic acids research 49*, D1, D458-D460.

LI, J., LIN, L., LI, H., TIAN, C., AND MA, Y. 2014. Transcriptional comparison of the filamentous fungus *Neurospora crassa* growing on three major monosaccharides D-glucose, D-xylose and L-arabinose. *Biotechnol Biofuels 7*, 1, 31.

LI, J., LIU, Q., LI, J., LIN, L., LI, X., ZHANG, Y., AND TIAN, C. 2021. RCO-3 and COL-26 form an external-to-internal module that regulates the dual-affinity glucose transport system in *Neurospora crassa*. *Biotechnol Biofuels 14*, 1, 33. https://biotechnologyforbiofuels.biomedcentral.com/articles/10.1186/s13068-021-01877-2.

LI, L., AND BORKOVICH, K.A. 2006. GPR-4 is a predicted G-protein-coupled receptor required for carbon source-dependent asexual growth and development in *Neurospora crassa*. *Eukaryotic Cell 5*, 8, 1287–1300.

LI, Z., YAO, G., WU, R., GAO, L., KAN, Q., LIU, M., YANG, P., LIU, G., QIN, Y., SONG, X., ZHONG, Y., FANG, X., AND QU, Y. 2015. Synergistic and Dose-Controlled Regulation of Cellulase Gene Expression in *Penicillium oxalicum*. *PLOS Genetics 11*, 9, e1005509.

LIN, L., CHEN, Y., LI, J., WANG, S., SUN, W., AND TIAN, C. 2017. Disruption of non-anchored cell wall protein NCW-1 promotes cellulase production by increasing cellobiose uptake in *Neurospora crassa*. *Biotechnol Lett 39*, 4, 545–551. https://link.springer.com/article/10.1007/s10529-016-2274-1.

LIN, L., SUN, Z., LI, J., CHEN, Y., LIU, Q., SUN, W., AND TIAN, C. 2018. Disruption of *gul-1* decreased the culture viscosity and improved protein secretion in the filamentous fungus *Neurospora crassa*. *Microbial cell factories 17*, 1, 96.

LIN, L., WANG, S., LI, X., HE, Q., BENZ, J.P., AND TIAN, C. 2019. STK-12 acts as a transcriptional brake to control the expression of cellulase-encoding genes in Neurospora crassa. *PLOS Genetics 15*, 11, e1008510.

LIU, Q., LI, J., GAO, R., LI, J., MA, G., AND TIAN, C. 2019. CLR-4, a novel conserved transcription factor for cellulase gene expression in ascomycete fungi. *Molecular microbiology 111*, 2, 373–394.

LIU, W., XIE, Y., MA, J., LUO, X., NIE, P., ZUO, Z., LAHRMANN, U., ZHAO, Q., ZHENG, Y., ZHAO, Y., XUE, Y., AND REN, J. 2015. IBS: an illustrator for the presentation and visualization of biological sequences. *Bioinformatics (Oxford, England) 31*, 20, 3359–3361.

LIU, Y., NAKATSUKASA, K., KOTERA, M., KANADA, A., NISHIMURA, T., KISHI, T., MIMURA, S., AND KAMURA, T. 2011. Non-SCF-type F-box protein Roy1/Ymr258c interacts with a Rab5-like GTPase Ypt52 and inhibits Ypt52 function. *Molecular biology of the cell 22*, 9, 1575–1584.

LOBO, D.S., PEREIRA, I.B., FRAGEL-MADEIRA, L., MEDEIROS, L.N., CABRAL, L.M., FARIA, J., BELLIO, M., CAMPOS, R.C., LINDEN, R., AND KURTENBACH, E. 2007. Antifungal *Pisum sativum* defensin 1 interacts with *Neurospora crassa* cyclin F related to the cell cycle. *Biochemistry 46*, 4, 987–996.

LOCKINGTON, R.A., AND KELLY, J.M. 2002. The WD40-repeat protein CreC interacts with and stabilizes the deubiquitinating enzyme CreB *in vivo* in *Aspergillus nidulans*. *Molecular microbiology 43*, 5, 1173–1182. https://onlinelibrary.wiley.com/doi/full/10.1046/j.1365-2958.2002.02811.x.

LOVE, M.I., HUBER, W., AND ANDERS, S. 2014. Moderated estimation of fold change and dispersion for RNA-seq data with DESeq2. *Genome Biol 15*, 12, 550. https://genomebiology.biomedcentral.com/articles/10.1186/s13059-014-0550-8?ref=https://githubhelp.com.

MALIHA, A., AND ABU-HIJLEH, B. 2022. A review on the current status and post-pandemic prospects of third-generation biofuels. *Energy Syst*, 1–32. https://link.springer.com/article/10.1007/s12667-022-00514-7.

MASI, A., MACH, R.L., AND MACH-AIGNER, A.R. 2021. The pentose phosphate pathway in industrially relevant fungi: crucial insights for bioprocessing. *Appl Microbiol Biotechnol 105*, 10, 4017–4031. https://www.ncbi.nlm.nih.gov/pmc/articles/PMC8140973/.

MCCLUSKEY, K., WIEST, A., AND PLAMANN, M. 2010. The Fungal Genetics Stock Center: a repository for 50 years of fungal genetics research. *Journal of biosciences 35*, 1, 119–126.

METZGER, M.B., HRISTOVA, V.A., AND WEISSMAN, A.M. 2012. HECT and RING finger families of E3 ubiquitin ligases at a glance. *J Cell Sci 125*, Pt 3, 531–537. https://journals.biologists.com/jcs/article/125/3/531/32708/HECT-and-RING-finger-families-of-E3-ubiquitin.

METZGER, M.B., PRUNEDA, J.N., KLEVIT, R.E., AND WEISSMAN, A.M. 2014. RING-type E3 ligases: master manipulators of E2 ubiquitin-conjugating enzymes and ubiquitination. *Biochimica et biophysica acta 1843*, 1, 47–60.

MEYER, V., BASENKO, E.Y., BENZ, J.P., BRAUS, G.H., CADDICK, M.X., CSUKAI, M., VRIES, R.P. DE, ENDY, D., FRISVAD, J.C., GUNDE-CIMERMAN, N., HAARMANN, T., HADAR, Y., HANSEN, K., JOHNSON, R.I., KELLER, N.P., KRAŠEVEC, N., MORTENSEN, U.H., PEREZ, R., RAM, A.F.J., RECORD, E., ROSS, P., SHAPAVAL, V., STEINIGER, C., VAN DEN BRINK, H., VAN MUNSTER, J., YARDEN, O., AND WÖSTEN, H.A.B. 2020. Growing a circular economy with fungal biotechnology: a white paper. *Fungal Biol Biotechnol 7*, 1, 5. https://fungalbiolbiotech.biomedcentral.com/articles/10.1186/s40694-020-00095-z.

MOHNEN, D. 2008. Pectin structure and biosynthesis. *Current opinion in plant biology 11*, 3, 266–277. https://pubmed.ncbi.nlm.nih.gov/18486536/.

MYLYK, O.M., BARRY, E.G., AND GALEAZZI, D.R. 1974. New isogenic wild types in *N. crassa*. *Fungal Genetics Reports 21*, 1.

NEER, E.J., SCHMIDT, C.J., NAMBUDRIPAD, R., AND SMITH, T.F. 1994. The ancient regulatory-protein family of WD-repeat proteins. *Nature 371*, 6495, 297–300. https://www.nature.com/articles/371297a0.

OKOYE, C.N., ROWLING, P.J.E., ITZHAKI, L.S., AND LINDON, C. 2022. Counting Degrons: Lessons From Multivalent Substrates for Targeted Protein Degradation. *Frontiers in physiology 13*, 913063.

ORLICKY, S., TANG, X., WILLEMS, A., TYERS, M., AND SICHERI, F. 2003. Structural basis for phosphodependent substrate selection and orientation by the SCF^{Cdc4} ubiquitin ligase. *Cell 112*, 2, 243–256.

OSMAN, A.I., CHEN, L., YANG, M., MSIGWA, G., FARGHALI, M., FAWZY, S., ROONEY, D.W., AND YAP, P.-S. 2023. Cost, environmental impact, and resilience of renewable energy under a changing climate: a review. *Environ Chem Lett 21*, 2, 741–764. https://link-springer-com.eaccess.tum.edu/article/10.1007/s10311-022-01532-8.

ØSTBY, H., HANSEN, L.D., HORN, S.J., EIJSINK, V.G.H., AND VÁRNAI, A. 2020. Enzymatic processing of lignocellulosic biomass: principles, recent advances and perspectives. *J Ind Microbiol Biotechnol 47*, 9-10, 623–657. https://link.springer.com/article/10.1007/s10295-020-02301-8.

PARK, Y.-C., SAN, K.-Y., AND BENNETT, G.N. 2007. Characterization of alcohol dehydrogenase 1 and 3 from *Neurospora crassa* FGSC2489. *Appl Microbiol Biotechnol 76*, 2, 349–356. https://link.springer.com/article/10.1007/s00253-007-0998-5.

PAYSAN-LAFOSSE, T., BLUM, M., CHUGURANSKY, S., GREGO, T., PINTO, B.L., SALAZAR, G.A., BILESCHI, M.L., BORK, P., BRIDGE, A., COLWELL, L., GOUGH, J., HAFT, D.H., LETUNIĆ, I., MARCHLER-BAUER, A., MI, H., NATALE, D.A., ORENGO, C.A., PANDURANGAN, A.P., RIVOIRE, C., SIGRIST, C.J.A., SILLITOE, I., THANKI, N., THOMAS, P.D., TOSATTO, S.C.E., WU, C.H., AND BATEMAN, A. 2023. InterPro in 2022. *Nucleic acids research 51*, D1, D418-D427.

PEREZ-RIBA, A., AND ITZHAKI, L.S. 2019. The tetratricopeptide-repeat motif is a versatile platform that enables diverse modes of molecular recognition. *Current Opinion in Structural Biology 54*, 43–49. https://www.sciencedirect.com/science/article/pii/S0959440X18301647.

PERTEA, M., PERTEA, G.M., ANTONESCU, C.M., CHANG, T.-C., MENDELL, J.T., AND SALZBERG, S.L. 2015. StringTie enables improved reconstruction of a transcriptome from RNA-seq reads. *Nat Biotechnol 33*, 3, 290–295. https://www.nature.com/articles/nbt.3122.

POTUSCHAK, T., STARY, S., SCHLÖGELHOFER, P., BECKER, F., NEJINSKAIA, V., AND BACHMAIR, A. 1998. PRT1 of *Arabidopsis thaliana* encodes a component of the plant N-end rule pathway. *Proceedings of the National Academy of Sciences of the United States of America 95*, 14, 7904–7908.

PRIEBE, S., KREISEL, C., HORN, F., GUTHKE, R., AND LINDE, J. 2015. FungiFun2: a comprehensive online resource for systematic analysis of gene lists from fungal species. *Bioinformatics (Oxford, England) 31*, 3, 445–446.

RADFORD, A. 2004. Metabolic Highways of *Neurospora crassa* Revisited. In *Advances in Genetics*. Academic Press, 165–207.

RAVID, T., AND HOCHSTRASSER, M. 2008. Diversity of degradation signals in the ubiquitin-proteasome system. *Nat Rev Mol Cell Biol 9*, 9, 679–690.

REITSMA, J.M., LIU, X., REICHERMEIER, K.M., MORADIAN, A., SWEREDOSKI, M.J., HESS, S., AND DESHAIES, R.J. 2017. Composition and Regulation of the Cellular Repertoire of SCF Ubiquitin Ligases. *Cell 171*, 6, 1326-1339.e14. https://www.cell.com/cell/pdf/S0092-8674(17)31238-2.pdf.

REN, J., WEN, L., GAO, X., JIN, C., XUE, Y., AND YAO, X. 2009. DOG 1.0: illustrator of protein domain structures. *Cell Res 19*, 2, 271–273. https://www.nature.com/articles/cr20096.

RIES, L., PULLAN, S.T., DELMAS, S., MALLA, S., BLYTHE, M.J., AND ARCHER, D.B. 2013. Genome-wide transcriptional response of *Trichoderma reesei* to lignocellulose using RNA sequencing and comparison with *Aspergillus niger*. *BMC Genomics 14*, 541.

RIES, L.N.A., BEATTIE, S.R., ESPESO, E.A., CRAMER, R.A., AND GOLDMAN, G.H. 2016. Diverse Regulation of the CreA Carbon Catabolite Repressor in *Aspergillus nidulans*. *Genetics 203*, 1, 335–352.

RUEPP, A., ZOLLNER, A., MAIER, D., ALBERMANN, K., HANI, J., MOKREJS, M., TETKO, I., GÜLDENER, U., MANNHAUPT, G., MÜNSTERKÖTTER, M., AND MEWES, H.W. 2004. The FunCat, a functional annotation scheme for systematic classification of proteins from whole genomes. *Nucleic acids research 32*, 18, 5539–5545.

SALAS-LLORET, D., AND GONZÁLEZ-PRIETO, R. 2022. Insights in Post-Translational Modifications: Ubiquitin and SUMO. *International Journal of Molecular Sciences 23*, 6.

SÁNCHEZ, C. 2009. Lignocellulosic residues: biodegradation and bioconversion by fungi. *Biotechnology Advances 27*, 2, 185–194. https://www.sciencedirect.com/science/article/pii/S0734975008001092.

SARIKAYA BAYRAM, Ö., BAYRAM, Ö., KARAHODA, B., MEISTER, C., KÖHLER, A.M., THIEME, S., ELRAMLI, N., FRAWLEY, D., MCGOWAN, J., FITZPATRICK, D.A., SCHMITT, K., ASSIS, L.J. DE, VALERIUS, O., GOLDMAN, G.H., AND BRAUS, G.H. 2022. F-box receptor mediated control of substrate stability and subcellular location organizes cellular development of *Aspergillus nidulans*. *PLOS Genetics 18*, 12, e1010502. https://journals.plos.org/plosgenetics/article?id=10.1371/journal.pgen.1010502.

SCHEFFNER, M., NUBER, U., AND HUIBREGTSE, J.M. 1995. Protein ubiquitination involving an E1-E2-E3 enzyme ubiquitin thioester cascade. *Nature 373*, 6509, 81–83. https://www.nature.com/articles/373081a0.

SCHMIDT, M.W., MCQUARY, P.R., WEE, S., HOFMANN, K., AND WOLF, D.A. 2009. F-box-directed CRL complex assembly and regulation by the CSN and CAND1. *Molecular Cell 35*, 5, 586–597. https://www.sciencedirect.com/science/article/pii/S1097276509005565.

SCHMOLL, M., TIAN, C., SUN, J., TISCH, D., AND GLASS, N.L. 2012. Unravelling the molecular basis for light modulated cellulase gene expression - the role of photoreceptors in *Neurospora crassa*. *BMC Genomics 13*, 1, 127. https://bmcgenomics.biomedcentral.com/articles/10.1186/1471-2164-13-127.

SCHOLS, H.A., POSTHUMUS, M.A., AND VORAGEN, A.G. 1990. Structural features of hairy regions of pectins isolated from apple juice produced by the liquefaction process. *Carbohydrate Research 206*, 1, 117–129. https://www.sciencedirect.com/science/article/pii/000862159084011I.

SCHULMAN, B.A., CARRANO, A.C., JEFFREY, P.D., BOWEN, Z., KINNUCAN, E.R., FINNIN, M.S., ELLEDGE, S.J., HARPER, J.W., PAGANO, M., AND PAVLETICH, N.P. 2000. Insights into SCF ubiquitin ligases from the structure of the Skp1-Skp2 complex. *Nature 408*, 6810, 381–386. https://www.nature.com/articles/35042620.

SEIBERT, V., PROHL, C., SCHOULTZ, I., RHEE, E., LOPEZ, R., ABDERAZZAQ, K., ZHOU, C., AND WOLF, D.A. 2002. Combinatorial diversity of fission yeast SCF ubiquitin ligases by homo- and heterooligomeric assemblies of the F-box proteins Pop1p and Pop2p. *BMC Biochemistry 3*, 22. https://www.ncbi.nlm.nih.gov/pmc/articles/PMC128837/.

SEN, A., ACOSTA-SAMPSON, L., ALVARO, C.G., AHN, J.S., CATE, J.H.D., AND THORNER, J. 2016. Internalization of Heterologous Sugar Transporters by Endogenous α-Arrestins in the Yeast *Saccharomyces cerevisiae*. *Applied and environmental microbiology 82*, 24, 7074–7085.

SHEAR, C.L., AND DODGE, B.O. 1927. *Life histories and heterothallism of the red bread-mold fungi of the Monilia sitophila group*. US Government Printing Office Washington, DC.

SIEVERS, F., WILM, A., DINEEN, D., GIBSON, T.J., KARPLUS, K., LI, W., LOPEZ, R., MCWILLIAM, H., REMMERT, M., SÖDING, J., THOMPSON, J.D., AND HIGGINS, D.G. 2011. Fast, scalable generation of high-quality protein multiple sequence alignments using Clustal Omega. *Molecular systems biology 7*, 539.

SKAAR, J.R., PAGAN, J.K., AND PAGANO, M. 2013. Mechanisms and function of substrate recruitment by F-box proteins. *Nat Rev Mol Cell Biol 14*, 6, 369–381. https://www.nature.com/articles/nrm3582.

SKOWYRA, D., CRAIG, K.L., TYERS, M., ELLEDGE, S.J., AND HARPER, J.W. 1997. F-box proteins are receptors that recruit phosphorylated substrates to the SCF ubiquitin-ligase complex. *Cell 91*, *2*, 209–219.

SOMERVILLE, C., BAUER, S., BRININSTOOL, G., FACETTE, M., HAMANN, T., MILNE, J., OSBORNE, E., PAREDEZ, A., PERSSON, S., RAAB, T., VORWERK, S., AND YOUNGS, H. 2004. Toward a systems approach to understanding plant cell walls. *Science (New York, N.Y.) 306*, 5705, 2206–2211.

SUN, J., AND GLASS, N.L. 2011. Identification of the CRE-1 cellulolytic regulon in *Neurospora crassa*. *PLoS ONE 6*, 9, e25654.

SZILÁGYI, M., MISKEI, M., KARÁNYI, Z., LENKEY, B., PÓCSI, I., AND EMRI, T. 2013. Transcriptome changes initiated by carbon starvation in *Aspergillus nidulans*. *Microbiology (Reading, England) 159*, Pt 1, 176–190.

SZŐKE, A., SÁRKÁNY, O., SCHERMANN, G., KAPUY, O., DIERNFELLNER, A.C.R., BRUNNER, M., GYÖNGYÖSI, N., AND KÁLDI, K. 2023. Adaptation to glucose starvation is associated with molecular reorganization of the circadian clock in *Neurospora crassa*. *eLife 12*.

TAIZ, L., AND ZEIGER, E. 2002. *Plant physiology*. W. H. Freeman, New York.

THE UNIPROT CONSORTIUM. 2023. UniProt: the Universal Protein Knowledgebase in 2023. *Nucleic acids research 51*, D1, D523-D531.

THIEME, N. 2019. *Plant polysaccharide perception and its molecular regulation – with a focus on pectin degradation – in Neurospora crassa*. Dissertation, Technische Universität München.

THIEME, N., WU, V.W., DIETSCHMANN, A., SALAMOV, A.A., WANG, M., JOHNSON, J., SINGAN, V.R., GRIGORIEV, I.V., GLASS, N.L., SOMERVILLE, C.R., AND BENZ, J.P. 2017. The transcription factor PDR-1 is a multi-functional regulator and key component of pectin deconstruction and catabolism in *Neurospora crassa*. *Biotechnol Biofuels 10*, 1, 149. https://biotechnologyforbiofuels.biomedcentral.com/articles/10.1186/s13068-017-0807-z.

THOMAS, P.D., EBERT, D., MURUGANUJAN, A., MUSHAYAHAMA, T., ALBOU, L.-P., AND MI, H. 2022. PANTHER: Making genome-scale phylogenetics accessible to all. *Protein science : a publication of the Protein Society 31*, 1, 8–22.

THOMPSON, L.L., RUTHERFORD, K.A., LEPAGE, C.C., AND MCMANUS, K.J. 2021. The SCF Complex Is Essential to Maintain Genome and Chromosome Stability. *International Journal of Molecular Sciences 22*, 16.

THROWER, J.S., HOFFMAN, L., RECHSTEINER, M., AND PICKART, C.M. 2000. Recognition of the polyubiquitin proteolytic signal. *The EMBO Journal 19*, 1, 94–102. https://pubmed.ncbi.nlm.nih.gov/10619848/.

TIAN, C., BEESON, W.T., IAVARONE, A.T., SUN, J., MARLETTA, M.A., CATE, J.H.D., AND GLASS, N.L. 2009. Systems analysis of plant cell wall degradation by the model filamentous fungus *Neurospora crassa*. *Proceedings of the National Academy of Sciences of the United States of America 106*, 52, 22157–22162.

TISCH, D., AND SCHMOLL, M. 2010. Light regulation of metabolic pathways in fungi. *Appl Microbiol Biotechnol 85*, 5, 1259–1277. https://link.springer.com/article/10.1007/s00253-009-2320-1.

TODD, R.B., LOCKINGTON, R.A., AND KELLY, J.M. 2000. The *Aspergillus nidulans creC* gene involved in carbon catabolite repression encodes a WD40 repeat protein. *Molecular & general genetics : MGG 263*, 4, 561–570.

TREITEL, M.A., AND CARLSON, M. 1995. Repression by SSN6-TUP1 is directed by MIG1, a repressor/activator protein. *Proceedings of the National Academy of Sciences of the United States of America 92*, 8, 3132–3136.

TYANOVA, S., TEMU, T., SINITCYN, P., CARLSON, A., HEIN, M.Y., GEIGER, T., MANN, M., AND COX, J. 2016. The Perseus computational platform for comprehensive analysis of (prote)omics data. *Nat Methods 13*, 9, 731–740. https://www.nature.com/articles/nmeth.3901.

VAN DEN BOSCH, S., KOELEWIJN, S.-F., RENDERS, T., VAN DEN BOSSCHE, G., VANGEEL, T., SCHUTYSER, W., AND SELS, B.F. 2018. Catalytic Strategies Towards Lignin-Derived Chemicals. *Topics in current chemistry (Cham) 376*, 5, 36. https://link-springer-com.eaccess.tum.edu/article/10.1007/s41061-018-0214-3.

VARNER, J.E., AND LIN, L.S. 1989. Plant cell wall architecture. *Cell 56*, 2, 231–239. https://www.sciencedirect.com/science/article/pii/0092867489908969.

VARSHAVSKY, A. 1991. Naming a targeting signal. *Cell 64*, 1, 13–15.

VIJAY-KUMAR, S., BUGG, C.E., AND COOK, W.J. 1987. Structure of ubiquitin refined at 1.8 A resolution. *Journal of molecular biology 194*, 3, 531–544.

VOGEL, H.J. 1956. A convenient growth medium for *Neurospora* (Medium N). *Microb Genet Bull*, 13, 42–43.

WANG, B., LI, J., GAO, J., CAI, P., HAN, X., AND TIAN, C. 2017. Identification and characterization of the glucose dual-affinity transport system in *Neurospora crassa*: pleiotropic roles in nutrient transport, signaling, and carbon catabolite repression. *Biotechnology for biofuels 10*, 17.

WANG, M., WU, M., AND HUO, H. 2007. Life-cycle energy and greenhouse gas emission impacts of different corn ethanol plant types. *Environ. Res. Lett. 2*, 2, 24001.

WANG, X.S., COTTON, T.R., TREVELYAN, S.J., RICHARDSON, L.W., LEE, W.T., SILKE, J., AND LECHTENBERG, B.C. 2023. The unifying catalytic mechanism of the RING-between-RING E3 ubiquitin ligase family. *Nat Commun 14*, 1, 168. https://www.nature.com/articles/s41467-023-35871-z.

WELCHMAN, R.L., GORDON, C., AND MAYER, R.J. 2005. Ubiquitin and ubiquitin-like proteins as multifunctional signals. *Nat Rev Mol Cell Biol 6*, 8, 599–609. https://www.nature.com/articles/nrm1700.

WENZEL, D.M., LISSOUNOV, A., BRZOVIC, P.S., AND KLEVIT, R.E. 2011. UBCH7 reactivity profile reveals parkin and HHARI to be RING/HECT hybrids. *Nature 474*, 7349, 105–108. https://www.nature.com/articles/nature09966.

WESTERGAARD, M., AND MITCHELL, H.K. 1947. *Neurospora* V. A synthetic medium favouring sexual reproduction. *American Journal of Botany*. https://www.semanticscholar.org/paper/NEUROSPORA-V.-A-SYNTHETIC-MEDIUM-FAVORING-SEXUAL-Westergaard-Mitchell/17576757e0384e921462c7c3c889d985e9816740.

WILLEMS, A.R., SCHWAB, M., AND TYERS, M. 2004. A hitchhiker's guide to the cullin ubiquitin ligases: SCF and its kin. *Biochimica et biophysica acta 1695*, 1-3, 133–170.

WILSON, K., AND LEE, A.F. 2016. Catalyst design for biorefining. *Philosophical transactions. Series A, Mathematical, physical, and engineering sciences 374*, 2061, 1–23.

WINSTON, J.T., KOEPP, D.M., ZHU, C., ELLEDGE, S.J., AND HARPER, J.W. 1999. A family of mammalian F-box proteins. *Current biology : CB 9*, 20, 1180–1182.

WU, V.W., THIEME, N., HUBERMAN, L.B., DIETSCHMANN, A., KOWBEL, D.J., LEE, J., CALHOUN, S., SINGAN, V.R., LIPZEN, A., XIONG, Y., MONTI, R., BLOW, M.J., O'MALLEY, R.C., GRIGORIEV, I.V., BENZ, J.P., AND GLASS, N.L. 2020. The regulatory and transcriptional landscape associated with carbon utilization in a filamentous fungus. *Proceedings of the National Academy of Sciences of the United States of America 117*, 11, 6003–6013. https://www.pnas.org/doi/full/10.1073/pnas.1915611117.

WU, W., KASUGA, T., XIONG, X., DI MA, AND FAN, Z. 2013. Location and contribution of individual β-glucosidase from Neurospora crassa to total β-glucosidase activity. *Arch Microbiol 195*, 12, 823–829. https://link.springer.com/article/10.1007/s00203-013-0931-5.

XIONG, Y., SUN, J., AND GLASS, N.L. 2014. VIB1, a link between glucose signaling and carbon catabolite repression, is essential for plant cell wall degradation by *Neurospora crassa*. *PLOS Genetics 10*, 8, e1004500.

ZHANG, Y., NADA, B., BAKER, S.E., EVANS, J.E., TIAN, C., BENZ, J.P., AND TAMAYO, E. 2024. Unveiling a classical mutant in the context of the GH3 β-glucosidase family in *Neurospora crassa*. *AMB Expr 14*, 1, 4. https://amb-express.springeropen.com/articles/10.1186/s13568-023-01658-0.

ZHENG, N., SCHULMAN, B.A., SONG, L., MILLER, J.J., JEFFREY, P.D., WANG, P., CHU, C., KOEPP, D.M., ELLEDGE, S.J., PAGANO, M., CONAWAY, R.C., CONAWAY, J.W., HARPER, J.W., AND PAVLETICH, N.P. 2002. Structure of the Cul1-Rbx1-Skp1-F boxSkp2 SCF ubiquitin ligase complex. *Nature 416*, 6882, 703–709. https://www.nature.com/articles/416703a.

ZHENG, N., AND SHABEK, N. 2017. Ubiquitin Ligases: Structure, Function, and Regulation. *Annual review of biochemistry 86*, 129–157. https://pubmed.ncbi.nlm.nih.gov/28375744/.

ZNAMEROSKI, E.A., CORADETTI, S.T., ROCHE, C.M., TSAI, J.C., IAVARONE, A.T., CATE, J.H.D., AND GLASS, N.L. 2012. Induction of lignocellulose-degrading enzymes in *Neurospora crassa* by cellodextrins. *Proceedings of the National Academy of Sciences of the United States of America 109*, 16, 6012–6017.

ZNAMEROSKI, E.A., LI, X., TSAI, J.C., GALAZKA, J.M., GLASS, N.L., AND CATE, J.H.D. 2014. Evidence for transceptor function of cellodextrin transporters in *Neurospora crassa*. *The Journal of biological chemistry 289*, 5, 2610–2619. https://www.sciencedirect.com/science/article/pii/S0021925819747838.

Acknowledgements

First of all, I want to thank Prof. Dr. J. Philipp Benz and Prof. Dr. Gustavo H. Goldman. Without both of you, this dissertation would not have been possible! Thank you Prof. Dr. J. Philipp Benz for giving me the opportunity to conduct the dissertation at your professorship, for keeping always the door open to talk about science and for your support throughout the whole process. Thank you Prof. Dr. Gustavo H. Goldman for your inspiring ideas, for being always supportive and always being ready for a meeting (virtually and in person) even if many miles and different time zones are in between Brazil and Germany. Muito obrigada!
Thank you both for your supervision and your advice. It was a pleasure to work with you.

Furthermore, I want to thank Dr. Karin Pritsch for being my mentor. I enjoyed our free, informal and joyful exchange a lot.

A special thanks goes to everyone from the Professorship of Fungal Biotechnology in Wood Science! I want to thank the post-docs Dr. Tanja Karl, Dr. Elisabeth Tamayo Martinez and Dr. Maria Augusta C. Horta for their guidance and support. Eli, thank you for always trying to shovel free time to give me advice, especially throughout the writing process. Maria, thank you for your support, especially with *in silico* analytics concerning the *fbx* ortholog search and RNA-sequencing data processing and thank you for being always ready to help, although you left the professorship during my doctorate (that was a heavy loss).

To all the doctoral candidates: Keep on going, you will get there!

I want to thank everyone from the lab group, not only for being the greatest colleagues you could wish for, also for becoming good friends. You have enriched my time here.
Thank you peers for the mutual support in every matter: Kevin Schmitz, Christina Hach, Yuxin Zhang, Manfred Reppke, Pia Stange, Marcel Rüllke, Basant Nada and Marcello Nussbaumer. Also, I want to thank Christina and Kevin for your precious advice! You helped me a lot in the beginning of my doctorate to get started and to grow into this challenge.
I would like to express a big thank you to our technical assistances Sabrina Klasen and Petra Arnold. You are the heart of the lab and have always kept everything running!

This dissertation would not be what it is without the help of collaborators!
Thank you very much Dr. Christina Ludwig, Franziska Hackbarth and Hermine Kienberger for teaching me the tryptic in-gel digestion, which I was allowed to perform at the Bavarian

Center for Biomolecular Mass Spectrometry (BayBioMS) in Weihenstephan, Freising. It was not a matter of course that I was allowed to do this there, therefore: Thank you so much!
Thank you very much Prof. Dr. Gerhard Braus, Dr. Kerstin Schmitt and Dr. Oliver Valerius for performing the mass spectrometry at Göttingen. It was a pleasure to collaborate with you.
I also want to thank Caroline Batchelor for helping with the Proteome Discoverer Software.
Thank you Dr. Leandro de Assis for your advice concerning the qualitative analysis of mass spectrometry data and Miriam Abele for your advice concerning the quantitative analysis of the mass spectrometry data.
Thank you Dr. Christine Wurmser for the preparation of the RNA-sequencing library. Thank you Dr. Stephanie Herzog for your advice and ideas concerning protein-protein interaction approaches.

Last but not least:
Ich möchte meiner Familie und meinen Freunden danken, für eure Unterstützung, euer Verständnis und die vielen schönen Momente, die wir gemeinsam verbracht haben.
Ich möchte insbesondere meinen Eltern danken! Ohne euch wäre ich nicht wer ich heute bin, und wo ich heute bin. Danke, dass ihr mir immer alles ermöglicht habt und mich gelehrt habt, an mich selbst zu glauben.

Zum Abschluss möchte ich mich bei einem der wichtigsten Menschen in meinem Leben bedanken: meinem Mann Stefan. Danke, dass du immer für mich da bist, mir immer die Kraft gegeben hast weiterzumachen, mich immer unterstützt und motiviert hast. Danke, dass du mit deiner ungezwungenen und fröhlichen Art so viel Freude in mein Leben bringst.